

Isotropic and Patchy Colloids with Engineered Surface Functionality



Universiteit Utrecht

Cover design: Ruben Heijbroek & Bas van Ravensteijn

ISBN: 978-94-623-3110-5

Subject headings: Colloids / patchy particles / colloidal dumbbells / Atom Transfer Radical Polymerization (ATRP) / thermo-reversible aggregation / out-of-equilibrium assembly / charge inversion / transfer hydrogenation.

Isotropic and Patchy Colloids with Engineered Surface Functionality

Isotrope en ‘Patchy’ Colloïden met Ontworpen
Oppervlakte Functionaliteiten

(met een samenvatting in het Nederlands)

Proefschrift

ter verkrijging van de graad van doctor aan de
Universiteit Utrecht op gezag van de rector magnificus,
prof. dr. G. J. van der Zwaan, ingevolge het besluit van het
college voor promoties in het openbaar te verdedigen
op woensdag 18 november 2015 des middags te 2.30 uur

door

Bas Gijsbertus Paulus van Ravensteijn

geboren op 18 april 1988 te Eindhoven

Promotor: Prof. dr. W. K. Kegel

Het in dit proefschrift beschreven onderzoek werd gefinancierd door het gebied Chemische Wetenschappen (CW) van de Nederlandse Organisatie voor Wetenschappelijk Onderzoek (NWO).

Contents

Chapter 1	Introduction	1
Part 1	Synthesis of Shape and Chemically Anisotropic Colloids	
Chapter 2	General Route toward Chemically Anisotropic Colloids	15
Chapter 3	Synthesis of Anisotropic Colloids from Chlorinated Seed Particles	35
Part 2	Colloidal Surface Modifications using ATRP	
Chapter 4	Atom Transfer Radical Polymerization (ATRP) on Colloidal Particles	69
Chapter 5	Thermo-reversible Aggregation of pNIPAM Grafted Colloids	127
Chapter 6	Site-specific Surface Modification of Patchy Colloids using Atom Transfer Radical Polymerization	149
Chapter 7	Out-of-equilibrium Aggregation of Colloidal Building Blocks	185
Part 3	Colloids with Tunable Surface Charge	
Chapter 8	Charge Inversion of Chlorinated Colloids in Dimethylformamide	209
Chapter 9	Colloids with Continuously Tunable Surface Charge	221
Part 4	Colloids for Catalysis	
Chapter 10	The Immobilization of a Transfer Hydrogenation Catalyst	251
	Summary	277
	Samenvatting in het Nederlands	281
	Acknowledgments	293
	List of Publications	297
	Curriculum Vitae	299

1

Introduction

Abstract

In this thesis the synthesis and (self-)assembly of a variety of chemically anisotropic or patchy colloidal particles is described. This Introduction chapter provides a motivation for the use of patchy colloids and the basic design criteria that need to be considered when a bottom-up structure formation route is applied. Moreover, the aim and scope of each chapter is highlighted.

1.1. Colloids as building blocks for self-assembly

The spontaneous formation of (functional) structures starting from a disordered situation is a common feature in biological systems.¹⁻³ These ordering phenomena can be spontaneous or driven by the input of (chemical) energy. The energy-driven or so-called dissipative systems will be treated in more detail in Section 1.2. The spontaneous assembly processes occur without energy consumption, since the total free energy of the system is lowered by arranging the building blocks in the appropriate manner.⁴⁻⁶ Therefore, the formed structure exists in a (local) free energy minimum and is consequently (meta)stable. Examples include the formation of virus capsids from proteins,⁷⁻⁹ cell membranes from phospholipids,^{10,11} and folding of proteins.¹²⁻¹⁴ The first two examples start from a random solution of individual building blocks, while folding of proteins starts during the formation of a single polymer that transforms from a random coil into a macromolecule with well-defined three-dimensional structure.

Capturing the physics behind self-assembly processes involved in these systems is not a trivial task due to two fundamental reasons. Firstly, the individual building blocks are of molecular dimensions and therefore not easily visualized. Hence, direct probing the dynamics of structure formation is practically impossible. Indirect methods, such as light scattering techniques, can provide information about the assembly processes, although interpretation is often cumbersome and does not always yield conclusive results. The second difficulty arises from the fact that the interactions between the building blocks are complex and compose of various contributions, e.g. electro-statics, hydrophobic interactions, steric repulsion and hydrogen bonding.^{3,8,9} The importance of each individual contribution is generally difficult to extract from experimental results, since independent variation of contributions is usually not possible.

In this context, the use of colloidal particles as analogues for molecular building blocks is an attractive option. Colloids are objects with at least one dimension in the order of 1 nm – 1 μ m, that are dispersed in a continuous medium.¹⁵ At low colloid density and/or small time scales, thermal fluctuations result in constant, uncorrelated movements of the colloids. This so-called Brownian motion counteracts sedimentation ensuring similar behavior as atoms and molecules.¹⁵ However, due to the relatively large dimensions of colloids compared to atoms and molecules, the dynamics are much slower. The large size and related slow dynamics facilitate direct visualization and therefore studying structure formation upon assembly of colloidal building blocks.

An additional advantage of using colloidal systems over their molecular or atomic counterparts is that inter-particle interactions and particle shape are tunable to a large extent. In contrast to molecular systems where interactions are ultimately determined by the atoms, colloidal interactions are tunable in magnitude and range by physical and/or chemical alternations. This allows for the rational design of particles

to either mimic the self-assembly of existing (molecular) structures or the formation of new assemblies with tailored properties. Systematic variation of either shape or interactions can in principle reveal the minimal complexity required to form a desired superstructure.

Colloids with relatively simple geometries and hard interactions, i.e. (hardly) no attraction between the individual particles, were extensively studied during the past decades.^{16–21} Colloidal spheres, rods and platelets were the main workhorses of colloidal self-assembly.^{16–21} These particles organize themselves into different (liquid) crystals as function of the particle volume fraction (Figure 1.1a and b). Although these structures are fundamentally intriguing and find applications as, for example,

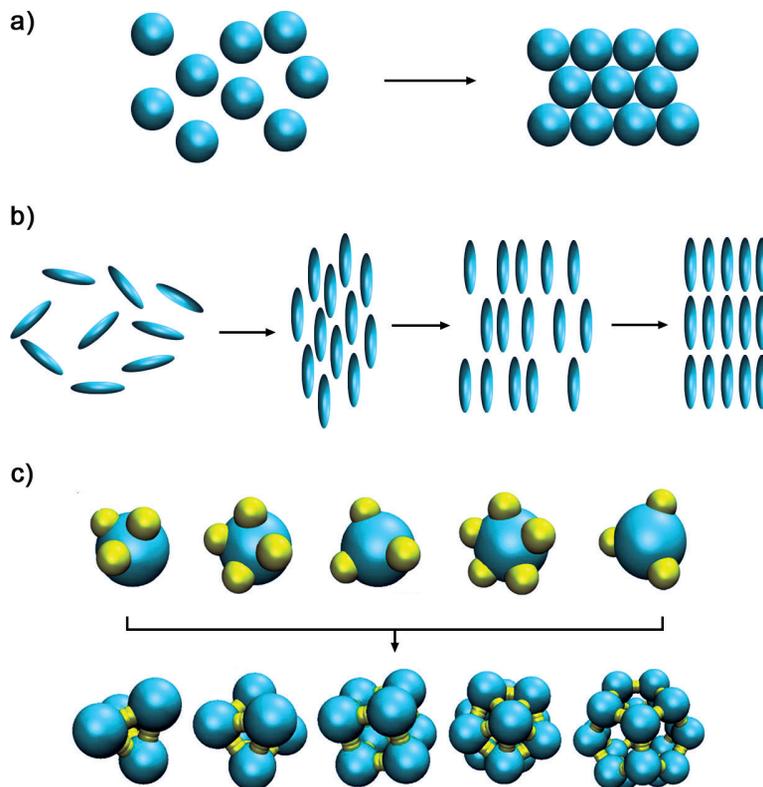


Figure 1.1. (a) Schematic representation of the spontaneous crystallization of colloidal hard spheres into hexagonal crystals with long-range order. (b) Formation of liquid crystals (middle two images) and crystals (right) of anisotropic rod/platelets. (c) Self-assembly of patchy particles into finite-size colloidal clusters. The resulting cluster geometry is dependent on both the number as well as the orientation of the patches (shown in yellow) with respect to each other.

optical/photonic materials^{22–24} and masks for lithograph,^{25,26} the achievable structural complexity with these elementary building blocks is limited. To move (slightly) towards the biological examples mentioned at the beginning of this Introduction, new designs of building blocks are required. The most straightforward way of altering the structure obtained after (self-)assembly, is by changing the geometry of the colloids. Similar to the volume fraction induced crystallization of hard spheres; different shaped particles without any attraction are expected to form crystals as well. Obviously, the details of the crystal depend on the geometry of the individual particles. Therefore, control over only particle geometry in principle enables formation of new long-rang ordered materials. Experimental and simulation examples include colloidal crystals prepared from faceted/polyhedral particles,^{27–31} dumbbell-shaped particles³² and peanut-shaped colloids.³³

However, if asymmetric or low coordination number assemblies are desired, hard particles with just excluded volume interactions are not sufficient. The symmetry of the building blocks in terms of inter-particle interactions needs to be broken. Only in this way, preferred particle alignments can be forced into the system. One needs to move from particles with isotropic interactions to building blocks with anisotropic interactions, similar to directional bonding observed between atoms and molecules facilitated by anisotropic orbitals.^{34,35} Colloids that meet these requirements are usually referred to as patchy particles. These particles contain regions (patches) that are attractive or repulsive towards patches present on other building blocks. By introducing these patches, the interactions between the particles become directional, i.e. colloids bind to each other in a preferred orientation, similar to preferred orientation of, for example, proteins in virus capsids (Figure 1.1c).^{7–9,36,37}

The structure that is formed upon self-assembly of patchy particles depends in principle on the number and size of patches and the distribution of patches over the particle surface (Figure 1.1c). The importance of these parameters is intuitively evident, but was also confirmed by numerous simulations on the self-assembly behavior of this type of colloids.^{38–42} Experimental realizations of truly patchy particles and their assembly are still limited.^{43–47} Despite the enormous progress in colloid syntheses procedures, two main factors remain challenging. Firstly, preparing colloids that can be modified in a site-specific fashion is difficult to achieve with conventional colloidal syntheses methods. To gain control over the distribution of functional patches, more elaborate procedures such as lithography,^{48,49} microfluidics,^{50,51} and site-specific deposition^{52,53} are usually employed. Although these procedures provide good control over building block formation, the yield is often low. This low yield hampers systematic study of the self-assembly behavior. In this thesis, the use of bulk, wet-chemical colloidal syntheses procedures were exploited for the preparation of patchy colloids on a large scale (Chapter 2 and 3).

Secondly, being able to prepare colloids with functional patches is not sufficient for successful self-assembly. The interactions between the patches need to be carefully designed. If patch-patch interactions are too strong, disordered structures are likely formed, since the colloids get stuck into the orientation they meet. This prevents reaching the intended equilibrium structure. In the other limit, too weak interactions will not lead to assembly at all. For successful self-assembly, the ratio of attractive and repulsive interactions between the particles requires optimization in such a way that a net weak attraction is generated. Relatively weak attractions allow for bond reversibility or adjustability which ensures that the building blocks can find their optimal position inside the assembling structure. Reversible bonds between colloids typically rely on hydrogen bonding,^{43,54–56} host-guest interactions,^{57,58} hydrophobic interactions^{53,59} and metal-ion coordination.^{47,60} The strength of these bonds is generally dependent on temperature, redox potential and solvent quality.

Instead of relying on spontaneous adjustability of the building blocks inside a growing assembly, attractions between particles/patches can also be triggered on demand, by for example deliberately changing the temperature of the whole system^{43,54} or by applying magnetic/electric external fields.^{61–65} By cyclic switching between the attractive and the non-attractive/repulsive mode of the patch, assembly defects can be annealed out, even if the attractions are significantly stronger than the thermal energy.

Since control over the interactions between the patches is essential for successful self-assembly, a large part of this thesis will focus on chemical strategies to control these interactions by modifying the surface properties of the colloidal building blocks (**Chapter 4–6, 8, 9**).

By combining appropriate strategies to induce reversible interactions with wet-chemical procedures for the preparation of colloids with functional patches, colloidal systems which can self-assemble into complex structures are within reach. The insights obtained from the assembly dynamics of these colloids may lead to new design principles in macromolecular systems, such as block-copolymers and proteins.

1.2. Equilibrium versus non-equilibrium assembly

It must be noted that although structurally, colloidal assemblies might mimic biological analogues, the details and pathways of assembly can be completely different (Figure 1.2). As mentioned in the beginning of the Introduction, a variety of processes in biology are driven by consumption of energy rich molecules, such as adenosine triphosphate (ATP) and guanosine-5'-triphosphate (GTP).^{1–3} Examples include the continuous formation and collapse of micro-tubules^{66,67} tread milling of actin filaments,⁶⁸ and the action of molecular motors.^{69,70} The attractions responsible for structure formation, represented by the blue dots in Figure 1.2, are only present upon energy dissipation/fuel consumption. Depletion of chemical fuel stops the assembly

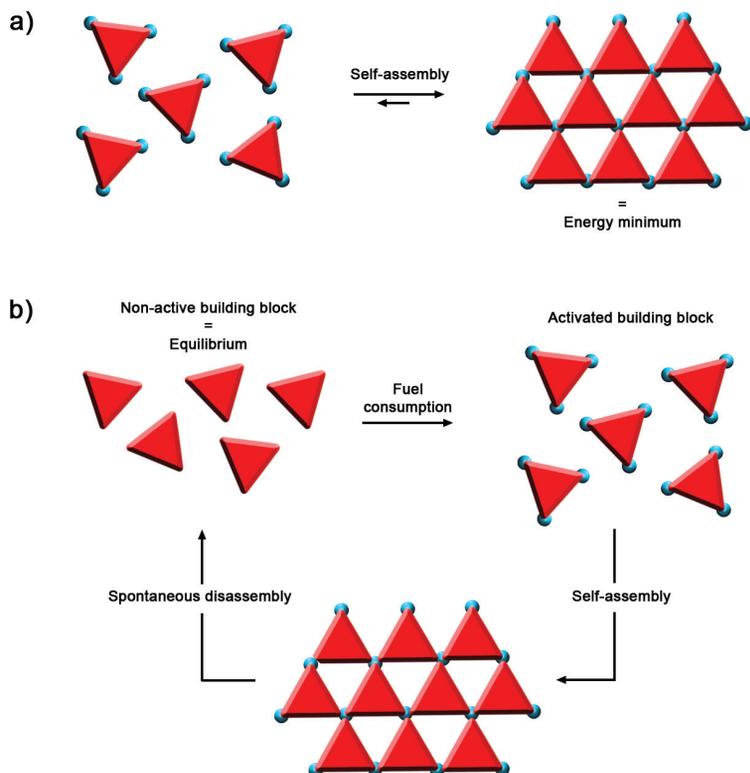


Figure 1.2. (a) Schematic representation of the equilibrium self-assembly strategy. The colloidal building blocks (red triangles) are prepared with attractive sites (blue dots). Alignment of the attractive sites lowers the free energy of the system, which drives structure formation. The final structure exists in a (local) energy minimum. (b) Schematic representation of out-of-equilibrium self-assembly. Non-active building blocks (red triangles) are first activated by consumption of chemical fuel. These activated building blocks carry the attractive sites (blue dots) required for self-assembly and structure formation is triggered. Upon fuel depletion, the attractive interactions between the building blocks vanish and the formed assembly disintegrates. The assembled structure only exists if fuel is supplied.

process and triggers spontaneous disintegration of previously formed structures. Therefore, these processes operate far from equilibrium.^{4,5} This is in sharp contrast to the generally applied self-assembly strategies in the colloidal regime. Colloidal self-assembly is usually driven by lowering the free energy of the total system upon forming the intended superstructure which represents the lowest energy, equilibrium situation (Figure 1.2a). Synthetic systems that capture the dissipative essence and capability to adapt to environmental triggers characteristic for many biological systems are only sparsely found in literature.^{71–73} In **Chapter 7**, we show the first example of

a colloidal system showing out-of-equilibrium assembly. With this system as starting point, colloidal self-assembly can be taken to a new level in which not only equilibrium structures, but also highly dynamic molecular superstructure formation can be studied with colloids as model system.

1.3. Scope of this thesis

This thesis is divided in four parts in which different particle syntheses and surface modification procedures are discussed.

In **Part 1** we focus on the preparation of shape and chemically anisotropic colloids. In **Chapter 2** we show that functional chlorinated polystyrene colloids can be converted to dumbbell-shaped colloids by formation of protrusions onto these seed particles. During protrusion formation, the functional chlorine groups remain localized on the lobe originating from the seed particle. This results into particles that contain two lobes of which only one is chemically modifiable. As proof of principle, site-specific surface modifications were conducted using click chemistry as orthogonal functionalization method. In **Chapter 3**, the influence of the experimental conditions and properties of the chlorinated seed particles on the geometric shape of the resulting chemically anisotropic dumbbells is systematically investigated. The size of the protrusion compared to the functional seed is tunable, resulting in the preparation of a family of chemically anisotropic colloids.

In **Part 2**, Surface-Initiated Atom Transfer Radical Polymerization (SI-ATRP) is applied for modification of (anisotropic) colloidal particles. SI-ATRP allows for the growth/grafting of polymer brushes from solid surfaces, in this case the surface of colloidal particles. We show that the physical properties of the polymers in the grafted brush can be translated to the physical behavior of the colloidal particles. The theoretical background of ATRP is treated in **Chapter 4**. These theoretical considerations are illustrated by experimental results on the grafting of a variety of (functional) polymers to spherical colloids. The basics of grafting via ATRP are exploited in the remaining chapters of this part. In **Chapter 5** thermo-responsive polymers are grafted onto spherical polystyrene particles. The thermo-reversible chain-to-globule transition of the grafted polymers translated into a colloidal dispersion showing reversible aggregation. **Chapter 6** combines grafting of these responsive brushes with the chemically anisotropic colloids obtained from the syntheses procedures described in Chapter 2 and 3. This combination yields dumbbell-shaped colloids of which only one lobe is grafted with a polymer brush. These particles are used for the assembly of finite-sized colloidal clusters. Part 2 is concluded with **Chapter 7**, which focuses on dissipative aggregation of polymer grafted colloidal particles. Assembly of these particles is induced by addition of a chemical fuel. Upon fuel depletion, aggregation stops and spontaneous redispersion of the colloids occurs.

Part 3 comprises two chapters which focus on charge inversion of colloidal particles. In **Chapter 8** an unexpected (at least at first sight) surface reaction between negatively charged chlorinated colloids and dimethylformamide (DMF) is reported. The surface reactions results in formation of positively charged quaternary amines. The colloids can be completely overcharged and stable, positively charged particles could be obtained. In **Chapter 9**, the phenomena observed in Chapter 8 are used to devise a more controlled surface reaction to tune the surface charge of polystyrene colloids. The obtained positively charged particles are subsequently used in electrostatic driven assembly, to form hybrid organic–inorganic colloidal clusters.

Finally, in **Part 4** functional colloids are employed as carrier for a molecular transfer hydrogenation catalyst. The catalytically active colloids are able to convert ketones into the corresponding alcohols. Catalyst immobilization on colloids ensures easy recovery and recyclability of the catalyst (**Chapter 10**).

References

- [1] B. Alberts, A. Johnson, J. Lewis, M. Raff, K. Roberts, P. Walter, In *Molecular Biology of the Cell*, 4th ed.; Garland Science, New York, 2002.
- [2] R. Phillips, J. Kondev, J. Theriot, H. Garcia, In *Physical Biology of the Cell*, 2nd ed.; Garland Science, New York, 2012.
- [3] D. J. Kushner, Self-assembly of biological structures. *Bacteriol Rev.* **1969**, *33*, 302–345.
- [4] G. M. Whitesides, M. Boncheva, Beyond molecules: Self-assembly of mesoscopic and macroscopic components. *Proc. Natl. Acad. Sci. U.S.A.* **2002**, *99*, 4769–4774.
- [5] G. M. Whitesides, B. Grzybowski, Self-assembly at all scales. *Science* **2002**, *295*, 2418–2421.
- [6] J. D. Halley, D. A. Winkler, Consistent concepts of self-organization and self-assembly. *Complexity* **2008**, *14*, 10–17.
- [7] A. Zlotnick, Theoretical aspects of virus capsid assembly. *J. Mol. Recognit.* **2005**, *18*, 479–490.
- [8] A. J. Olson, Y. H. E. Hu, E. Keinan, Chemical mimicry of viral capsid self-assembly. *Proc. Natl. Acad. Sci. U.S.A.* **2007**, *104*, 20731–20736.
- [9] W. K. Kegel, P. van der Schoot, Competing hydrophobic and screened-Coulomb interactions in Hepatitis B virus capsid assembly. *Biophys J.* **2004**, *86*, 3905–3913.
- [10] P.-A. Monnard, D. W. Deamer, Membrane self-assembly processes: Steps toward the first cellular life. *Anat. Rec.* **2002**, *268*, 196–207.

-
- [11] H. T. McMahon, J. L. Gallop, Membrane curvature and mechanisms of dynamic cell membrane remodeling. *Nature* **2005**, *438*, 590–596.
- [12] C. M. Dobson, A. Šali, M. Karplus, Protein folding: A perspective from theory and experiment. *Angew. Chem., Int. Ed.* **1998**, *37*, 868–893.
- [13] C. M. Dobson, Protein folding and misfolding. *Nature* **2003**, *426*, 884–890.
- [14] K. A. Dill, J. L. MacCallum, The protein-folding problem, 50 years on. *Science* **2012**, *338*, 1042–1046.
- [15] R. J. Hunter, In *Foundations of Colloid Science*, 2nd ed.; Oxford University Press: New York, 2009.
- [16] P. N. Pusey, W. van Meegen, Phase behaviour of concentrated suspensions of nearly hard colloidal spheres. *Nature* **1986**, *320*, 340–342.
- [17] P. N. Pusey, W. van Meegen, P. Bartlett, B. J. Ackerson, J. G. Rarity, S. M. Underwood, Structure of crystals of hard colloidal spheres. *Phys. Rev. Lett.* **1989**, *63*, 2753–2756.
- [18] Z. Cheng, W. B. Russel, P. M. Chaikin, Controlled growth of hard-sphere colloidal crystals. *Nature* **1999**, *401*, 893–895.
- [19] G. J. Vroege, H. N. W. Lekkerkerker, Phase transitions in lyotropic colloidal and polymer liquid crystals. *Rep. Prog. Phys.* **1992**, *55*, 1241–1309.
- [20] F. M. van der Kooij, K. Kassapidou, H. N. W. Lekkerkerker, Liquid crystal phase transitions in suspensions of polydisperse plate-like particles. *Nature* **2000**, *406*, 868–871.
- [21] D. Frenkel, H. N. W. Lekkerkerker, A. Stroobants, Thermodynamic stability of a smectic phase in a system of hard rods. *Nature* **1998**, *332*, 822–823.
- [22] Y. Xia, B. Gates, Y. Yin, Y. Lu, Monodispersed colloidal spheres: Old materials with new applications. *Adv. Mater.* **2000**, *12*, 693–713.
- [23] H. Cong, B. Yu, J. Tang, Z. Li, X. Liu, Current status and future developments in preparation and application of colloidal crystals. *Chem. Soc. Rev.* **2013**, *42*, 7774–7800.
- [24] S.-H. Kim, S. Y. Lee, S.-M. Yang, G.-R. Yi, Self-assembled colloidal structures for photonics. *NPG Asia Materials* **2011**, *3*, 25–33.
- [25] S.-M. Yang, S. G. Jang, D.-G. Choi, S. Kim, H. K. Yu, Nanomachining by colloidal lithography. *Small* **2006**, *2*, 458–475.
- [26] J. Zhang, B. Yang, Patterning colloidal crystals and nanostructure arrays by soft lithography. *Adv. Funct. Mater.* **2010**, *20*, 3411–3424.
- [27] R. Ni, A. P. Gantapara, J. de Graaf, R. van Roij, M. Dijkstra, Phase diagram of colloidal hard superballs: From cubes via spheres to octahedral. *Soft Matter* **2012**, *8*, 8826–8834.
- [28] U. Agarwal, F. A. Escobedo, Mesophase behaviour of polyhedral particles. *Nat. Mater.* **2001**, *10*, 230–235.

- [29] A. P. Gantapara, J. de Graaf, R. van Roij, M. Dijkstra, Phase diagram and structural diversity of a family of truncated cubes: Degenerate close-packed structures and vacancy-rich states. *Phys. Rev. Lett.* **2013**, *111*, 015501.
- [30] L. Rossi, V. Soni, D. J. Ashton, D. J. Pine, A. P. Philipse, P. M. Chaikin, M. Dijkstra, S. Sacanna, W. T. M. Irvine, Shape-sensitive crystallization in colloidal superball fluids. *Proc. Natl. Acad. Sci. U.S.A.* **2015**, *112*, 5286–5290.
- [31] G. van Anders, N. K. Ahmed, R. Smith, M. Engel, S. C. Glotzer, Entropically patchy particles: Engineering valence through shape entropy. *ACS Nano* **2014**, *8*, 931–940.
- [32] J. D. Forster, J.-G. Park, M. Mittal, H. Noh, C. F. Schreck, C. S. O’Hern, H. Cao, E. M. Furst, E. R. Dufresne, Assembly of optical-scale dumbbells into dense photonic crystals. *ACS Nano* **2011**, *5*, 6695–6700.
- [33] S. H. Lee, S. J. Gerbode, B. S. John, A. K. Wolfgang, F. A. Escobedo, I. Cohen, C. M. Liddell, Synthesis and assembly of nonspherical hollow silica colloids under confinement. *J. Mater. Chem.* **2008**, *18*, 4912–4916.
- [34] F. Li, D. P. Josephson, A. Stein, Colloidal assembly: The road from particles to colloidal molecules and crystals. *Angew. Chem., Int. Ed.* **2011**, *50*, 360–388.
- [35] A. van Blaaderen, Colloidal molecules and beyond. *Science* **2003**, *301*, 470–471.
- [36] G.-R. Yi, D. J. Pine, S. Sacanna, Recent progress on patchy colloids and their self-assembly. *Phys.: Condens. Matter* **2013**, *25*, 193101.
- [37] A. B. Pawar, I. Kretzschmar, Fabrication, assembly, and application of patchy particles. *Macromol. Rapid Commun.* **2010**, *31*, 150–168.
- [38] A. W. Wilber, J. P. K. Doye, A. A. Louis, Self-assembly of monodisperse clusters: Dependence on target geometry, *J. Chem. Phys.* **2009**, *131*, 175101.
- [39] A. W. Wilber, J. P. K. Doye, A. A. Louis, E. G. Noya, M. A. Miller, P. Wong, Reversible self-assembly of patchy particles into monodisperse icosahedral clusters. *J. Chem. Phys.* **2007**, 085106.
- [40] E. Bianchi, P. Tarlaglia, E. Zaccarelli, F. Sciortino, Theoretical and numerical study of the phase diagram of patchy colloids: Ordered and disordered patch arrangements, *J. Chem. Phys.* **2008**, *128*, 144504.
- [41] Z. Zhang, S. C. Glotzer, Self-assembly of patchy particles. *Nano Lett.* **2004**, *4*, 1407–1413.
- [42] A. Giacometti, F. Lado, J. Largo, G. Pastore, F. Sciortino, Effects of patch size and number within a simple model of patchy colloids. *J. Chem. Phys.* **2010**, *132*, 174110.
- [43] Y. Wang, Y. Wang, D. R. Breed, V. N. Manoharan, L. Feng, A. D. Hollingsworth, M. Weck, D. J. Pine, Colloids with valence and specific directional bonding. *Nature* **2013**, *491*, 51–56.

- [44] Q. Chen, J. K. Whitmer, S. Jiang, S. C. Bae, E. Luijten, S. Granick, Supracolloidal reaction kinetics of Janus spheres. *Science* **2011**, *331*, 199–202.
- [45] D. J. Kraft, R. Ni, F. Smalenburg, M. Hermes, K. Yoon, D. A. Weitz, A. van Blaaderen, J. Groenewold, M. Dijkstra, W. K. Kegel, Surface roughness directed self-assembly of patchy particles into colloidal micelles. *Proc. Natl. Acad. Sci. U.S.A.* **2012**, *109*, 10787–10792.
- [46] J. R. Wolters, G. Avvisati, F. Hagemans, T. Vissers, D. J. Kraft, M. Dijkstra, W. K. Kegel, Self-assembly of “Mickey Mouse” shaped colloids into tube-like structures: Experiments and simulations. *Soft Matter* **2015**, *11*, 1067–1077.
- [47] Y. Wang, A. D. Hollingsworth, S. K. Yang, S. Patel, D. J. Pine, M. Weck, Patchy particle self-assembly via metal coordination. *J. Am. Chem. Soc.* **2013**, *135*, 14064–14067.
- [48] C. Bae, J. Moon, H. Shin, J. Kim, M. M. Sung, Fabrication of monodisperse asymmetric colloidal clusters by using contact area lithography (CAL). *J. Am. Chem. Soc.* **2007**, *129*, 14232–14239.
- [49] Y. Yu, B. Ai, H. Möhwald, Z. Zhou, G. Zhang, B. Yang, Fabrication of binary and ternary hybrid particles based on colloidal lithography. *Chem. Mater.* **2012**, *24*, 4549–4555.
- [50] K.-H. Roh, D. C. Martin, J. Lahann, Biphasic Janus particles with nanoscale anisotropy. *Nat. Mater.* **2005**, *4*, 759–763.
- [51] K. P. Yuet, D. K. Hwang, R. Haghgooeie, P. S. Doyle, Multifunctional superparamagnetic Janus particles. *Langmuir* **2010**, *26*, 4281–4287.
- [52] A. B. Pawar, I. Kretzschmar, Patchy particles by glancing angle deposition. *Langmuir* **2008**, *24*, 355–358.
- [53] Q. Chen, S. C. Bae, S. Granick, Directed self-assembly of a colloidal kagome lattice. *Nature* **2011**, *469*, 381–384.
- [54] I. de Feijter, L. Albertazzi, A. R. A. Palmans, I. K. Voets, Stimuli-responsive colloidal assembly driven by surface-grafted supramolecular moieties. *Langmuir* **2015**, *31*, 57–64.
- [55] F. M. Bayer, K. Hiltrop, K. Huber, Hydrogen-bond-induced heteroassembly in binary colloidal systems. *Langmuir* **2010**, *26*, 13815–13822.
- [56] H. Mori, A. H. E. Müller, J. E. Klee, Intelligent colloidal hybrids via reversible pH-induced complexation of polyelectrolyte and silica nanoparticles. *J. Am. Chem. Soc.* **2003**, *125*, 3712–3713.
- [57] X. Y. Ling, I. Y. Phang, C. Acikgoz, M. D. Yilmaz, M. A. Hempenius, G. J. Vancso, J. Huskens, Janus particles with controllable patchiness and their chemical functionalization and supramolecular assembly. *Angew. Chem., Int. Ed.* **2009**, *48*, 7677–7682.

- [58] G. Chen, M. Jiang, Cyclodextrin-based inclusion complexation bridging supramolecular chemistry and macromolecular self-assembly. *Chem. Soc. Rev.* **2011**, *40*, 2254–2266.
- [59] L. Hong, A. Cacciuto, E. Luijten, S. Granick, Clusters of amphiphilic colloidal spheres. *Langmuir* **2008**, *24*, 621–625.
- [60] M. B. Bannwarth, T. Weidner, E. Eidmann, K. Landfester, D. Crespy, Reversible redox-responsive assembly/disassembly of nanoparticles mediated by metal complex formation. *Chem. Mater.* **2014**, *26*, 1300–1302.
- [61] S. Sacanna, L. Rossi, D. J. Pine, Magnetic click colloidal assembly. *J. Am. Chem. Soc.* **2012**, *134*, 6112–6115.
- [62] D. Zerrouki, J. Baudry, D. Pine, P. Chaikin, J. Bibette, Chiral colloidal clusters. *Nature* **2008**, *455*, 380–382.
- [63] J. Yan, S. C. Bae, S. Granick, Colloidal superstructures programmed into magnetic Janus particles. *Adv. Mater.* **2015**, *27*, 874–879.
- [64] S.-R. Yeh, M. Seul, B. I. Shraiman, Assembly of ordered colloidal aggregates by electric-field-induced fluid flow. *Nature* **1997**, *386*, 57–59.
- [65] M. E. Leunissen, H. R. Vutukuri, A. van Blaaderen, Directing colloidal self-assembly with biaxial electric fields. *Adv. Mater.* **2009**, *21*, 3116–3120.
- [66] A. Desai, T. J. Mitchison, Microtubule polymerization dynamics. *Annu. Rev. Cell Dev. Biol.* **1997**, *13*, 83–117.
- [67] T. Mitchison, M. Kirschner, Dynamic instability of microtubule growth. *Nature* **1984**, *312*, 237–242.
- [68] T. D. Pollard, G. G. Borisy, Cellular motility driven by assembly and disassembly of actin filaments. *Cell* **2003**, *112*, 453–465.
- [69] J. Howard, Molecular motors: Structural adaptations to cellular functions. *Nature* **1997**, *389*, 561–567.
- [70] K. Kinbara, T. Aida, Toward intelligent molecular machines: Directed motions of biological and artificial molecules and assemblies. *Chem. Rev.* **2005**, *105*, 1377–1400.
- [71] M. Fialkowski, K. J. M. Bishop, R. Klajn, S. K. Smoukov, C. J. Campbell, B. A. Grzybowski, Principles and implementations of dissipative (dynamic) self-assembly. *J. Phys. Chem. B* **2006**, *110*, 2482–2496.
- [72] J. Boekhoven, A. M. Brizard, K. N. K. Kowligi, G. J. M. Koper, R. Eelkema, J. H. van Esch, Dissipative self-assembly of a molecular gelator using a chemical fuel. *Angew. Chem., Int. Ed.* **2010**, *49*, 4825–4828.
- [73] J. Boekhoven, W. E. Hendriksen, G. J. M. Koper, R. Eelkema, J. H. van Esch, Transient assembly of active materials fuelled by a chemical reaction. *Science* **2015**, *349*, 1075–1079.

Part 1

**Synthesis of Shape and Chemically
Anisotropic Colloids**

2

General Route toward Chemically Anisotropic Colloids

Abstract

We report a versatile emulsion-based synthesis for the preparation of nanometer-sized dumbbell-shaped particles that contain two chemically different patches. One patch consists of solely polystyrene and is therefore chemically inert toward most chemical reactions. The other patch contains reactive surface chlorine groups. To achieve this, we prepared seed particles with a chlorinated surface that were transformed into dumbbell-shaped particles by introducing a liquid styrene protrusion on the surface, which was polymerized to form a solid, anisotropic colloidal particle. The chlorinated layer on the seed particles provides both sufficient hydrophilicity to set a finite contact angle between the liquid protrusion and the seed particle and a chemical handle for further site-specific modification of the reactive patch. The chlorine groups can be easily converted to other functionalities, making these particles an ideal platform for the preparation of colloids with complex (surface) properties. As an example, it is shown that this patch can participate in copper-catalyzed Huisgen 1,3-dipolar cycloaddition reactions after conversion of the chlorines to azides. This very robust form of click chemistry allows us to decorate the reactive patch with a wide variety of molecules.

2.1. Introduction

Currently there is an increasing interest in colloidal particles with anisotropic shape or surface properties.¹⁻³ These can be considered as building blocks that potentially self-assemble into complex structures. Preparing particles with functional patches, e.g. DNA or magnetic material, is of particular interest because this leads to directional interactions between the colloids and more advanced superstructures.⁴⁻⁶ The synthetic procedures generally applied to prepare particles with functional patches, such as selective deposition, surface templating, and lithography, are difficult to perform and suffer from low yields, which makes it hard to study these systems systematically. To circumvent these problems, emulsion-based syntheses can be used. A number of papers have reported this type of procedure to synthesize polymeric or polymeric/inorganic hybrid dumbbell-shaped particles.⁷⁻¹⁸ The general strategy relies on the internal phase separation of a monomer-swollen, cross-linked polymer particle.¹⁹⁻²⁰ Upon swelling of the polymer network of a cross-linked particle, an elastic stress is induced. This stress can be relieved by heating the swollen particles, which results in a contraction of the polymer network. Upon contraction, excess monomer is expelled from the particle. If the surface properties of the colloid are tuned well, i.e. if there is a finite contact angle between the expelled monomer and the surface of the polymer particle, the monomer will form a liquid protrusion on the surface. Polymerization of this liquid droplet results in solid, dumbbell-shaped colloids. Tuning of the contact angle is usually achieved by adding hydrophilic layers of poly(vinyl acetate) or poly(acrylic acid) onto the surface of the seed particles.⁷⁻⁹

In this chapter, we show that a functional, slightly hydrophilic coating of vinylbenzyl chloride (VBC) can be applied to the surface of cross-linked polystyrene particles. These functional chlorinated particles were successfully used as seeds for the formation of dumbbell-shaped colloids. The resulting particles contain a well-defined chlorinated and therefore, reactive patch that allows for localized, site-specific modification of the nano-sized colloids. The chlorine functionality provides a versatile chemical handle that is the starting point for surface modifications via a wide variety of chemistries. This provides the possibility to introduce virtually any desired molecule onto the surface of the reactive patch. As an example, we show that the particles can be modified using click chemistry, further expanding the possibilities for tuning the patch characteristics.

2.2. Experimental Section

2.2.1. Materials. Styrene (St, 99%), divinylbenzene (DVB, 55% mixture of isomers, tech. grade), vinylbenzyl chloride (VBC, $\geq 90\%$, tech. grade), fluoresceinamine (for fluorescence, mixture of isomers, $\geq 75\%$), dimethylformamide (DMF, $\geq 99\%$), bromotris(triphenylphosphine) copper(I) [$\text{Cu}(\text{PPh}_3)_3\text{Br}$, 98%], *N,N*-

diisopropylethylamine (DIPEA, $\geq 98\%$), 4-pentynoic acid (95%), propargyl alcohol (99%), and propargylamine (98%) were obtained from Sigma-Aldrich. Hydroquinone (99%) was purchased from Riedel-de Haën, sodium azide (NaN_3 , 99%) from VWR, and sodium dodecyl sulfate (SDS) from BDH. Potassium persulfate (KPS, $> 99\%$ for analysis), sodium bisulfite (NaHSO_3 , ACS reagent) and azobis(isobutyronitrile) (AIBN, 98%) were purchased from Acros Organics. All chemicals were used as received. The water used throughout all syntheses was purified using a Milli-Q water purification system.

2.2.2. Synthesis of chlorinated seed particles. Cross-linked polystyrene (CPs) particles were synthesized using a standard emulsion polymerization method described in literature.⁷ A 500 mL round-bottom flask equipped with magnetic stir bar was placed in an oil bath at 80 °C. Water (200 mL) was charged into the reactor and allowed to reach the bath temperature. Styrene (21.15 g), DVB (0.635 g), and SDS (0.25 g) dissolved in water (50 mL) were added. The complete mixture was allowed to heat up to the temperature of the bath. Finally, the addition of KPS (0.39 g dissolved in 37.5 mL water) initiated the polymerization. The reaction was allowed to continue for 24 h at 80 °C. The resulting latex had a solid content of 7% (measured gravimetrically). The resulting particles had a radius of 125 nm with a polydispersity of 3.8% as determined with transmission electron microscopy (TEM).

The synthesized particles were used as seeds in the second step, in which chlorine groups were introduced at the colloidal surface.²¹ Crude seed dispersion (25 mL) and water (10 mL) were introduced into a 50 mL round-bottom flask equipped with a magnetic stir bar. The mixture was degassed with nitrogen for 30 min. VBC (1 mL premixed with 20 μL of DVB) was added under inert atmosphere. The seeds were swollen for 1 h at 30 °C, after which the temperature was raised to 60 °C. When this temperature was reached, KPS (0.04 g) and sodium bisulfite (0.03 g) dissolved in water (2.5 mL) were added. The reaction was allowed to run for 4 h. The particles were washed by centrifugation and redispersion in water. The solid content of the resulting dispersion was adjusted to 5%. A particle radius of 155 nm and polydispersity of 4.4% were measured using TEM. The presence of the chlorine groups was confirmed using Fourier transform infrared spectroscopy (FT-IR, ATR) and X-ray photoelectron spectroscopy (XPS).

2.2.3. Synthesis of anisotropic particles based on chlorinated seeds. The spherical chlorinated seed particles were converted to anisotropic colloids using a method described by Kraft et al.^{7,8} SDS (84 mg) was introduced into a small reactor tube containing a magnetic stir bar. To this tube, chlorinated seeds (2.5 mL, solid content = 5%) and water (2.5 mL) were added. The particles were swollen for 48 h with a mixture consisting of styrene (550 μL) and DVB (20 μL) (swelling ratio ≈ 5 ; the mass of added monomer divided by the mass of polymer in the seed particles). After

this swelling period, the mixture was heated at 80 °C for 2 h, causing the formation of a liquid protrusion at the surface of the seed particles. After the 2 h period, the mixture was allowed to cool to room temperature. To polymerize this liquid protrusion, AIBN (4.8 mg) dissolved in styrene (230 μ L) was added, as well as 0.5 mL of a hydroquinone solution (46 mg in 50 mL water). Hydroquinone was added to prevent polymerization in the aqueous phase. The reaction was allowed to continue for 24 h at 80 °C. The resulting particles were washed using centrifugation and redispersion in water to remove unwanted aggregates and secondary nuclei. The washed dispersion had a solid content of 1%. The particle size and shape were investigated with TEM. The majority of the particles was dumbbell-shaped, consisting of nearly equally sized lobes (\approx 185 nm radius). Besides the dumbbells, a small fraction of dimers of dumbbells was also observed, in agreement with ref. 7. No attempts to separate the dumbbells from the dimers were performed.

2.2.4. Covalent attachment of fluoresceinamine to chlorinated dumbbells. To prove that only one side of the dumbbells contained chlorine groups, fluoresceinamine was coupled to the reactive patch of the dumbbells via a reaction between the surface chlorine groups and the amine functionality of the dye. A 1 mL aliquot of the dispersion containing the dumbbell-shaped particles (solid content = 1%) was used. First, water was replaced by DMF by centrifugation and redispersion (three times). Fluoresceinamine (3.5 mg) was added to the DMF dispersion, and the mixture was heated to 90 °C for 24 h. The particles were washed with DMF and ethanol to remove excess dye, and finally the particles were redispersed in water. Confocal microscopy was used to investigate the distribution of the fluorescence signal over the particles.

2.2.5. Conversion of chlorine groups to azides on dumbbells. NaN_3 (13.5 mg) was added to a dispersion of chlorinated dumbbells in DMF (6 mL, solid content = 1%). The mixture was heated for 24 h at 70 °C. After this, the emulsion was washed with DMF and water to remove excess NaN_3 . Substitution of chlorines by azides was monitored with FT-IR (ATR). TEM was used to confirm that the particle shape remained unaffected during the reaction.

2.2.6. Click chemistry on azide-functionalized dumbbells. $\text{Cu}(\text{PPh}_3)_3\text{Br}$ (12.5 mg) was introduced into a 10 mL round-bottom flask equipped with a magnetic stir bar. To this, DIPEA (26 μ L) and 4-pentynoic acid (6 mg) or propargylamine (5 μ L) were added. Finally, a dispersion containing azide-functionalized particles in DMF (2.5 mL, solid content = 1%) was injected. The reaction was allowed to run for 24 h under gentle stirring at 70 °C. After 24 h, the reaction was stopped, and the mixture was washed with DMF. FT-IR (ATR) was used to probe the chemical composition of the resulting colloids. TEM confirmed the presence of the original dumbbell-shaped particles.

2.2.7. Characterization. Transmission electron microscopy (TEM) pictures were taken with a Philips Technai10 electron microscope typically operating at 100 kV. The samples were prepared by drying a drop of diluted aqueous particle dispersion on top of polymer-coated copper grids.

The X-ray photoelectron spectroscopy (XPS) measurements were conducted with a Thermo Scientific K-Alpha spectrometer equipped with a monochromatic small-spot X-ray source and a 180° double-focusing hemispherical analyzer with a 128-channel detector. Spectra were obtained using an aluminium anode (Al K α = 1486.6 eV) operating at 72 W and a spot size of 400 μm . Survey scans were measured at a constant pass energy of 200 eV and region scans at 50 eV. The background pressure was 2×10^{-9} mbar and during measurement the argon pressure was 3×10^{-7} mbar because of the charge-compensation dual-beam source.

Infrared (IR) spectra were obtained using a PerkinElmer Frontier FT-IR/FIR spectrometer. The attenuated total reflectance (ATR) mode was used. Measurements were performed on powders obtained by drying the particle dispersion.

Confocal images were recorded on a Leica SP8 microscope. The microscope was equipped with a Plan Apo 100 \times oil immersion lens with a numerical aperture of 1.4. Samples were illuminated by a laser beam with a wavelength of 488 nm selected from a white-light laser by means of an acousto-optical beam splitter (AOBS). The scanning was unidirectional at a scanning speed of 600 Hz. The pinhole size was 151.7 μm (airy disk). We used varying line and frame averaging. Images were captured by combining two imaging channels, one recorded in reflection mode and the other in fluorescence mode. The excitation wavelength of 488 nm was close to the excitation maximum of the dye coupled to the particles. To visualize the lobes that were not labeled, we took advantage of their Mie scattering: the particles were immersed in immersion oil ($n = 1.52$) which is not perfectly index matched with polystyrene ($n = 1.59$). The two channels were recorded in different 8 bit color look-up tables so as to distinguish them: reflection mode in cyan and fluorescence mode in red 'glow'.

2.3. Results and Discussion

We synthesized cross-linked spherical polystyrene colloids (CPs)⁷ that were coated with a thin, cross-linked layer of vinylbenzyl chloride (step a, Scheme 2.1). The chlorine groups of vinylbenzyl chloride (VBC) ensure a slightly hydrophilic character of the seed surface and at the same time, provide a chemical handle for further surface modification. A core-shell approach was used to ensure that the majority of the added VBC actually ended up at the surface of the particles.²¹ Potassium persulfate (KPS) was used in combination with sodium bisulfite as an initiator system in the shell formation step. The addition of sodium bisulfite shifts the mechanism for radical formation from a thermal to a redox process in which the bisulfite ion acts as a reductor.²² In this

way, the polymerization could be conducted at a lower temperature, suppressing the undesired hydrolysis of the relatively labile chlorine functionality of VBC. Successful incorporation of the chlorine functionality was provided by both infrared spectroscopy (IR) and X-ray photoelectron spectroscopy (XPS).

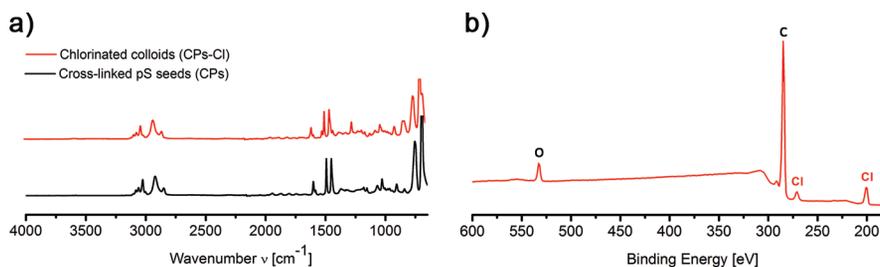
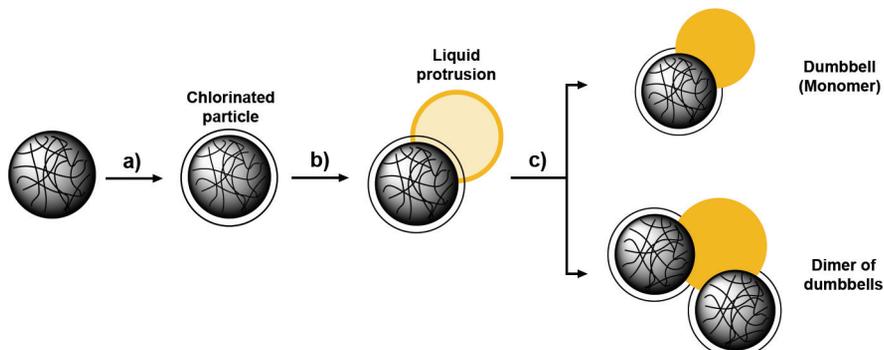


Figure 2.1. (a) Infrared (IR) spectra of bare cross-linked polystyrene seeds (black) and the chlorinated seeds (red). (b) X-ray photoelectron spectrum (XPS) of chlorinated particles.

Comparison of the IR spectra of the bare polystyrene seeds (CPs) and the chlorinated particles showed the appearance of a new signal at 1266 cm^{-1} , which corresponds to the $-\text{CH}_2\text{-Cl}$ vibration of the incorporated VBC (Figure 2.1a). In the XPS spectrum, binding energies of 200 and 270 eV corresponding to chlorine were detected (Figure 2.1b), providing additional proof that chlorine groups were indeed present at the surface, as XPS is a surface elemental analysis technique with a penetration depth of only 1–10 nm. The binding energy measured at 530 eV was attributed to oxygen originating from the initiator system that was used to start the polymerization. The intense signal at 285 eV was obviously caused by the carbon atoms of polystyrene.

In the second step, the chlorinated seed particles were used for the preparation of dumbbells (step b, Scheme 2.1). To this end, the particles were swollen with a mixture of styrene (St) and divinylbenzene (DVB). Because a chlorinated seed was used, we expected that the resulting dumbbells would consist of one lobe covered with surface chlorine groups, while the other lobe (originating from the liquid protrusion) would be built up solely from polystyrene (note: there might be SDS present on this lobe, as SDS was added to stabilize the liquid protrusion during synthesis). It is not likely that the chlorine groups would distribute over the whole dumbbell, since the chlorine groups were covalently attached to the seed. This argument was also used by Mock and Zukoski when they prepared dumbbells containing lobes with different charges on the surface using a different procedure from the one reported here.²³ Wang et al. recently used a procedure in which VBC acted as swelling monomer for non-functionalized polystyrene seeds.¹⁴ In that case it can not be ruled out that a small fraction of residual

Scheme 2.1. Schematic representation of the synthetic procedure to obtain anisotropic particles with chlorinated patches.^a



^a Step (a): introduction of a chlorinated shell (in white) on cross-linked polystyrene particles. Step (b): swelling of the chlorinated seeds with a mixture of divinylbenzene and styrene, and subsequent heating to form a liquid protrusion. Step (c): polymerization of the liquid protrusion by addition of an oil-soluble radical initiator (AIBN) to form solid dumbbell-shaped colloids. If fusion of the liquid protrusion occurs before polymerization, dimers of dumbbells are formed.

VBC remained inside the seed particles, thereby limiting the chemical anisotropy.

Figure 2.2 shows a representative TEM picture of the colloids after formation and polymerization of the liquid protrusion. Anisotropic colloids based on our chlorinated seeds were clearly obtained and the synthesis yielded dumbbell-shaped particles with two well-defined patches. Dumbbell-shaped particles were the most abundant species, although also dimers of dumbbells were observed to a lesser extent (5–10%). These

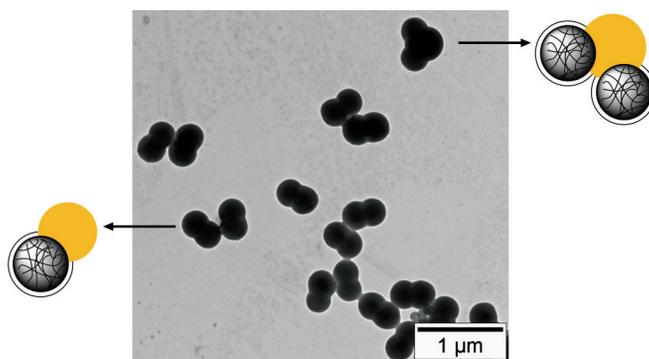


Figure 2.2. Transmission electron microscopy (TEM) picture of the anisotropic particles synthesized using chlorinated seeds. The majority of the particles are monomeric dumbbells. A small percentage of dimers was observed.

dimer particles were formed when the liquid protrusions of two particles fused together before polymerization.^{7,8} The fraction of dimers depends on the size of the liquid protrusion, the amount of surfactant to stabilize the oil–water interface of the protrusion, and most likely also on the time between formation of the liquid protrusions and actual polymerization of these monomer droplets. In our synthesis, polymerization was induced directly after protrusion formation to minimize the number of dimer particles. Nevertheless, a small fraction of dimers was formed, which is inherent to the synthetic procedure. Dumbbells and dimers (or even higher-order aggregates) can be separated using density gradient centrifugation, as shown by Kraft et al.⁷ This provides a method to obtain dispersions containing solely dumbbells or dimers.

For all dumbbells, the size of the protrusion is almost equal to the size of the seed particle. The contact angle between the protrusion and the seed is very pronounced, indicating that the expelled monomer mixture only partially wets the chlorinated surface. In other words, the introduction of the chlorine functionalities at the surface of the seed particles provides sufficient hydrophilicity to prevent full wetting of the colloidal surface by the apolar protrusion. IR analysis of these particles confirmed that the chlorine functionality was still present (see Figure 2.4). This signal decreased in intensity compared to the chlorine signal observed for the spherical particles (Figure 2.1a) because of doubling of the amount of polystyrene after protrusion formation.

TEM analysis (Figure 2.2) convincingly showed the formation of shape anisotropic particles, but obviously we cannot conclude anything about the distribution of chlorine groups over the particle surface and therefore the chemical anisotropy of the colloids. To visualize the chlorine distribution and test our hypothesis that the chlorine groups are immobile during protrusion formation, a dye with an amino group (fluoresceinamine) was mixed with the obtained dumbbells. The reaction between the surface chlorine groups and the amino group ensures covalent attachment of the fluorescent label. A large excess of dye was used to saturate the particle surface with dye. Non-reacted or aspecific absorbed dye was washed off after the reaction. High resolution confocal microscopy was used to analyze the fluorescence of the obtained particles (Figure 2.3). The red signal corresponds to fluorescence, while the scattered signal is shown in cyan. Overlaying the two signals revealed that the particles showed significant fluorescence at only one lobe of each particle. The asymmetric fluorescence signal proved that the chlorine groups were asymmetrically distributed across the particles and therefore did not migrate to the protrusion.

The ability to prepare dumbbell-shaped colloids of which only one lobe contains chlorine groups opens the way to site-specific modification reactions. The chlorines on the surface can be easily converted to other functionalities by straightforward organic chemistry, such as nucleophilic displacements with functional amines or reactive

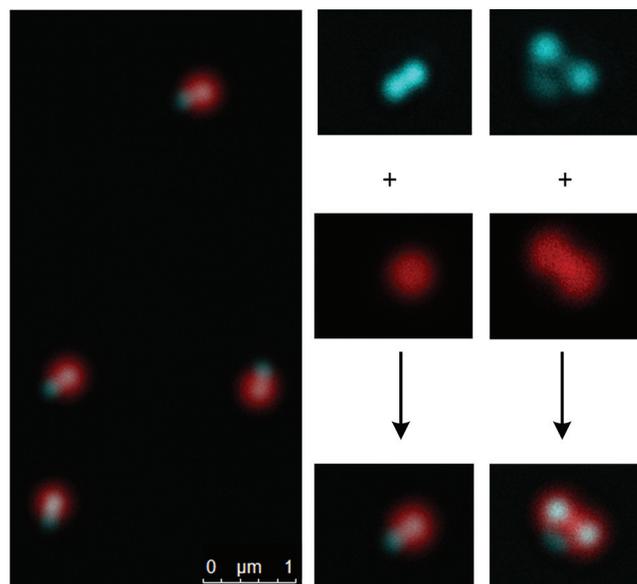
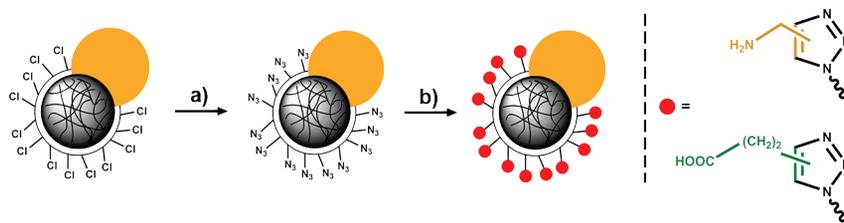


Figure 2.3. Confocal images of dumbbell-shaped particles after functionalization of the chlorinated patch with fluoresceinamine. Left: Image captured by combining two imaging channels, one recording in reflection mode (cyan) and the other in fluorescence mode (red). Right: enlargement of the two separate imaging channels for both a monomeric dumbbell-shaped particle and a dimer particle. Overlaying the separate channels reveals the asymmetric distribution of dye and therefore the chemical anisotropy of the colloids.

anions of metal salts, i.e. KOH. Numerous examples of possible applications of these particles can be envisioned. Dumbbells with a hydrophobic and a hydrophilic patch can be synthesized and used for very efficient stabilization of oil–water interfaces.^{12,13,24,25} The introduction of well-designed molecules could lead to directional interactions between the particles,^{7–9} and self-propelling particles are accessible in large quantities when proper catalytic complexes are attached on the reactive lobes.²⁶ The synthesized particles are therefore a versatile platform for the preparation of a wide variety of complex colloidal systems.

As a proof of principle, the copper-catalyzed Huisgen 1,3-dipolar cycloaddition (in the remainder of the chapter termed ‘click chemistry’) was chosen because of its orthogonal character.^{27–29} The surface reactions were first performed on spherical chlorinated seeds to optimize the reaction conditions. Click chemistry was previously used to modify the surface of polystyrene particles.³⁰ However, our synthesis is an improvement of the previously reported method in terms of surface coverage and tunability of the number of functional groups. The results and proof of successful modification of the chlorinated spheres are shown in the Appendix.

Scheme 2.2. Schematic representation of the site-specific functionalization of dumbbell-shaped colloids using click chemistry.^a



^aStep (a): substitution of surface chlorine groups with azides by addition of sodium azide (NaN_3) in DMF. Step (b): coupling of propargylamine (orange) or 4-pentynoic acid (green) to the surface using the copper-catalyzed Huisgen 1,3-dipolar cycloaddition reaction.

To use click chemistry for modification, the chlorine groups were first transformed into azides by addition of sodium azide to a dispersion of dumbbells in dimethylformamide (DMF). DMF is known for its poor ability to solvate anions.³¹ Therefore, dissolving sodium azide in DMF results in ‘naked’, i.e. non-hydrated azide ions. These ions are highly reactive and ensure high conversion of chlorines to azides. Cross-linking of both the seed and protrusion of the dumbbells prevents dissolution of the particles in DMF. IR spectroscopy showed the disappearance of the chlorine signal and the appearance of a relatively strong azide signal at 2096 cm^{-1} (Figure 2.4) after reaction with NaN_3 .

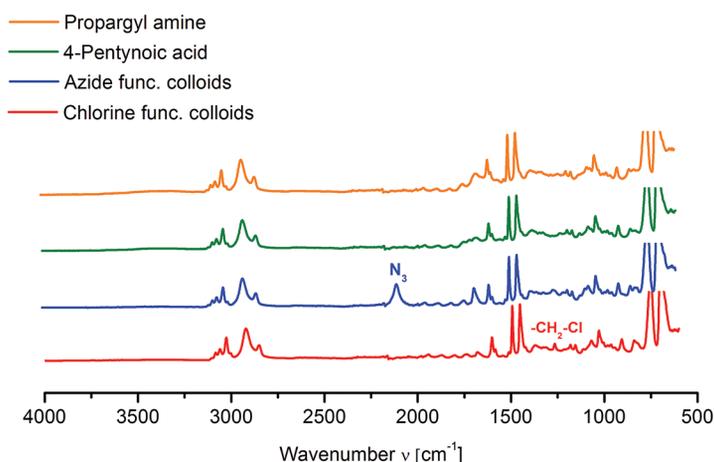


Figure 2.4. Infrared (IR) spectra of dumbbells with a chlorinated patch (red) or an azide-functionalized patch (blue) and the spectra obtained after surface functionalization via click chemistry with 4-pentynoic acid (green) or propargylamine (orange).

After successful introduction of the azide functionality, two click reactions were conducted with two small alkyne-containing molecules, namely, propargylamine and 4-pentynoic acid (Scheme 2.2). The reactions were performed with a conventional catalytic system consisting of bromo-tris(triphenylphosphine)copper(I) [Cu(PPh₃)₃Br] and *N,N*-diisopropylethylamine (DIPEA). After the click reactions, IR analysis showed the complete disappearance of the azide signal (Figure 2.4), which is a strong indication that attachment of the alkyne precursors was successful. Unfortunately, no characteristic alkyne precursor signals could be observed in the IR spectra. This in contrast to the spectra obtained after click functionalization of the spherical particles (see Appendix, Figure 2.9). The lack of these signals is attributed to the fact that the dumbbells contain roughly twice the amount of polystyrene compared to the spherical seeds. Furthermore, a part of the surface functionalities are buried under the protrusion after dumbbell formation. The resulting number of functional groups is too low to give a signal of reasonable intensity compared to the strong polystyrene related vibrations originating from the bulk of each particle.

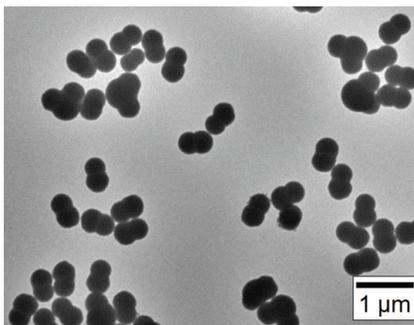


Figure 2.5. Transmission electron microscopy (TEM) picture of dumbbell-shaped colloids with a patch functionalized with propargylamine via the copper-catalyzed Huisgen 1,3-dipolar cycloaddition reaction.

Finally, the particles were imaged after the complete reaction sequence to verify the robustness of the colloids. A TEM picture of particles functionalized with propargylamine (Figure 2.5) clearly shows that the particles maintained their anisotropic shape, making click chemistry indeed suitable for site-specific patch modifications.

2.4. Conclusions

We have developed a synthesis route toward anisotropic particles that contain chemically inert and reactive chlorinated lobes. The synthesis is emulsion-based, allowing for the preparation of these complex particles in large quantities, which in itself is a significant advantage compared with available methods to date. The chlorine

functionality opens the way for further site-specific functionalization reactions. As an example, surface modification of the reactive lobe using click chemistry was shown. The combination of click chemistry and the developed synthesis method provides a route for the preparation of anisotropic particles with a wide variety of functionalities and morphologies.

Acknowledgments

I would like to thank Marlous Kamp for confocal microscopy analysis and Judith van Wijk for facilitating the XPS analysis at the Eindhoven University of Technology. This chapter is reprinted with kind permission from [33]. Copyright 2013 American Chemical Society

Appendix 1 – Click chemistry on spherical chlorinated colloids

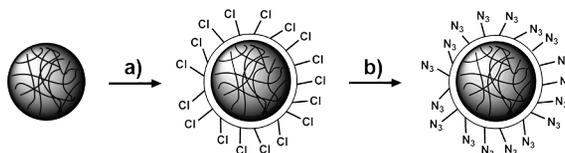
A1.1. Experimental

A1.1.1. Nucleophilic substitution of surface chlorines by azides. The CPs-Cl particles were first transferred from water to DMF by centrifugation and redispersion (three times). The solid content was kept at 5% during this process. NaN_3 (32 mg) was weighed into a reaction tube and the DMF-dispersion (5 mL) was added. The resulting dispersion was heated for 24 h at 70 °C. After this, the particles were washed with DMF to remove excess NaN_3 . The conversion of the chlorine functionality to azides was confirmed by FT-IR (ATR) and XPS. The same reaction was also conducted in an aqueous environment.

A1.1.2. Click chemistry on spherical, azide functionalized colloids (CPS- N_3). $\text{Cu}(\text{PPh}_3)_3\text{Br}$ (25 mg) was introduced in a 25 mL round-bottom flask equipped with a magnetic stir bar. DMF (4 mL) was added to dissolve the catalyst. To this solution, DIPEA (52 μL) and an alkyne precursor was added either directly or from a stock solution of the precursor in DMF. If a stock solution was used, the amount of DMF used to dissolve the catalyst was reduced to keep the total reaction volume constant throughout all click reactions. Finally, the CPs- N_3 dispersion (1 mL in DMF, solid content = 1%) was added. The reaction was allowed to run for 24 h under gentle stirring at 70 °C (flask was equipped with water cooler to prevent any evaporation). After the reaction, the particles were washed with DMF. FT-IR (ATR) and XPS were used to show successful surface modification.

A1.2. Results and Discussion

The overall synthetic strategy toward particles which are able to participate in click chemistry reactions is shown in Scheme 2.3. The first step comprises the synthesis of cross-linked polystyrene colloids (CPs) using a straightforward

Scheme 2.3. Schematic overview of the synthesis of azide functionalized colloids.^a

^a Step (a): introduction of cross-linked chlorinated shell on a cross-linked polystyrene core. Step (b): substitution of surface chlorine groups with azides by addition of sodium azide (NaN_3) in water or DMF.

emulsion polymerization of styrene with divinylbenzene as cross-linker. In the next step (a), a chlorinated shell was grown around the seed particles in a similar fashion as discussed in the main text. The surface chlorine groups were subsequently converted into azides by a nucleophilic substitution reaction with sodium azide (b).

The preparation of the cross-linked polystyrene colloids was performed as described in ref. 7 and resulted in monodisperse particles which could be used directly in the second step, namely, the addition of a chlorinated and cross-linked shell.²¹ Successful incorporation of the chlorine functionality was confirmed by both IR spectroscopy (Figure 2.6) and XPS (Figure 2.8). The resulting chlorinated particles were monodispers and spherical, as was observed with TEM (Figure 2.7).

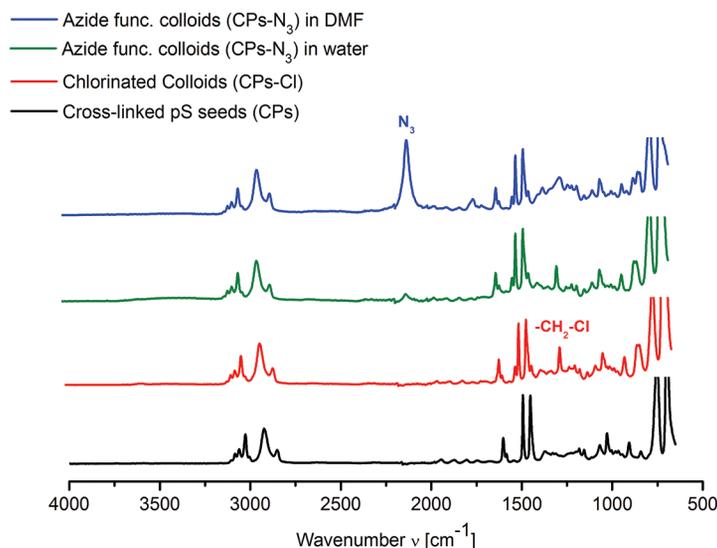


Figure 2.6. Infrared (IR) spectra of cross-linked polystyrene particles (black), chlorinated particles (red) and azide functionalized particle obtained after reaction with NaN_3 in water (green) and DMF (blue).

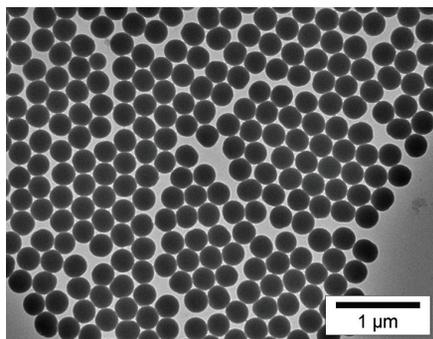


Figure 2.7. Transmission electron microscope (TEM) picture of chlorinated cross-linked polystyrene particles.

With these particles at hand, we moved on to the introduction of azides to the colloidal surface. Following Breed et al.,³⁰ attempts were conducted to perform substitution reactions with sodium azide in an aqueous environment. However, this resulted in very low conversions of chlorines to azides as determined from the low intensity azide signal (2096 cm^{-1}) observed in the IR spectrum (Figure 2.6, green spectrum). Increasing the number of equivalents of sodium azide significantly was not possible due to salt induced aggregation of the charge stabilized colloids.

To circumvent aggregation and increase the number of surface azides, DMF was chosen as solvent. DMF is known for its poor ability to solvate anions.³¹ Therefore, dissolving sodium azide in DMF results in ‘naked’, i.e. non-hydrated azide ions.

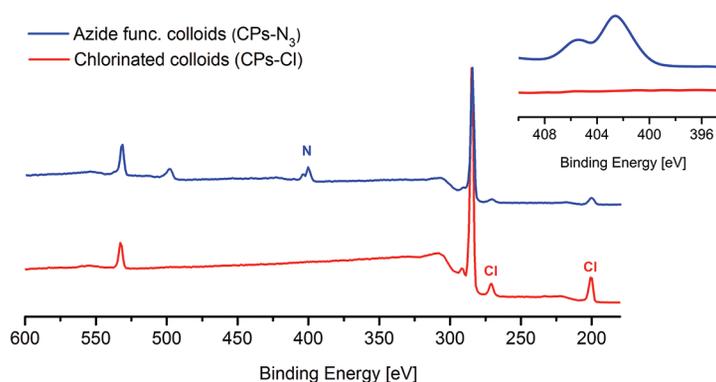


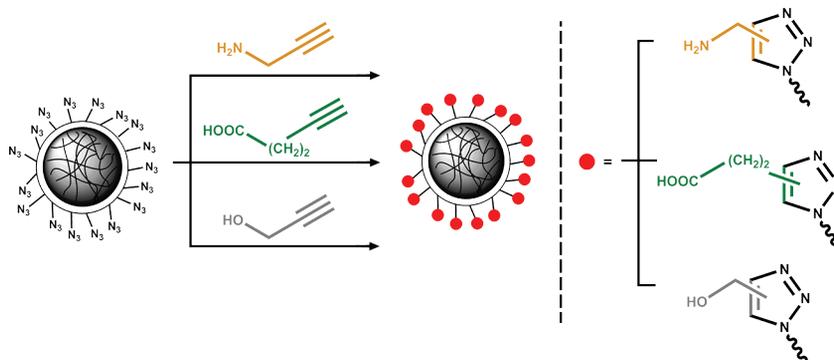
Figure 2.8. X-ray photoelectron spectra (XPS) of the chlorinated particles (red) and the azide functionalized particles obtained after reaction with NaN_3 in DMF (blue). An enlargement of the nitrogen signal is shown in the inset.

These ions are highly reactive ensuring high chlorine conversions after addition of only one equivalent of NaN_3 . IR spectroscopy (Figure 2.6, blue spectrum) showed complete disappearance of the $-\text{CH}_2\text{-Cl}$ signal at 1266 cm^{-1} and the appearance of a strong $-\text{N}_3$ vibration at 2096 cm^{-1} . XPS (Figure 2.8) showed complementary results: the intensity of the chlorine signals decreased significantly after the substitution reaction. The signal does not completely disappear, because a part of the chlorine groups is probably buried just under the particle surface. These buried chlorines cannot be reached by the azide anion, simply because these charged species do not penetrate into the hydrophobic interior of the polystyrene colloids.

Furthermore, the spectrum also shows a split nitrogen signal at 401 and 406 eV. This peak splitting indicates the presence of two nitrogen species and reflects the differently charged nitrogen atoms in a covalently bound azide group.³²

Successful introduction of the azide functionality opens the way to surface modifications with click chemistry. $\text{Cu}(\text{PPh}_3)_3\text{Br}$ in combination with DIPEA was used as catalytic system, because this system is soluble in the reaction medium DMF.

Scheme 2.4. Synthetic strategy for the surface modification of spherical colloids via click chemistry.^a



^a Coupling of propargylamine (top, orange), 4-pentynoic acid (middle, green) and propargyl alcohol (bottom, gray) to the surface of azide functionalized polystyrene particles using copper-catalyzed Huisgen 1,3-dipolar cycloaddition reaction. The alkyne precursors are linked to the particle surface via triazole moieties drawn on the right.

Three alkyne precursors with different types of functional groups (pentynoic acid = COOH , propargyl alcohol = OH and propargylamine = NH_2) were employed as model molecules for surface modification. The reactions are schematically depicted in Scheme 2.4.

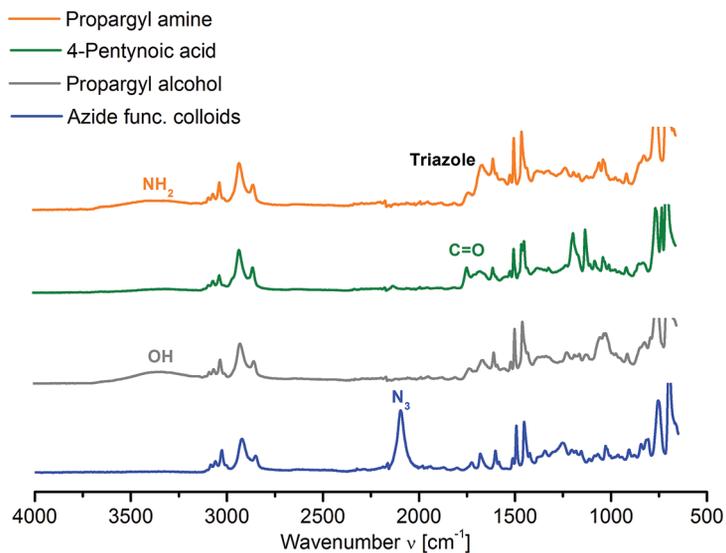


Figure 2.9. Infrared (IR) spectra of the azide functionalized particles (CPs- N_3) before (blue) and after surface modification with propargyl alcohol (gray), 4-pentynoic acid (green) or propargylamine (orange) using click chemistry.

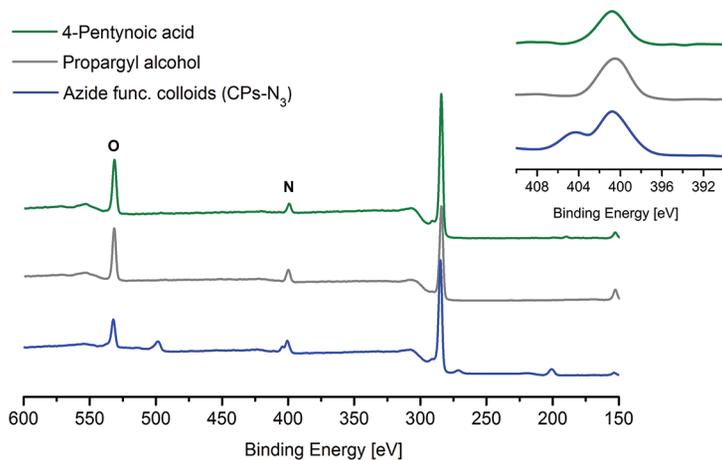


Figure 2.10. X-ray photoelectron spectra (XPS) of the azide functionalized particles (CPs- N_3 , blue) and the particles after click reaction with propargyl alcohol (gray) and 4-pentynoic acid (green). An enlargement of the nitrogen signal is shown in the inset.

The chemical composition of the particles obtained after click chemistry reactions were analyzed using IR spectroscopy (Figure 2.9). Regardless of the functionality present in the alkyne precursor, the IR spectra showed no azide signal (2096 cm^{-1}) anymore. This is a clear indication that most free azides have reacted to form the triazole moiety (Figure 2.9). The signal of the triazole group itself is hard to detect, but in all three spectra a new signal appeared around 1650 cm^{-1} , which possibly originates from the formed triazoles. On top of this, all three spectra contained the IR signals corresponding to the functionality of the specific alkyne precursor that was added.

XPS analysis was conducted on the particles functionalized with 4-pentynoic acid and propargyl alcohol (Figure 2.10). For both samples an increase in the oxygen content (543 eV) was observed corresponding to the oxygen atoms present in the bound carboxylic and hydroxyl functionalities. The oxygen signal present before click chemistry is attributed to sulfate or sulfonate groups produced by the initiator system.

Besides this enrichment in oxygen, the split nitrogen signal in the azide functionalized particles was merged into one signal after the click reactions. As pointed out in ref. 32, this merging is observed if free azides are converted to triazoles.

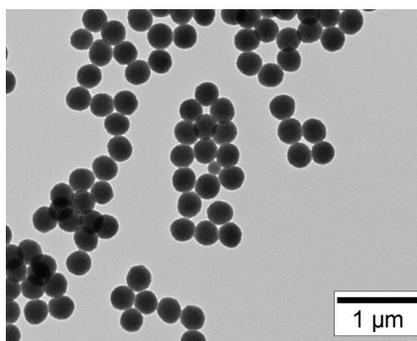


Figure 2.11. Transmission electron microscopy (TEM) image of the colloids obtained after functionalization with propargyl alcohol via click chemistry.

The results obtained from IR spectroscopy and XPS show that the surface modifications were successful on the chemical level. However, for these reactions to be useful as surface modifications for colloids, it is of course necessary that the particles stay intact during the whole procedure. Usually particle integrity is not an issue, because most reported reactions are performed in water. In this case however, both introduction of azides and subsequent click chemistry reactions are performed in DMF at elevated temperatures. Although linear polystyrene is soluble in DMF, upon cross-linking this solubility diminishes. To investigate if the cross-linking density of

the employed particles was high enough to prevent dissolution of the particles, the modified colloids were imaged using TEM. Figure 2.11 shows the particles modified with propargyl alcohol. The particle morphology was unaffected by the modification procedure, since a similar morphology was observed for the chlorinated colloids (Figure 2.7). From these results we concluded that the surface modifications via click chemistry were successful, both on the chemical and the colloidal level.

References

- [1] S. C. Glotzer, M. J. Solomon, Anisotropy of building blocks and their assembly into complex structures. *Nat. Mater.* **2007**, *6*, 557–562.
- [2] A. B. Pawar, I. Kretzschmar, Fabrication, assembly, and application of patchy particles. *Macromol. Rapid Commun.* **2010**, *31*, 150–168.
- [3] F. Wurm, A. F. M. Kilbinger, Polymeric Janus particles. *Angew. Chem., Int. Ed.* **2009**, *48*, 8412–8421.
- [4] Y. Wang, Y. Wang, D. R. Breed, V. N. Manoharan, L. Feng, A. D. Hollingsworth, M. Weck, D. J. Pine, Colloids with valence and specific directional bonding. *Nature* **2013**, *491*, 51–56.
- [5] Q. Chen, J. K. Whitmer, S. Jiang, S. C. Bae, E. Luijten, S. Granick, Supracolloidal reaction kinetics of Janus spheres. *Science* **2011**, *331*, 199–202.
- [6] G.-R. Yi, D. J. Pine, S. Sacanna, Recent progress on patchy colloids and their self-assembly. *Phys.: Condens. Matter* **2013**, *25*, 193101.
- [7] D. J. Kraft, W. S. Vlug, C. M. van Kats, A. van Blaaderen, A. Imhof, W. K. Kegel, Self-assembly of colloids with liquid protrusions. *J. Am. Chem. Soc.* **2009**, *131*, 1182–1186.
- [8] D. J. Kraft, J. Groenewold, W. K. Kegel, Colloidal molecules with well-controlled bond angles. *Soft Matter* **2009**, *5*, 3823–3826.
- [9] E. B. Mock, H. De Bruyn, B. S. Hawkett, R. G. Gilbert, C. F. Zukoski, Synthesis of anisotropic nanoparticles by seeded emulsion polymerization. *Langmuir* **2006**, *22*, 4037–4043.
- [10] J.-G. Park, J. D. Forster, E. R. J. Dufresne, High-yield synthesis of monodisperse dumbbell-shaped polymer nanoparticles. *J. Am. Chem. Soc.* **2010**, *132*, 5960–5961.
- [11] J.-W. Kim, R. J. Larson, D. A. Weitz, Uniform nonspherical colloidal particles with tunable shapes. *Adv. Mater.* **2007**, *19*, 2005–2009.
- [12] J.-W. Kim, J. L. Ryan, D. A. Weitz, Synthesis of nonspherical colloidal particles with anisotropic properties. *J. Am. Chem. Soc.* **2006**, *128*, 14374–14377.
- [13] J.-W. Kim, D. Lee, H. C. Shum, D. A. Weitz, Colloid surfactants for emulsion stabilization. *Adv. Mater.* **2008**, *20*, 3239–3243.

- [14] Y. Wang, W. Huang, L. Huang, S. Zhang, D. Hua, X. Zhu, Synthesis of walnut-like polystyrene particles using a “giant” surfactant and its superhydrophobic property. *Polym. Chem.* **2013**, *4*, 2255–2259.
- [15] J. Parvole, I. Chaduc, K. Ako, O. Spalla, A. Thill, S. Ravaine, E. Duguet, M. Lansalot, E. Bourgeat-Lami, Efficient synthesis of snowman- and dumbbell-like silica/polymer anisotropic heterodimers through emulsion polymerization using a surface-anchored cationic initiator. *Macromolecules* **2012**, *45*, 7009–7018.
- [16] C. Tang, C. Zhang, J. Liu, X. Qu, J. Li, Z. Yang, Large scale synthesis of Janus submicrometer sized colloids by seeded emulsion polymerization. *Macromolecules* **2010**, *43*, 5114–5120.
- [17] B. Liu, J. Liu, F. Liang, Q. Wang, C. Zhang, X. Qu, J. Li, D. Qiu, Robust anisotropic composite particles with tunable Janus balance. *Macromolecules* **2012**, *45*, 5176–5184.
- [18] K. Yoon, D. Lee, J. W. Kim, J. Kim, D. A. Weitz, Asymmetric functionalization of colloidal dimer particles with gold nanoparticles. *Chem. Commun.* **2012**, *48*, 9056–9058.
- [19] H. R. Sheu, M. S. El-Aasser, J. W. J. Vanderhoff, Uniform nonspherical latex particles as model interpenetrating polymer networks. *Polym. Sci., Part A: Polym. Chem.* **1990**, *28*, 653–667.
- [20] W. K. Kegel, D. Breed, M. Elsesser, D. J. Pine, Formation of anisotropic polymer colloids by disparate relaxation times. *Langmuir* **2006**, *22*, 7135–7136.
- [21] M. K. Maurer, I. K. Lednev, S. A. Asher, Photoswitchable spirobenzopyran-based photochemically controlled photonic crystals. *Adv. Funct. Mater.* **2005**, *15*, 1401–1406.
- [22] J. R. Ebdon, T. N. Huckerby, T. C. Hunter, Free-radical aqueous slurry polymerizations of acrylonitrile: 2. End-groups and other minor structures in polyacrylonitriles initiated by potassium persulfate/sodium bisulfite. *Polymer* **1994**, *35*, 4659–4664.
- [23] E. B. Mock, C. F. Zukoski, Emulsion polymerization routes to chemically anisotropic particles. *Langmuir* **2010**, *26*, 13747–13750.
- [24] B. P. Binks, P. D. I. Fletcher, Particles adsorbed at the oil–water interface: A theoretical comparison between spheres of uniform wettability and “Janus” particles. *Langmuir* **2001**, *17*, 4708–4710.
- [25] N. Glaser, D. J. Adams, A. Böker, G. Krausch, Janus particles at liquid–liquid interfaces. *Langmuir* **2006**, *22*, 5227–5229.
- [26] R. Golestanian, T. B. Liverpool, A. Ajdari, Propulsion of a molecular machine by asymmetric distribution of reaction products. *Phys. Rev. Lett.* **2005**, *94*, 220801.

-
- [27] H. C. Kolb, M. G. Finn, K. B. Sharpless, Click Chemistry: Diverse chemical function from a few good reactions. *Angew. Chem., Int. Ed.* **2001**, *40*, 2004–2021.
- [28] W. H. Binder, R. Sachsenhofer, ‘Click’ Chemistry in polymer and materials science. *Macromol. Rapid Commun.* **2007**, *28*, 15–54.
- [29] S. Lal, S. J. Díez- González, [CuBr(PPh₃)₃] for azide–alkyne cycloaddition reactions under strict click conditions. *Org. Chem.* **2011**, *76*, 2367–2373.
- [30] D. R. Breed, R. Thibault, F. Xie, Q. Wang, C. J. Hawker, D. J. Pine, Functionalization of polymer microspheres using Click Chemistry. *Langmuir* **2009**, *25*, 4370–4376.
- [31] M. A. Fox, J. K. Whitesell, In *Organic Chemistry*, 3rd ed.; Jones and Bartlett Publishers: Sudbury, MA, 2003; pp 373–375.
- [32] C. Haensch, S. Hoepfener, U. S. Schubert, Chemical surface reactions by Click Chemistry: Coumarin dye modification of 11-bromoundecyltrichlorosilane monolayers. *Nanotechnology* **2008**, *19*, 1–7.
- [33] B. G. P. van Ravensteijn, M. Kamp, A. van Blaaderen, W. K. Kegel, General route toward chemically anisotropic colloids. *Chem. Mater.* **2013**, *25*, 4348–4353.

3

Synthesis of Anisotropic Colloids from Chlorinated Seed Particles

Abstract

Dumbbell-shaped colloids are prepared starting from a cross-linked polymer seed particle which is swollen by a monomer (mixture). Upon heating of this swollen network, an elastic contraction is induced leading to the formation of a liquid protrusion on the surface of the seed particles. Subsequent polymerization of this liquid protrusion results in solid, dumbbell-shaped colloids. The wetting properties of the seed particles are key in this process. The surface of the seed particles should be slightly wettable by the expelled monomer to form particles with two well-separated lobes. Complete wetting or non-wetting is not desired, since this will lead to the formation of spherical particles or fully detached protrusions, respectively. Hence, a slightly hydrophilic coating should be present on the seeds.

Here we present a systematic study on the preparation of dumbbell-shaped colloids starting from seed particles with a reactive chlorinated coating. We explore the effects of the experimental conditions during protrusion formation as well as the seed properties on the geometry of the resulting colloids.

3.1. Introduction

Emulsion-based syntheses of anisotropic particles are promising routes towards the large scale production of such particles. Several authors reported on the preparation of dumbbell-shaped colloids using this type of syntheses leading to a variety of particles where the particle shape and size can be tuned in a controlled fashion.^{1–13}

Sheu et al. pioneered this field and demonstrated that raising the temperature of monomer-swollen cross-linked polystyrene particles causes the monomer to phase-separate from the seed particle as a liquid protrusion.^{14,15} Subsequent polymerization of the monomer inside this protrusion yields anisotropic dumbbell-shaped colloids. A thermodynamic model was provided that accounts for swelling as a result of balancing the free energy of mixing the monomer with the polymer (ΔG_m), the elastic energy resulting from stretching the cross-linked polymer network in the seed particles (ΔG_{el}), and the surface tension of the particle with the aqueous phase (ΔG_t) (Eq. 3.1). Substituting the Flory-Huggins expression^{16,17} for ΔG_m (free-energy change of mixing the monomer with the polymer), the Flory-Rehner equation¹⁸ for ΔG_{el} (dominated by an entropy term associated with a decrease in the number of configurations due to stretching of the polymer network upon swelling), and the Morton equation¹⁹ for ΔG_t (increase in surface area on swelling), the following equation was derived

$$\begin{aligned}\Delta\bar{G}_{m,p} &= \Delta\bar{G}_m + \Delta\bar{G}_{el} + \Delta\bar{G}_t \\ &= RT [\ln(1 - \nu_p) + \nu_p + \chi\nu_p^2] + RTNV_m(\nu_p^{1/3} - \nu_p/2) + \frac{2V_m\gamma}{r}\end{aligned}\quad (3.1)$$

Here, R is the ideal gas constant, T is the temperature, ν_p is the volume fraction of polymer in the swollen seed particle, χ is the monomer-polymer interaction parameter, N is the effective number of chains in the network per unit volume, V_m is the monomer molar volume, γ is the interfacial tension between the particle and water, and r is the radius of the swollen seed particle.

From this equation we learn that ΔG_{el} and ΔG_t restrict the swelling process (positive contribution to $\Delta G_{m,p}$) while ΔG_m promotes the swelling by a negative contribution to $\Delta G_{m,p}$. Intuitively this is easy to understand since it is energetically unfavorable for a cross-linked polymer network to expand because it creates elastic stress. Furthermore, swelling the particle leads to a larger interfacial area between the particle surface and the continuous phase, hence a higher surface free energy. On the other hand, transporting hydrophobic monomer from the continuous aqueous phase to the hydrophobic interior of the seed particles is energetically favorable, thus promoting the swelling process. Swelling proceeds until an equilibrium situation is reached, i.e. the sum of all three contributions equals zero.

To form a liquid protrusion, the monomer needs to phase separate from the

swollen particles. This phase separation is driven by relaxation of the polymer network generating an elastic retractile force that pushes out the monomer. This relaxation is in principle a spontaneous process,¹³ although the rate of monomer expulsion can be slow. This process can be sped up considerably if the swollen particles are heated.^{14,15} Heating causes an increase in the elastic free energy (ΔG_{el}) leading to a positive value of $\Delta G_{m,p}$, i.e. the system is in a unfavorable state, promoting the phase separation between the monomer and the polymer network. Expulsion of the monomer continues until a new equilibrium condition is reached. Sheu et al. showed that the initial monomer droplet which is expelled is rather small. The protrusion grows during the polymerization, since monomer is withdrawn from the swollen seed particle by an imbalance of the chemical potential of the monomer. The swollen seed effectively acts as a monomer reservoir.^{14,15} The formation of the additional lobe therefore follows a nucleation and growth type of mechanism (Scheme 3.3). After completing the polymerization of the monomer, well-defined dumbbell-shaped colloids are obtained. Recently, this model for the formation of dumbbells was slightly revised. Kraft et al. suggested the formation of large liquid protrusions, which could fuse together to form colloidal molecules.^{1,2} Both mechanisms lead eventually to the same end product.

The work of Sheu et al. focused on the use of micron-sized seed particles (2–8 μm diameter). It was concluded that the degree of phase separation increases with increasing size of the seeds. Using particles with a diameter on the order of 500 nm did not result in the formation of a protrusion. This can be easily understood if we consider the third contribution in Eq. 3.1. The Morton equation states that the interfacial pressure at the swollen particle/water interface is inversely proportional to the radius of the particles. If the particle size becomes small enough, a point is reached where the sum of the interfacial force and the mixing force exceed the thermo-induced elastic-retractile force. In this situation, no phase separation will occur and spherical particles are produced.

More recently, Mock et al. confirmed this by using seed particles with sizes between 200 and 500 nm. Instead of well-defined dumbbells, egg-shaped colloids were obtained, i.e. the degree of phase separation was low.²⁰ However, Mock et al. provided a solution for this by coating the seed particles with a thin hydrophilic layer consisting of poly(vinyl acetate) or poly(acrylic acid).²⁰ In fact, it is the ratio between the surface tension and the particle radius that determines the weight of the Morton contribution in Eq. 3.1. Effectively, this coating procedure lowers the surface tension between the swollen particle/water interface. This causes a decreasing contribution of the Morton equation to $\Delta G_{m,p}$ and hence promotes the tendency for monomer phase separation. An additional effect is that the polymer lobes are separated by a well-defined contact angle. The contact angle (θ) between the expelled monomer and the particle can be expressed by Young's law:^{20,21}

$$\theta = \cos^{-1} \left[\frac{\gamma_{p,a} - \gamma_{p,m}}{\gamma_{m,a}} \right] \quad (3.2)$$

with $\gamma_{p,a}$ the interfacial tension between the particle and the aqueous phase, $\gamma_{p,m}$ between the particle and the monomer and $\gamma_{m,a}$ between the monomer and the aqueous phase. The contact angle increases, i.e. the liquid protrusion will be more separated from the seed, if the difference between $\gamma_{p,a}$ and $\gamma_{p,m}$ decreases. Applying the hydrophilic coating ensures a larger mismatch between the hydrophobic monomer and the particle surface thereby increasing $\gamma_{p,m}$ and decreasing the difference between $\gamma_{p,a}$ and $\gamma_{p,m}$. Mock et al. also showed experimentally that by applying these hydrophilic coatings, dumbbells with sizes in the order of 200–500 nm with well-defined protrusions could be obtained. The degree of anisotropy could even be tuned by the thickness of the hydrophilic layer which was deposited onto the seed particles. In addition to the hydrophilic coating, seed particles with a significantly higher cross-link density were required to maximize the elastic-retractile force generated upon heating the swollen particles.

In the previous chapter we already showed an extension of this synthesis procedure by substituting the poly(vinyl acetate) or poly(acrylic acid) coating by a reactive poly(vinylbenzyl chloride) (pVBC) coating.⁵ Dumbbells were formed with these chlorine modified seed particles yielding shape and chemically anisotropic colloids. These particles can be modified site-specifically using the benzyl chloride groups present on the seed side of the dumbbell-shaped particles.

In this chapter we explore which particle geometries are accessible using chlorinated seed particles and how the seeds properties influence the protrusion formation step. Being able to tune the particles shape is an important step towards functional particles which can be used in self-assembly studies, where the final structure heavily depends on the geometry of the building blocks.^{22–24}

3.2. Experimental Section

3.2.1. Materials. Styrene (St, 99%), divinylbenzene (DVB, 55% mixture of isomers, tech. grade) and vinylbenzyl chloride (VBC, $\geq 90\%$, tech. grade) were obtained from Sigma-Aldrich. Hydroquinone (99%) was purchased from Riedel-de Haën. Sodium dodecyl sulfate (SDS) from BDH was used. Potassium persulfate (KPS, $> 99\%$ for analysis) and azobis(isobutyronitrile) (AIBN, 98%) were purchased from Acros Organics. All chemicals were used as received. The water used for all syntheses was purified using a Milli-Q water purification system.

3.2.2. Synthesis of cross-linked polystyrene colloids (CPs). Typically, cross-linked polystyrene colloids were prepared as described in Chapter 2 via conventional emulsion polymerization. This standard synthesis procedure yielded particles with a

cross-link density of 3%. Here, the cross-link density of these seed particles was varied by changing the ratio of divinylbenzene and styrene in the monomer feed. Particles containing cross-link densities of up to 18% were prepared.

3.2.3. Synthesis of chlorinated core-shell colloids (CPs-Cl). The previously synthesized particles (CPs) were used as seeds in the second step, in which chlorine groups were introduced at the colloidal surface.⁵ Crude seed dispersion (25 mL) and water (10 mL) were introduced into a 50 mL round-bottom flask equipped with a magnetic stir bar. The mixture was degassed with nitrogen for 30 min. VBC (1 mL premixed with 20 μ L of DVB) was added under an inert atmosphere. The seeds were swollen for 1 h at 30 °C, after which the temperature was raised to 60 °C. When this temperature was reached, KPS (0.04 g) and sodium bisulfite (0.03 g) dissolved in water (2.5 mL) were added. The reaction was allowed to run for 4 h. The particles were washed with ethanol and water by centrifugation and after the final washing step redispersed in water. The solid content of the resulting dispersion was adjusted to 5%. This procedure yielded particles with a radius of 155 nm and polydispersity of 4.4% as determined with transmission electron microscopy (TEM). The presence of the chlorine groups was confirmed using Fourier transform infrared spectroscopy (FT-IR, ATR) and X-ray photoelectron spectroscopy (XPS) (see Chapter 2; Figure 2.1).

Variations on this synthesis procedure to tune the shell thickness and the composition of the shell were conducted. The shell thickness was systematically controlled by variation of the volume of VBC which was added to a fixed amount of CPs particles. In all cases, the VBC that was added contained 3% DVB. Monomer volumes and the resulting shell thicknesses are listed in Table 3.2.

The shell composition was tuned by growing shells around CPs particles using monomer mixtures containing both styrene and VBC. Also here, all monomer mixtures contained 3% DVB to cross-link the formed shells. The percentages of VBC in the monomer feed are listed in Table 3.2.

3.2.4. Synthesis of non-chlorinated core-shell particles (CPs-St). The core-shell approach as described in Section 3.2.3 was also applied to prepare non-chlorinated particles. The crude CPs dispersion (25 mL) and water (10 mL) were introduced in a 50 mL three-neck flask equipped with a magnetic stir bar (submerged in a thermostated oil bath). This dispersion was bubbled with nitrogen for 30 min at room temperature (needle through a septum). After this 30 min, a mixture of styrene (1 mL) and DVB (20 μ L) was injected under inert atmosphere. After 1 h of swelling, the temperature was increased to 60 °C. When this temperature was reached, the initiator solution (0.04 g KPS and 0.03 g sodium bisulfite dissolved in 2.5 mL water) was injected. After 4 h, the reaction was quenched and the particles were washed with water and ethanol. After the final centrifugation step, the particles were dispersed in water and the solid content was adjusted to 5%.

3.2.5. Procedure for the synthesis of anisotropic particles based on chlorinated seeds. Typically, the spherical chlorinated seed particles (CPs-Cl) were converted to anisotropic colloids using the method described by Kraft et al.^{1,2} and in the previous chapter.⁵ SDS (42 mg) was introduced into a 25 mL elongated reactor tube containing a magnetic stir bar. To this tube a dispersion containing the chlorinated seeds (1.25 mL, solid content = 5%) and water (1.25 mL) were added. The particles were swollen for 48 h with a mixture consisting of styrene (420 μ L) and DVB (10 μ L). These volumes lead to a swelling ratio of approximately 6. The swelling ratio is here defined as the mass of added monomer divided by the mass of polymer in the seed particles. After this swelling period, the dispersion was heated at 80 °C for 2 h, causing the formation of a liquid protrusion at the surface of the seed particles. After 2 h, the dispersion was cooled to room temperature. To polymerize this liquid protrusion, AIBN (2.4 mg) dissolved in styrene (115 μ L) was added, as well as 0.25 mL of a hydroquinone solution (46 mg in 50 mL water). Hydroquinone was added to prevent polymerization in the aqueous phase. The reaction was allowed to continue for 24 h at 80 °C. The resulting particles were washed using centrifugation and redispersion in water to remove unwanted aggregates and secondary nuclei. The washed dispersion had a solid content of 1%.

Variations on this synthesis procedure can be found in Table 3.1 and Table 3.2 where the swelling ratio, cross-link density of the seed/protrusion, SDS concentration in the reaction mixtures and (chemical) properties of the seeds particles were varied to investigate the influence of these parameters on the resulting particle shape.

3.2.6. Characterization. Transmission electron microscopy (TEM) pictures were taken with a Philips Technai10 electron microscope typically operating at 100 kV. The samples were prepared by drying a drop of diluted aqueous particle dispersion on top of polymer-coated copper grids. Scanning electron microscopy (SEM) images were obtained using a FEI XL30 FEG microscope operating at 5 kV. The samples were prepared by sticking a TEM grid (prepared as described before) on a stub using a conductive carbon sticker. The samples were not coated with platinum in order to reveal subtle surface characteristics of the colloids.

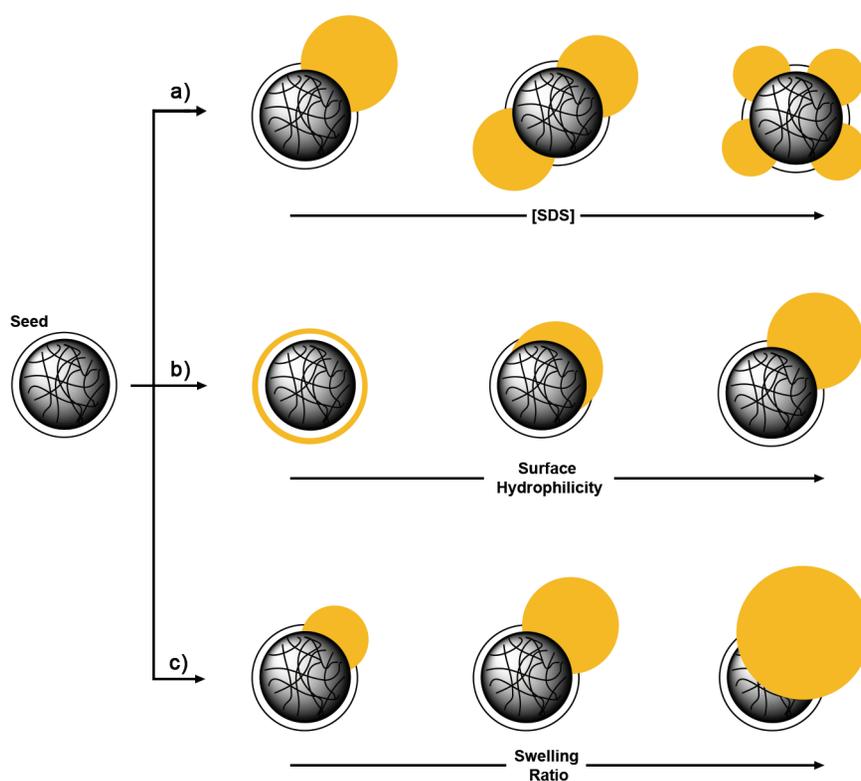
Infrared (IR) spectra were obtained using a PerkinElmer Frontier FT-IR/FIR spectrometer. The attenuated total reflectance (ATR) mode was used. All the measurements were performed on powders obtained by drying particle dispersions.

Dynamic light scattering (DLS) measurements were performed using a Malvern Zetasizer Nano instrument using highly diluted aqueous dispersions at 25 °C. The DLS measurements were taken in seven runs of 15 individual measurements in backscatter mode (173°). The sizes of the colloids are reported as Z-average diameters and the corresponding polydispersity index (PDI). These values were obtained by using the cumulant method as described in ref. 25.

3.3. Results and Discussion

In this chapter we explore to what extent we can tune the particle geometry of dumbbell-shaped colloids based core-shell seed particles which consist of a cross-linked polystyrene core and a cross-linked vinylbenzyl chloride outer layer. The results obtained by Kraft et al. who used poly(vinyl acetate) coated polystyrene particles and poly(*N*-isopropylacrylamide) (pNIPAM) particles as seeds act as guidelines.¹⁻³

Scheme 3.1. Schematic representation of the accessible particle geometries after protrusion formation by variation of the surfactant concentration (a), surface hydrophilicity of the seed particles (b) and the swelling ratio (c).



Kraft et al. studied the influence of the swelling ratio and the surfactant (SDS) concentration present during the protrusion formation on the resulting particle shape. As expected, higher swelling ratios yielded particles with a larger protrusion. The protrusion size could be varied between approximately half the volume of the seed particle to several times the volume of the seed.

The concentration of surfactant determines the extent to which the liquid protrusion is stabilized against merging. It was found that increasing the SDS

concentration led to the formation of multiple protrusions on a single seed.³ The hypothesis was that during heating of the swollen seeds, multiple liquid protrusions are formed. These protrusions merge, i.e. decrease the oil–water interface, until they are sufficiently stabilized by surfactants that adsorb onto this oil–water interface. A higher initial surfactant concentration will therefore limit this merging, giving rise to multiple protrusions per seed particle. A low surfactant concentration promotes merging of the individual protrusions leading to particles with one well-defined lobe. Besides determining the number of protrusions on the surface, also the extent to which the liquid protrusions of other particles fuse together to form higher order patchy particles is determined by this surfactant concentration. Intuitively, the formation of these more complex particles also depends on the time between formation and actual polymerization of the (fused) protrusions and the size of the liquid protrusions. The chance that two liquid protrusions will meet each other increases if particles with liquid protrusion on their surface are allowed to diffuse over a longer period or if the surface area of a protrusion is increased. This increased chance translates in a large fraction of these colloidal molecules in the final particle dispersion.

Finally, Kraft et al.^{1–3} showed that the seed surface has to be (slightly) hydrophilic in order to obtain a protrusion with a pronounced contact angle and prevent full wetting of the seeds by the hydrophobic swelling monomers, in line with the findings of Mock et al.²⁰ Furthermore, the coating applied to induce the surface hydrophilicity facilitates the swelling process due to a decreased surface tension between the particle and the aqueous phase as described in the Introduction.²⁰ The particle geometries obtained experimentally by Kraft et al. are schematically depicted in Scheme 3.1.^{1–3}

Besides these factors, also the effect of the cross-linking density in both the chlorinated seeds and the protrusion on the resulting particle geometry will be investigated to complete the experimental parameter space.

As a starting point, chlorinated core-shell colloids were prepared in a two-step synthesis procedure as previously described in Chapter 2. The presence of the chlorine groups on the surface of the colloids was confirmed using both IR spectroscopy and XPS measurements (Figure 2.1). The seeds and dumbbells prepared in Chapter 2 serve as a reference synthesis throughout this chapter (entry 1, Table 3.1). This synthesis yielded nearly symmetric dumbbell-shaped colloids with a pronounced contact angle between seed and protrusion (Figure 3.1a and b). SEM analysis of these particles revealed that one lobe of the dumbbells is slightly textured (bottom lobe of dumbbell in Figure 3.1d, only barely visible in the TEM images). We attribute this effect to the presence of the chlorinated outer layer. This layer is in principle cross-linked with the same density as the seed. However, if the actual densities deviate slightly from each other, the degree of swelling will also be different. The shell remains attached to the core during the swelling process. In doing so it might be possible that this

shell needs to buckle slightly after protrusion formation, which results in the observed surface roughness (Figure 3.1c and d). Such surface structure is not observed on the protrusions, since these lobes consist of only one polymer network. This subtle surface structure can be used to deduce which lobe of the dumbbells originated from the seed and which lobe was formed as a protrusion.

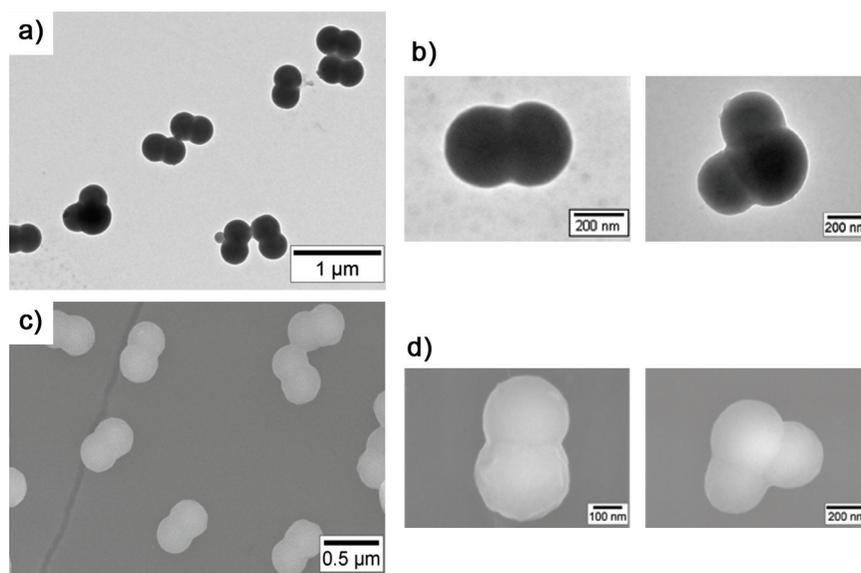
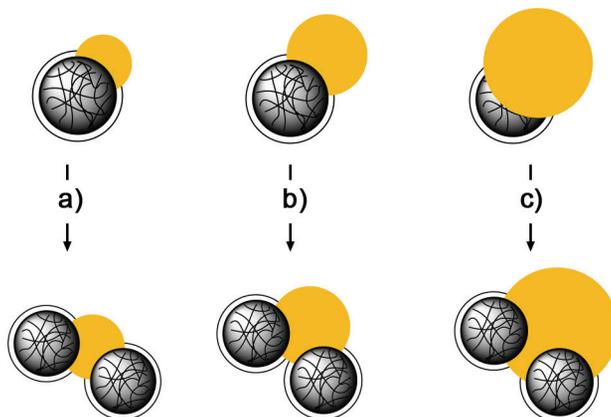


Figure 3.1. (a) Transmission electron microscopy (TEM) image of the dumbbell-shaped colloids resulted from the reference synthesis. (b) TEM image of a single dumbbell (left) and dimer of dumbbells (right). (c) Scanning electron microscopy (SEM) image of the dumbbell-shaped colloids resulting from the reference synthesis. (d) SEM image of a single dumbbell (left) and dimer of dumbbells (right).

In the reaction product of our reference synthesis, a small fraction of larger clusters was observed. These clusters consist of two seed particles and one central lobe originating from the fusion of the (partially) liquid protrusion of the individual dumbbells. These clusters will be referred to as dimers. The shape of these dimers will also be used to determine which lobe of the dumbbell originates from the seed and which is the protrusion. Since these dimers are formed by fusion of liquid or partially polymerized protrusions of two individual dumbbells, the volume of the central lobe is equal to two times the volume of a protrusion. If the protrusion is smaller than the seed a more linear dimer will be formed (Scheme 3.2a), while a large protrusion will give rise to more spherical dimers with a significantly larger central lobe (Scheme 3.2c).^{1,2,7}

Scheme 3.2. Schematic representation of the expected geometry of dimers of dumbbells (bottom) based on the size of the protrusion of a single dumbbell (top). Smaller protrusions lead to the formation of more linear dimers.



In the next sections the results of the dumbbell formation reactions will be discussed as a function of the previously mentioned experimental variables.

3.3.1. Necessity of chlorine functionality. The first experiments were performed to verify that the chlorine groups originating from the vinylbenzyl chloride (VBC) coating on our seeds were indeed necessary to obtain well-defined protrusions. In contrast to the system used by Kraft et al., who used solely potassium persulfate (KPS) to initiate the polymerization of the hydrophilic coating, we used a combination of KPS and sodium bisulfite (NaHSO_3). Possibly this leads to a higher content of charged groups (sulfate and sulfonate) at the surface and therefore a more hydrophilic surface.²⁶ Core-shell particles with a shell consisting of styrene and divinylbenzene were prepared using exactly the same method as used to prepare the chlorinated seeds. Therefore the only difference is the absence of the chlorine groups at the surface of these particles. Subsequently, a dumbbell synthesis was conducted with these non-functionalized seeds (entry 2, Table 3.1). TEM images of the resulting particles are depicted in Figure 3.2.

Although the particles are slightly elongated, no clear protrusions were formed. This suggests a very small contact angle between the seed and the expelled monomer. Therefore, the charged groups on the surface provide some hydrophilicity, but not enough to yield particles with clearly separated lobes. The chlorines increase the surface hydrophilicity just enough to yield a well-defined contact angle and a large degree of phase separation, which is in agreement with previously obtained results.²⁰ These experiments underline the dual function of VBC which provides both surface hydrophilicity as well as a versatile chemical handle for further surface modification.

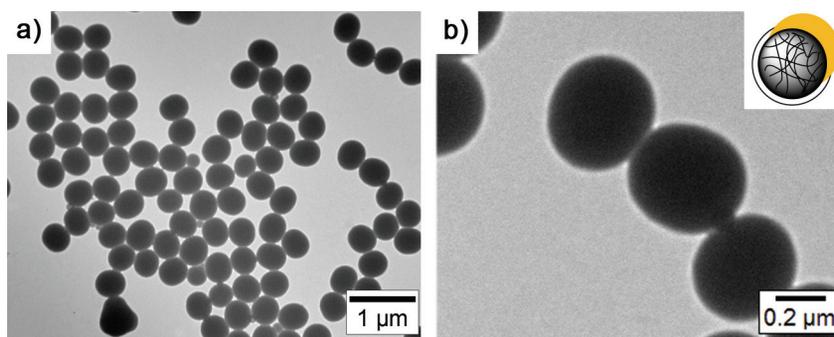


Figure 3.2. (a) Transmission electron microscopy (TEM) image of the resulting colloids after an attempt to introduce protrusions on non-functionalized polystyrene seeds. (b) Enlargement of the same colloids as shown in (a), revealing a slightly elongated particle shape.

3.3.2. Effect of the cross-link density of the seed particles. As discussed in the Introduction, the formation of a (liquid) protrusion on a seed particle is induced by an elastic contraction of the cross-linked polymer network inside the seed particle. A higher degree of cross-linking of this network results in the generation of a larger elastic-retractile force. With this larger force, more monomer can be expelled from the monomer-swollen seed particles, which leads to the formation of larger protrusions. Sheu et al. also pointed out that a minimal cross-link density is required, such that the elastic-retractile force which is generated exceeds the sum of the mixing and interfacial forces.^{14,15} If this criterion is not fulfilled, no phase separation will occur, which results in spherical particles after polymerization. Based on these arguments one would conclude that a higher cross-link density is favored if large protrusions are desired. However, there are practical limits to the maximum value of the cross-link density. First, polymer networks with high degrees of cross-linking are known to be inhomogeneous.^{14,15} If phase separation between monomer and these networks occurs, the contraction of the network will be localized within the regions containing the weakest spots. This leads to the formation of particles with multiple, ill-defined protrusions ('popcorn-like' particles). The second limiting factor is that if the cross-linking density increases, the flexibility of the network decreases. Consequently, the amount of monomer that can be taken up by the seeds in the swelling stage decreases as well. Therefore, it is expected that there exists an optimal cross-link density which results in the formation of the largest possible well-defined protrusions. Our reference synthesis was performed with seeds containing a cross-link density of 3% (entry 1, Table 3.1) and a swelling ratio of 6. The first experiments focused on decreasing the cross-link density of both the polystyrene core and the shell to 1 and 2% by changing the ratio between styrene and DVB. The resulting particles were of comparable size as

the reference seeds as measured with DLS (see Table 3.1). Also the chlorine content of the particles as probed with IR spectroscopy was comparable to the seeds used in the reference synthesis. Subsequently, both the particles with a 1 and 2% cross-link density were used to prepare dumbbell-shaped colloids. Swelling ratios of 6 and 10 were applied for both seeds (entries 3–6, Table 3.1). TEM images of the particles prepared with swelling ratio 6 and 10 are shown in Figure 3.3a,b and Figure 3.4a,b, respectively.

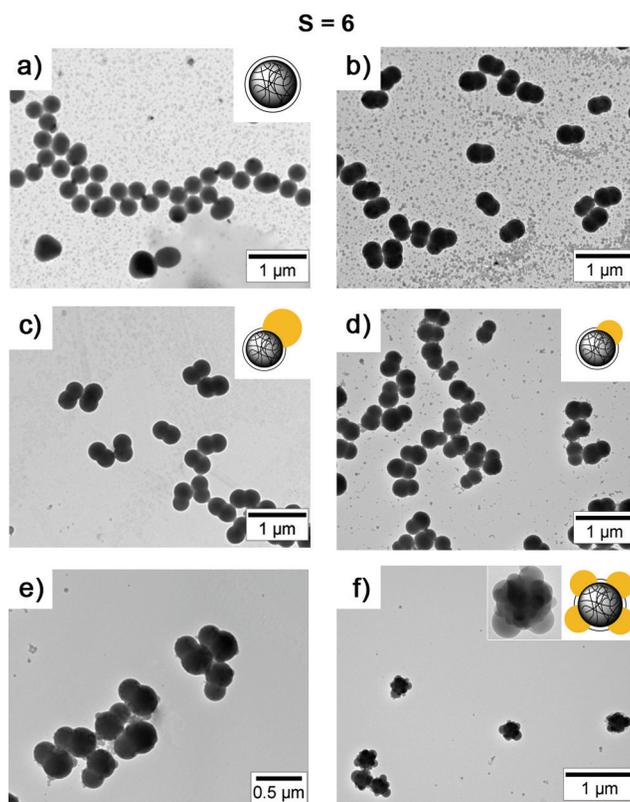


Figure 3.3. Transmission electron microscopy (TEM) images of anisotropic particles prepared using seed particles with cross-link densities of (a) 1%, (b) 2%, (c) 3%, (d) 5%, (e) 10% and (f) 18%. All reactions were carried out with a swelling ratio of 6.

Clearly, a cross-link density of 1% did not lead to the formation of well-defined dumbbell-shaped colloids. Especially for a swelling ratio of 6 the particles are still relatively spherical. A fraction of larger aggregates was observed. These most probably form when the swollen, and therefore soft, colloidal particles bump into each other and get stuck during the polymerization. Roughly the same situation is observed using a swelling ratio equal to 10, although the obtained particles are slightly more anisotropic

(egg-shaped). This indicates that a little monomer was expelled during the protrusion formation/polymerization due to the low elastic-retractile force which was generated by the lightly cross-linked network. If the particles take up more monomer in the swelling step, the stress on the polymer network is larger. This translates into a larger elastic force upon heating and therefore a slightly more pronounced phase separation.

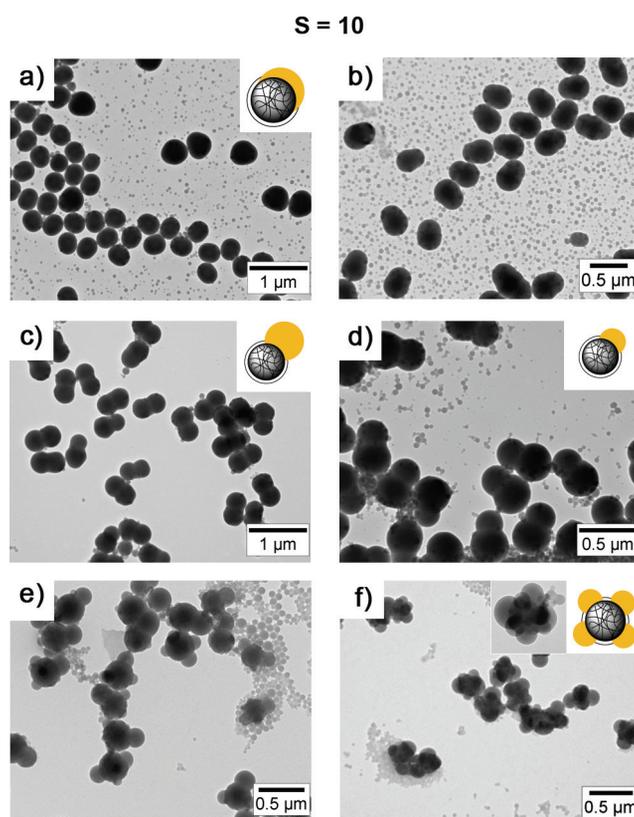


Figure 3.4. Transmission electron microscopy (TEM) images of anisotropic particles prepared using seed particles with cross-link densities of (a) 1%, (b) 2%, (c) 3%, (d) 5%, (e) 10% and (f) 18%. All reactions were carried out with a swelling ratio of 10.

Increasing the cross-link density to 2% leads to the formation of well-defined dumbbells that are of similar shape as the particles obtained in the reference synthesis (cross-link density = 3%). The cross-link density of 2% appears to be the minimal density required to induce a sufficient degree of phase separation and to prepare these dumbbells. This small increase in the cross-link density illustrates that the resulting particle geometry is highly sensitive towards this experimental variable.

For seed particles with a cross-link density of 2%, the geometry of the dumbbells

is limited to symmetrical dumbbells regardless the swelling ratio. The fact that we have not been able to prepare dumbbell-shaped colloids with a larger protrusion than the size of the seed, could be due to the limited elastic force that can be generated using these weakly cross-linked seed particles. Using our reference seeds with a cross-link density of 3% and a swelling ratio of 10 did not change this result and still symmetrical dumbbells were obtained (entry 7, Table 3.1).

Increasing the cross-link density to 5, 10 and 18% did also not result in particles with larger protrusions either. In contrast, the dumbbells prepared using the seed particles with a cross-link density of 5% showed the formation of asymmetric particles in which the protrusion is smaller than the corresponding seed particle for both swelling ratios (entry 8 and 9, Table 3.1, Figure 3.3d and Figure 3.4d). Apparently, increasing the cross-link density from 3 to 5% leads to a reduction in monomer uptake. As mentioned before, this limited swelling capability originates from a decreased network flexibility. Increasing the cross-link density even further to 10 and 18% (entry 11–13, Table 3.1) resulted in the formation of the predicted ‘popcorn-like’ particles (Figure 3.3f and Figure 3.4e and f). Several protrusions were identified on these particles, which makes these seeds not useful for the preparation of well-defined colloidal dumbbells.

To conclude, the expected maximum in the protrusion size as a function of the cross-link density was obtained using seeds with a cross-link density between 2 and 3%. Seed particles with these densities formed protrusions of sizes comparable to that of the employed seeds. Lowering the cross-link density might increase the swelling capability, but results in insufficient elastic force upon heating to form liquid protrusions. Increasing the cross-link density to increase the magnitude of this elastic force yielded particles with smaller protrusion compared to the seed due to limited monomer uptake. Using seeds with cross-link densities beyond 10% yielded undefined particles with multiple protrusions generated due to inhomogeneities in the polymer network.

3.3.3. Cross-linking of the protrusion. The chlorines present on the colloids provide a reactive chemical handle. However the particles need to be resistant against the conditions under which this chemical handle is converted into the desired (end-) functionality. A vast majority of the organic chemistry transformations based on the chlorine groups are not possible and/or effective in water, but are commonly carried out in organic solvents. One example was already shown in Chapter 2, where the chlorinated lobe was functionalized via click chemistry using dimethylformamide (DMF) as solvent. Without cross-linking the protrusion, the linear polystyrene would completely dissolve leaving only the spherical seed particle behind (Figure 3.5). Cross-linking the protrusion is achieved by a straightforward procedure; instead of swelling solely with styrene, a mixture of styrene and DVB is used. Subsequent polymerization directly leads to a cross-linked protrusion.

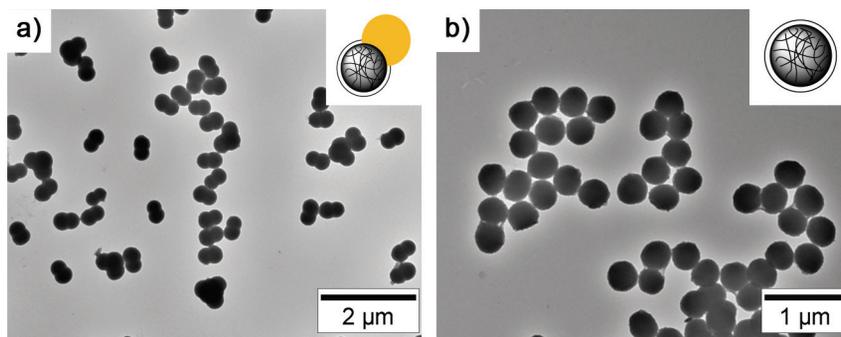


Figure 3.5. (a) Dumbbell-shaped colloids containing a protrusion which is not cross-linked dispersed in water. (b) The same colloidal dumbbells as shown in (a), after redispersion in dimethylformamide (DMF). The protrusion was completely dissolved under these conditions.

Results presented in Chapter 2 already confirmed that this cross-linking procedure is effective, since we showed that colloids were functionalized in DMF without loss of their anisotropic shape. Here we investigate the effect of the DVB concentration in the swelling solution on the resulting particle geometry. Therefore, dumbbells were prepared by swelling seeds with styrene containing 0, 3, 6 and 12% DVB (entry 15, 1, 17 and 18, Table 3.1). In all cases, the total swelling ratio was kept constant at a value equal to 6.

From Figure 3.6, we observed that the contact angle becomes less pronounced at intermediate cross-link densities (3 and 6%) compared to the particles with non-cross-linked protrusions. If one draws a circle around the seed and protrusion, one finds that the centers of these circles are much farther apart if the protrusion is not cross-linked. In other words, the degree of phase separation between the seed particles and protrusions is higher. Nevertheless, the dumbbells prepared at these intermediate cross-link densities are well-defined and consist of clearly separated lobes. Going to the highest cross-link density of 12% resulted in a smaller protrusion compared to the syntheses performed with swelling solutions containing less or no DVB.

These observations can be explained if we consider the protrusion formation mechanism proposed by Sheu et al.^{14,15} They showed that the contraction of the elastic network initially generates only a small liquid protrusion while the remaining monomer stays inside the swollen seed particle. As soon as the polymerization of the protrusion starts, monomer is consumed and an osmotic flow of monomer is generated from the swollen seed to the protrusion. This process occurs until the monomer is depleted, or more precisely, if osmotic balance is regained, and the final protrusion size is obtained. Sheu et al. made the distinction between semi-interpenetrating networks (semi-IPNs) and full-interpenetrating networks (full-IPNs) which were prepared by swelling

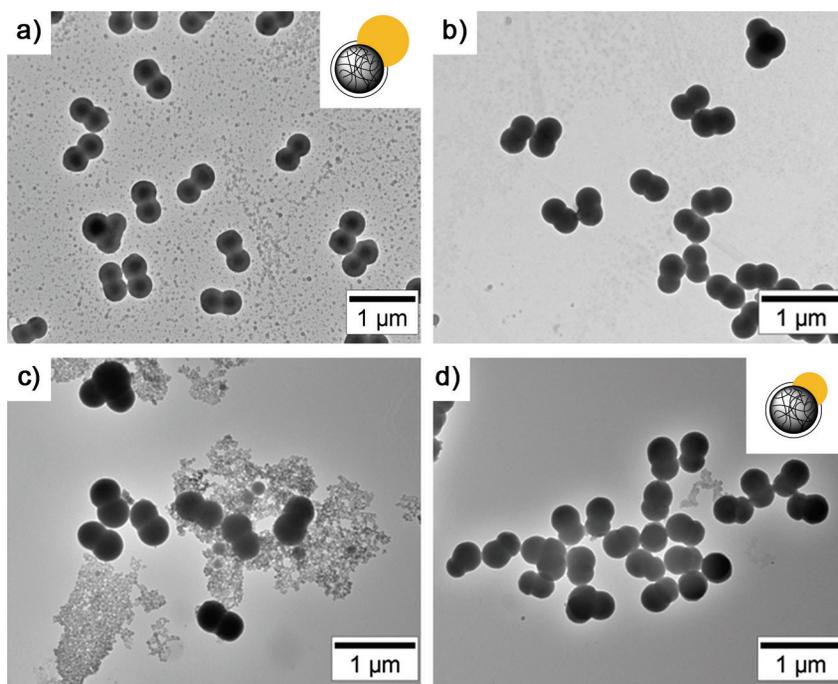
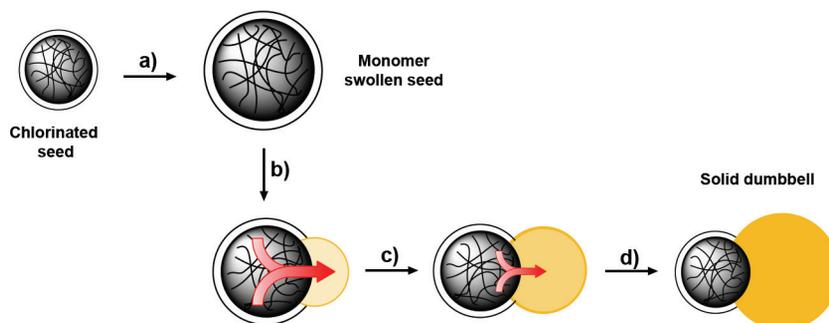


Figure 3.6. Transmission electron microscopy (TEM) images of anisotropic particles prepared by using swelling solutions containing 0% (a), 3% (b), 6% (c) and 12% (d) divinylbenzene (DVB) to form a cross-linked protrusion.

cross-linked seed particles with only monomer (semi-IPN) or with a mixture of monomer and cross-linker (full-IPN), respectively. When the content of cross-linker in the swelling solution was high enough, the preparation of the full-IPNs resulted in dumbbell-shaped particles with a smaller protrusion. This observation was attributed to an increased viscosity at higher degrees of chains entanglements which hinders the flow of monomer into the newly formed polymer bulge during the polymerization process.^{14,15}

The results obtained by Sheu et al.^{14,15} seem in line with our results obtained after swelling with a monomer solution containing 12% DVB. A lower degree of chain entanglements and lower viscosity also accounts for the observation that the semi-IPN particles (no cross-linker added in the swelling step) have a larger degree of phase separation compared to the full-IPN particles. Cross-link densities obtained after swelling with 3 and 6% DVB are apparently high enough to prevent a high degree of phase separation, but insufficient to significantly slow down the monomer feed to the forming protrusion. Therefore, at these intermediate cross-link densities, dumbbell-shaped particles with reasonable separated lobes were still obtained.

Scheme 3.3. Schematic representation of the mechanism for protrusion formation proposed by Sheu et al.^a



^aStep (a): swelling of the cross-linked seed particles by monomer. Step (b): heating of the monomer swollen seeds resulting in a contraction of the polymer network. The generated elastic-retractile force causes the phase separation of a small liquid monomer bulge on the surface of the seed particle. Step (c): upon polymerizing the liquid protrusion, monomer is consumed leading to the formation of a monomer flow from the monomer swollen seed to the protrusion. Step (d): the supply of monomer from the seeds continues until the monomer is depleted. Polymerization proceeds in the newly formed lobe until maximum conversion is reached. The final solid dumbbell-shaped colloid is formed.

3.3.4. Effect of SDS concentration. Dumbbell syntheses were conducted in aqueous media containing 0, 1 and 7 times the critical micelle concentration (CMC) of SDS (entry 19, 20 and 1, Table 3.1) to investigate how the particle shape is altered upon changing the surfactant concentration. The dumbbells were prepared with a swelling ratio of 6 and the results are summarized in Figure 3.7.

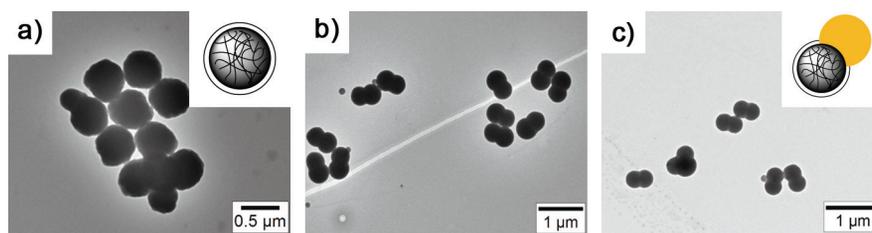


Figure 3.7. Transmission electron microscopy (TEM) images of dumbbell-shaped colloids prepared in solution containing SDS concentrations equal to (a) 0 \times , (b) 1 \times and (c) 7 \times the critical micelle concentration (CMC).

The only clear conclusion which can be drawn from these results is that at least some SDS in the reaction mixture is required to obtain dumbbell-shaped colloids. In the absence of this surfactant irregularly shaped particles were obtained with no

protrusions (Figure 3.8a). This is in agreement with the proposed mechanism which states that the oil–water interface of the protrusion needs to be stabilized.^{1–3,10,20} Phase separation between monomer and styrene is facilitated in the presence of surfactant. The decrease in surface tension of the oil–water interface makes it energetically less costly to create new interface, in this case a liquid protrusion. Experimentally the decreased surface tension translates into the formation of colloids with well-defined and well-separated lobes. Within the experimental window we did not observe any dependence of the protrusion size or the number of protrusions (Figure 3.7b and c) on the SDS concentration. This observation suggests that the lowest SDS concentration was already sufficient to stabilize all the oil–water interface present in the system. Kraft et al. did observe a distinct influence of the SDS concentration on the number of protrusions that were formed per particle.³ In our system, the formation of multiple protrusions is probably more dependent on the homogeneity of the polymer network in the seed particles. As mentioned in Section 3.3.2, a high cross-link density promotes the formation of multiple protrusions. If in such a situation sufficient SDS is present, all the formed protrusions will be stabilized against merging into one single protrusion, resulting in the formation of ‘popcorn-like’ particles. Since the effect of the SDS concentration was probed using particles with a cross-link density of only 3% we do not expect an inhomogeneous network and therefore the formation of multiple protrusions should not occur.

Finally, we did not observe an enhanced formation of dimers or higher aggregates of dumbbells upon lowering the surfactant concentration from 7 times to 1 time the CMC. This is another indication that the formed protrusions are already fully stabilized even at SDS concentrations equal to the CMC and do not merge. Decreasing the surfactant concentrations below the CMC might induce the formation of higher order aggregates, but these low concentrations were not applied in this study.

3.3.5. Effect of the swelling ratio. The most straightforward way to alter the size ratio between seed and protrusion is by varying the swelling ratio, since this is directly related to the size of the resulting protrusion. The lower limit of the protrusion size is determined by the minimal amount of monomer required to swell the seed to such extent that enough elastic force can be generated to push out the initial monomer upon contraction of the polymer network.^{14,15} The upper limit is obviously set by the amount of monomer the seeds can take up. Polystyrene colloids can be swollen with volumes of styrene up to several times their own volume.^{14,15} Consequently, protrusions much larger than the seeds can in principle be grown. These statements were experimentally verified for small seed particles coated with a thin, non-cross-linked layer of poly(vinyl acetate)^{1,2,20} and micron-sized particles.^{14,15} To investigate if these statements also hold for the chlorinated particles, we prepared dumbbell-shaped colloids with three different swelling ratios (4, 6 and 10, entry 14–16, Table

3.1). The formed protrusions in these experiments were not cross-linked (swelling solution consisted of pure styrene; semi-IPN). Representative TEM images of the resulting colloidal particles are shown in Figure 3.8. At a swelling ratio equal to 4, slightly asymmetric dumbbells were prepared where the protrusion was smaller than the seed (Figure 3.8a). We deduced this by the approximately linear geometry of the dimers of dumbbells that were present in the sample. According to the schematic representation shown in Scheme 3.2a this must imply a dumbbell-shaped colloid with a protrusion smaller than the seed. Furthermore, the dumbbells clearly show that the larger lobe is characterized by some surface structure and is less spherical, originating from the core-shell structure of the seeds (Figure 3.1). In contrast, the protrusions are smooth and spherical.

Going up to swelling ratios as high as 10 resulted in the formation of larger protrusions, but the limiting size of the protrusion seems to be comparable to the size of the seed particle (Figure 3.8b and c).

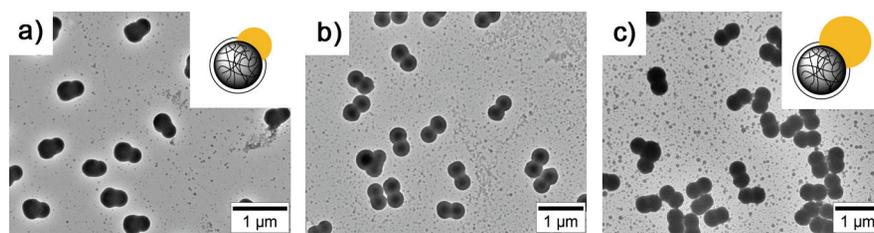


Figure 3.8. Transmission electron microscopy (TEM) images of dumbbell-shaped colloids prepared with a swelling ratio of (a) 4, (b) 6 and (c) 10. In all cases the protrusions were not cross-linked.

For each swelling ratio, the obtained protrusion is significantly smaller than expected purely based on the volume of monomer that was added to the seeds. Together with the observation that the seed particles were of comparable size before and after protrusion formation, we concluded that not all monomer was taken up by the seeds. The excess monomer is converted into unwanted secondary nucleation.

3.3.6. Effect of the shell properties on dumbbell formation. As mentioned before, it would greatly widen the practical use of the anisotropic particles based on the chlorinated seed particles if the functional patches were (much) smaller than the non-functionalized regions (see Chapter 6). The changes in the obvious experimental parameters (Section 3.3.1–3.3.5) did not enable us to synthesize this type of particles, since only asymmetric dumbbells with a small protrusion or symmetric dumbbells (equally sized lobes) were obtained.

The only significant difference between the reported systems and the seed particles used in this chapter is the rather thick (≈ 30 nm) chlorinated layer, which is also cross-linked. The influence of the properties of the chlorinated layer on the

dumbbell formation are therefore investigated in the upcoming sections.

The limited protrusion growth is most probably caused by limited swelling capacity of the seed particles (Section 3.3.1–3.3.5). Below we list potential synthetic strategies to increase the monomer uptake of the seed particles and to overcome the narrow range of accessible particle geometries:

I) Decrease the thickness of the chlorinated shell.

Due to the hydrophilic character of this shell, it is possible that the shell limits the diffusion of styrene into the seeds particles upon swelling. The chlorinated layer which was typically used was much thicker than the poly(vinyl acetate) coating employed by Kraft et al. and Mock et al.^{1–3,20} In principle these thick coatings are not necessary, since only surface chlorines are required to provide surface hydrophilicity and functionality.

II) Change the shell composition.

Another option to enhance the diffusion of monomer into the particle is to synthesize shells using a mixture of styrene, VBC and DVB instead of solely VBC and DVB. Increasing the percentage of styrene into the monomer feed should result in a more hydrophobic shell which facilitates the swelling process.

3.3.7. Effect of shell thickness on dumbbell formation. As a first attempt, chlorinated layers consisting of cross-linked p(VBC), ranging from 8 to 65 nm were introduced on the same batch of seed particles (entry 1–9, Table 3.2). The cross-link density was again 3%, since this density resulted in the formation of the largest protrusions as described in Section 3.3.2. The thicknesses of the chlorinated layers were estimated from DLS data by measuring the increase in hydrodynamic radius compared to the seed particles (Figure 3.9a). All syntheses yielded monodisperse particles. Furthermore, IR spectroscopy showed a clear increase in chlorine content ($-\text{CH}_2\text{-Cl}$ vibration at 1266 cm^{-1}) with increasing shell thickness (Figure 3.9b, highlighted in grey).²⁷ The seeds used in the reference synthesis (entry 1, Table 3.1 or 3.2) had a p(VBC) layer of 33 nm.

For each of the seeds, two dumbbell syntheses were performed with swelling ratios equal to 6 and 10. The results are shown in Figure 3.10 and remarkably, we found that the thickness of the cross-linked chlorinated shell has a distinct influence on the size of the protrusions that are formed. The particles with the thinnest shell (8 nm, entry 8 and 9, Table 3.2), did not yield dumbbell-shape particles, but rather spherical colloids for both swelling ratios (Figure 3.10a and b). This result contradicts our previous hypothesis where we stated that a thinner shell promotes particles swelling.

Increasing the shell thickness to 27 nm (entry 6 and 7, Table 3.2) led to the formation of asymmetric dumbbell-shaped particles with a slightly better defined contact angle

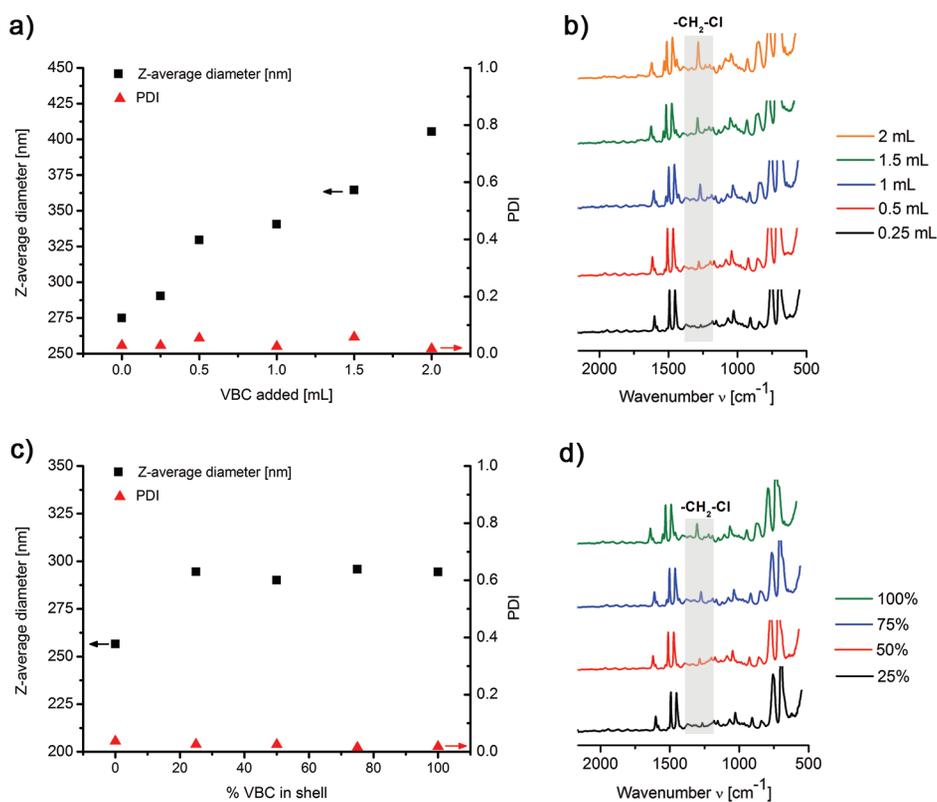


Figure 3.9. (a) Dynamic light scattering (DLS) results of the core-shell seed particles prepared by the addition of a variable amount of vinylbenzyl chloride (VBC) to a fixed amount of cross-linked polystyrene particles. The VBC added to the core particles contained 3% divinylbenzene (DVB) in each synthesis. The Z-average sizes are shown in black squares and polydispersity indices (PDI's) in red triangles. (b) Infrared (IR) spectra obtained from the core-shell seed particles with variable chlorinated shell thickness. The highlighted signal at 1266 cm^{-1} corresponds to the $-\text{CH}_2\text{-Cl}$ signal. (c) DLS results of the core-shell seed particles prepared by the addition of a mixture of styrene and VBC to a fixed amount of core particles. The volume percentage of VBC in the feed ranged from 25–100%. All monomer mixtures contained 3% DVB. The Z-average sizes are shown in black squares and polydispersity indices (PDI's) in red triangles. (d) IR spectra obtained from the core-shell seed particles with variable shell composition. The signal at 1266 cm^{-1} corresponds again to the $-\text{CH}_2\text{-Cl}$ signal.

(Figure 3.10b and c). The formed protrusion was smaller than the seed particle, deduced from the shape of the dimer particles as mentioned before. The reference synthesis conducted with particles with a shell thickness of 33 nm led to the formation of well-defined symmetric dumbbells (Figure 3.10e and f). Increasing the thickness

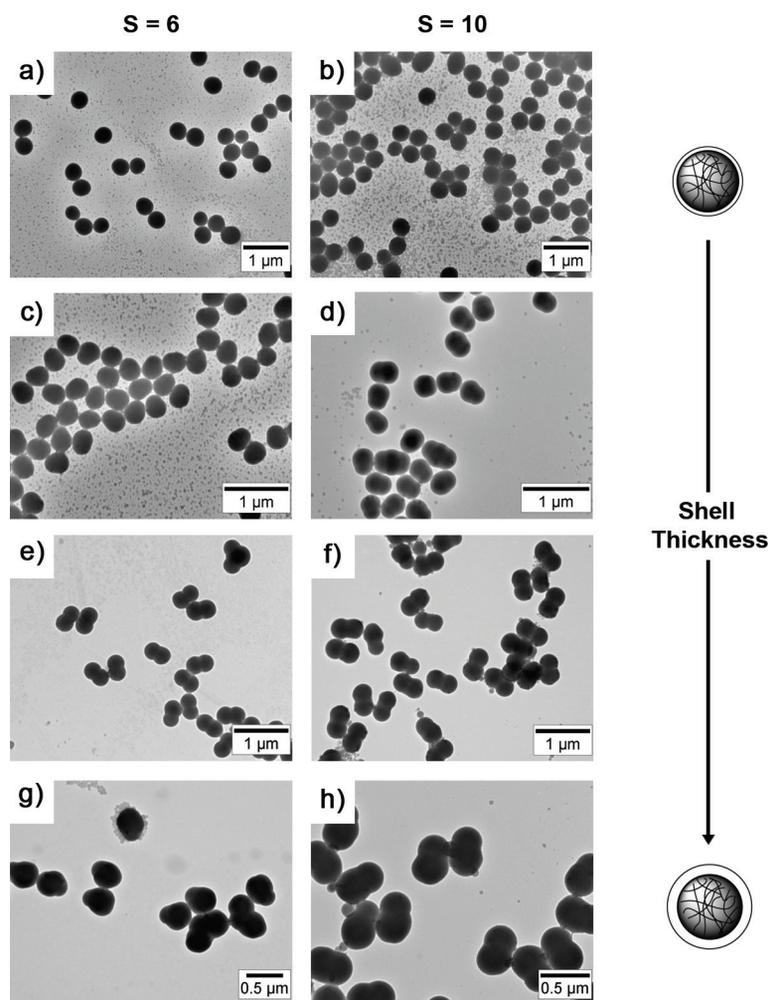


Figure 3.10. Transmission electron microscopy (TEM) images of dumbbell-shaped colloids prepared by using core-shell seed particles with variable chlorinated shell thicknesses at swelling ratio 6 and 10. Swelling ratio of 6 in combination with shell thickness (a) 8 nm, (c) 27 nm, (e) 33 nm and (g) 45 nm. Swelling ratio of 10 in combination with shell thickness (b) 8 nm, (d) 27 nm, (f) 33 nm and (h) 45 nm.

of the chlorinated shell even further resulted in the formation of ill-defined seed particles. The surface of these particles is rough as observed with TEM. Dumbbells prepared starting from particles with a layer thickness of 45 nm were asymmetric (smaller protrusion) at a swelling ratio of 6 (Figure 3.10g, entry 4, Table 3.2) and symmetrical if this ratio was 10 (Figure 3.10h, entry 5, Table 3.2). For the particles with the thickest shell (65 nm, entry 2 and 3, Table 3.2), only asymmetric dumbbells with

smaller protrusions were formed. From this set of experiments it follows that a shell thickness of 33 nm yield dumbbells with the maximum protrusion size.

These results suggest that for the chlorinated core-shell colloids it is not the core, but only the shell that is actively involved in the protrusion formation. The thickness of the shell sets the limit for the amount of monomer that can be accommodated inside the particles and not the core of these colloids. At a shell thickness of 33 nm, 50% of the particle volume is present in the shell. In this situation still a large volume is available for taking up monomer. However, if the shell becomes thinner the relative volume of the shell and consequently the swelling capacity decreases.

A possible explanation for this observation can be provided if the structure of the core-shell seed particles is examined in more detail. Nieuwenhuis et al.²⁸ showed by means of scattering techniques that the cross-link density in a latex particle is non-uniform. In the core of the particles this density is high, while the outer shell of the particle is more lightly cross-linked. McPhee et al.²⁹ confirmed this picture by measuring the efficiency of cross-linking monomer incorporation into growing particles during an emulsion polymerization and concluded that a large portion of the cross-links were incorporated during the initial growth of the particles. This is not surprising, as the solubility of a polymer chain decreases with increasing molecular weight; addition of cross-linking monomer facilitates a substantial increase in the polymer length and therefore its insolubility. If we expand this view to the core-shell particles, we obtain the following picture: the grey area in Figure 3.11 represents the polystyrene core while the chlorinated shell is depicted as the white outer layer. Both layers are cross-linked

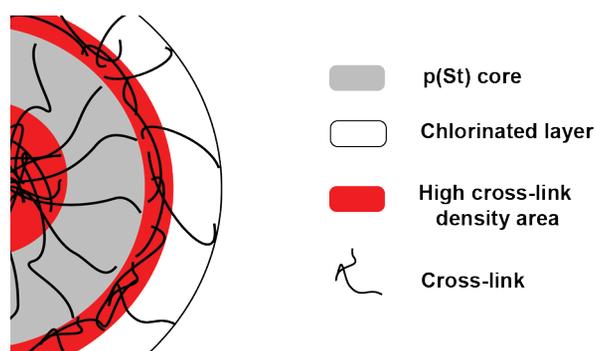


Figure 3.11. Schematic representation of variations in cross-link density in the chlorinated core-shell colloids. Cross-links are depicted by the black lines. The grey area represents the polystyrene core and the white outer ring the chlorinated layer. Higher cross-link density areas are highlighted in red and are located in the center of the particle and on the interface between the core and the outer chlorinated layer.

as indicated by the presence of the black lines. The areas with the highest cross-link density are highlighted in red and these are the inner part of the polystyrene core and the interfacial layer between the grey polystyrene core and the chlorinated outer layer. Note that the introduction of the chlorinated shell was performed in a separate reaction step. Also in this reaction step, more cross-links will be formed at the start of the polymerization leading to the picture schematically drawn in Figure 3.11.

Naively, one might argue that when these particles are swollen with hydrophobic monomers the highly cross-linked interfacial region between the seed and the shell acts as a barrier for the monomer to penetrate into the core due to a locally increased viscosity. In effect the actual swelling capacity of the seed particle as a whole is only determined by the volume of the outer shell. This reasoning also explains the limiting increase in size that is observed after swelling the particles with the thin shells in which no protrusion was formed (Figure 3.10a and b). Furthermore, if the size of the swollen network decreases, i.e. the shell thickness decreases, the elastic-retractile force generated upon heating will also be smaller which further hampers protrusion formation. For the particles with thicker shells (> 33 nm) these arguments do not seem to hold anymore. The physical principle behind this observation is not clear. The irregular shape of colloids which shells > 33 nm suggests that these particles are not ideal model systems for studying the effect of the shell thickness on the protrusion formation process.

To make solid statements about the role of the shell and its cross-link density, a systematic study should be conducted in which the cross-link density of the shell is varied while keeping the core properties constant. Another interesting experiment would be to prepare particles which consist of only one polymer network and a gradient in VBC content. In this type of particles there is no densely cross-linked layer which can interfere with the monomer uptake in the swelling stage. These particles are accessible by performing one-pot emulsion polymerizations in which VBC is added to the reaction at moderate to high styrene conversions. These experiments have not been performed during this study and are recommended for future follow-up research.

3.3.8. Effect of shell composition on dumbbell formation. With the experimental observation that only the shell participates in swelling and subsequent dumbbell formation (Section 3.3.7), we tried to increase the swelling ability of these layers by using mixtures of styrene and VBC as shell monomers. Using styrene as comonomer leads to a more hydrophobic shell which should then be able to take up more monomer in the swelling step. Since VBC is slightly more hydrophilic than styrene we still expect that the majority of this monomer will be located at the particle surface to provide both the chemical handle and the slightly enhanced surface hydrophilicity.

Based on cross-linked polystyrene particles, four different seed particles were prepared with shells consisting of 25, 50, 75 and 100% VBC (entry 10–15, Table

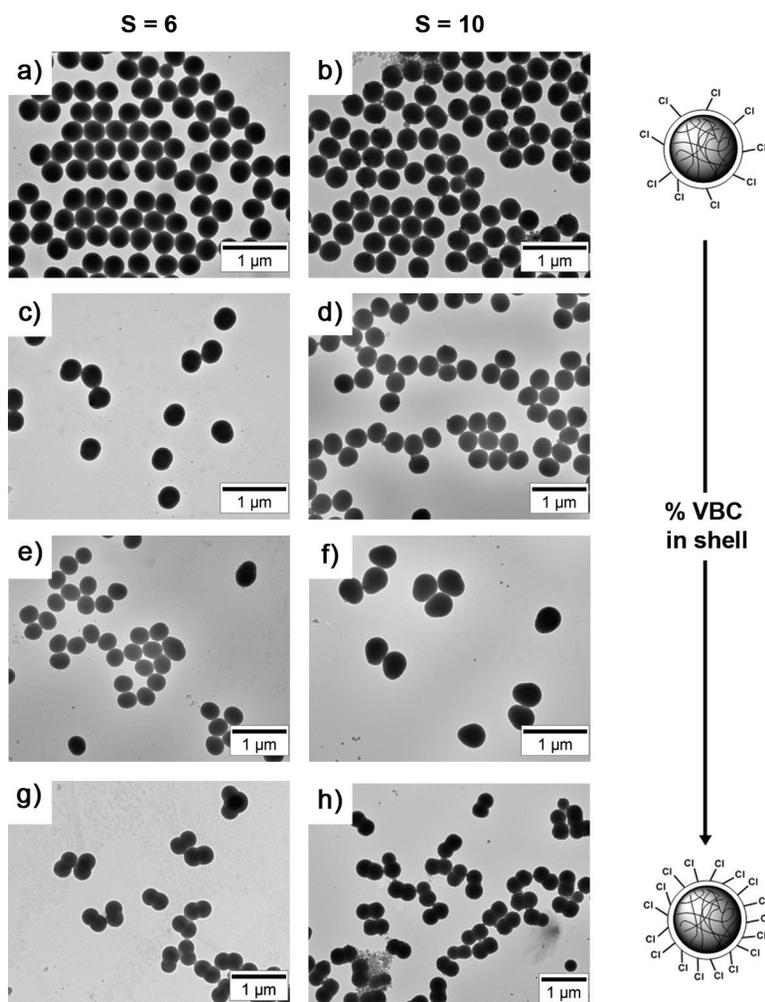


Figure 3.12. Transmission electron microscopy (TEM) images of dumbbell-shaped colloids prepared by using core-shell seed particles equipped with shells consisting of various mixtures of styrene and vinylbenzyl chloride (VBC) at swelling ratio 6 and 10. Swelling ratio of 6 in combination with shell composition (a) 25% VBC, (c) 50% VBC, (e) 75% VBC and (g) 100% VBC. Swelling ratio of 10 in combination with shell composition (b) 25% VBC, (d) 50% VBC, (f) 75% VBC and (h) 100% VBC.

3.2). The particles with a shell consisting of solely VBC and DVB were our reference colloids (entry 1, Table 3.1 or 3.2). In all syntheses, the shell was cross-linked by adding 3% DVB to the monomer phase. The total monomer volume added to the polystyrene cores was kept constant. DLS measurements showed that we obtained core-shell

particles with a shell thickness of approximately 30 nm and that this thickness was independent of the shell composition (Figure 3.9c). All seeded emulsion polymerization yielded monodisperse particles, making it an ideal series to test the influence of shell composition. IR spectroscopy confirmed an increasing chlorine content if higher ratios of VBC:St were used to grow the shell (Figure 3.9d). In other words, the composition of the monomer feed was directly transferred into the composition of the shell.

Also in this case each type of chlorinated seed was used to prepared dumbbell-shaped colloids using swelling ratios 6 and 10. Representative TEM pictures of the obtained particles are shown in Figure 3.12. Using particles equipped with a shell that contained only 25 (entry 14 and 15, Table 3.2) or 50% (entry 12 and 13, Table 3.2) of VBC did not result in clear dumbbell-shaped colloids (Figure 3.12a–d). Especially the particles with the lowest chlorine content resulted in spherical particles regardless of the swelling ratio. This observation can be easily explained by the fact that the surface is just not hydrophilic enough to prevent (almost) full wetting of the expelled monomer (Section 3.1). One could also claim that the seeds are just not capable of taking up enough monomer to form a protrusion. However, if we measure the increase in volume of the seeds after the attempted protrusion formation we find that the increase would be sufficient to form protrusions with similar size as the seeds (radius $\approx 150\text{--}175$ nm). This indicates that the low degree of surface hydrophilicity most likely causes the lack of protrusions on these particles. For the particles equipped with a polymeric shell consisting of 75% VBC and 25% styrene we observed that with a swelling ratio of 10 (entry 11, Table 3.2) asymmetric dumbbells were obtained. In this case the protrusion corresponds to the larger lobe of the particle, since the dimers of dumbbells that were present in the sample showed a very large central lobe compared to the size of the seeds (Figure 3.13). The contact angle between seed and protrusion is not very pronounced compared to the reference synthesis. This again was attributed to the lower surface hydrophilicity of the shell due to the lower VBC content. However, it seems that the shell composition of 75% VBC and 25% styrene is the right balance between swelling capacity and surface hydrophilicity, although the size difference between seed and protrusion is still limited. Increasing the asymmetry of the particles further will not be trivial, since most of the experimental parameters involved in this reaction were optimized for obtaining a large protrusion. Increasing the swelling ratio even further will probably not result in a higher degree of swelling. At these high swelling ratios free styrene was observed even after 48 h of swelling, indicating that not all monomer is taken up by the seed particles. Increasing the amount of styrene in the swelling step will only lead to the formation of more secondary nucleation and coagulum. As mentioned before, the use of seed particles consisting of a single continuous cross-linked network might be the solution if one aims for particles with a larger asymmetry.

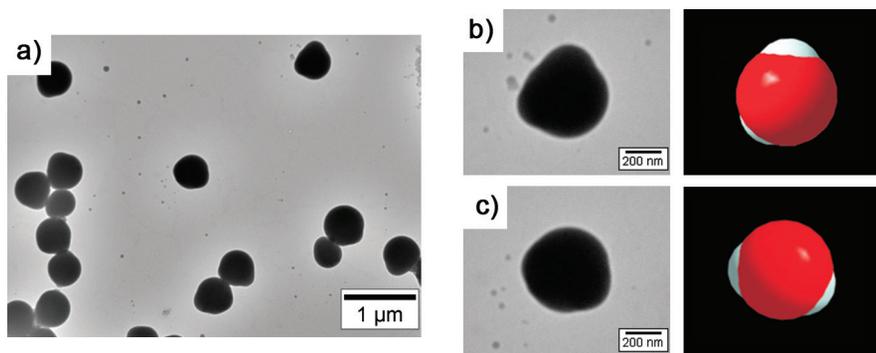


Figure 3.13. (a) Transmission electron microscopy (TEM) images of dimers of dumbbells observed after protrusion formation of core-shell seed particles equipped with a shell consisting of 75% VBC and 25% styrene. (b) Enlarged TEM picture of 2 dimers and their corresponding 3D models to clarify the particle geometry. In the 3D model the red center resembles the fused protrusions while the chlorinated seeds are shown in white.

3.4. Conclusions

In this chapter we showed that the preparation of anisotropic colloidal particles based on chlorinated polystyrene seeds is possible. These seeds consist of a cross-linked core and an outer cross-linked chlorinated layer. The chlorine groups on the outer surface of these particles provide sufficient surface hydrophilicity to prevent full wetting of the expelled monomer and therefore for the formation of well-defined dumbbell-shaped colloids. Dumbbells with protrusions smaller or equal to the size of the seed particles are easily accessible by tuning experimental parameters such as swelling ratio and cross-link density of the seed and/or protrusion. Moreover, the shell properties of the seed particles have a major influence on the resulting particle geometry. The protrusion size increases with increasing shell thickness. This suggests that only the cross-linked shell is actively involved in the protrusion formation. Increasing the hydrophobicity of the shell by incorporating styrene results in a situation where surface hydrophilicity (provided by the chlorine groups) and swelling capacity are optimized leading to the formation of particles with protrusions larger than the corresponding seeds. Although the size difference between the seed and protrusion remained limited, we show that a reasonable variation in particle geometry is accessible based on these chlorinated particles. This gives rise to a family of chemically anisotropic colloids with tunable particle shape.

Acknowledgments

Sonja Castillo is thanked for providing the SEM pictures of the dumbbells and Antara Pal for preparing the polystyrene seeds with cross-link densities of 1 and 18%.

Appendix 1 – Overview of syntheses to prepare dumbbells

Table 3.1. Overview of the syntheses conducted to prepare dumbbell-shaped particles.

Entry	Surface func. of seed	Cross-link density seed [%]	Diameter [nm] / PDI [-]	[SDS] × CMC	Swelling ratio	wt% DVB in swelling solution	Resulting particle shape
1	Chlorine	3	341 / 0.029	7	6	3	Symmetric dumbbell
2	None	3	336 / 0.066	7	6	3	Slightly elongated egg
3	Chlorine	1	309 / 0.05	7	6	3	No dumbbells; spherical
4	Chlorine	1	309 / 0.05	7	10	3	Slightly elongated egg
5	Chlorine	2	350 / 0.072	7	6	3	Symmetric dumbbell; ill pronounced lobe
6	Chlorine	2	350 / 0.072	7	10	3	Symmetric dumbbell; ill pronounced lobe
7	Chlorine	3	341 / 0.029	7	10	3	Symmetric dumbbell
8	Chlorine	5	301 / 0.094	7	6	3	Asymmetric dumbbells; smaller protrusion
9	Chlorine	5	301 / 0.094	7	10	3	Asymmetric dumbbells; smaller protrusion
10	Chlorine	10	353 / 0.089	7	6	3	Asymmetric dumbbells; smaller protrusion
11	Chlorine	10	353 / 0.089	7	10	3	Particles with multiple protrusions
12 ¹	Chlorine	18	291 / 0.053	7	6	3	Particles with multiple protrusions
13 ¹	Chlorine	18	291 / 0.053	7	10	3	Particles with multiple protrusions
14	Chlorine	3	341 / 0.029	7	4	0	Asymmetric dumbbell; smaller protrusion
15	Chlorine	3	341 / 0.029	7	6	0	Symmetric dumbbell; highly separated lobes
16	Chlorine	3	341 / 0.029	7	10	0	Symmetric dumbbell; highly separated lobes
17	Chlorine	3	341 / 0.029	7	6	6	Symmetric dumbbell
18	Chlorine	3	341 / 0.029	7	6	12	Asymmetric dumbbell; smaller protrusion
19	Chlorine	3	341 / 0.029	0	6	3	Ill-defined particle; no dumbbells
20	Chlorine	3	341 / 0.029	1	6	3	Symmetric dumbbell

¹ Entries 12, 13 were carried out with 233 nm seeds compared to 275–280 nm used for the remaining entries.

Appendix 2 – Variations of chlorinated particles & dumbbell formation

Table 3.2. Overview of variations in thickness and composition of the shell of the seed particles and subsequent dumbbell formations.

Entry* ¹	Thickness		Volume monomer for shell [mL]	Vol% VBC in shell	Diameter [nm]/ PDI [-]	Swelling ratio	Resulting particle shape
	shell [nm]	monomer for shell [mL]					
1	33	1	100	341 / 0.029	6	Symmetric dumbbell	
2	65	2	100	405 / 0.017	6	Asymmetric dumbbell; smaller protrusion. Rough seed	
3	65	2	100	405 / 0.017	10	Asymmetric dumbbell; smaller protrusion. Rough seed	
4	45	1.5	100	365 / 0.058	6	Asymmetric dumbbell; smaller protrusion	
5	45	1.5	100	365 / 0.058	10	Symmetric dumbbell	
6	27	0.5	100	330 / 0.054	6	Egg-shaped colloids; no clear contact angle	
7	27	0.5	100	330 / 0.054	10	Egg-shaped colloids; no clear contact angle	
8	7.5	0.25	100	290 / 0.029	6	No dumbbells; spherical	
9	7.5	0.25	100	290 / 0.029	10	No dumbbells; spherical	
10 ²	20	1	75	296 / 0.015	6	Egg-shaped colloids; no clear contact angle	
11	20	1	75	296 / 0.015	10	Egg-shaped; protrusion > seed	
12	17	1	50	290 / 0.025	6	Egg-shaped colloids; no clear contact angle	
13	17	1	50	290 / 0.025	10	Egg-shaped colloids; no clear contact angle	
14	19	1	25	295 / 0.026	6	No dumbbells; spherical	
15	19	1	25	295 / 0.026	10	No dumbbells; spherical	

*¹ All particles have a cross-link density of 3% (both core and chlorinated shell). Dumbbell syntheses were carried out with [SDS] = 7× the critical micelle concentration (CMC) and a swelling solution consisting of 3% DVB. *² Entries 10–15 were carried out with a different batch of seeds with a diameter of 256 nm instead of 280 nm particles used in the rest of the chapter.

References

- [1] D. J. Kraft, W. S. Vlug, C. M. van Kats, A. van Blaaderen, A. Imhof, W. K. Kegel, Self-assembly of colloids with liquid protrusions. *J. Am. Chem. Soc.* **2009**, *131*, 1182–1186.
- [2] D. J. Kraft, J. Groenewold, W. K. Kegel, Colloidal molecules with well-controlled bond angles. *Soft Matter* **2009**, *5*, 3823–3826.
- [3] D. J. Kraft, J. Hilhorst, M. A. P. Heinen, M. J. Hoogenraad, B. Luigjes, W. K. Kegel, Patchy polymer colloids with tunable anisotropy dimensions. *J. Phys. Chem. B* **2011**, *115*, 7175–7181.
- [4] B. Peng, H. R. Vutukuri, A. van Blaaderen, A. Imhof, Synthesis of fluorescent monodisperse non-spherical dumbbell-like model colloids. *J. Mater. Chem.* **2012**, *22*, 21893–21900.
- [5] B. G. P. van Ravensteijn, M. Kamp, A. van Blaaderen, W. K. Kegel, General route toward chemically anisotropic colloids. *Chem. Mater.* **2013**, *25*, 4348–4353.
- [6] C. Tang, C. Zhang, J. Liu, X. Qu, J. Li, Z. Yang, Large scale synthesis of Janus submicrometer sized colloids by seeded emulsion polymerization. *Macromolecules* **2010**, *43*, 5114–5120.
- [7] J.-G. Park, J. D. Forster, E. R. Dufresne, Synthesis of colloidal particles with the symmetry of water molecules. *Langmuir* **2009**, *25*, 8903–8906.
- [8] J.-W. Kim, R. J. Larson, D. A. Weitz, Uniform nonspherical colloidal particles with tunable shapes. *Adv. Mater.* **2007**, *19*, 2005–2009.
- [9] J.-W. Kim, J. L. Ryan, D. A. Weitz, Synthesis of nonspherical colloidal particles with anisotropic properties. *J. Am. Chem. Soc.* **2006**, *128*, 14374–14377.
- [10] E. B. Mock, C. F. Zukoski, Emulsion polymerization routes to chemically anisotropic particles. *Langmuir* **2010**, *26*, 13747–13750.
- [11] M. Yang, G. Wang, H. Ma, An efficient approach for production of polystyrene/poly(4-vinylpyridine) particles with various morphologies based on dynamic control. *Chem. Commun.* **2011**, *47*, 911–913.
- [12] J.-G. Park, J. D. Forster, E. R. J. Dufresne, High-yield synthesis of monodisperse dumbbell-shaped polymer nanoparticles. *J. Am. Chem. Soc.* **2010**, *132*, 5960–5961.
- [13] W. K. Kegel, D. Breed, M. Elsesser, D. J. Pine, Formation of anisotropic polymer colloids by disparate relaxation times. *Langmuir* **2006**, *22*, 7135–7136.
- [14] H. R. Sheu, M. S. El-Aasser, J. W. J. Vanderhoff, Phase separation in polystyrene latex interpenetrating polymer networks. *Polym. Sci., Part A: Polym. Chem.* **1990**, *28*, 629–651.
- [15] H. R. Sheu, M. S. El-Aasser, J. W. J. Vanderhoff, Uniform nonspherical latex particles as model interpenetrating polymer networks. *Polym. Sci., Part A: Polym. Chem.* **1990**, *28*, 653–667.

-
- [16] P. J. Flory, Thermodynamics of high polymer solutions. *J. Chem. Phys.* **1942**, *10*, 51–61.
- [17] M. L. Huggins, Some properties of solutions of long-chain compounds. *J. Phys. Chem.* **1942**, *46*, 151–158.
- [18] P. J. Flory, J. Rehner, Statistical mechanics of cross-linked polymer networks II. Swelling. *J. Chem. Phys.* **1943**, *11*, 521–526.
- [19] M. Morton, S. Kaizerman, M.W. Altier, Swelling of latex particles. *J. Colloid Sci.* **1954**, *9*, 300–312.
- [20] E. B. Mock, H. De Bruyn, B. S. Hawkett, R. G. Gilbert, C. F. Zukoski, Synthesis of anisotropic nanoparticles by seeded emulsion polymerization. *Langmuir* **2006**, *22*, 4037–4043.
- [21] T. Young, An essay on the cohesion of fluids. *Phil. Trans. R. Soc. Lond.* **1805**, *95*, 65–87.
- [22] S. C. Glotzer, M. J. Solomon, Anisotropy of building blocks and their assembly into complex structures. *Nat. Mater.* **2007**, *6*, 557–562.
- [23] A. B. Pawar, I. Kretzschmar, Fabrication, assembly, and application of patchy particles. *Macromol. Rapid Commun.* **2010**, *31*, 150–168.
- [24] G. Avvisati, T. Vissers, M. Dijkstra, Self-assembly of patchy colloidal dumbbells. *J. Chem. Phys.* **2015**, *142*, 084905.
- [25] J. C. Thomas, The determination of log normal particle size distributions by dynamic light scattering. *J. Colloid Interface Sci.* **1987**, *117*, 187–192.
- [26] J. R. Ebdon, T. N. Huckerby, T. C. Hunter, Free-radical aqueous slurry polymerizations of acrylonitrile: 2. End-groups and other minor structures in polyacrylonitriles initiated by potassium persulfate/sodium bisulfite. *Polymer* **1994**, *35*, 4659–4664.
- [27] G. Socrates, In *Infrared and Raman Characteristic Groups Frequencies*, 3rd ed.; John Wiley & Sons Ltd: Chichester, England, 2001.
- [28] E. A. Niewenhuis, A. Vrij, Light scattering of PMMA latex particles in benzene: Structural effects. *J. Colloid Interface Sci.* **1979**, *72*, 321–341.
- [29] W. McPhee, K. C. Tam, R. Pelton, Poly(*N*-isopropylacrylamide) latices prepared with sodium dodecyl sulfate. *J. Colloid Interface Sci.* **1993**, *156*, 24–30.

Part 2

**Colloidal Surface Modifications using
Atom Transfer Radical Polymerization**

4

Atom Transfer Radical Polymerization (ATRP) on Colloidal Particles

Abstract

In this chapter we elaborate on Atom Transfer Radical Polymerization (ATRP). This type of controlled radical polymerization offers ample opportunities for tuning macromolecular architectures and allows for the preparation of a wide variety of functional polymers. Exploiting ATRP to graft polymers to solid surfaces (Surface-Initiated ATRP; SI-ATRP), for example a colloidal particle, opens the way for the synthesis of colloidal brush particles in which the physical properties and chemical functionalities are tunable to a large extent.

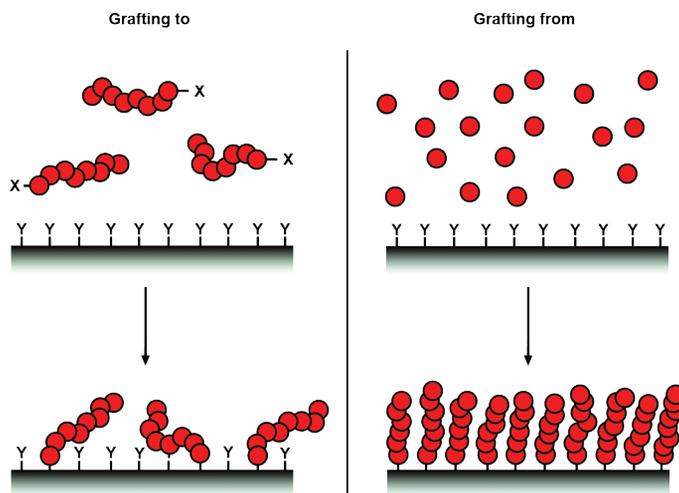
Here, the theoretical aspects and synthetic possibilities of (SI-) ATRP are presented. These features are illustrated by a variety of experiments in which colloidal particles were grafted with a variety of (block-co)polymers. To broaden the scope of these grafted polymers, post-polymerization functionalization reactions were carried out with model compounds. The results provide a starting point for the development of colloidal systems with tailored properties, for example described in Chapters 5–7 of this thesis.

4.1. Introduction

4.1.1. Surface immobilization of polymers. The properties of colloidal surfaces and hence the physical behavior of colloidal particles can be extensively tuned by the attachment of polymers. A classic example is steric stabilization of colloidal particles by polymers linked to the particle surface. More sophisticated examples include the introduction of stimuli responsive inter-particle interactions, controllable adhesion of proteins or other target molecules, and the fabrication of hybrid materials with superior properties.^{2,3}

Polymers can be attached to the surface by covalent and non-covalent interactions, such as Van der Waals forces, hydrogen bonding and electrostatics. The covalent linking of polymers has the obvious advantage that the functionalization reactions are permanent and no desorption of the polymers will occur. There are two basic strategies for the covalent attachment of polymers, namely the ‘grafting to’ and the ‘grafting from’ approach (Scheme 4.1).¹

Scheme 4.1. Schematic representation of surface modification with polymers using a) the ‘grafting to’ and b) the ‘grafting from’ approach. *X* represents the functional groups on the polymers which can be coupled to the surface tether points denoted with *Y* using the ‘grafting to’ approach.



The ‘grafting to’ approach has the advantage that it is an easy procedure. Pre-existing, end-functionalized polymers are attached by simple coupling reactions which directly leads to a functionalized surface. The disadvantage of this approach is that the grafting density, defined as the number of attached polymer chains per surface area, is usually rather low. The chance that a single end-group in a polymer will find the

surface and undergoes successful binding is small.¹ On top of that, if several polymers are attached, they will distribute over the surface and then block other tethering sites.

In contrast, the ‘grafting from’ approach leads to much higher grafting densities or in other words, the formation of dense polymer brushes. This strategy relies on growing polymers from a grafting point located at the surface. Polymers are slowly built up during this process, ensuring that the whole brush increases gradually in thickness. To obtain the highest degree of control over the brush formation, the ‘grafting from’ approach is usually combined with a controlled or living polymerization.⁴ These include anionic,^{5,6} cationic,^{5,7} ring opening,^{8,9} and radical based polymerization techniques.^{10,11} The last category of polymerizations includes Nitroxide Mediated Polymerizations (NMP),¹² Reversible Addition-Fragmentation chain-Transfer polymerization (RAFT),^{13,14} and Atom Transfer Radical Polymerization (ATRP).^{15,16} These techniques are generally preferred over the ionic polymerizations due to their high tolerance towards functional monomers and impurities.

In Chapter 5–7 we will use ATRP as the grafting method of choice to synthesize colloidal systems whose physical properties are dictated by the type of polymers that are attached to the particles. Since the chemical mechanism and principles behind this polymerization technique are rather unknown in the field of physical and colloid chemistry, we want to provide a theoretical framework which supports the upcoming ATRP experiments. Therefore, this chapter contains the following aspects: we will start by treating the fundamental aspects of controlled radical polymerizations on the molecular scale and compare it to conventional free radical polymerizations. With this background, the mechanistic details of ATRP are discussed and a concise review is given to show what is achievable using this type of radical polymerization. Special attention is given to colloidal systems which exploit the use of ATRP. This theoretical part is largely based on four review papers written by Matyjaszewski et al.^{17–20}

Finally, the (molecular) theoretical claims are translated to colloidal systems by using polystyrene particles as colloidal initiators. These particles are grafted with different types of (block-co)polymers. Model reactions for subsequent functionalization of the grafted hairs are discussed to give an idea about the possibilities when combining ATRP with colloidal systems.

4.1.2. Conventional free radical polymerization versus controlled radical polymerization. Free radical polymerization (FRP) is one of the mostly used techniques for preparing polymers.^{18,22,23} Especially on an industrial scale FRP proved its significance, since approximately 50% of all produced polymers are synthesized via this technique.¹⁸ FRP reactions are typically initiated by peroxides, diazo compounds or redox systems which slowly produce radicals when the system is heated or exposed to high energy radiation. The generated radicals are the active centers in these polymerizations and undergo propagation reactions with the monomer to

form the corresponding polymer. A wide variety of polymers including polystyrene, polyvinylchloride, polyethylene, polyacrylates, polyvinyl alcohol and fluorinated polymers can be prepared.¹⁸ These examples underline the robustness of FRP towards functional moieties present in the polymerizable monomers. Due to the high reactivity of the propagating centers, FRP reactions are not very sensitive towards impurities contributing greatly to the ease of operation. Besides polymerization in bulk monomer or solvent, FRP can be conducted in dispersed media to yield polymer products in the form of particles.²³

These attractive aspects of FRP are accompanied by two fundamental drawbacks, which limit control over the formed polymer in terms of molecular structure and molecular weight distribution. The first disadvantage originates from the high reactivity of the propagating radicals. Radicals are prone to termination reactions, which occur either via coupling of two growing chains or via disproportionation.^{22,23} Termination reactions are very fast and essentially diffusion controlled (reaction constant $k_t > 10^8 \text{ M}^{-1} \cdot \text{s}^{-1}$). The unavoidable consequence of this fast termination is the limited life-time of growing polymers and the fact that most polymer chains in a FRP are present as dead chains. In a typical FRP reaction, the life-time does not exceed a couple of seconds.^{18,23} Synthetic manipulations, end-functionalization or the polymerization of a second monomer to synthesize a block-copolymer are therefore impossible.

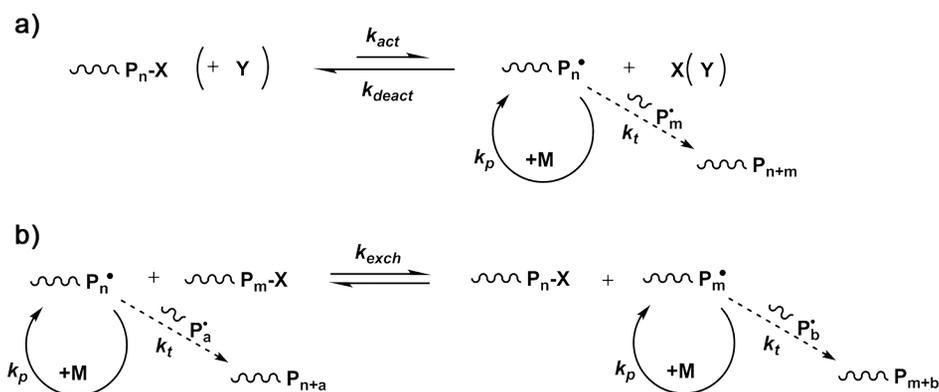
The second drawback is caused by the slow radical production (rate constant $k_d \approx 10^{-5} \text{ s}^{-1}$).^{22,23} In a FRP, polymer chains are continuously formed. The ill-defined initiation period, i.e. the time frame in which new chains are formed, limits control over the polydispersity (PDI) of the formed product. The molecular weight distribution broadens even further due to chain transfer reactions, in which radicals are shuffled between active propagating chain ends and other components in the system, such as solvent, monomer and formed polymer. In a FRP these transfers are irreversible and cause polymer branching or the initiation of new chains and hence the observed broadening of the PDI.^{22,23}

Consequently, free radical polymerizations are not the technique of choice if polymers with well-defined chemical structure or low polydispersity are required. In order to gain more control over the formed polymer architecture, a polymerization should be performed in the absence of irreversible chain transfer and termination reactions. Furthermore, initiation reactions should be (extremely) fast to ensure that all chains form at the same time, leading to a narrow molecular weight distribution. Polymerization techniques that meet these criteria are so-called living polymerizations. Examples are anionic, cationic, coordination and ring-opening polymerizations. These polymerizations will not be treated in this chapter. Detailed reviews can be found in references 24–28. Living polymerization techniques provide tremendous control over the polymerization. Theoretically, termination reactions are absent, hence the term

living polymerization, allowing for chain extension and chain-end functionalization reactions. The drawback of the living polymerizations lies in the very limited tolerance towards monomers with functional groups and impurities in the reaction mixture.

To overcome this limited scope of monomers and the stringent reaction conditions required for the classical living polymerizations, radical based analogues were developed.^{17–19,29–36} These so-called controlled radical polymerization combine the high level of control from living polymerizations with the robustness of conventional radical polymerizations. However, the combination of fast initiation and absence of termination/irreversible chain transfer reactions is contradictory for radical based systems as discussed before. To circumvent this, controlled radical polymerizations make use of a rapid dynamic equilibrium between a minute amount of propagating radicals and a large amount of dormant species. Radicals are reversibly trapped in a deactivation/activation process or they can be involved in a reversible transfer degenerate exchange process. Both processes are schematically depicted in Scheme 4.2.¹⁸

Scheme 4.2. Schematic representation of the two classes of controlled radical polymerizations. a) Represents polymerizations in which the required dynamic equilibrium between active (P_n^\bullet) and dormant species (P_n-X) is established to gain control over the polymerization by reversibly trapping active species in a deactivation/activation process. b) Represents polymerizations which make use of a 'reversible transfer' degenerate exchange process to establish a dynamic equilibrium.



Nitroxide Mediated Polymerization (NMP),^{30,31} Cobalt Mediated Radical Polymerization (CMRP),³⁵ and ATRP^{17,19} follow Scheme 4.2a. The situation shown in Scheme 4.2b is representative for Reversible Addition Fragmentation chain-Transfer Polymerization (RAFT)^{32–34} and degenerative polymerization (DT).³⁶

For the remaining discussion we will focus on establishing equilibrium through a deactivation/activation process (Scheme 4.2a). In this situation the established equilibrium is shifted far to the ‘dormant side’, implying that propagating radicals (P_n^\bullet) are rapidly trapped by a deactivation mechanism (rate constant = k_{deact}). In turn, the dormant species (P_n-X) can be activated again to regain the active centers. The active centers undergo propagation (rate constant = k_p) and termination (rate constant = k_t) reactions, analogous to those observed for a conventional free radical polymerization.^{17–21} The life-time of a chain in the active state in a controlled radical process is in fact comparable to that of a propagating chain in conventional FRP, but this life-time is now divided in short active periods separated by long dormant periods. Since chain propagation occurs via the same reactions as in conventional FRP, the same degrees of stereoselectivity (preference for the formation of a specific stereoisomer), regioselectivity (preference of one direction of chemical bond making or breaking over all other possible directions) and chemoselectivity (selective reactivity of one functional group in the presence of others) are obtained for the controlled radical polymerization procedures.¹⁸ In practice, ATRP has poor stereoselectivity, but rather good regio- and chemoselectivity. This behavior originates from minimization of the steric repulsion between adjacent monomers in a polymer backbone, which is realized by a strong preference for head-to-tail monomer attachment.²²

The fundamental difference between truly living polymerization systems and the controlled radical polymerizations is that termination reactions are not completely absent.^{17–21} Termination by recombination of radicals cannot be prevented. This is in contrast to, for example, anionic polymerizations, where two growing chain-ends electrostatically repel each other.^{24,25} However, since the equilibria depicted in Scheme 4.2 are shifted far towards the dormant side, the steady state concentration of radicals, set by the dynamic equilibrium, is low. As a result, the contribution of termination reactions is negligible.

Based on the discussion above, we can define four features of a controlled radical polymerization, namely first-order kinetic behavior, a pre-determinable degree of polymerization, a designed (usually narrow) molecular weight distribution and the presence of long-lived polymer chains with preserved end-functionalities.^{18,19,37} These features are in principle valid for all the controlled polymerizations, regardless of which mechanism shown in Scheme 4.2 is applied. In the upcoming section these four hallmarks will be explained.

1) First order kinetics.

The rate of polymerization is in fact nothing more than the rate of monomer consumption ($-d[M]/dt$) and should be equal to^{19,22,23,37,38}

$$R_p = -\frac{d[M]}{dt} = k_p[M][P_n^\bullet] \quad (4.1)$$

where $[P_n^\bullet]$ is the concentration of propagating species and $[M]$ the monomer concentration. Eq. 4.1 can be integrated yielding the following result

$$\ln \frac{[M]_0}{[M]} = \ln \left(\frac{1}{1-p} \right) = k_p[P_n^\bullet]t \quad (4.2)$$

where p represents the monomer conversion. The integration is done under the assumption that $[P_n^\bullet]$ is constant over time, which is equivalent to the assumption that termination reactions are absent. As mentioned in the previous discussion, a system is regarded controlled if termination reactions are not occurring.

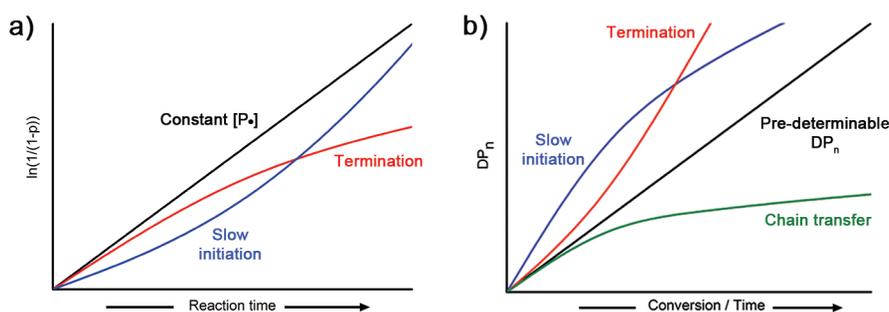


Figure 4.1. (a) Semi-logarithmic plot of $\ln(1/(1-p))$ (p = monomer conversion) versus the reaction time. For a controlled radical polymerization, this graph should yield a straight line (black curve) which implies a constant number of active species. If termination plays a role, a downwards bending curve is observed (red curve) as a result of a decreasing number of active centers. Slow initiation is characterized by an upwards bending curve (blue curve). This is caused by an increase in propagating radicals. (b) Plot of the average degree of polymerization (DP_n) versus conversion/reaction time. The black, straight line represents the pre-determinable degree of polymerization for a controlled radical polymerization. If termination by coupling occurs, a steeper increase in DP_n is observed (red curve). Slow initiation is characterized by a fast increase in molecular weight, but levels off after the initiation period is finished (blue curve). Chain transfer decreases the molecular weight, which is more pronounced at higher conversion (green curve).

Therefore, a straight line is expected when plotting $\ln(1/(1-p))$ against time for a controlled radical polymerization (Figure 4.1a, black line). Deviations from a straight line provide information about the reaction mechanisms causing decreased control

over the polymerization reaction. If termination reactions are involved, the graph will show a downwards curvature caused by the decrease in $[P_n^\bullet]$ (Figure 4.1a, red line). Reactions with slow initiation are characterized by an upwards curvature of this plot, since $[P_n^\bullet]$ increases during a prolonged period (Figure 4.1a, blue line).^{37,38}

Conversions are experimentally easy to measure. Extracting information about the degree of control via the shape of these curves is therefore a common strategy. However, one has to be careful to conclude if a system is controlled, based solely on these curves. The rearrangement of radicals caused by chain-transfer reactions is not visible in the semi-logarithmic plot, because these processes do not alter the free radical concentration $[P_n^\bullet]$. The effect of chain-transfer reactions is expressed in the second feature of controlled radical polymerizations, the pre-determinable degree of polymerization.^{37,38}

II) Pre-determinable degree of polymerization.

For a truly controlled/living polymerization, the average degree of polymerization (DP_n) is set by the ratio between monomer and initiator which are added at the start of the polymerization^{37,38}

$$DP_n = \frac{[M]_0}{[I]_0} \quad (4.3)$$

Obviously, this linear relation between the average molecular weight and the conversion is only valid if initiation is fast, ensuring that all chains start growing at the same moment (Figure 4.1b, black curve). Furthermore, chain transfer reactions that increase the number of propagating chains must be absent. Termination reactions are only reflected in the average degree of polymerization versus conversion plot if a significant portion of the chains terminate by recombination or coupling. The ideal behavior and the effect of slow initiation (blue curve), coupling (red curve) and transfer reactions (green curve) are schematically depicted in Figure 4.1b.^{37,38}

Experimentally, the average molecular weight can be measured as a function of reaction time. If the linear relation between the molecular weight and the conversion is found together with a linear semi-logarithmic plot, the system is truly controlled.

III) Narrow molecular weight distribution.

The existence of a narrow molecular weight distribution is actually not a prerequisite for a controlled reaction. Nevertheless, these narrow distributions are often aimed for, since they are only achievable with living or controlled polymerizations. Low dispersities are obtained if the rate of initiation is fast compared to propagation, the exchange between active and dormant species is faster than propagation, and the

polymerization is an irreversible process. Fulfilling these requirements results in a Poisson distribution for the polydispersity³⁷⁻⁴⁰

$$PDI = \frac{[M]_w}{[M]_n} \cong 1 + \frac{1}{DP_n} \quad (4.4)$$

The polydispersity goes down with increasing degree of polymerization. Typically values below 1.5 are reachable. This is in sharp contrast with FRP where the PDI is generally above 3 and increases significantly with increasing monomer conversions.^{22,23}

IV) Long-lived polymer chains with preserved end-functionality.

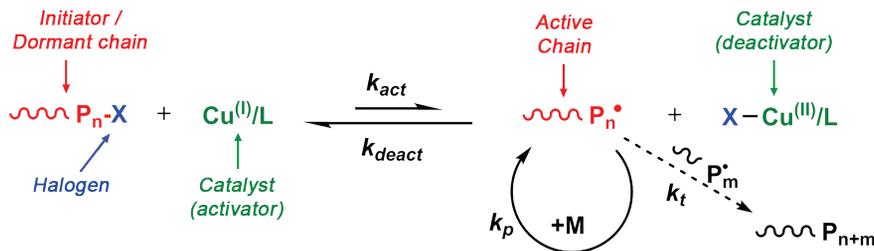
Since the contributions of irreversible termination and chain-transfer reactions are negligible, the chains remain end-capped by the reversibly cleavable group (X in Scheme 4.2) after consumption of the monomer.^{37,41} This allows for synthetic manipulations, including chain-end functionalization or chain extension to form block-copolymers.

In summary, a controlled radical polymerization relies on a rapid dynamic equilibrium between propagating and dormant species. This equilibrium is shifted towards the dormant side ensuring low radical concentrations to prevent irreversible termination. If this feature is combined with fast initiation and prevention of chain transfer reactions, a truly controlled system is obtained and the preparation of low dispersity polymers with tunable architecture is possible.

4.1.3. Mechanism of Atom Transfer Radical Polymerization (ATRP). In the previous section, the general principles of a controlled radical polymerization were discussed. We will now use these general arguments to explain the ATRP reaction in more detail.

A typical mechanism for the ATRP reaction is shown in Scheme 4.3.¹⁷⁻²¹ Compared to Scheme 4.2a, a transition metal complex (activator, $Cu(I)/L$) appears in the reaction scheme, which catalyzes the periodic formation of active radical species through a reversible redox reaction. This complex undergoes a one-electron oxidation which is accompanied by the abstraction of a (pseudo)halogen (X) from the dormant species (P_n-X). Pseudo-halogens are polyatomic analogues of a halogen and include SCN , N_3 and CN . The rate of halogen abstraction reaction is characterized by the rate constant for activation, k_{act} . This reaction results in the formation of a deactivator ($X-Cu(I)/L$), which is basically the (pseudo)halogenated version of the transition metal complex, and an active radical species ($P_n\bullet$). These radical species undergo propagation reactions and termination reactions, although the contribution of termination

Scheme 4.3. Schematic representation of an Atom Transfer Radical Polymerization (ATRP). A rapid dynamic equilibrium between dormant species (P_n-X) and active species (P_n^\bullet) is established by the presence of a (copper based) catalytic complex ($Cu(I)/L$). This complex reversibly abstracts a halogen atom (X) from the dormant chain, forming its halogenated counterpart ($X-Cu(II)/L$). In the active state, the chain ends undergo radical mediated propagation reactions (reaction rate = k_p) and possibly termination reactions (reaction rate = k_t).



reactions is minimized due to the low concentration of propagating radicals (Section 4.1.2). The deactivator reacts with the propagating radical in a reverse reaction (k_{deact}) to form the dormant species and the activator again.

The rate of polymerization for an ATRP reaction can be expressed in terms of the concentrations of the reactants as depicted in Scheme 4.3. This leads to the following equation¹⁷⁻²¹

$$R_p = -\frac{d[M]}{dt} = k_p[M][P_n^\bullet] = k_p K_{ATRP} \left(\frac{[P_n X][Cu^I/L]}{[X - Cu^{II}/L]} \right) \quad (4.5)$$

Here, K_{ATRP} is equal to the ratio of the rate of activation (k_{act}) and deactivation (k_{deact}). Typically, this equilibrium constant is directly proportional to the reaction rate: a larger value of K_{ATRP} translates to a higher rate of polymerization and vice versa. Higher monomer or initiator concentration increase the rate of polymerization. An important feature of specifically ATRP is that the rate of polymerization depends on the ratio of activator and deactivator. This allows for conducting polymerizations at very low catalyst loadings without affecting the molecular weight of the formed polymer.

The minimal amount of catalyst that is used mainly depends on the desired PDI. Litvinenko et al. derived an expression for the PDI in an ATRP reaction⁴⁰

$$PDI = \frac{M_w}{M_n} = 1 + \frac{1}{DP_n} + \left(\frac{k_p[P_n X]}{k_{deact}[X - Cu^{II}/L]} \right) \left(\frac{2}{p} - 1 \right) \quad (4.6)$$

From this expression it becomes immediately clear that if the deactivation rate of the catalytic species is high, polymers with a lower dispersity will be obtained. This underlines the necessity of an equilibrium that lies far to the dormant side in order to prepare monodisperse polymers. Shifting this equilibrium to the dormant side can be achieved by increasing the concentration of deactivator for example by the addition of Cu(II)-halide salts. However, addition of Cu(II)-halide salts is unavoidably accompanied with a decrease in polymerization rate. Other means to decrease the PDI is by aiming for low molecular weight polymers or going to high conversions, since k_p is monomer-dependent and hardly tunable by experimental parameters.

For certain applications, such as tuning the micro-phase separation of block-copolymers, a broader PDI is desired.⁴² Eq. 4.6 can then be used to choose the reaction conditions such that the PDI meets the requirements.

Finally, Zhong et al.⁴¹ derived an expression for the dead chain fraction (*DCF*) based on the reaction mechanism depicted in Scheme 4.3. A dead chain in this context is defined as a polymer which is no longer end-capped with a (pseudo)halogen. The fraction of dead chains is easily derived assuming a constant radical concentration during the reaction. This assumption is valid for a controlled radical polymerization, since termination is prevented to a large extent and first-order kinetics are typically observed.

$$DCF = \frac{[T]}{[R-X]_0} = \frac{2(DP_n)k_t[\ln(1-p)]^2}{[M]_0k_p^2t} \quad (4.7)$$

In this equation, $[T]$ represents the concentration of terminated chains and $[R-X]_0$ the concentration of added initiator. To minimize the *DCF*, one can either prolong the reaction time (t) by: decreasing the rate of polymerization, playing with the reaction temperature or pressure, preventing the polymerization from reaching high monomer conversions, aiming for lower average degrees of polymerization (DP_n), increasing the initial monomer concentration or use monomers with lower ratios of $k_t/(k_p)^2$.

Knowledge of the *DCF* is of importance if one aims for the synthesis of end-functionalized polymers or the formation of multi-block-copolymers by subsequential introduction of monomers. Chemical end-group modifications or chain extension reactions are only possible on chains that are still ‘alive’, i.e. when they are end-capped with an (pseudo)halogen. The possibilities of chemical end-group modifications are discussed in the Section 4.1.5.

4.1.4. Structure-reactivity correlations in ATRP reactions. As discussed in the previous section, the rate of polymerization depends on the value of K_{ATRP} , which is equal to the quotient of the rate constant for activation and the rate constant

bonds of the adjacent methyl groups with the singly occupied p -orbital of the carbon bearing the radical.⁴³

A second factor that determines the bond energy is the polarizability of the halogen atom involved. The reactivity order that is observed follows the leaving group capability of the halogen, $I > Br > Cl$. This is partially the result of the increase in size going down in the periodic table, which causes the contribution of an extra electron to be distributed over a larger volume.

Additionally, the stability of the formed radical can be further enhanced by using a carbon center that is substituted with activating groups, such as an α -cyano or ester moieties. Activation occurs either by stabilization using lone pair orbitals for electron-donating groups or via the π -electron system from electron-withdrawing substituents.

Lastly, resonance structures can also stabilize the formed radicals. The stabilizing group order with respect to initiating activity is roughly $CN > C(O)R > C(O)OR > Ph > Cl > Me$.¹⁷⁻¹⁹

All these observations are summarized in Figure 4.2, which ranks a wide variety of initiators on their k_{act} while arranging them based on their chemical structure as well.¹⁷

II) Catalytic complex.

Most of the catalytic complexes used for ATRP reactions are based on copper, although also other transition metals like Ru, Fe, Mo and Os can be used as well.¹⁹ The complexes are formed by addition of ligands to the system. These ligands are nitrogen based as depicted in Figure 4.3. The use of phosphorus based ligands is also reported, but not in combination with copper.¹⁹ Ligands must be chosen such that stable complexes are formed. If the ligands are strongly bound to the copper center ligand substitution with other components (solvent, monomer, and polymer) which are present in the system is prevented. Furthermore, robust complexes allow for the use low catalyst concentrations without disintegrating into loose metal ions and dissolved ligands.

Unsurprisingly, it has been shown that the activity of a catalytic system depends on the redox potential, which is a measure for the tendency to acquire electrons.^{18,19} The rate constants in ATRP depend heavily on the structure of the ligands that are used. The overall activity of a catalyst is determined by factors like the number of carbons bridging the nitrogen atoms ($C2 > C3 > C4$), the topology of the ligand (branched $>$ cyclic/linear), the chemical nature/binding mode, and steric bulk of the ligand.¹⁷⁻¹⁹

It must be noted that an effective catalyst is not only characterized by a large value of k_{act} . The deactivation rate is equally important, because a fast deactivation is required for a controlled polymerization. A fast rearrangement from $L/Cu(II)-X$ to $L/Cu(I)$ is therefore necessary and can be obtained by using bulky, highly coordinating ligands such as Me_6TREN or cyclam-B.

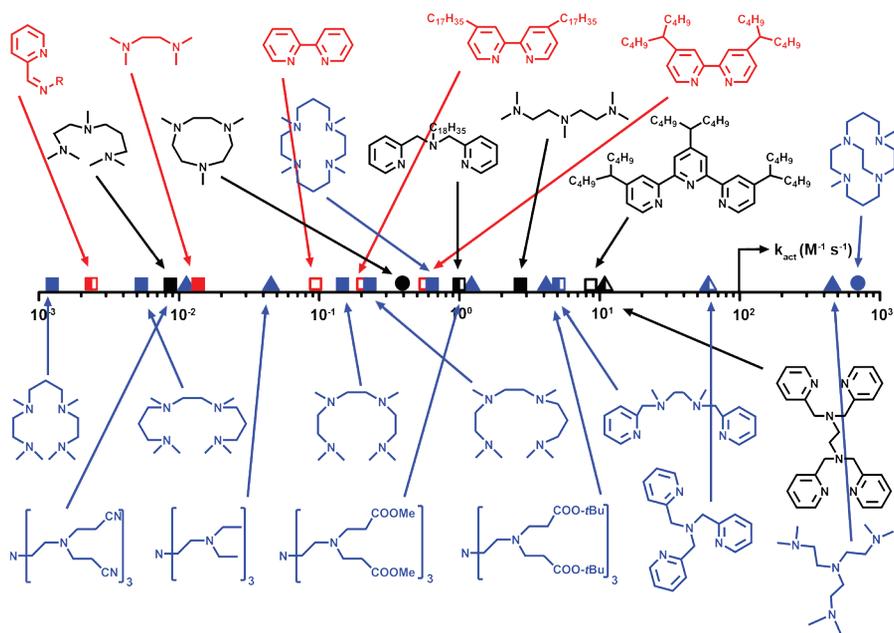


Figure 4.3. ATRP activation constants for a variety of ligands using ethyl 2-bromo-2-methylpropanoate as initiator in the presence of Cu(I)Br in MeCN at 35 °C as model system. The ligands are color-coded based on the number of nitrogen atoms in the following way: N2 = red, N3 = black, N4 = blue. The filling of the symbols represent the overall chemical structure of the ligand: amine/imine = solid, pyridine = open, mixed structure = left-half filled. The shape of this symbol represents the topology of the ligand as follows: branched = \blacktriangle , linear = \square , cyclic = \circ . Figure adapted from ref. 17.

An overview of common ligands is shown in Figure 4.3.¹⁷ The ligands are arranged based on their value of k_{act} (at fixed reaction conditions; see caption) and divided according to their chemical structure, topology and coordination mode.¹⁷

III) Solvents.

Generally, propagation reactions in free radical polymerizations are not very sensitive towards the type of solvent. The active radicals are extremely reactive and capable of reacting with monomers regardless of the solvent around the active center. This is in contrast to, for example, ionic polymerizations in which the character of the reactive ionic chain-end is strongly influenced by the degree of solvation. Since the propagation reactions in ATRP are the same as in a conventional FRP, the choice of solvent will not play a major role here. However, the solvent has tremendous effect on the equilibrium depicted in Scheme 4.3.¹⁷ The main reason for the strong dependency of the solvent on the overall reaction rate is that the Cu(I) species are much less polar

than the cationic Cu(II) complexes.^{17,18} Therefore, a more polar solvent will result in a higher value of K_{ATRP} , since the equilibrium is shifted towards the active side. Water, being one of the most polar solvents, can be used as reaction medium. However, in these polar protic media, hydrolysis of the $Cu(II)-X$ complexes by solvation of the individual ions occurs at significant rates. This will lead to a decrease of deactivator concentration and hence a faster reaction and less controlled polymerization. To suppress this deactivator loss, halide salts should be added to the reaction.^{17,18}

Another drawback of water as solvent is the disproportionation reaction of two Cu(I) centers to a Cu(II) and a Cu(0) species, leading to the loss of active catalyst. To counteract this effect, appropriate ligands should be chosen in such a way that water-stable complexes are formed.¹⁷⁻¹⁹ Finally, polar solvents are known to assist the elimination of HX from radical species. This elimination results in the formation of unsaturated chain ends and the loss of chain-end functionality, preventing further monomer additions and hence limiting the reachable molecular weight.¹⁷⁻¹⁹

Lastly, a solvent should be selected that is not an active chain transfer agent or does not interfere with the catalytic systems, e.g. by replacing the ligands.

IV) Monomers.

A wide variety of monomers are polymerizable using ATRP. These include (functionalized) styrene derivatives, (meth)acrylates, (meth)acrylamides, dienes and acrylonitrile.^{17,19} The feature that all these monomers have in common is the presence of substituents that stabilize the active radical chain-end during propagation reactions. Since the chemical structure of the active chain-end is determined by the structure of the monomer, it is difficult to extract general trends on combinations between monomers and other components of the system. Optimization in terms of catalytic complex, reaction temperature and solvent for each monomer is therefore usually required.

Two types of monomer deserve a special note. Firstly, (meth)acrylamides can be polymerized using ATRP, however, the control over these reactions is rather poor. This is mainly due to catalyst inactivation by the forming polymer and displacement of the terminal halogen from the polymer by the amide group.¹⁹

Secondly, (meth)acrylic acids are notoriously difficult to polymerize using ATRP. The acid moieties in these monomers coordinate strongly to the transition metal, thereby destroying the catalyst. Additionally, if the pH drops due to the acidic groups, nitrogen-based ligands become protonated, leading to disintegration of the catalyst as well.¹⁹ To prevent these issues, the preferred route is to polymerize monomers which bear a protected carboxylic acid group, for example, in the form of an ester. After the ATRP reaction, the protecting group is cleaved off, yielding well-defined poly((meth)acrylic) polymers.^{19,44,45} This strategy will be illustrated experimentally in Section 4.3.6.

4.1.5. Synthetic scope of ATRP: Polymer topology and functionality.

Since ATRP allows for control over the molecular weight and the livingness of the reaction, the way is open to prepare polymers with controlled architectures. This control is expressed in three basic ways, namely topology, composition and polymer functionality.^{17–19}

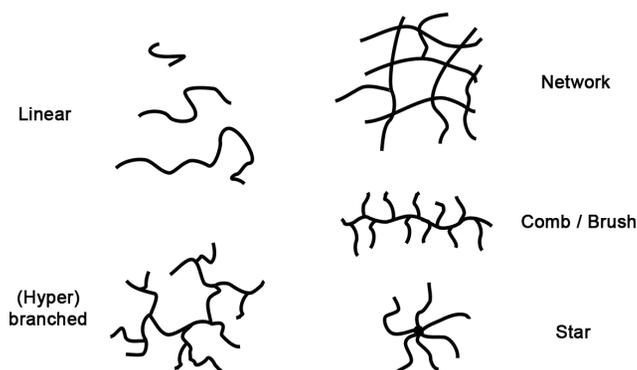


Figure 4.4. Examples of accessible polymer topologies via ATRP.

Topology of the synthesized polymers refers to their shape. Several examples are shown in Figure 4.4.¹⁷ The most straightforward topological change is the length of linear polymers. This is easily achieved by tuning the ratio between monomer and initiator or the allowed monomer conversion (Eq. 4.3). More sophisticated polymer structures can be obtained by, for example, using multifunctional initiators or a combination of ATRP with grafting methods. Topologies obtained via these routes include star-shaped polymers, bottlebrushes and comb polymers (Figure 4.4).^{17,20}

These topologies are surely not limited to homopolymers. If chain-ends remain functional after polymerizing the first monomer, a second monomer can be added to perform a chain extension reaction. This sequential monomer addition can be repeated multiple times to form multi-block-copolymers.^{17,46} If well-defined blocks are desired, the reactivity order of monomers should be taken into account. For ATRP this sequence is acrylonitrile > methacrylates > styrene \approx acrylates > acrylamides \gg vinyl chloride > vinyl acetate.^{17–21} If this order is not followed, initiation might not occur simultaneously, leading to the formation of a second block with a larger polydispersity. If the order needs to be altered, one should make use of halogen exchange.^{18,46} Together with the second, more active monomer, CuCl is added to a brominated pre-formed polymer. The bromine will be substituted by the Cl, causing a decrease in propagation rate compared to the activation rate (K_{ATRP} of alkyl chlorides is much smaller than for the corresponding bromide). This deceleration of the reaction

results in better control and hence lower polydispersities of the second block.

Control over the composition is not limited to linear block-copolymers, but graft-copolymers, random/statistical, periodic and gradient copolymers are within reach (Figure 4.5).^{17,20} All these variations in polymer composition can be combined with the more elaborate topologies discussed before.

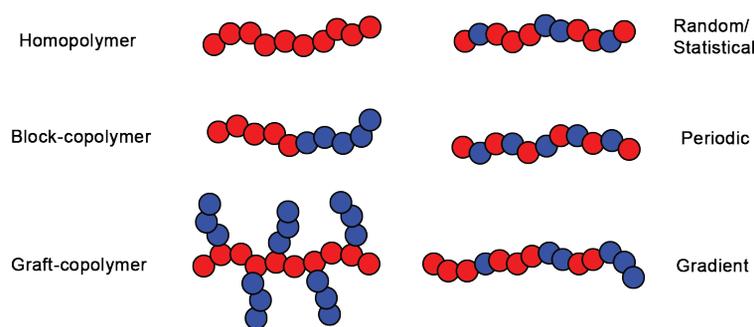


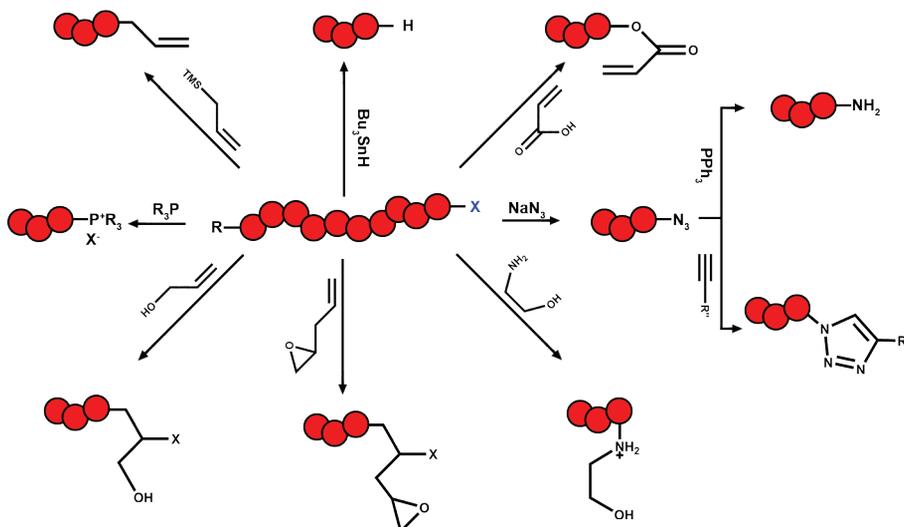
Figure 4.5. Examples of polymers with different controlled compositions accessible via ATRP. The blue and red spheres represent two different monomers.

The final form of a controlled polymer architecture is the incorporation of chemical functionality on demand. These functionalities can be located anywhere in the structure: polymers with one or two functional end-groups (telechelics) or polymers which contain functionalities along (a part) or their backbone.^{17,20} Functionalities can be introduced in several ways.

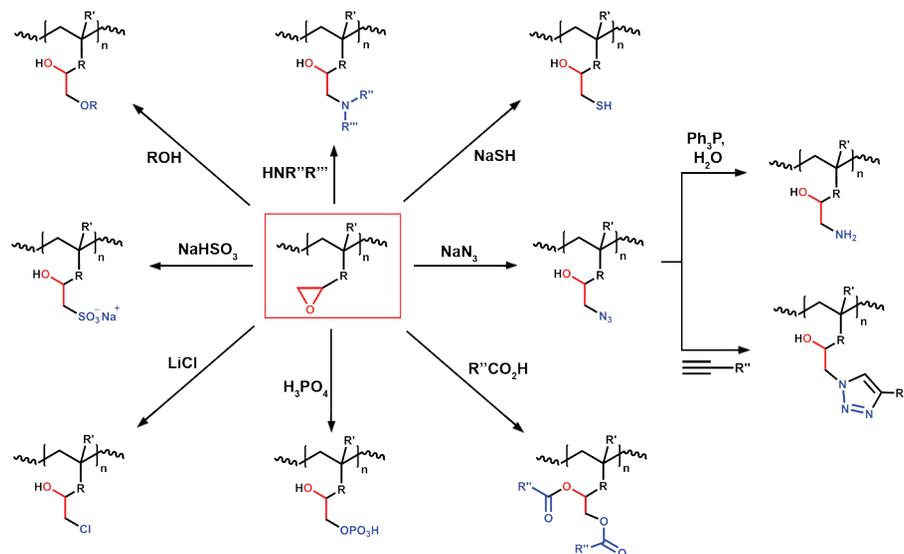
The use of a functional initiator, which directly leads to the formation of end-functionalized polymers (R in Scheme 4.4) is one option. Also the halogens present on the polymers after the ATRP reaction can be regarded as functional groups. These halogens can be further modified by nucleophilic substitution reactions or electrophilic addition reactions. The nucleophilic substitutions are especially useful for acrylates and styrene derivatives, however, less efficient for tertiary halogens in for example poly(methacrylates). A brief summary of reported halogen substitution reactions are depicted in Scheme 4.4, showing the wide variety of accessible chain-end functionalities.^{17,19,20}

The last straightforward strategy for creating functional polymers that will be treated is the use of functional monomers. ATRP is highly tolerant towards functional groups and monomers containing for example, amines, hydroxyls, sulfonates, cyano and epoxide moieties have been successfully polymerized.^{17–21} Special attention

Scheme 4.4. Schematic representation of end-group modifications accessible based on (pseudo)halogen (X) end-capped polymers prepared using ATRP. R represents the (functional) initiator fragment from which the polymer grows.



Scheme 4.5. Schematic representation of post-polymerization functionalization reactions based on the ring opening of pending epoxide moieties (in red) along the polymer backbone. The introduced functionalities are highlighted in blue.



goes to the use of epoxide functionalized monomers, such as glycidyl methacrylate (GMA). The epoxide ring is a versatile starting point for further functionalization by ring opening reactions as is shown in Scheme 4.5. We also exploit GMA as functional monomer in Sections 4.3.3 and 4.3.5.

4.1.6. Combining ATRP with colloids. In this last section of the theoretical background on ATRP, we show how ATRP can be combined with colloidal particles and what type of hybrid materials are within reach by using this combination. We will not focus on the preparation of particles using, for example, ATRP in dispersed systems,^{37,47–51} but rather on ATRP-based modifications of existing particles.

Combining ATRP, or any other polymerization technique, with (particles) surfaces is in principle easily realized by immobilization of the initiator species onto the corresponding surface.^{2–4,10} After immobilization, each initiator molecule will act as a grafting point. ATRP reactions to graft polymers from the surface are commonly referred to as Surface Initiated-ATRP (SI-ATRP) reactions. Immobilization procedures of the initiator species rely obviously on the type of surface that is chosen. A vast amount of literature reports the use of silica particles and the corresponding silane coupling chemistry to attach initiator fragments to the surface.^{15,16,52–55} Polymer particles can be decorated with ATRP initiators by employing inimers. These molecules are composed of an ATRP initiator fragment (ini) and a polymerizable double bond (mer), with which the inimer is directly attached to a polymer colloid in any particle forming free-radical polymerization procedure.^{15,56–60} Metallic (nano)particles are typically functionalized by the adsorption of ATRP initiator molecules which are equipped with moieties that have high affinity for the metal particle.^{60–64} An example is the use of initiators with sulfur containing groups that adsorb readily onto gold nanoparticles.

Non-functionalized surfaces can be activated using plasma or ozone treatments, which yield surface hydroxyl groups which are further functionalized towards the desired ATRP initiator.^{3,10} If functional groups are already present on the target surface, corresponding coupling procedures can be selected to introduce the initiators.^{3,10,17} Examples include the use of click chemistry for azide functionalized surfaces, ester formation for hydroxyl or activated carboxylic acid containing surfaces, and the use of maleimide chemistry for thiolated surfaces.³ For a complete overview of immobilization techniques we refer to ref. 10.

The mechanistic principles discussed in Sections 4.1.2–4.1.4 are still valid, since the polymerization mechanism is not changed upon initiator immobilization. However, in some cases extra precautions are necessary to retain control over the polymerization, especially if the surface density of initiating groups is low.^{3,15} In this case, also the concentration of deactivator will be low, resulting in a poorly controlled polymerization. To compensate for this drawback, sacrificial initiators or deactivators are usually added to increase the $[X-Cu(II)/L]$ concentration and consequently gain

more control over the ATRP reaction. Measures to prevent high radical concentrations might be even more important in SI-ATRP reactions compared to the molecular analogue. The reason for this is that the local surface concentration of radical species might be quite high, because all the initiator molecules are confined on the surface. Termination by recombination might therefore be a more important mechanism for termination compared to the molecular ATRP reactions. Furthermore, termination by recombination can also occur in an inter-particle fashion, leading to irreversible aggregation or even gelation of the system.^{3,15}

However, the previously mentioned problems are (easily) solvable and the hallmarks of ATRP (controllable molecular weight, tunable monomer composition and incorporation of functionality) can still be exploited. Consequently, well-defined (hybrid) particle systems are formed in which interactions between particles and their surroundings are highly tunable.^{2-4,10,15}

Besides the degrees of freedom discussed for homogenous ATRP, the experimental parameter space in SI-ATRP is even bigger. Grafting polymers from a colloidal particle leads to the formation of a polymer brush. The properties of these brushes are heavily dependent on the grafting density, but also on the height of the polymer brush compared to the curvature of the carrier colloid. We will not go into the physics of polymer brushes here, but the picture provided by a scaling model of Daoud and Cotton is worth mentioning.⁶⁵

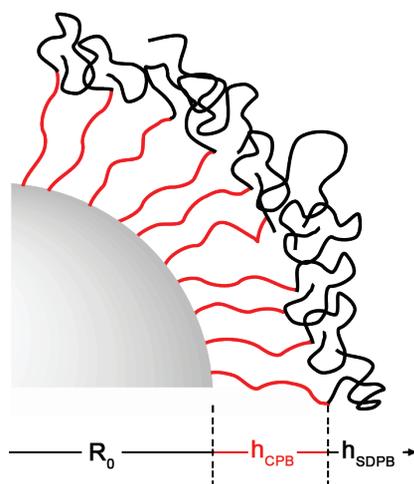


Figure 4.6. Schematic representation of the two polymer conformation regimes present in spherical brushes. The concentrated particle brush (CPB, red) is located inside the brush. Polymers are predominantly in an extended configuration due to dominating excluded volume interactions. On the outer rim, a semi-diluted brush (SDPB, black) is present. In this regime, the polymer conformations are more relaxed.

According to this model, a polymer brush consists of two parts: an inner concentrated particle brush (CPB) and a semi-dilute particle brush (SDPB) on the outside of the complete brush (Figure 4.6). In the CPB (red region in Figure 4.6), polymer chains possess stretched conformations due to dominating excluded volume interactions. In the SDPB, chain conformations are more relaxed (black region in Figure 4.6). The distinction between the two regions also appears in the effective particle interactions. Particles grafted with CPBs are characterized by a hard-core repulsion, while soft brush-overlap and chain entanglements take over in the outer corona of the brush in a SDPB.³

Other strategies to tune interactions between particles is the growth of polymer brushes consisting of polymers that are responsive to external triggers, such as temperature, pH or ionic strength. Combinations of these triggers are also possible, leading to double or even triple responsive systems.^{54,56,58,66,67}

The use of immobilized block-copolymers is also a promising strategy for self-assembly studies, since the organization of the colloidal particles is in principle guided by the micro-phase separation between the two polymers blocks present in the brush.⁶⁸

The attachment of polymers is of course not limited by the tethering of only one type of polymer. Multiple polymers could be grafted and their spatial arrangement over the particle surface can be altered, e.g. a Janus particle that consists of two different, well-separated polymer brushes on the same colloid. These Janus particles have shown to exhibit interesting self-assembly behavior.^{66,69}

Lastly, materials composed of particles equipped with a polymer brush show superior properties compared to materials prepared using the bare colloids. Examples are the formation of crack-free colloidal crystals with excellent mechanical strength due to inter-twining of the polymer brushes.⁷⁰ These types of particles can also be used for the preparation of hybrid materials if an inorganic cores are used. The polymeric shell enables high compatibility with a polymer matrix, so these particles act as excellent fillers to further boost the properties of coatings and plastics.^{71,72}

In summary, we conclude that the combination of ATRP and colloids is a powerful concept. ATRP is easily extendable to SI-ATRP by numerous immobilization procedures of initiators. By exploiting the features of ATRP on colloids, systems arise that show unmatched properties as a function of the chain characteristics, the architecture of the grafted polymers, and the morphology of the polymer brush. This field of research has shown potential in both fundamental sciences and practical applications. We contribute to this emerging field with the work presented in Chapters 5–7.

The remainder of this chapter contains experimental results to illustrate the theoretical background treated in the Introduction. Polystyrene particles were exploited

as colloidal initiators and grafted with different types of (block-co)polymers. Model reactions for subsequent functionalization of the grafted hairs are discussed to give an idea about the possibilities when combining ATRP with colloidal systems.

4.2. Experimental Section

4.2.1. Materials. Styrene (St, 99%), divinylbenzene (DVB, 55% mixture of isomers, tech. grade), vinylbenzyl chloride (VBC, $\geq 90\%$), 2-bromoisobutryl bromide (BiBb, 98%), 2-hydroxyethyl acrylate (HEA, 96%, contains 200–650 ppm monomethyl ether hydroquinone as inhibitor), *N*-hydroxyethyl acrylamide (HEAA, 97%), *t*-butyl acrylate (*t*-BuA, 98%), methyl methacrylate (MMA, $\geq 99\%$), sodium sulfate (Na_2SO_4 , ACS reagent, $\geq 99\%$, anhydrous), copper bromide (Cu(I)Br , 98%), 2,2'-bipyridyl (Bpy, Reagentplus, $\geq 99\%$), *N,N,N',N',N''*-pentamethyldiethylenetriamine (PMDTA, 99%), fluoresceinamine (mixtures of isomers, $\geq 75\%$), dimethylformamide (DMF, $\geq 99\%$), propargylamine (Prp-NH_2 , 98%), 2-(*N*-morpholino)ethanesulfonic acid (MES, $\geq 99\%$), sodium phosphate dibasic (Na_2HPO_4 , BioXtra, $\geq 99.0\%$), sodium phosphate monobasic dihydrate ($\text{NaH}_2\text{PO}_4 \cdot 2\text{H}_2\text{O}$, $> 99\%$) and trifluoroacetic acid (TFA, Reagentplus, 99%) were obtained from Sigma-Aldrich. Glycidyl methacrylate (GMA, $\geq 97.0\%$) and 1-ethyl-3-(3 dimethylaminopropyl) carbodiimide hydrochloride (EDC, $\geq 98.0\%$) from Fluka Analytical were used. Potassium persulfate (KPS, $> 99\%$ for analysis), sodium bisulfite (NaHSO_3 , ACS reagent), pyridine ($> 99\%$) and dimethyl sulfoxide (DMSO, 99.7%) were purchased from Acros Organics. Methanol (MeOH, exceeds ACS specifications) was obtained from J.T. Baker and dichloromethane (DCM, peptide synthesis) from Biosolve. Sodium azide (NaN_3 , 99%) and ammonium chloride (NH_4Cl , Suprapur) were obtained from VWR. All chemicals were used as received. The water used for all syntheses was purified using a Milli-Q water purification system.

4.2.2. Synthesis of 2-(2-bromoisobutyryloxy) ethyl acrylate (BIEA). The synthesis of BIEA was adapted from ref. 73. A solution of 2-hydroxyethyl acrylate (40 mL, 348 mmol) and pyridine (31 mL, 383 mmol) in DCM (250 mL) was stirred and cooled in an ice bath. Under nitrogen atmosphere, a solution of 2-bromoisobutryl bromide (36.45 mL, 348 mmol) in DCM (50 mL) was added drop wise over the course of 1 h. During the addition a white precipitate was formed (HBr-pyridine). After complete addition of the BiBb solution, the reaction mixture was stirred an additional 3 h at room temperature.

The precipitate was filtered off and DCM was evaporated under reduced pressure. A yellow oil and additional precipitate was formed. The additional precipitate was filtered off and washed with DCM. The DCM from washing and the yellow oil were combined and washed with water (3 times, 50 mL per washing step). The oil phase was dried over Na_2SO_4 and finally, the DCM was evaporated under reduced pressure. The resulting yellow oil was distilled to complete the purification procedure yielding a

colorless oil. $^1\text{H-NMR}$: 400 MHz (CDCl_3) δ : 6.43 (d, 1H); 6.14 (dd, 1H); 5.85 (d, 1H); 4.4 (s, 4H); 1.9 (s, 6H).

4.2.3. Synthesis of chlorinated colloidal initiators (CPs-Cl). The chlorinated colloids (CPs-Cl) were prepared using the same core-shell approach as described in Chapter 2.⁷⁴ This synthesis consisted of two steps, namely the synthesis of a cross-linked polystyrene core (CPs) followed by the introduction of a cross-linked chlorinated shell. The shell was grown by the addition of VBC and DVB. Surface benzyl chloride functionalities can act as ATRP initiators (Section 4.2.5). The synthetic procedure yielded particles with a radius of 155 nm and a polydispersity of 4.4% as determined using transmission electron microscopy (TEM). The presence of the chlorine groups was confirmed using Fourier transform infrared spectroscopy (FT-IR) (1266 cm^{-1}) and X-ray photoelectron spectroscopy (XPS) [200 and 270 eV (Cl)].

4.2.4. Synthesis of brominated colloidal initiators (CPs-Br). Analogous to the method described in Section 4.2.3 to prepare the chlorinated initiator colloids, a core-shell approach was chosen in which the CPs particles served as seed particles for brominated core-shell particles. The crude seed dispersion (25 mL) was introduced in a 100 mL round-bottom flask, together with water (25 mL). The dispersion was heated to 70 °C and purged with nitrogen for 30 min. After degassing, a mixture of styrene (1 mL) and DVB (20 μL) was added. The dispersion was stirred for 10 min after which BIEA (0.75 g) was injected. After 5 min of stirring, the polymerization was started by the addition of a degassed, aqueous KPS solution (32 mg in 5 mL water). The polymerization was allowed to run for 6 h after which the reaction was stopped by removing the flask from the oil bath. The particles were washed with water and ethanol three times. FT-IR (ATR) spectroscopy was used to confirm successful surface modification. Dynamic light scattering (DLS) showed a Z-average radius of 184 nm and a polydispersity index (PDI) of 0.028.

A similar method was also used to prepare larger BIEA-p(St) core-shell colloids, which could be visualized with (fluorescence) microscopy. In this case a larger cross-linked seed was used. They were prepared using the same method as described above, but by lowering the amount of SDS to 0.125 gram (see Chapter 2, Section 2.2.2). The resulting particles had a radius of 225 nm and a PDI of 0.031 as determined with DLS. The BIEA coated particles based on these seeds had a hydrodynamic radius of 255 nm and a PDI of 0.030.

4.2.5. Typical ATRP procedure using CPs-Cl as colloidal initiators. The experimental conditions were adapted from ref. 75. MMA (100 mg, 1 mmol), Cu(I)Br (13 mg, 0.09 mmol) and 2,2'-bipyridyl (28 mg, 0.18 mmol) were weighed into a small, oven-dried Schlenk flask. The CPs-Cl dispersion (1 mL, solid content = 1% in DMF or DMSO) was added. Upon mixing, the mixture became dark brown. The mixture was carefully degassed by evacuation and refilling with nitrogen. The reaction flask was

placed in a 90 °C oil bath for 24 h. After this period, the ATRP reaction was quenched by exposing the mixture to air. The resulting particles (CPs-MMA-Cl) were washed several times with MeOH, 50 mM NaHSO₃ solution (removal of copper complexes) and MilliQ water. Successful grafting was confirmed using IR spectroscopy (1732 cm⁻¹) and DLS measurements. Similar ATRP reactions were performed with different monomer concentrations to tune the brush thickness. The same reactions were also conducted with glycidyl methacrylate (GMA) as monomer to grow polymer brushes with pending epoxide groups along the polymer backbone (CPs-GMA-Cl).

The ATRP reactions were monitored in time by extracting samples from the reaction mixture by a syringe. The samples were directly quenched and washed before analysis with both IR spectroscopy (1732 cm⁻¹ and 907 cm⁻¹) and DLS.

An identical ATRP reaction of MMA was conducted in the presence of non-functionalized CPs colloids to confirm that the benzyl chloride moieties were indeed required to initiate the brush formation.

4.2.6. Typical ATRP procedure using CPs-Br as colloidal initiators. The brominated initiators were exploited for surface initiated ATRP reactions using two different monomers, namely hydroxyethyl acrylate (HEA) or *N*-hydroxyethyl acrylamide (HEAA). In a typical experiment, monomer (1 mmol) and Cu(I)Br (13 mg, 0.09 mmol) were weighed and transferred directly into an oven-dried Schlenk flask. A MeOH/H₂O mixture (7:3, v/v) (0.5 mL) was added and the solution was stirred for 5 min to dissolve Cu(I)Br. A light green solution was obtained. After complete dissolution, PMDETA (63 μL, 0.3 mmol) was injected, resulting in a blue/green mixture. The monomer/catalyst mixture was degassed by evacuation and refilling with nitrogen (three cycles).

In a separate Schlenk flask, the BIEA-colloids dispersed in the same MeOH/H₂O mixture (0.5 mL, 2 wt %) were degassed by evacuation and refilling with nitrogen (three cycles). After degassing, the mixture was injected into the monomer/catalyst mixture under inert atmosphere. The resulting reaction mixture was white/green. The ATRP reaction was allowed to run for 4 h at room temperature. The reaction was terminated by exposing the mixture to air which resulted in the formation of an intense blue color. The particles were washed several times with MeOH, 50 mM NaHSO₃ solution (removal of copper complexes) and MilliQ water. Successful grafting of the polymer was confirmed using IR spectroscopy: 1732 cm⁻¹ for p(HEA) and 3300 cm⁻¹ (N-H vibration), 1640 cm⁻¹ (amide I; carbonyl stretching) and 1536 cm⁻¹ (amide II N-H deformation) for p(HEAA).

If, however, a block-copolymer was desired, a monomer mixture dissolved in the MeOH/H₂O mixture (7:3, v/v) was degassed in a separate flask and injected in the reaction mixture 2 h after the start of the polymerization of the first monomer. End-blocks of glycidyl methacrylate (GMA) and *t*-butyl acrylate (*t*-BuA) were introduced.

After addition of the second monomer, the resulting mixture was allowed to react overnight under inert atmosphere. The obtained dispersions were washed in a similar fashion as described for the particles equipped with polymer brushes consisting of solely HEA or HEAA. The block-copolymer structure of the grafted polymers was confirmed after the attachment of probe molecules (Section 4.2.8–4.2.10). The ATRP reactions were monitored in time by extracting samples from the reaction mixture by a syringe. The samples were directly quenched and washed before analysis.

4.2.7. End-functionalization of particles equipped with p(MMA) brushes (CPs-MMA-Cl). NaN_3 (4.5 mg) was dissolved in DMF (0.5 mL). To this solution, a dispersion containing the CPs-MMA-Cl colloids was added (0.5 mL, solid content = 1% based on CPs). The complete mixture was allowed to stir for 24 h at 70 °C. After the reaction, the particles were washed with water to remove excess NaN_3 and analyzed using IR spectroscopy to confirm the presence of the azide signal (2096 cm^{-1}). This reaction was performed for particles in which the ATRP reaction (as described in Section 4.2.5) was run for 1.5 h and 23 h to probe the effect of decreasing chain-end functionality at elevated monomer conversions.

4.2.8. Ring opening of epoxides on particles equipped with p(GMA) brushes. CPs-Cl colloids that were grafted with GMA homopolymers (CPs-GMA-Cl) were functionalized by ring opening either with propargylamine or NaN_3 . In case of ring opening with propargylamine, a dispersion containing the CPs-GMA-Cl particles (0.5 mL, solid content = 1% based on CPs) was transferred to DMF by three centrifugation and redispersion cycles. After the last centrifugation step, the supernatant was replaced with a solution of propargylamine dissolved in DMF (2.5 mL, 1 M). The particles were redispersed and heated to 60 °C, while stirring.

The ring opening of CPs-GMA-Cl with NaN_3 was conducted by transferring a dispersion of CPs-GMA-Cl particles (0.25 mL, solid content = 1% based on CPs) to DMF (2.5 mL) by three centrifugation and redispersion cycles. The resulting DMF dispersion was added to a reaction tube which contained NaN_3 (48 mg, 0.75 mmol) and NH_4Cl (40 mg, 0.75 mmol). The resulting mixture was stirred and heated in an oil bath of 50 °C for 24 h.⁷⁶

Colloids equipped with a block-copolymer brush with a terminal epoxide block (CPs-HEA-*co*-GMA-Br and CPs-HEAA-*co*-GMA-Br) were reacted with fluoresceinamine or NaN_3 in analogous reactions as described for the CPs-GMA-Cl colloids. In both reactions, the amount of $\text{NaN}_3/\text{NH}_4\text{Cl}$ or fluoresceinamine was scaled to the maximum number of epoxide groups present in the reaction mixtures.

All particles were extensively washed with DMF and water after completion of the reaction. After the final centrifugation step, the particles were redispersed in water and analyzed using IR spectroscopy (2100 cm^{-1}) or fluorescence microscopy in the case of fluoresceinamine functionalized polymer brushes.

4.2.9. Functionalization of particles equipped with *t*-BuA end-block via amide formation. Functionalized amines were coupled to the poly(*t*-butyl acrylate) block of colloids equipped with polymers consisting of a poly(*N*-hydroxyethyl acrylamide) inner block and a terminal poly(*t*-butyl acrylate) block (p(HEAA-*co-t*-BuA)) via a synthesis inspired by Merchand-Brynaert et al.⁷⁷ In the first step, the esters in the *t*-BuA block were hydrolyzed by redispersing the colloids in a TFA:water mixture (9:1 v/v, 1 mL, solid content = 2%). The particles were allowed to react for 20 h at room temperature and were then centrifuged after addition of MeOH/H₂O (7:3, v/v, 4 mL). The particles were extensively washed with water. After the last washing step an aqueous dispersion with a solid content of 1 wt% was obtained.

In the second step, the obtained carboxylic acids were activated by coupling of 1-ethyl-3-(3-dimethylaminopropyl)carbodiimide (EDC). To conduct this activation, the dispersion (1 mL) was centrifuged and the sediment was redispersed in MES buffer (pH 3.5, 0.974 g MES in 50 mL water) and EDC (17.5 mg) was added. This dispersion was tumbled for 1 h at room temperature. Subsequently, the dispersion was washed with MES and water. After the last centrifugation step the particles were redispersed in phosphate buffer (1.5 mL, pH 8.2, 1.344 g Na₂HPO₄, 0.0819 g NaH₂PO₄·2H₂O in 50 mL).

In the last reaction step, the activated esters reacted with the primary amine of fluoresceinamine. The dispersion obtained from the second step was transferred to a vial containing excess fluoresceinamine and allowed to react for 20 h at room temperature. The mixture was then washed with phosphate buffer and water. The particles were characterized with IR spectroscopy and (fluorescence) microscopy.

4.2.10. Functionalization of particles equipped with *t*-BuA end-block via direct aminolysis. Colloids grafted with polymers consisting of a poly(*N*-hydroxyethyl acrylamide) inner block and a terminal poly(*t*-butyl acrylate) block (p(HEAA-*co-t*-BuA)) were functionalized via direct aminolysis of the poly(*t*-butyl acrylate) segment.⁷⁸ The colloids were transferred to DMSO (0.5 mL, resulting solid content = 0.5%) and introduced into a reaction flask containing fluoresceinamine (6.0 mg). The dispersion was flushed with nitrogen and then placed in a 120 °C oil bath. The mixture was allowed to react for 48 h. The resulting particles were washed with a mixture of DMSO/ethanol and water in which the particles were redispersed after the final washing step. The particles were characterized by IR spectroscopy and fluorescence microscopy.

4.2.11. Characterization. Dynamic light scattering (DLS) and ζ potential measurements were performed using a Malvern Zetasizer Nano using highly diluted aqueous dispersions (approximately 20 μ L of a 1 wt% dispersion in 2 mL water). DLS measurements were conducted using glass sample cells. The measurements were carried out in MilliQ water at 20 °C and consisted of 7 runs of 15 individual measurements in

backscatter mode (173°). An equilibration time of 5 min was applied to ensure that the dispersions were at the right temperature. The sizes of the colloids or aggregates are reported as a *Z*-average diameter and the corresponding polydispersity index (PDI).

For the ζ potential measurements, 7 runs of at least 50 individual measurements were used to obtain a statistically reliable potential. The electrophoretic mobilities were measured in MilliQ water. To measure the ζ potential as function of the pH, a MPT-2 Autotitrator attached to the Malvern Zetasizer Nano was used.

$^1\text{H-NMR}$ spectra were recorded using a Varian MRF400 400 MHz NMR machine. CDCl_3 was used as solvent.

Infrared (IR) spectra were obtained using a Perkin Elmer FT-IR/FIR Frontier Spectrometer in attenuated total reflectance (ATR) mode. The measurements were performed on powders obtained by drying the corresponding particle dispersion.

Optical microscopy images were obtained using a Nikon Eclipse Ti-E inverted microscope equipped with a Hamatsu Orca Flash 4.0 V2 Digital Camera. A Nikon CFI Apo TIRF objective ($100\times$ magnification, N.A. 1.49) was used. Pictures were either recorded in bright field or fluorescent mode using a Semrock FITC-3540C filter.

4.3. Results and Discussion

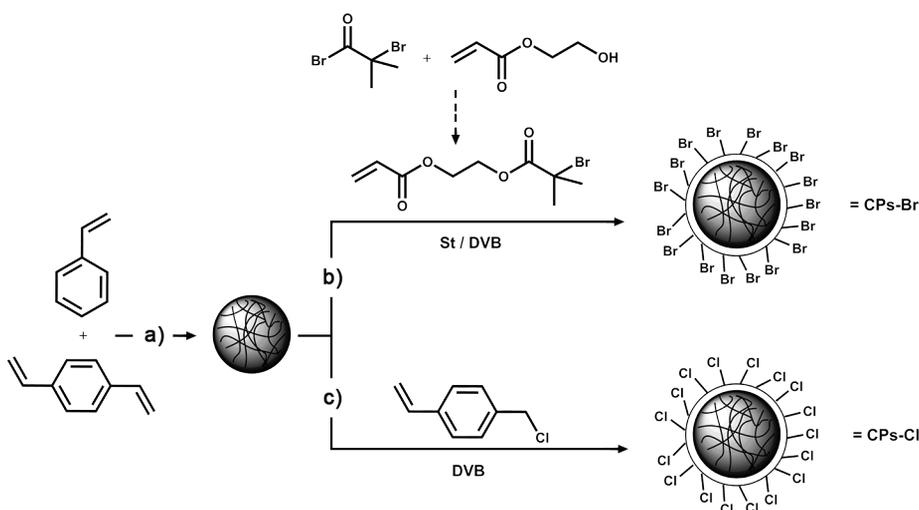
In this section, the synthesis of colloidal particles equipped with ATRP initiators on their surface will be discussed. These colloidal initiators were subsequently used in a variety of Surface-Initiated-ATRP (SI-ATRP) reactions to illustrate some of the important aspects discussed in the Theory section (Section 4.1). The focus will be on the preparation of chemical functional polymer brushes by end-group modifications, incorporation of functional monomers, and the use of post-polymerization functionalization methods. In this way, we illustrate that a wide variety of brushes can be tethered to colloidal systems. This section will be concluded by a comparison between polyacrylic and polyacrylamide hairs with respect to the measurable surface charge.

4.3.1. Synthesis of chlorinated and brominated colloidal initiators.

Both chlorinated and brominated colloidal initiators were synthesized in a two-step procedure as schematically depicted in Scheme 4.6. In the first step (step a, Scheme 4.6), cross-linked core particles (CPs) were synthesized in a straightforward emulsion polymerization of styrene (St) and divinylbenzene (DVB). Crosslinking of both core and shell is of importance, since a significant part of the subsequent reactions were conducted in solvents capable of dissolving linear polystyrene. Crosslinking the network prevents this dissolution and ensures that the colloids remain intact during the whole procedure. Monodisperse particles were obtained with a diameter of approximately 280 nm and polydispersities of 3–4%. These particles served as cores for the introduction of the actual ATRP initiators via a

seeded emulsion procedure (step b and c, Scheme 4.6). The core-shell geometry of the colloids was used to maximize the number of initiators directly on the surface. For the chlorinated particles (CPs-Cl), vinylbenzyl chloride (VBC) was used as shell monomer (route c in Scheme 4.6), while brominated particles (CPs-Br) were obtained by using a mixture of styrene and 2-(2-bromoisobutyryloxy) ethyl acrylate (BIEA) (route b, Scheme 4.6). BIEA was synthesized by coupling of 2-hydroxyethyl

Scheme 4.6. Synthetic strategy applied to prepare colloidal initiators for surface-initiated ATRP.^a



^a Step (a): emulsion polymerization of styrene (St) and divinylbenzene (DVB) to prepare cross-linked seed particles. Step (b): seeded emulsion polymerization to grow a shell consisting of St, DVB and 2-(2-bromoisobutyryloxy) ethyl acrylate (BIEA) on the core particles obtained in step a) which resulted in brominated colloidal initiators (CPs-Br). Step (c): seeded emulsion polymerization to grow a shell consisting of vinylbenzyl chloride (VBC) and DVB on the core particles obtained in step a) which yields chlorinated colloidal initiators (CPs-Cl).

acrylate to 2-bromoisobutyryl bromide according to ref. 73. Styrene was added to the shell formation reaction in case of the brominated particles to facilitate incorporation of BIEA. The addition of extra styrene proved to be unnecessary for introducing a chlorinated shell, probably due to large similarities in chemical structure and hydrophobicity between VBC and styrene. In both cases, the shells were cross-linked by addition of DVB during the seeded emulsion polymerizations.

The particles were analyzed using infrared (IR) spectroscopy to probe their chemical composition. The results are shown in Figure 4.7. After the seeded emulsion

procedure to introduce the initiator-shells on the colloids, a clear signal at 1266 cm^{-1} is observed for the chlorinated particles (Figure 4.7, red spectrum), corresponding to the $-\text{CH}_2\text{-Cl}$ vibration. The brominated particles are characterized by the presences of a carbonyl vibration ($\text{C}=\text{O}$) at 1732 cm^{-1} (Figure 4.7, blue spectrum), corresponding to the two ester moieties present in BIEA. Signals of both functional groups were not observed in the spectrum of the bare core particles (Figure 4.7, black spectrum).

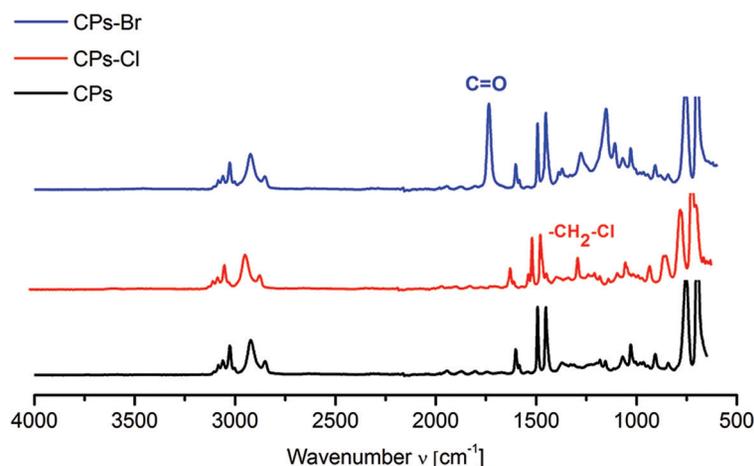


Figure 4.7. Infrared (IR) spectra from the polystyrene seed particles (black), the chlorinated colloidal initiators (CPs-Cl, red) and the brominated colloidal initiators (CPs-Br, blue).

Dynamic light scattering (DLS) measurements revealed that the initiator particles were monodisperse and slightly larger than the CPs particles. An increase of approximately 80 nm in diameter was measured for both the chlorinated and the brominated particles. The increase in size is in line with the introduction of a shell onto the CPs core particles.

The benzyl chloride fragments on the CPs-Cl particles are not a very active ATRP initiator (Figure 4.2). Nevertheless, we would like to explore the use of this initiator, since VBC is a cheap and commercially available molecule. The brominated particles are expected to be much more efficient initiators (Figure 4.2), capable to conduct ATRP reactions under much milder conditions. The minor disadvantage compared to the chlorinated colloids is that BIEA must be synthesized before use.

With both colloidal initiators in hand, we proceeded to the SI-ATRP reactions to introduce polymer brushes onto these particles.

4.3.2. SI-ATRP of methyl methacrylate using CPs-Cl. As a first attempt, the chlorinated colloids were exploited as colloidal initiators for the grafting of

a poly(methyl methacrylate) (p(MMA)) brush. MMA is an easily polymerizable monomer, since the propagating species is a stable tertiary radical. Reaction conditions were adapted from Teare et al.⁷⁵ The brush thickness was varied using two basic strategies, namely by changing the initial monomer concentration ($[MMA]_0$) or the reaction time, i.e. the extent of monomer conversion. Washed reaction products or samples were analyzed using IR spectroscopy to probe the chemical composition of the colloids. DLS was used to estimate the brush thickness by measuring the increase in hydrodynamic diameter after the SI-ATRP reaction.

Results of the experiments in which the initial monomer concentration was varied are shown in Figure 4.8. All IR spectra are normalized with respect to the polystyrene signal (695 cm^{-1}) to fairly compare the p(MMA) content, represented by the carbonyl signal located at 1732 cm^{-1} . Increasing $[MMA]_0$ from 0.25 to 1 M leads to a tremendous increase in the intensity of the carbonyl signal (Figure 4.8a and b). A linear relation between the intensity of the normalized carbonyl signal and $[MMA]_0$ was obtained (Figure 4.8c), implying that the monomer feed is quantitatively transferred to the resulting particles and that the hair length is indeed easily tunable by $[MMA]_0$. Increasing the initial monomer concentration to 1.5 M resulted in an aggregated system (note the break on the y -axis in Figure 4.8d). This aggregation behavior was attributed to either a too large hydrophobic contribution of the p(MMA) brush or to inter-particle termination reactions where two propagating polymers attached to different particles terminate by recombination. These reactions are more likely to occur if the polymers grow longer. If the charges on the core-particles are not effective in repelling particles over distances comparable to the polymer length, these reactions contribute considerably to aggregation by the formation of covalent links between the colloids.

However, if the monomer concentration is equal or lower than 1 M, stable colloidal systems were obtained, as concluded from the DLS results depicted in Figure 4.8d. The polydispersity indices (PDI's) of the dispersions remain low, indicating that the particles are well-dispersed and of similar size. Consistent with the IR spectroscopy results, an increase in hydrodynamic radius with increasing $[MMA]_0$ is observed.

In the second set of experiments, the reaction with a $[MMA]_0 = 0.5\text{ M}$ was repeated and samples were withdrawn from the reaction mixture to probe the brush formation in time. The same IR and DLS analyses as described before were performed.

The IR spectra show a gradual increase in the intensity of the carbonyl vibration (Figure 4.9a). Since this carbonyl signal was representative for the fraction of MMA converted to p(MMA) during the grafting procedure, the height of this signal is a measure for the monomer conversion (p). Here we assume that the signal intensity obtained after 24 h of reaction represents full conversion. Plotting the normalized C=O signal as a function of time yields the graph plotted in Figure 4.9b (black dots). The obtained graph shows the characteristic shape of a conversion

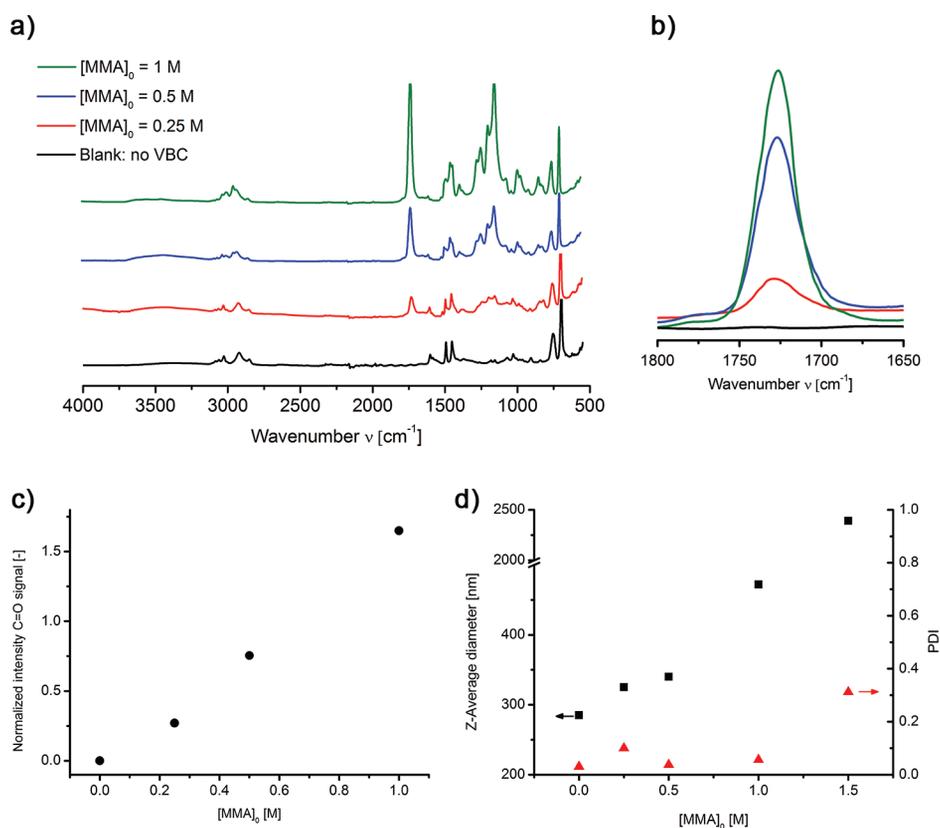


Figure 4.8. (a) Infrared (IR) spectra of colloidal particles after grafting poly(methyl methacrylate) (p(MMA)) on the surface of chlorinated colloidal initiators (CPs-Cl). The black spectrum was obtained after an ATRP reaction on non-functionalized polystyrene seed particles. The red, blue and green spectra are obtained after ATRP reactions with initial MMA concentrations of 0.25, 0.5 and 1 M, respectively. (b) Overlay of the carbonyl vibrations (1732 cm^{-1}) observed after grafting of p(MMA) on CPs-Cl. (c) Plot of the normalized intensity of the carbonyl vibrations (shown in b)) versus the initial MMA concentration. (d) Dynamic light scattering (DLS) results of the chlorinated colloidal initiators and the particles obtained after ATRP reaction. The size of the colloids is reported as the Z-average diameter (black squares). The polydispersity (PDI) of particles is depicted by the red triangles.

versus time plot for a reaction following first order kinetics. Rearranging the data and plotting $\ln(1/(1-p))$ versus time results in a straight line up to 4 h of reaction (Figure 4.9b, red triangles). As explained in Section 4.1.2 (Eq. 4.2), obtaining a straight semi-logarithmic plot indicates a controlled polymerization; it implies a constant number of propagating species and therefore, the absence of termination reactions.

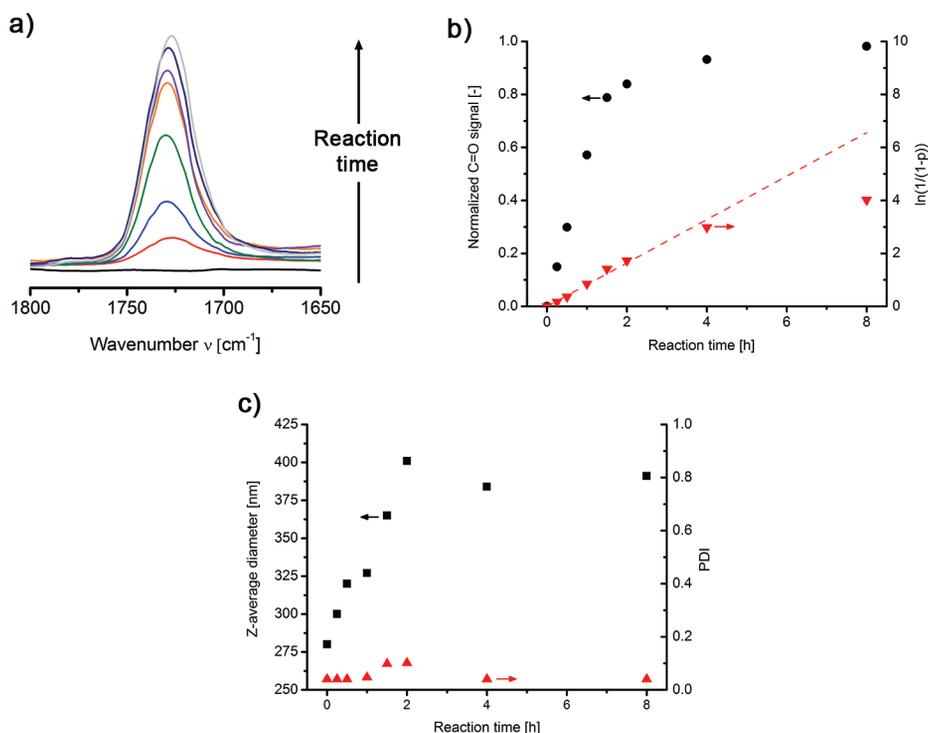


Figure 4.9. (a) Overlay of the carbonyl vibrations (1732 cm^{-1}) observed in infrared (IR) spectra during the grafting of p(MMA) on chlorinated colloidal initiators (CPs-Cl). (b) Black circles: plot of the normalized intensity of the carbonyl vibrations (shown in a)) versus reaction time (black circles). Red triangles: semi-logarithmic kinetic plot based on monomer conversions determined from the carbonyl vibrations. The straight line indicates the theoretical curve for a controlled radical polymerization. (c) Dynamic light scattering (DLS) results of the chlorinated colloidal initiators during the grafting of p(MMA). The size of the colloids is reported as the Z-average diameter (black squares). The polydispersity (PDI) of particles is depicted by the red triangles.

Furthermore, obtaining a straight line indicates fast initiation. After 4 h, when maximum conversion is almost reached, the measured curve deviates with respect to the theoretical straight line by a downwards curvature indicating the occurrence of termination reactions. Nevertheless, the reaction seems controlled up to at least 90% of the maximum conversion.

However, to claim full control over the polymerization, the average degree of polymerization as function of monomer conversion should also be measured. A linear dependence between the degree of polymerization and the conversion is expected. Only if this linear dependence is observed, the contribution of chain transfer reactions is negligible and full control can be claimed (see Section 4.1.2). These measurements

are not performed here, since the exact molecular weight of the grafted polymer is not of interest. Furthermore, the analysis of the molecular weight distribution is not trivial if polymers are grafted onto a substrate. If the initiator fragments by which the polymers are attached to the surface possess a chemically liable bond, the polymers can be cleaved off and analyzed separately.⁵⁷ For the current system this strategy is not applicable, since no cleavable bonds are present in the tethering points of the polymers.

The results of the DLS analysis of the p(MMA) brush particles are shown in Figure 4.9c. Plotting the hydrodynamic diameter versus reaction time shows that the hydrodynamic size increases the first 2 h of the reaction, after which the size levels off. As expected, the point where the size levels off is reached slightly earlier than the point of maximum conversion (Figure 4.9b). If the polymer hairs grow farther away from the surface, the grafted polymers get increasingly more freedom. This originates from the spherical geometry of the grafting surface which allows for more relaxed, i.e. non-stretched configurations only farther away from the surface (Figure 4.6). Regardless of the conversion, the PDI (red triangles, Figure 4.9c) of the dispersion remained low. This showed that the particles remain stable during the whole polymerization and no significant aggregation occurred.

To prove that the chlorine groups are really necessary to graft polymers onto the colloids, a blank ATRP reaction was conducted in which non-functionalized polystyrene particles were used as supposedly non-active colloidal initiators. This experiment was also used to prove that the measured carbonyl signals with IR spectroscopy and the increase in hydrodynamic radius are not caused by adsorbed p(MMA). The particles were treated in the same fashion as the chlorinated analogues and afterwards characterized with IR spectroscopy. The resulting spectrum is plotted in Figure 4.8 (black spectrum). As expected, no p(MMA) signal (1732 cm^{-1}) was observed, proving that the chlorine functionalities acted as ATRP initiators and therefore, as grafting points of the formed p(MMA).

4.3.3. Introduction of functionality to polymers grafted to CPs-Cl. As discussed in the Theory Section (Section 4.1), the polymers grown by ATRP are in principle end-capped by a halogen atom which originates from the initiator (Scheme 4.3 and 4.4) or the added cuprous salt. From the previously measured IR spectra (Figure 4.8) it is not possible to observe these chlorine/bromine functionalities to verify if the polymers are still functional. However, the end-groups can be made visible by conducting a nucleophilic substitution reaction with sodium azide (NaN_3). The azide groups are easily detectable in IR spectroscopy and show up at a wavenumber of 2100 cm^{-1} where there will be no overlap with signals originating from the polystyrene core or the p(MMA) brush. According to Coessens et al.,^{79,80} the esters in the backbone of p(MMA) are not able to react with the azide ions under the reaction conditions

which were used. This ensures that only end-group modifications will take place and the intensity of the azide signal in the IR spectra of the obtained products will be a good measure for the effectiveness of these modifications.

Substitution reactions were performed on two different brush particles, namely particles obtained after reaching the maximum conversion of MMA and brush particles obtained after reaching approximately 50% of the maximum conversion. Based on the discussions in Section 4.1.3 and the results shown in Figure 4.9b, which indicates the occurrence of termination reactions at elevated conversions, we expect a higher fraction of halogen end-capped chains for a lower monomer conversion.

After the nucleophilic substitution, the particles were washed to remove any unreacted sodium azide and the products were analyzed with IR spectroscopy. The spectra are shown in Figure 4.10. In both spectra an azide signal (2100 cm^{-1}) was observed. To compare the intensities of the azide signals fairly, the spectra were normalized to the signal of the polystyrene core (695 cm^{-1}). The p(MMA) related signals cannot be used as reference due to the difference in monomer conversion and hence p(MMA) content of the colloids.

In agreement with Eq. 4.7, the azide signal intensity observed in the spectrum obtained from the particles with the limited conversion (Figure 4.10, red spectrum) is significantly higher compared to the signal intensity measured for the particles obtained after maximum MMA conversion (Figure 4.10, black spectrum).

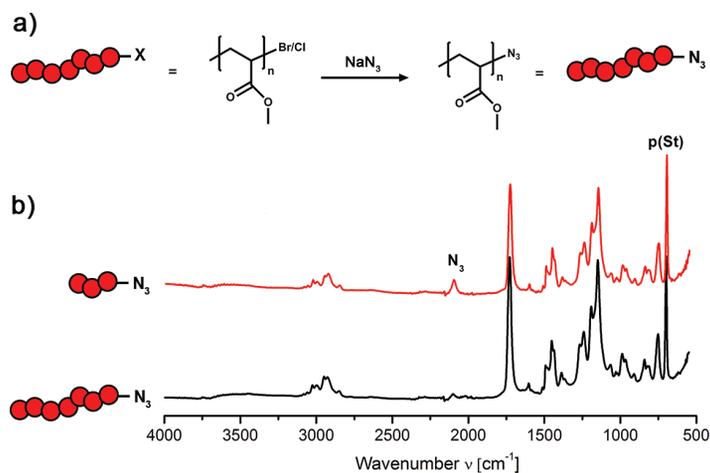


Figure 4.10. (a) Schematic representation of end-group modification of poly(methyl methacrylate) (p(MMA)) using azide anions as nucleophiles. (b) Infrared (IR) spectra of p(MMA) after substitution of the terminal halogens by azides. The substitution reaction was performed on polymers obtained from an ATRP reaction which was allowed to go to maximum conversion (black) and quenched at approximately 50% MMA conversion (red). Both spectra are normalized to the signal of the polystyrene core (695 cm^{-1}).

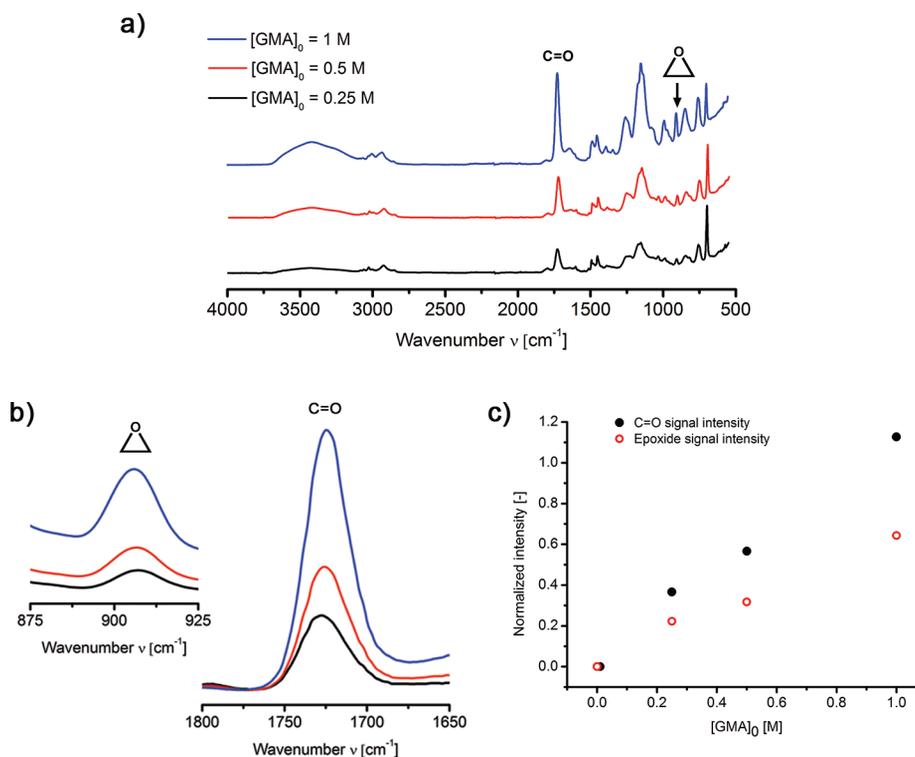


Figure 4.11. (a) Infrared (IR) spectra of colloidal particles after grafting poly(glycidyl methacrylate) (p(GMA)) onto the surface of chlorinated particles (CPs-Cl). The black, red and blue spectra are obtained after ATRP reactions with initial GMA concentrations of 0.25, 0.5 and 1 M, respectively. (b) Overlay of the carbonyl (1732 cm⁻¹) and epoxide (907 cm⁻¹) vibrations observed after grafting of p(GMA) on CPs-Cl. (c) Plot of the normalized intensity of the carbonyl (black filled circles) and epoxide (red open circles) vibrations (shown in b)) versus the initial GMA concentration.

As mentioned before in the Theory section, the use of acrylates or styrene derivatives facilitates end-group modifications.^{17,79,80} The lower reactivity of the terminal halogen atom of methacrylate polymers arises from the fact that the terminal halogen is a tertiary group in most polymer chains due to the relatively high preference for head-to-tail attachment of the monomers. Polyacrylates and styrene derivatives do not suffer from these rather inactive chain ends, making these polymers preferable if end-functionalization is required. Nevertheless, if the nucleophile is in large excess, as is the case in these experiments, substitution reactions on p(MMA) brushes are effective enough and end-functionalized brushes are still accessible via this route.⁷⁹

The substitution reactions are obviously not limited to NaN₃, but several

functionalities are easily reachable as depicted in Scheme 4.4.

If a larger density of functional groups is required, a logical strategy is to substitute MMA by a functional monomer. For these model reactions we selected the use of glycidyl methacrylate (GMA). This monomer has an epoxide moiety which is susceptible towards ring opening in post-polymerization reactions. As shown in Scheme 4.5, a wide variety of functionalities can be introduced based on this monomer.

To graft the p(GMA) on the CPs-Cl colloids, a similar approach was applied as for the p(MMA) brushes. The initial GMA concentration was varied between 0.25 and 1 M to verify that also for this monomer we could grow well-defined brushes. The IR spectra of the resulting colloids are shown in Figure 4.11a and b. In all spectra, both the carbonyl (1732 cm^{-1}) and the epoxide signal (907 cm^{-1}) were present. Plotting the normalized intensities of both signals against the initial monomer concentration reveals that both carbonyl and epoxide intensities scale linearly with respect to the added monomer (Figure 4.11c). Analogous to the SI-ATRP reactions with MMA, the results plotted in Figure 4.11c show that the brush thickness is tunable with the initial monomer concentration. Additionally, the epoxide remains intact during the ATRP reaction, allowing for further modifications.

Two simple ring opening reactions were conducted to illustrate the post-functionalization methods. NaN_3 and propargylamine were used to conduct these

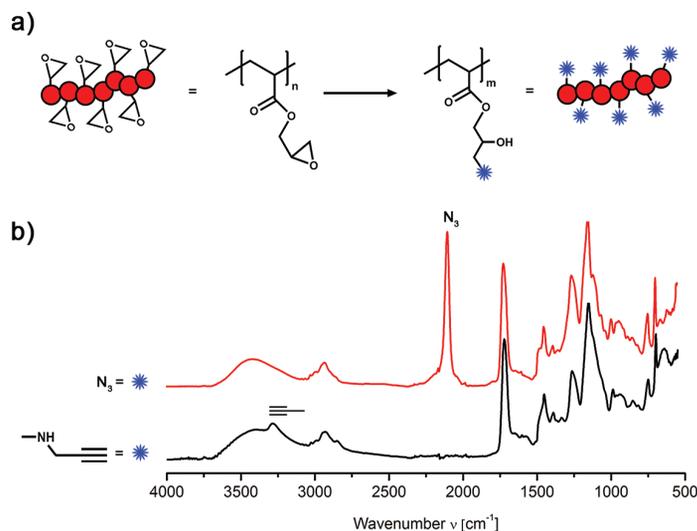


Figure 4.12. (a) Schematic representation of ring opening reactions to functionalize the pending epoxides in grafted poly(glycidyl methacrylate) (p(GMA)). The blue star represents the introduced functionality. (b) Infrared (IR) spectra of the p(GMA) grafted colloids after ring opening of the epoxide groups with propargylamine (black spectrum) and sodium azide (red spectrum).

reactions. The functionalization is schematically depicted in Figure 4.12a. Polymer hairs with either azides (Figure 4.12b, red spectrum, 2100 cm^{-1}) or with alkyne (Figure 4.12b, black spectrum, sharp signal at 3300 cm^{-1}) moieties were obtained, as concluded from the IR spectra of the obtained products. In both spectra, no epoxide signals were observed, underlining the effectiveness of this functionalization method. The prepared brushes can be used in click chemistry reactions to increase the molecular complexity of the brushes even further.⁷⁶ As mentioned before, the pending epoxides are versatile and reactive handles, rendering these brushes the ideal starting point for the preparation of chemically complex grafted polymers.

4.3.4. Grafting under milder conditions using CPs-Br. The grafting reactions that were discussed in Sections 4.3.2 and 4.3.3 were all performed under relatively harsh conditions (in DMF or DMSO at $90\text{ }^{\circ}\text{C}$ for periods of 8–24 h). For monomers that are susceptible to auto-initiation or are thermally liable these harsh grafting conditions are therefore not optimal. To be able to use more ambient reaction conditions, the brominated colloidal initiators were used in SI-ATRP reactions. Methanol (MeOH)/water mixtures were used as solvent and maximum monomer conversion was typically reached after 4 h of reaction at room temperature. The use of MeOH/water mixtures as continuous phase has the advantage that non-cross-linked colloids can also be applied as colloidal initiators without dissolving the particles, which does happen if DMF or DMSO are applied as solvents.

For the SI-ATRP reactions at ambient conditions, the brominated colloidal initiators were used in combination with 2-hydroxyethyl acrylate (HEA) as monomer. This hydrophilic monomer was selected to avoid solubility problems of the formed polymers, since hydrophobic polymers such as p(MMA) are not soluble in the water/MeOH mixture. A reaction with an initial HEA concentration of 0.6 M was performed. Samples were withdrawn from the mixture to follow the increase in p(HEA) content using both IR spectroscopy and DLS. Figure 4.13b shows the conversion versus time plot, revealing that nearly maximum conversion was already reached after 2 h. This plot was constructed using the normalized carbonyl vibrations extracted from IR spectra (Figure 4.13a) as explained in Section 4.3.2. Compared to the minimal 8 h at $90\text{ }^{\circ}\text{C}$ required for the chlorinated particles, this system reacts much faster and under significantly milder conditions, even when less active acrylates are used as monomer.

Determination of the level of control via a kinetic plot (Figure 4.13b) was complicated by the presence of a carbonyl vibration before grafting. This initial carbonyl vibrations originates from the ester moieties present in BIEA. Subtracting the intensity at $t = 0$ and using the obtained intensities as measure for the conversion yielded a reasonable straight curve, which indicates good control over the reaction. Full claim for a controlled reaction can again not be made without analyzing the molecular weight of the polymers as function of the conversion.

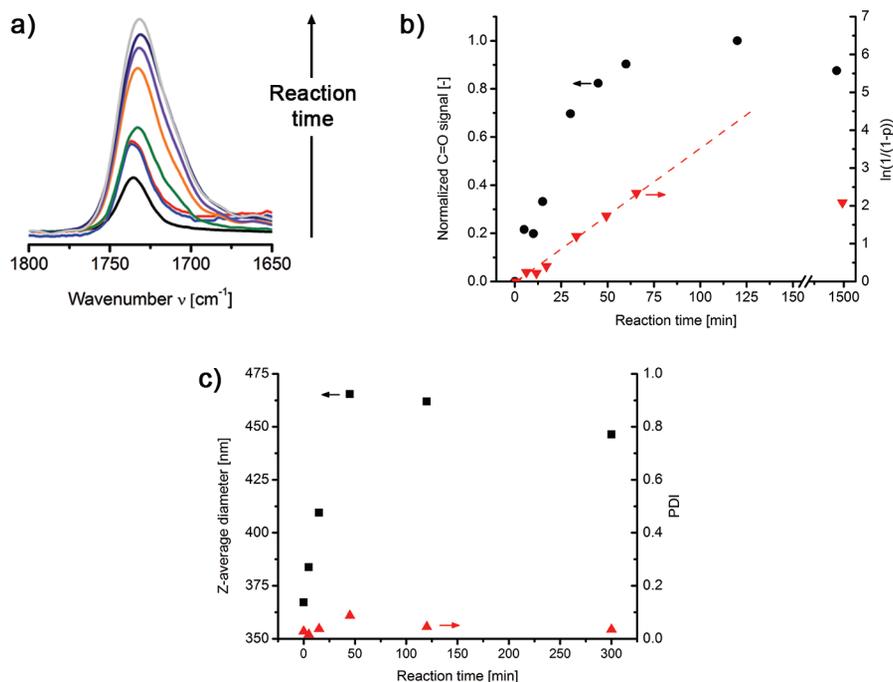


Figure 4.13. (a) Overlay of the carbonyl vibrations (1732 cm^{-1}) observed in infrared (IR) spectra during the grafting of poly(2-hydroxyethyl acrylate) (p(HEA)) on brominated colloidal initiators (CPs-Br). (b) Black circles: plot of the normalized intensity of the carbonyl vibrations (shown in a) versus reaction time (black circles). Red triangles: semi-logarithmic kinetic plot based on monomer conversions determined from the carbonyl vibrations. The straight line indicates the theoretical curve for a controlled radical polymerization. (c) Dynamic light scattering (DLS) results of the brominated colloidal initiators during the grafting of p(HEA). The size of the colloids is reported as the Z-average diameter (black squares). The polydispersity (PDI) of particles is depicted by the red triangles.

These measurements were not performed in this study. DLS measurements reveal that the hydrodynamic radius levels off after 1 h of reaction (Figure 4.13c, black squares). The measured PDIs of the colloidal particles remain low, reflecting the colloidal stability of the system during the polymerization (Figure 4.13c, red triangles).

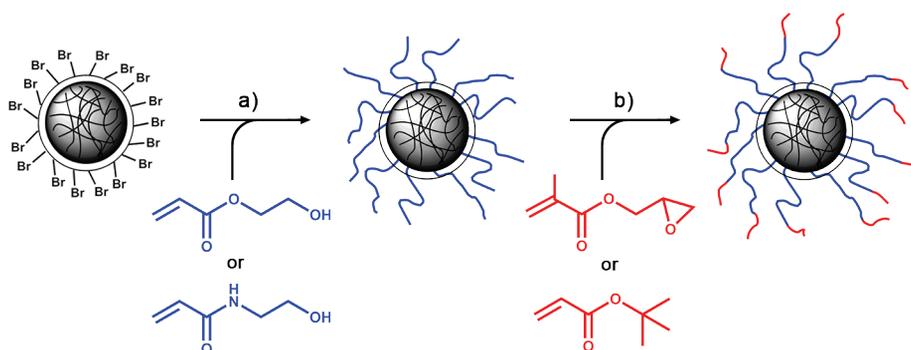
4.3.5. Grafting of poly(2-hydroxyethyl acrylate)-based block-copolymers using CPs-Br. The formed p(HEA) polymers are likely to extend into the solution when particles are dispersed in polar media. These polymers are therefore capable to act as spacers between the colloidal surface and a functionality attached to the end of these polymers. The hydrophilic brush shields the attached functional group from the

colloidal surface and makes sure it is accessible from the continuous phase. A potential application is the attachment catalytic species to the colloidal brush as solid support. We speculate that the attached catalyst is then easy to recover from the reaction mixture, since it is bound to a relatively large carrier particle. These immobilized species resemble molecularly dissolved catalyst considerably more than complexes directly attached to a surface, possibly having a positive influence on the catalytic activity.

In the field of (reversible) assembly of colloids, the terminal end-blocks can be functionalized with attractive groups, for example hydrophobic molecules. The hydrophilic brush prevents these molecules from collapsing on the surface of the colloids, facilitating the inter-particle interactions based on hydrophobic attractions if the particles are suspended in a polar medium. In fact, this is a fully synthetic analogue to particles functionalized with single-stranded sticky DNA ends to mediate thermo-reversible interactions.^{81,82} This strategy will be applied in Chapter 7 to create reversibly aggregating systems.

To show that these possible applications are indeed within reach, we attempted to prepare colloidal particles grafted with block-copolymers. The block-copolymers consist of a hydrophilic block which is directly attached to the colloidal surface and a terminal block consisting of functional monomers, allowing for further modification reactions. The basic synthetic strategy is depicted in Scheme 4.7.

Scheme 4.7. Schematic representation of grafting of block-copolymers on the surface of brominated colloidal initiators (CPs-Br).^a



^a Step (a): surface-initiated ATRP reaction of 2-hydroxyethyl acrylate (HEA, top) or *N*-hydroxyethyl acrylamide (HEAA, bottom) to introduce a hydrophilic brush (blue) onto the brominated colloidal particles (CPs-Br). Step (b): chain extension reactions to introduce a functional terminal end-block (red) on the grafted polymers using glycidyl methacrylate (GMA, top) or *t*-butyl acrylate (*t*-BuA, bottom).

We will first focus on block-copolymers consisting of a poly(2-hydroxyethyl acrylate) (Scheme 4.7, step a, top blue molecule) inner segment and a terminal poly(glycidyl methacrylate) (Scheme 4.7, step b, top red molecule) block. These polymers are abbreviated with p(HEA-*co*-GMA) in the upcoming sections.

To ensure efficient chain extension, all chains should remain end-capped with a halogen atom, i.e. the polymers should still be 'living' after consumption of HEA. As mentioned before in the Theory section and illustrated by the end-group substitution reaction on CPs-MMA-Cl (Section 4.3.3), the fraction of dead chain ends increases with conversion. It is therefore recommended to simply add the second monomer just before complete conversion is reached. If a strict separation between the two blocks is required, the reaction should be quenched and residual monomer be removed. Here, we applied a simpler method, where the second monomer was injected into the reaction mixture just before reaching maximum conversion of the first monomer. This procedure leads to a block-copolymer in which the two polymer blocks are probably connected by a transition segment containing a gradient in monomer composition. The time after which the second monomer should be injected into the reaction mixture was determined using the kinetic data obtained from the grafting of p(HEA) on the brominated particles (Figure 4.13b).

As mentioned before, chain extension reactions were conducted with GMA. In theory, this chain extension reaction is not very controlled, since methacrylate monomers are more reactive than the previously polymerized acrylates. Controlled chain extensions can be conducted in combination with halogen exchange as discussed in the Section 4.1.5. However, for sake of simplicity, this method was not applied here.

Three chain extension reactions were performed in which the GMA concentration was varied such that the resulting block-copolymers consist of 4 to 12 mol% p(GMA). The incorporation of GMA could not be confirmed directly by IR spectroscopy due to two reasons. Firstly, the added number of repeating units of GMA in the outer segment is relatively small compared to the number of repeating units of HEA present in the inner polymer segment. Secondly, GMA is structurally very similar to HEA, so no new distinct IR vibrations will appear after the formation of the p(GMA) terminal block. Also DLS was not suitable for this purpose, since no increase in hydrodynamic size could be measured (squares, Figure 4.14). Based on the geometric argument mentioned in Section 4.3.2, this is not surprising, since increasingly more monomer needs to be incorporated into the brush due to the more relaxed polymer configuration far from the colloidal surface. The DLS data, however, does show that the particles remain stable after the incorporation of the end-block as reflected by the low PDI's (triangles, Figure 4.14). Increasing the amount of GMA to facilitate the analysis to confirm successful chain extension was not possible, since GMA contents above 12 mol% resulted in aggregation of the colloidal particles.

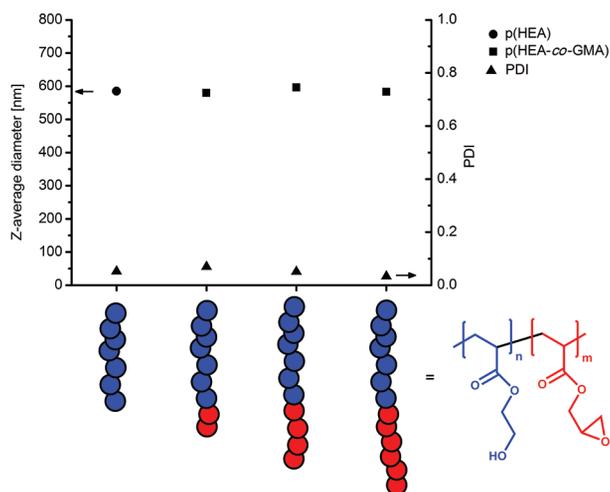


Figure 4.14. Dynamic light scattering (DLS) results of the brominated colloidal initiators (CPs-Br) before and after the grafting of block-copolymers consisting of a poly(2-hydroxyethyl acrylate) (p(HEA), blue) inner segment and a terminal poly(glycidyl methacrylate) (p(GMA), red) block. The size is measured as function of the amount of GMA added and is reported as the Z-average diameter (squares). The polydispersity (PDI) of particles is depicted by the triangles.

To circumvent the problematic p(GMA) detection, probe molecules were used which could be detected much easier and at significantly lower concentrations. This approach was already used in Section 4.3.3 to probe the presence of end-functionalities. In the current experiments, the epoxide side-groups of the present p(GMA) terminal blocks were ring opened with both sodium azide, facilitating IR spectroscopy analysis, and fluoresceinamine, enabling the use of fluorescence microscopy.

The IR spectra obtained after ring opening the epoxides with sodium azide are shown in Figure 4.15. The black spectrum shows the particles before reaction with sodium azide. The blue, green and orange spectra were obtained after ring opening the epoxide rings of the brush particles containing 4, 8 and 12 mol% of GMA in the polymer brush, respectively. In all these spectra an azide signal (2100 cm^{-1}) was observed. Unfortunately, no correlation between the length of the p(GMA) block and the azide intensity was measured. Probably, this is caused by the relatively small difference in azide content. The spectrum of the blank reaction (red spectrum), which was conducted with brush particles containing only the p(HEA), did not show the azide signal. The absence of this signal indicates that chain extension with GMA did lead to the incorporation of functional groups in the form of pending epoxides. Furthermore, the epoxides in the p(GMA) block were still reactive and end-functionalized block-

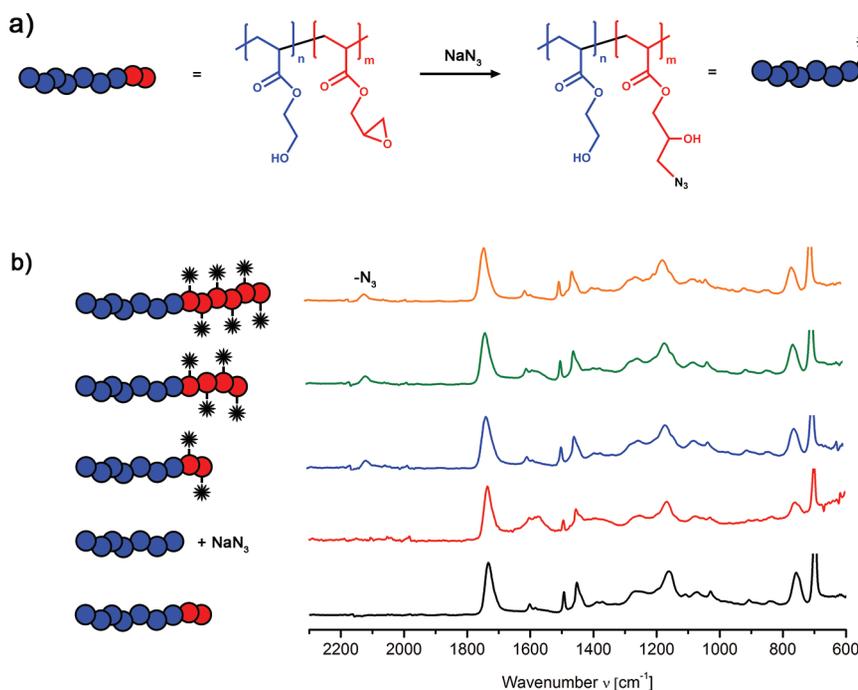
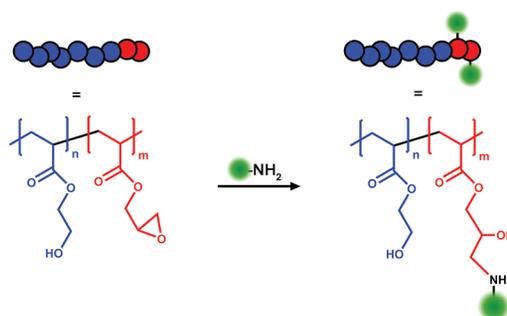


Figure 4.15. (a) Schematic representation of modification of the terminal poly(glycidyl methacrylate) (red, p(GMA)) by ring opening of the pending epoxides with sodium azide. The blue segment of the block-copolymer represents the poly(2-hydroxyethyl acrylate) (p(HEA)) block. The azide is depicted as a star. (b) Infrared (IR) spectra obtained after the ring opening reaction depicted in a) for polymers with different lengths of the terminal p(GMA) block (blue, green and orange spectra). As blank, particles equipped with a p(HEA) homopolymer brush were treated with sodium azide as well (red spectrum). No ring opening can occur for these homopolymers. For comparison, the spectrum of the particles with a p(HEA-co-GMA) brush before the ring opening reaction (black) is shown.

copolymers were prepared, although these results are inconclusive to claim systematic variation of the length of the terminal p(GMA) segment.

The IR spectroscopy results were consistent with fluorescence microscopy results obtained after introduction of fluoresceinamine as probe molecule (Scheme 4.8). Figure 4.16a and b show bright field images of colloidal particles equipped with a p(HEA) brush and with a p(HEA-co-GMA) brush after reaction with fluoresceinamine, respectively. These images reveal that the colloids were stable and did not aggregate after incorporation of the hydrophobic dye. The corresponding images recorded in fluorescence mode are shown in Figure 4.16c and d. The particles with a homopolymer brush of p(HEA) are clearly not fluorescent. This is also reflected in the intensity

Scheme 4.8. Schematic representation of ring opening of the pending epoxides of the terminal poly(glycidyl methacrylate) (red, p(GMA)) with fluoresceinamine (green dot, (Flu-NH₂)). The blue segment of the block-copolymer represents the poly(2-hydroxyethyl acrylate) (p(HEA) block.



profile that was recorded by measuring the fluorescence intensity along a line crossing a single particle. The intensity profile shows that the measured fluorescence is negligible compared to the background signal (Figure 4.16f).

On the other hand, the particles which supposedly contain a GMA end-block did show a clear fluorescence signal. The fluorescence was evident both visually (Figure 4.16d) and from the intensity profile (Figure 4.16f). Furthermore, the highest intensity of the profile was measured at the outer rim of the particle. This is consistent with the particle topology, which dictates that the dye should be present at the terminal part of the polymer brush and therefore at the outside of the colloidal particles (Scheme 4.8).

4.3.6. Grafting of poly(*N*-hydroxyethyl acrylamide)-based block-copolymers using CPs-Br. Similar experiments as described in the previous section were conducted using poly(*N*-hydroxyethyl acrylamide) (p(HEAA)) as hydrophilic spacer (Scheme 4.7, step a, bottom blue molecule). To illustrate the versatility of ATRP and its combination with post-functionalization methods, we aimed for the preparation of a different block-copolymer with a terminal *t*-butyl acrylate (*t*-BuA) block (Scheme 4.7, step b, bottom red molecule). This monomer is basically a protected carboxylic acid, since the *t*-butyl moiety can be cleaved off rather easily. Deprotection is achieved using, for example, trifluoroacetic acid (TFA) (step a, Scheme 4.9) or treatment with (strong) bases. The formed carboxylic acids were used for further functionalization by formation of an amide bond with a functional amine. The amide is formed after activation of the carboxylic acid with 1-ethyl-3-(3-dimethylaminopropyl) carbodiimide hydrochloride (EDC) (step b, Scheme 4.9). These coupling procedures are highly efficient and can be conducted under mild conditions, enabling the coupling of sensitive materials such as proteins.⁸³

Another method to introduce functionality based on the terminal p(*t*-BuA) blocks

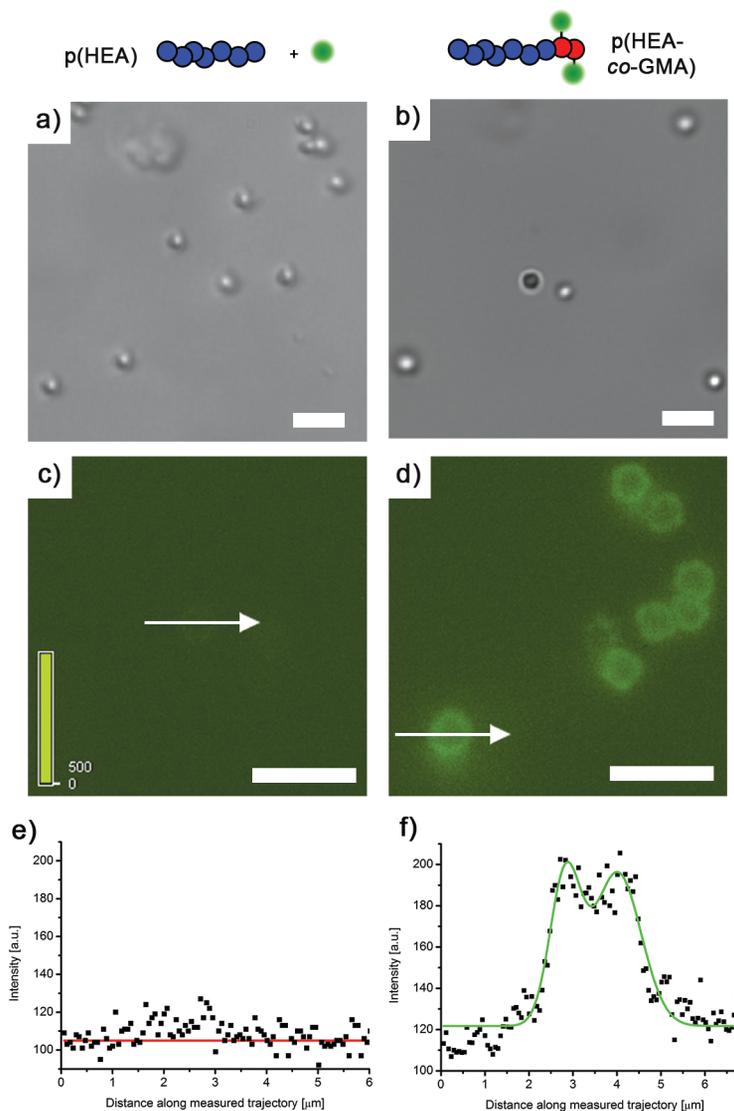
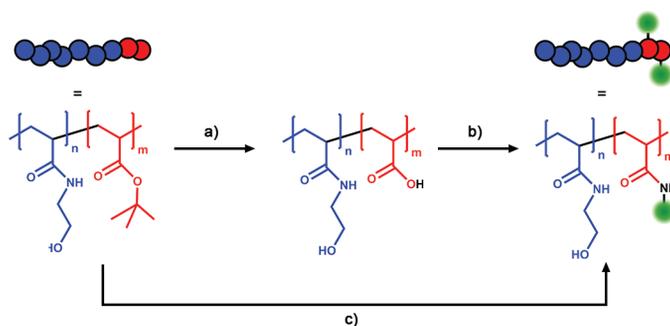


Figure 4.16. (a) Bright field microscopy images of particles equipped with a brush of homopolymer p(HEA). (b) Bright field microscopy images of particles equipped with a brush of p(HEA-co-GMA). (c) Fluorescence microscopy images of particles equipped with a brush of homopolymer p(HEA) after treatment with fluoresceinamine (Flu-NH₂). (d) Fluorescence microscopy images of particles equipped with a brush of p(HEA-co-GMA) after treatment with Flu-NH₂. (e) Fluorescence intensity measured along the arrow indicated in c). The particle underneath the arrow is hardly visible in fluorescence mode. (f) Fluorescence intensity measured along the arrow indicated in d). Scale bars are 5 μm for all subfigures.

Scheme 4.9. Schematic representation of the modification of block-copolymers consisting of a poly(*N*-hydroxyethyl acrylamide) (p(HEAA), blue) and a poly(*t*-butyl acrylate) (p(*t*-BuA), red) block via indirect (step a and b) and direct aminolysis (step c).^a



^a Step (a): cleavage of the *t*-butyl groups from the p(*t*-BuA) segment by treatment with trifluoroacetic acid (TFA). Step (b): coupling of fluoresceinamine (green dot) via activation of the formed carboxylic acid with 1-ethyl-3-(3 dimethylaminopropyl) carbodiimide hydrochloride (EDC). Step (c): direct aminolysis with fluoresceinamine in dimethyl sulfoxide (DMSO).

is a simple one-step reaction in which a functional amine reacts at high temperatures to directly form an amide bond by displacing the *t*-butyl group (step c, Scheme 4.9).⁷⁷ Both coupling strategies were applied to modify the colloidal particles and the suitability of both methods was compared. Since detection of the end-block by IR and DLS proved to be difficult, as discussed in the case of the p(HEA) brush particles, fluoresceinamine was again used as functional amine to probe if a block-copolymer was formed and if subsequent functionalizations were indeed possible.

The fluorescent microscopy results based on the deprotection and activation pathway (step a and b in Scheme 4.9) are shown in Figure 4.17d. Analogous to the results depicted in Figure 4.16, we observed clear fluorescence after the complete treatment with TFA, EDC and fluoresceinamine, both visually (Figure 4.17d) and by the intensity profile measured along the diameter of a single particle (Figure 4.17e).

When deprotection of the ester group by TFA addition was not performed, addition of fluoresceinamine did not result in the formation of an amide bond and hence no fluorescent particles were detected (Figure 4.17c). The results of this blank experiment underlines the effectiveness of this functionalization procedure.

The modification procedure based on the deprotection of the *t*-butyl acrylate and subsequent amide formation requires several steps, making this method rather complicated and time consuming. In literature, direct amide formation was reported.⁷⁷

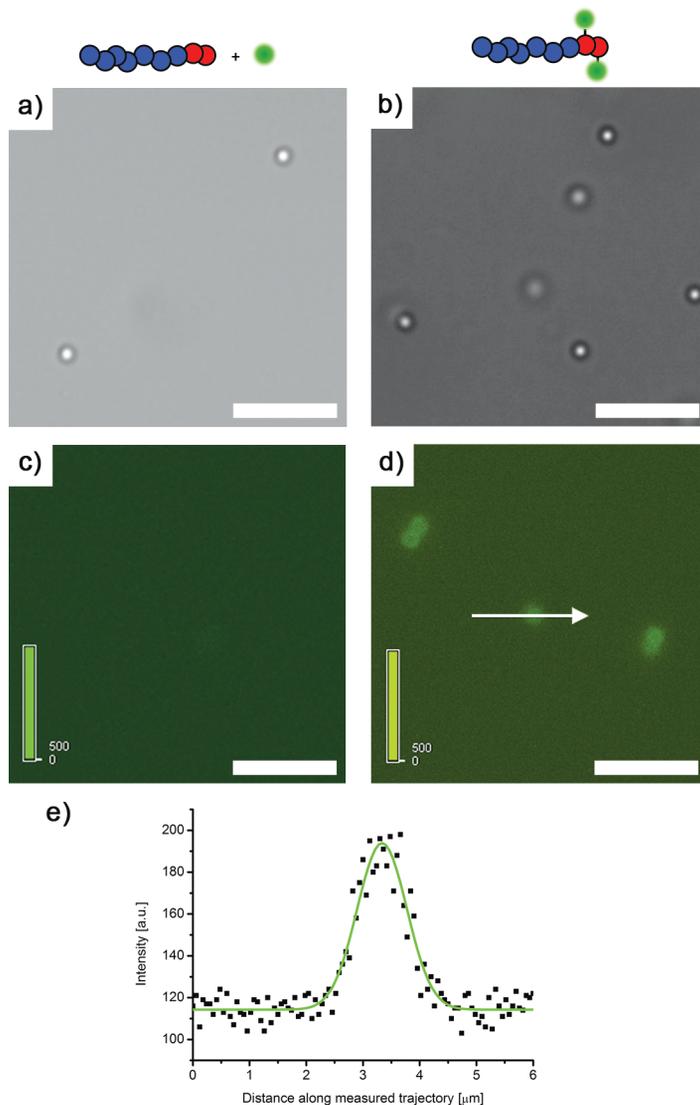


Figure 4.17. (a) Bright field microscopy images of particles equipped with a copolymer brush consisting of poly(*N*-hydroxyethyl acrylamide) and poly(*t*-butyl acrylate) (p(HEAA-*co-t*-BuA)) after treatment with fluoresceinamine (green dot, Flu-NH₂) without cleavage of the *t*-butyl group with trifluoroacetic acid (TFA) and subsequent activation with 1-ethyl-3-(3-dimethylaminopropyl) carbodiimide hydrochloride (EDC). (b) Bright field microscopy images of the same particles as depicted in a) after treatment with TFA and EDC and final functionalization with Flu-NH₂. (c) Fluorescence microscopy images of particles shown in a). (d) Fluorescence microscopy images of particles shown in b). (e) Fluorescence intensity measured along the arrow indicated in d). Scale bars are 10 μm for all subfigures.

This method was employed to functionalize the particles in a facile one-step procedure (step c, Scheme 4.9) under harsh conditions (48 h, 120 °C DMSO) in the presence of fluoresceinamine. The resulting colloids were highly fluorescent (Figure 4.18b), which suggest efficient functionalization. However, analysis of the resulting colloidal particles with IR spectroscopy showed that the intensity of the signal corresponding to the p(HEAA) brush (1650 cm^{-1}) decreased significantly after direct coupling of the dye (blue spectrum compared to black spectrum, Figure 4.18c).

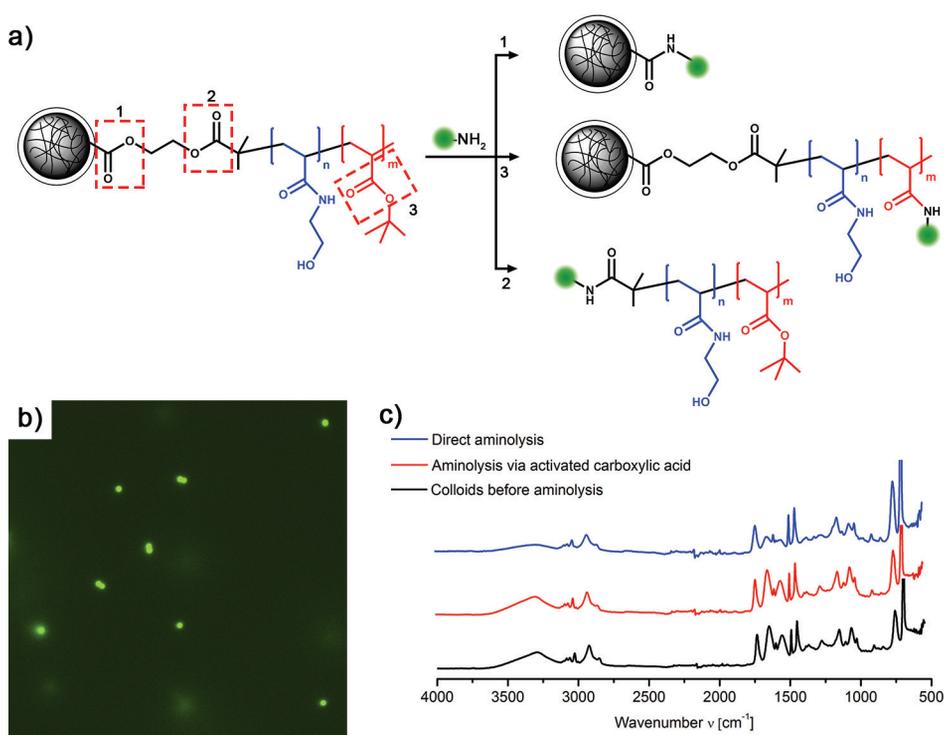


Figure 4.18. (a) Schematic representation of ester bonds present in the brominated colloidal initiators (CPs-Br) grafted with a copolymer of poly(*N*-hydroxyethyl acrylamide) and poly(*t*-butyl acrylate) (p(HEAA-*co-t*-BuA)). Products formed after cleavage of these ester bonds by fluoresceinamine (green dot, Flu-NH₂) in a direct aminolysis reaction are shown on the right. A combination of cleavage modes (reaction 1, 2 and 3) is possible, but not shown for clarity. (b) Fluorescence microscopy images of particles equipped with a p(HEAA-*co-t*-BuA) brush after direct aminolysis with Flu-NH₂. (c) Infrared (IR) spectra of the colloids with a brush of p(HEAA-*co-t*-BuA) before aminolysis (black), after indirect aminolysis (red) and direct aminolysis (blue). See Scheme 4.9 for the different aminolysis methods. Direct aminolysis clearly results in a lowering of the signal pHEAA signal at 1650 cm^{-1} , indicating polymer cleavage (reaction 1, Figure a).

The decrease in polymer related signals strongly suggest that the hairs were cleaved from the particles. This can be explained if the precise chemical structure of the used ATRP initiator (BIEA) is considered (Figure 4.18a). Two ester bonds are present in this molecule, which are in principle susceptible towards reaction with the amine, especially under the used reaction conditions. Apparently, reaction 1 depicted in Figure 4.18a occurs significantly since this pathway leads to the formation of fluorescent particles and cleavage of the polymer hairs.

In contrast, the IR spectrum of the particles functionalized using the extended deprotection, activation and amide formation procedure (step a and b, Scheme 4.8) did not show any polymer cleavage (Figure 4.18c, red spectrum). The intensity of the signal at 1650 cm^{-1} , which is indicative for the p(HEAA) hairs, did not decrease compared to the intensity measured before functionalization (Figure 4.18c, black spectrum). This indicates that coupling of functional amines preferentially occurs at the terminal activated esters derived from the butyl acrylate segment instead of the BIEA-related esters. Since cleavage of the polymer chains is obviously not desired, the deprotection/activation pathway (step a and b, Scheme 4.9) is preferred over the direct amide formation. However, it must be noted that the direct amide formation might be beneficial for polymers tethered to the particles via non-labile chemical bonds, for example the polymers grafted to the chlorinated seeds (Section 4.3.2 and 4.3.3).

The experiments presented in both Section 4.3.5 and 4.3.6 show that grafted block-copolymers are easily accessible via SI-ATRP. Incorporation of functional blocks based on epoxide bearing monomers as well as protected carboxylic acids opens the way for different types of post-functionalization procedures. Optimization in terms of monomer choice, monomer ratios and subsequent functionalization reactions is required to fully exploit this system. Nevertheless, the possibilities and versatility of these systems to prepare complex colloidal brush particles are evident.

4.3.7. Particle charges: Polyacrylates versus polyacrylamides. During the formation of polymer brushes consisting of p(HEA) (Section 4.3.4) we found that regardless of the brush thickness, the particles were strongly negatively charged ($\sim -40\text{ mV}$) as was observed from ζ potential measurements. For the bare particles, the negative charge originates from the sulfonate and sulfate groups introduced during the emulsion polymerization used to prepare these particles. However, we expected to measure a significantly higher (less negative) ζ potential for the particles equipped with a p(HEA) brush, since these brushes are built up from non-charged monomers. Consequently, the resulting brush particles could be modeled as particles with a hard charged core surrounded by a ‘fuzzy’, penetrable uncharged layer.^{84–86} Interpreting electro-kinetic data and converting it to reasonable values for surface charges is not trivial for these type of systems, although some general and basic understanding

can be extracted from the published literature. The ζ potential is the potential at the hydrodynamic shear surface. Behind this surface, charges are assumed to be immobile. For hard particles, this shear surface will be close to the actual surface of the particles. However, if a polymer brush is introduced, the hydrodynamic shear surface will shift outwards. Applying standard electro-kinetic models will lead to the potential at this apparent shear surface. The absolute ζ potential will therefore always be lower than the potential of the corresponding bare colloid. The precise position of the apparent shear surface, and therefore the measured ζ potential, is difficult to determine and depends on the hydrodynamic friction caused by the brush. This is in turn determined by the segment density distribution along the height of the polymer brush. Additional effects, such as a decrease in dielectric constant inside the polymer brush and decreased ion mobility, will alter the classical electro-kinetic picture of these systems even more.^{84–86} These subtle details will not alter the overall trend that lower absolute ζ potentials should be measured by the introduction of a non-charged polymer brush.

As mentioned before, for the colloids equipped with p(HEA) brushes these expectations were not met, since the introduction of the polymer brush did not lead to a decrease in the measured ζ potential. From these results we concluded that charges were introduced along the backbone of the grafted polymers. As a result the apparent shear plane is still located close to the charged species on the particles and hence, a more negative potential than expected was measured.

A possible explanation for the highly negative ζ potential is based on an observation made by Bories-Azeau et al.⁸⁷ and Connell et al.,⁸⁸ who reported the transesterification of the ester bond in p(HEA) to form methyl esters when the ATRP reaction was performed in MeOH (top reaction, Figure 4.19a). It is therefore reasonable to assume that in our case the analogous hydrolysis reaction will also occur, since a mixture of MeOH and water was used as continuous phase during the conducted ATRP reactions. This hydrolysis results in the formation of carboxylic acids, which provide the extra charges on the particles (bottom reaction, Figure 4.19b).

To support this hypothesis, ζ potentials were measured as function of pH. At pH values well below the pK_a of carboxylic acids ($pH \leq 4$),⁸⁹ the charges should vanish due to protonation (Figure 4.19a). Figure 4.19b depicts the results of a titration experiment where the ζ potentials was measured as function of the pH. At pH values above the pK_a the particles are clearly negatively charged. In agreement with the rough estimation of the pK_a , this negative charge starts to decrease if the pH drops below 4. Protonation, and therefore uncharging of the colloids, proceeds with decreasing pH until hardly any charge is left at the final pH of 2.5. In this final situation, the investigated system resembles the ideal case of a hard charged core with an uncharged ‘fuzzy’ layer, resulting in a significantly higher potential than the ζ potential of the bare particles (~ -50 mV).

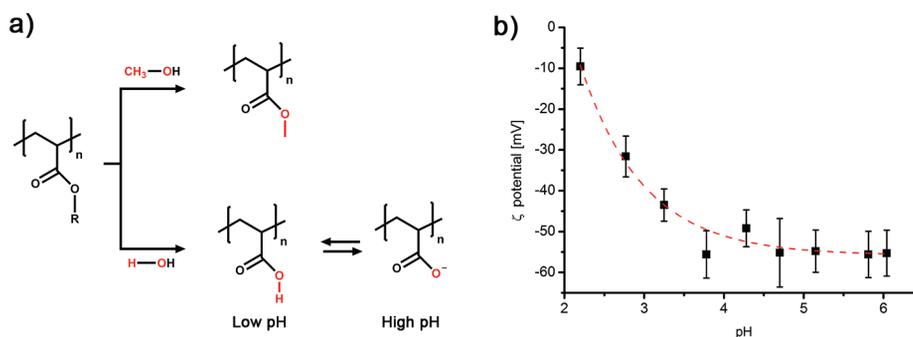


Figure 4.19. (a) Schematic picture of transesterification reactions which can occur during an ATRP reaction of 2-hydroxyethyl acrylate (HEA) in mixtures of methanol and water. Reaction with methanol leads to the formation of methyl esters (top), while hydrolysis produces carboxylic acids. (b) Titration curve of the ζ potential of colloids equipped with a p(HEA) brush prepared in methanol/water mixtures as function of pH.

The hydrolysis side reactions of (methyl)acrylates will also play a role in molecular ATRP reactions. However, to our knowledge, these reactions are never considered to be of significant importance. The degree of hydrolysis is harder to measure on a single polymer and might indeed be limited to only a small fraction of the incorporated monomers. In the presented colloidal system, where a large number of polymer chains are grafted on one single carrier colloid, the collective effect of all charges on the grafted polymers are measured simultaneously. This leads to the situation that a low degree of hydrolysis per polymer will already result in significant charging of the particles.

Physical properties of the colloidal particles are highly dependent on the surface charge. If charges on the polymers are not desired, the use of acrylates is therefore not recommended. In the previous section, particles with a p(HEAA) brush were also synthesized. These polyacrylamides have pending amides instead of esters. These amides are more stable and essentially non-hydrolysable,⁴³ which makes these grafted polymers more robust in aqueous media. The resulting system resembles the charged core surrounded by uncharged ‘fuzzy’ layers therefore much better. Regardless of the pH, we expect that the absolute ζ potential decreases with increasing brush thickness. To verify this, an ATRP reaction with HEAA as monomer was conducted. During this reaction, samples were withdrawn from the reaction mixture used to measure the ζ potential and the brush height as a function of reaction time. The results are shown in Figure 4.20a. The increase in brush thickness was estimated by an increase in hydrodynamic diameter (reported as Z-average size, Figure 4.20a, black squares). As expected, the brush height increases with increasing reaction time. The ζ potential shows the expected

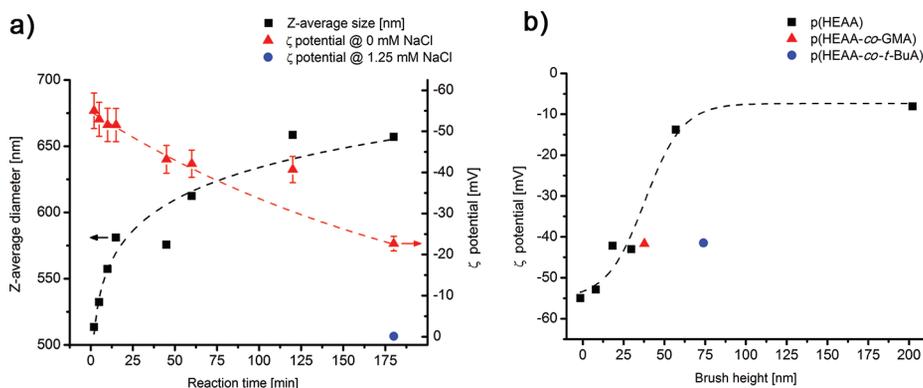


Figure 4.20. (a) Dynamic light scattering (DLS) results of particles during the formation of a poly(*N*-hydroxyethyl acrylamide) (p(HEAA)) brush. The black squares show the increase in *Z*-average diameter in time. The red triangles depict the ζ potential of the resulting particles as function of reaction time (or brush height). The blue circle shows the ζ potential of the particles obtained after 180 min of reaction dispersed in a 1.25 mM NaCl solution. (b) Plot of the brush height versus the ζ potential for p(HEAA) hairs (black squares), copolymer hairs consisting of poly(HEAA) and poly(glycidyl methacrylate) (p(HEAA-*co*-GMA)) (red triangle), and copolymer hairs consisting of poly(HEAA) and poly(*t*-butyl acrylate) (p(HEAA-*co*-*t*-BuA)) (blue dot).

opposite trend and decreases in time, i.e. with increasing brush height (Figure 4.20a, red triangles). Apparently, the brush thickness obtained after 180 min is not thick enough to push the apparent shear surface so far outwards that the charges located on the core do not contribute anymore.

If the particles are dispersed in 1.25 mM NaCl solution, the measured potential approaches zero. In this situation the charges are completely screened within the neutral polymer brush, or more precisely formulated, within the apparent shear surface.

Finally, also the ζ potentials of particles equipped with a p(HEAA) spacer and a polymethacrylate (GMA or *t*-BuA) end-block were measured (Figure 4.20b). In both cases a more negative potential was measured compared to the particles equipped with a homopolymer of p(HEAA) (Figure 4.20a). This clearly illustrates that incorporation of a small fraction of hydrolysable acrylates leads to the formation of enough charges to shift the ζ potential to large negative values.

From these results we concluded that the choice of monomer is crucial. Even when the unwanted reactions seem negligible in a molecular ATRP reaction, the collective effect of grafting a large amount of polymers on one carrier particle can lead to significant alternation of the physical properties of the resulting colloids.

4.4. Conclusions

In this chapter the theoretical aspects of ATRP were discussed, together with strategies to apply this polymerization technique for the grafting of polymers from (colloidal) surfaces. These theoretical considerations were illustrated by a set of experiments which shows the preparation of two types of colloidal ATRP initiators and subsequent grafting of a variety of (block-co)polymers onto the surface of these particles. Post-functionalization methods based on end-group substitutions and monomer modifications were shown to be effective for colloidal systems. These functionalizations and the formation of block-copolymers were conveniently visualized by the use of probe molecules. Lastly, it was shown that the choice of monomer and reaction conditions need to be matched to the colloidal system of interest to prevent brush cleavage or introduction of charges along the polymer backbone which alter the physical behavior of these systems.

Acknowledgments

I would like to thank Frans Dekker for performing a significant part of the experimental work presented in this chapter.

References

- [1] D. H. Napper, Steric stabilization. *J. Colloid Interface Sci.* **1977**, *58*, 390–407.
- [2] O. Azzaroni, Polymer brushes here, there, and everywhere: Recent advances in their practical applications and emerging opportunities in multiple research fields. *J. Polym. Sci., Part A: Polym. Chem.* **2012**, *50*, 3225–3258.
- [3] C. M. Hui, J. Pietrasik, M. Schmitt, C. Mahoney, J. Choi, M. R. Bockstaller, K. Matyjaszewski, Surface-initiated polymerization as an enabling tool for multifunctional (nano-)engineered hybrid materials. *Chem. Mater.* **2014**, *26*, 745–762.
- [4] S. Edmondson, V. L. Osborne, W. T. S. Huck, Polymer brushes via surface-initiated polymerizations. *Chem. Soc. Rev.* **2004**, *33*, 14–22.
- [5] R. Advincula, Polymer brushes by anionic and cationic surface-initiated polymerization. *Adv. Polym. Sci.* **2006**, *197*, 107–136.
- [6] R. Advincula, Q. Zhou, M. Park, S. Wang, J. Mays, G. Sakellariou, S. Pispas, N. Hadjichristidis, Polymer brushes by living anionic surface initiated polymerization on flat silicon (SiO_x) and gold surfaces: Homopolymers and block copolymers. *Langmuir* **2002**, *18*, 8672–8684.
- [7] R. Jordan, A. Ulman, Surface initiated living cationic polymerization of 2-oxazolines. *J. Am. Chem. Soc.* **1998**, *120*, 243–247.

- [8] M. Weck, J. J. Jackiw, R. R. Rossi, P. S. Weiss, R. H. Grubbs, Ring-opening metathesis polymerization from surfaces. *J. Am. Chem. Soc.* **1999**, *121*, 4088–4089.
- [9] K. J. Watson, J. Zhu, S. T. Nguyen, C. A. Mirkin, Hybrid nanoparticles with block copolymer shell structures. *J. Am. Chem. Soc.* **1999**, *121*, 462–463.
- [10] R. Barbey, L. Lavanant, D. Paripovic, N. Schüwer, C. Sugnaux, S. Tugulu, H.-A. Klok, Polymer brushes via surface-initiated controlled radical polymerization: Synthesis, characterization, properties, and applications. *Chem. Rev.* **2009**, *109*, 5437–5527.
- [11] S. G. Boyes, A. M. Granville, M. Baum, B. Akgun, B. K. Mirous, W. J. Brittain, Polymer brushes—surface immobilized polymers. *Surf. Sci.* **2004**, *570*, 1–12.
- [12] M. K. Brinks, A. Studer, Polymer brushes by nitroxide-mediated polymerization. *Macromol. Rapid Commun.* **2009**, *30*, 1043–1057.
- [13] M. Baum, W. J. Brittain, Synthesis of polymer brushes on silicate substrates via Reversible Addition-Fragmentation chain Transfer technique. *Macromolecules* **2002**, *35*, 610–615.
- [14] C. Li, B. C. Benicewicz, Synthesis of well-defined polymer brushes grafted onto silica nanoparticles via surface Reversible Addition-Fragmentation chain Transfer polymerization. *Macromolecules* **2005**, *38*, 5929–5936.
- [15] J. Pyun, T. Kowalewski, K. Matyjaszewski, Synthesis of polymer brushes using Atom Transfer Radical Polymerization. *Macromol. Rapid Commun.* **2003**, *24*, 1043–1059.
- [16] T. von Werne, T. E. Patten, Atom Transfer Radical Polymerization from nanoparticles: A tool for the preparation of well-defined hybrid nanostructures and for understanding the chemistry of controlled/“living” radical polymerizations from surfaces. *J. Am. Chem. Soc.* **2001**, *123*, 7497–7505.
- [17] K. Matyjaszewski, Atom Transfer Radical Polymerization (ATRP): Current states and future perspectives. *Macromolecules* **2012**, *45*, 4015–4039.
- [18] W. A. Braunecker, K. Matyjaszewski, Controlled/living radical polymerization: Features, developments and perspectives. *Prog. Polym. Sci.* **2007**, *32*, 93–146.
- [19] K. Matyjaszewski, J. Xia, Atom Transfer Radical Polymerization. *Chem. Rev.* **2001**, *101*, 2921–2990.
- [20] K. Matyjaszewski, N. V. Tsarevsky, Nanostructured functional materials prepared by Atom Transfer Radical Polymerization. *Nat. Chem.* **2009**, *1*, 276–288.
- [21] T. E. Patten, K. Matyjaszewski, Atom Transfer Radical Polymerization and the synthesis of polymeric materials. *Adv. Mater.* **1998**, *10*, 901–915.
- [22] A. Rudin, In *The elements of polymer science and engineering*, 2nd ed.; Academic Press: San Diego, 1999.

- [23] A. M. van Herk, In *Chemistry and technology of emulsion polymerisation*, 1st ed.; Blackwell Publishing Ltd, Oxford, UK, 2005.
- [24] N. Hadjichristidis, M. Pitsikalis, S. Pispas, H. Iatrou, Polymers with complex architecture by living anionic polymerization. *Chem. Rev.* **2001**, *101*, 3747–3792.
- [25] M. Szwarc, Living polymers and mechanisms of anionic polymerization. *Adv. Polym. Sci.* **1983**, *49*, 1–177.
- [26] S. Aoshima, S. Kanaoka, A renaissance in living cationic polymerization. *Chem. Rev.* **2009**, *109*, 5245–5287.
- [27] C. W. Bielawskia, R. H. Grubbs, Living ring-opening metathesis polymerization. *Prog. Polym. Sci.* **2007**, *32*, 1–29.
- [28] R. R. Schrock, Living ring-opening metathesis polymerization catalyzed by well-characterized transition-metal alkylidene complexes. *Acc. Chem. Res.* **1990**, *23*, 158–165.
- [29] M. Kamigaito, T. Ando, M. Sawamoto, Metal-catalyzed living radical polymerization. *Chem. Rev.* **2001**, *101*, 3689–3745.
- [30] C. J. Hawker, A. W. Bosman, E. Harth, New polymer synthesis by Nitroxide Mediated living radical Polymerizations. *Chem. Rev.* **2001**, *101*, 3661–3688.
- [31] J. Nicolas, Y. Guillaneuf, C. Lefay, D. Bertin, D. Gimes, B. Charleux, Nitroxide-Mediated Polymerization. *Prog. Polym. Sci.* **2013**, *38*, 63–235.
- [32] J. Chiefari, Y. K. Chong, F. Ercole, J. Krstina, J. Jeffery, T. P. T. Le, R. T. A. Mayadunne, G. F. Meijs, C. L. Moad, G. Moad, E. Rizzardo, S. H. Thang, Living free-radical polymerization by Reversible Addition-Fragmentation chain Transfer: The RAFT process. *Macromolecules* **1998**, *31*, 5559–5562.
- [33] A. Favier, M.-T. Charreyre, Experimental requirements for an efficient control of free-radical polymerizations via the Reversible Addition-Fragmentation chain Transfer (RAFT) process. *Macromol. Rapid Commun.* **2006**, *27*, 653–692.
- [34] S. Perrier, P. Takolpuckdee, Macromolecular design via Reversible Addition-Fragmentation chain Transfer (RAFT)/xanthates (MADIX) polymerization. *J. Polym. Sci., Part A: Polym. Chem.* **2005**, *43*, 5347–5393.
- [35] A. Debuigne, R. Poli, C. Jérôme, R. Jérôme, C. Detrembleur, Overview of cobalt-mediated radical polymerization: Roots, state of the art and future prospects. *Prog. Polym. Sci.* **2009**, *34*, 211–239.
- [36] B. M. Rosen, V. Percec, Single-electron transfer and single-electron transfer degenerative chain transfer living radical polymerization. *Chem. Rev.* **2009**, *109*, 5069–5119.
- [37] J. Qui, B. Charleux, K. Matyjaszewski, Controlled/living radical polymerization in aqueous media: Homogeneous and heterogeneous systems. *Prog. Polym. Sci.* **2001**, *26*, 2083–2134.

- [38] Features of Controlled/"Living" Radical Polymerizations - Matyjaszewski Polymer Group - Carnegie Mellon University. <http://www.cmu.edu/maty/crp/feature-development-crp/features.html>, April 2014.
- [39] B. D. Coleman, T. G. Fox, A multistate mechanism for homogeneous ionic polymerization. II. The molecular weight distribution. *J. Am. Chem. Soc.* **1963**, *85*, 1241–1244.
- [40] G. Litvinenko, A. H. E. Müller, General kinetic analysis and comparison of molecular weight distributions for various mechanisms of activity exchange in living polymerizations. *Macromolecules* **1997**, *30*, 1253–1266.
- [41] M. Zhong, K. Matyjaszewski, How fast can a CRP be conducted with preserved chain end functionality? *Macromolecules* **2011**, *44*, 2668–2677.
- [42] J. Listak, W. Jakubowski, L. Mueller, A. Plichta, K. Matyjaszewski, M. R. Bockstaller, Effect of symmetry of molecular weight distribution in block copolymers on formation of "metastable" morphologies. *Macromolecules* **2008**, *41*, 5919–5927.
- [43] M. A. Fox, J. K. Whitesell, In *Organic chemistry*, 3rd ed.; Jones and Bartlett Publishers: Sudbury, MA, 2003.
- [44] N. D. Treat, N. Ayres, S. G. Boyes, W. J. Brittain, A facile route to poly(acrylic acid) brushes using Atom Transfer Radical Polymerization. *Macromolecules* **2006**, *39*, 26–29.
- [45] K. A. Davis, K. Matyjaszewski, Atom Transfer Radical Polymerization of *tert*-butyl acrylate and preparation of block copolymers. *Macromolecules* **2000**, *33*, 4039–4047.
- [46] C. Boyer, A. H. Soeriyadi, P. B. Zetterlund, M. R. Whittaker, Synthesis of complex multiblock copolymers via a simple iterative Cu(0)-mediated radical polymerization approach. *Macromolecules* **2011**, *44*, 8028–8033.
- [47] N. V. Tsarevsky, B. M. Cooper, O. J. Wojtyna, N. M. Jahed, H. Gao, K. Matyjaszewski, Halogen exchange in Atom Transfer Radical Polymerization as a route to well-defined block copolymers. *Polym. Prepr.* **2005**, *46*, 249–250.
- [48] P. B. Zetterlund, Y. Kagawa, M. Okubo, Controlled/living radical polymerization in dispersed systems. *Chem. Rev.* **2008**, *108*, 3747–3794.
- [49] M. F. Cunningham, Controlled/living radical polymerization in aqueous dispersed systems. *Prog. Polym. Sci.* **2008**, *33*, 365–398.
- [50] J. Jiang, Y. Zhang, X. Guo, H. Zhang, Narrow or monodisperse, highly cross-Linked, and "living" polymer microspheres by Atom Transfer Radical Precipitation Polymerization. *Macromolecules* **2011**, *44*, 5893–5904.
- [51] V. L. Teo, B. J. Davis, N. V. Tsarevsky, P. B. Zetterlund, Successful miniemulsion ATRP using an anionic surfactant: Minimization of deactivator loss by addition of a halide salt. *Macromolecules* **2014**, *47*, 6230–6237.

- [52] C. Perruchot, M. A. Khan, A. Kamitsi, S. P. Armes, Synthesis of well-defined, polymer-grafted silica particles by aqueous ATRP. *Langmuir* **2001**, *17*, 4479–4481.
- [53] K. Ohno, T. Morinaga, S. Takeno, Y. Tsujii, T. Fukuda, Suspensions of silica particles grafted with concentrated polymer brush: Effects of graft chain length on brush layer thickness and colloidal crystallization. *Macromolecules* **2007**, *40*, 9143–9150.
- [54] T. Wu, Y. Zhang, X. Wang, S. Liu, Fabrication of hybrid silica nanoparticles densely grafted with thermoresponsive poly(*N*-isopropylacrylamide) brushes of controlled thickness via surface-initiated Atom Transfer Radical Polymerization. *Chem. Mater.* **2008**, *20*, 101–109.
- [55] B. Radhakrishnan, R. Ranjan, W. J. Brittain, Surface initiated polymerizations from silica nanoparticles. *Soft Matter* **2006**, *2*, 386–396.
- [56] J. N. Kizhakkedathu, R. Norris-Jones, D. E. Brooks, Synthesis of well-defined environmentally responsive polymer brushes by aqueous ATRP. *Macromolecules* **2004**, *37*, 734–743.
- [57] K. N. Jayachandran, A. Takacs-Cox, D. E. Brooks, Synthesis and characterization of polymer brushes of poly(*N,N*-dimethylacrylamide) from polystyrene latex by aqueous Atom Transfer Radical Polymerization. *Macromolecules* **2002**, *35*, 4247–4257.
- [58] M. Zhang, L. Liu, H. Zhao, Y. Yang, G. Fu, B. He, Double-responsive polymer brushes on the surface of colloid particles. *J. Colloid Interface Sci.* **2006**, *301*, 85–91.
- [59] G. Zheng, H. D. H. Stöver, Grafting of polystyrene from narrow disperse polymer particles by surface-initiated Atom Transfer Radical Polymerization. *Macromolecules* **2002**, *35*, 6828–6834.
- [60] V. Mittal, N. B. Matsko, A. Butté, M. Morbidelli, Functionalized polystyrene latex particles as substrates for ATRP: Surface and colloidal characterization. *Polymer* **2007**, *48*, 2806–2817.
- [61] T. K. Mandal, M. S. Fleming, D. R. Walt, Preparation of polymer coated gold nanoparticles by surface-confined living radical polymerization at ambient temperature. *Nano Lett.* **2002**, *2*, 3–7.
- [62] G. Li, J. Fan, R. Jiang, Y. Gao, Cross-linking the linear polymeric chains in the ATRP synthesis of iron oxide/polystyrene core/shell nanoparticles. *Chem. Mater.* **2004**, *16*, 1835–1837.
- [63] B. Wang, B. Li, B. Zhao, C. Y. Li, Amphiphilic Janus gold nanoparticles via combining “solid-state grafting-to” and “grafting-from” methods. *J. Am. Chem. Soc.* **2008**, *130*, 11594–11595.

- [64] E. M. Benetti, X. Sui, S. Zapotoczny, G. J. Vancso, Surface-grafted gel-brush/metal nanoparticle hybrids. *Adv. Funct. Mater.* **2010**, *20*, 939–944.
- [65] M. Daoud, J. P. Cotton, Star shaped polymers: A model for the conformation and its concentration dependence. *J. Phys.* **1982**, *43*, 531–538.
- [66] S. Berger, A. Synytska, L. Ionov, K.-J. Eichhorn, M. Stamm, Stimuli-responsive bicomponent polymer Janus particles by “grafting from”/“grafting to” approaches. *Macromolecules* **2008**, *41*, 9669–9676.
- [67] O. Azzaroni, A. A. Brown, W. T. S. Huck, Tunable wettability by clicking counterions into polyelectrolyte brushes. *Adv. Mater.* **2007**, *19*, 151–154.
- [68] X. Zhu, L. Wang, J. Lin, L. Zhang, Ordered nanostructures self-assembled from block copolymer tethered nanoparticles. *ACS Nano* **2010**, *4*, 4979–4988.
- [69] B. Liu, W. Wei, X. Qu, and Z. Yang, Janus colloids formed by biphasic grafting at a Pickering emulsion interface. *Angew. Chem., Int. Ed.* **2008**, *120*, 4037–4039.
- [70] J. Choi, C. M. Hui, J. Pietrasik, H. Dong, K. Matyjaszewski, M. R. Bockstaller, Toughening fragile matter: Mechanical properties of particle solids assembled from polymer-grafted hybrid particles synthesized by ATRP. *Soft Matter* **2012**, *8*, 4072–4082.
- [71] J. F. Moll, P. Akcora, A. Rungta, S. Gong, R. H. Colby, B. C. Benicewicz, S. K. Kumar. Mechanical reinforcement in polymer melts filled with polymer grafted nanoparticles. *Macromolecules* **2011**, *44*, 7473–7477.
- [72] Y. Li, P. Tao, A. Viswanath, B. C. Benicewicz, L. S. Schadler, Bimodal surface ligand engineering: The key to tunable nanocomposites. *Langmuir* **2013**, *29*, 1211–1220.
- [73] K. Matyjaszewski, S. G. Gaynor, A. Kulfan, M. Podwika, Preparation of hyperbranched polyacrylates by Atom Transfer Radical Polymerization. 1. Acrylic AB* monomers in “living” radical polymerizations. *Macromolecules* **1997**, *30*, 5192–5194.
- [74] B. G. P. van Ravensteijn, M. Kamp, A. van Blaaderen, W. K. Kegel, General route toward chemically anisotropic colloids. *Chem. Mater.* **2013**, *25*, 4348–4353.
- [75] D. O. H. Teare, D. C. Barwick, W. C. E. Schofield, R. P. Garrod, L. J. Ward, J. P. S. Badyal, Substrate-independent approach for polymer brush growth by surface Atom Transfer Radical Polymerization. *Langmuir* **2005**, *21*, 11425–11430.
- [76] N. V. Tsarevsky, S. A. Bencherif, K. Matyjaszewski, Graft copolymers by a combination of ATRP and two different consecutive click reactions. *Macromolecules* **2007**, *40*, 4439–4445.
- [77] J. Merchand-Brynaert, M. Deldime, I. Dupont, J. Dewez, Y. Schneider, Surface functionalization of poly(ethylene terephthalate) film and membrane by controlled wet chemistry: Chemical characterization of carboxylated surfaces. *J. Colloid Interface Sci.* **1995**, *173*, 236–244.

- [78] Z. S. Qureshi, R. DSouza, R. Mallampati, S. Valiyaveetil, Synthesis of amine functionalized block copolymers for nanopollutant removal from water. *J. Appl. Polym. Sci.* **2014**, *131*, 40943.
- [79] V. Coessens, K. Matyjaszewski, End group transformation of polymers prepared by ATRP, substitution to azides. *J. Macromol. Sci., Pure Appl. Chem.* **1999**, *36*, 667–679.
- [80] V. Coessens, T. Pintauer, K. Matyjaszewski, Functional polymers by Atom Transfer Radical Polymerization. *Prog. Polym. Sci.* **2001**, *26*, 337–377.
- [81] M.-P. Valignat, O. Theodoly, J. C. Crocker, W. B. Russel, P. M. Chaikin, Reversible self-assembly and directed assembly of DNA-linked micrometer-sized colloids. *Proc. Natl. Acad. Sci. U.S.A.* **2005**, *22*, 4225–4229.
- [82] M. E. Leunissen, R. Dreyfus, F. C. Cheong, D. G. Grier, R. Sha, N. C. Seeman, P. M. Chaikin, Switchable self-protected attractions in DNA-functionalized colloids. *Nat. Mater.* **2009**, *8*, 590–595.
- [83] N. Nakajima, Y. Ikada, Mechanism of amide formation by carbodiimide for bioconjugation in aqueous media. *Bioconjugate Chem.* **1995**, *6*, 123–130.
- [84] T. L. Doane, C.-H. Chuang, Reghan J. Hill, and Clemens Burda, Nanoparticle ζ -potentials. *Acc. Chem. Res.* **2012**, *45*, 317–326
- [85] R. J. Hill, D. A. Saville, W. B. Russel, Electrophoresis of spherical polymer-coated colloidal particles. *J. Colloid Interface Sci.* **2003**, *258*, 56–74.
- [86] M. R. Gittings, D. A. Saville, Electrophoretic behavior of bare and polymer-coated latices. *Langmuir* **2000**, *16*, 6416–6421.
- [87] X. Bories-Azeau, S. P. Armes, Unexpected transesterification of tertiary amine methacrylates during methanolic ATRP at ambient temperatures: A cautionary tale. *Macromolecules* **2002**, *35*, 10241–10243.
- [88] L. S. Connell, J. R. Jones, J. V. M. Weaver, Transesterification of functional methacrylate monomers during alcoholic copper-catalyzed Atom Transfer Radical Polymerization: Formation of compositional and architectural side products. *Polym. Chem.* **2012**, *3*, 2735–2738.
- [89] D. R. Lide, H. P. R. Frederikse, *CRC Handbook of Chemistry and Physics*, 76th ed.; CRC Press: Boca Raton, FL, 1995.

5

Thermo-reversible Aggregation of pNIPAM Grafted Colloids

Abstract

We report the synthesis of polystyrene colloids that are functionalized with a poly(*N*-isopropylacrylamide) (pNIPAM) corona. These ‘hairy’ colloids are prepared via Surface-Initiated Atom Transfer Radical Polymerization (SI-ATRP). The use of this controlled radical polymerization allows for easy control of the thickness of the pNIPAM brush. The resulting particles show thermo-reversible swelling and shrinking if dispersed in pure water. This behavior is caused by extension and collapse of the grafted pNIPAM polymers, which originates from the polymer’s lower critical solution temperature (LCST). Below this temperature the polymers are hydrophilic and extend into the aqueous continuous phase. Above the LCST, the polymers turn hydrophobic and collapse onto the polystyrene core.

If these hairy colloids are dispersed in an aqueous phase containing a slightly elevated ionic strength, the thermo-responsive behavior shifts to a completely different regime in which the particles show severe aggregation upon heating above the LCST of pNIPAM. This aggregation process is also reversible since cooling of the dispersion yields a colloidal stable dispersion again. This heating and cooling cycle can be repeated multiple times without significant signs of irreversible aggregation.

5.1. Introduction

Colloids can serve as building blocks for a variety of functional structures, such as photonic crystals,^{1,2} masks for lithography techniques,³ and templates for porous materials.⁴ Spontaneous formation of these structures is achievable using a self-assembly approach. Self-assembly requires careful design of the building blocks in terms of geometry and inter-particle interactions, and in turn enables great control over the final structure.^{5,6} Interactions between particles are tunable over a large range of strengths and even the directionality of the interaction can be controlled by making use of patchy or anisotropic colloids.⁷⁻⁹ Examples from recent literature include the use of DNA,⁹ depletion interaction,^{10,11} metal-ligand binding,¹² chemical triggers¹³ and supra-molecular hydrogen bonding¹⁴ to guide colloidal self-assembly. Some of these engineered colloidal interactions are also reversible, i.e. the interaction between the particles can be switched from repulsive to attractive by applying an external trigger, e.g. temperature or UV illumination. The reversibility of inter-particle interactions is a powerful tool if one aims for well-defined colloidal structures, since it is possible to anneal out defects by applying and turning off the specific trigger in a cyclic way. Despite the tremendous control over the fabrication of the building blocks, the self-assembly approach suffers from the non-trivial relation between building blocks and the final assembled structure.

The aforementioned methods to tune colloidal interactions suffer from the problem that the synthetic procedures required to prepare these systems are difficult and very labor intensive. Responsive polymers could be a possible candidate to overcome this problem and to guide the self-assembly behavior of the colloids in a more straightforward fashion. Many reported systems rely on the use of the thermo-responsive polymer poly(*N*-isopropylacrylamide) or in short pNIPAM. pNIPAM is well-known for its lower critical solution temperature (LCST): the polymer is water soluble below the LCST (≈ 35 °C) and becomes hydrophobic above this temperature.^{15,16} Therefore, this polymer could be a good candidate to trigger aggregation by a simple change of temperature. Although already several publications used pNIPAM polymers to steer the physical behavior of colloidal particles, most of these systems are rather ill-defined. The lack of control arises from the uncontrolled method for the introduction of pNIPAM by adsorption or direct copolymerization in the particle formation step.¹⁷⁻¹⁹ Especially the use of adsorption for the introduction of pNIPAM limits the applicability of this procedure to homogeneously interacting systems, since the polymer will distribute evenly over the surface of the colloids. This is a major disadvantage if directional or site-specific interactions are required (see Chapter 6). Additionally, often only swelling and shrinking of the pNIPAM brush is observed without altering the interactions between the particles sufficiently to induce aggregation.²⁰⁻²²

Inspired by the work of Kizhakkedathu et al.²⁰ and Jayachandran et al.²¹ we prepared charge stabilized polystyrene colloids functionalized with ATRP initiators onto their surface. A dense, covalently bound brush of pNIPAM was grafted on these colloids using Surface-Initiated Atom Transfer Radical Polymerization (SI-ATRP) of NIPAM. The thickness of the brush is easily controlled by the amount of monomer used in the ATRP reaction. We show that swelling and shrinking of the pNIPAM hairs is observed without loss of colloidal stability at low ionic strengths. Increasing the salt concentration gave rise to a completely different behavior: the particles show reversible aggregation if the temperature is raised and subsequently lowered again. This behavior is explained by an interplay between the temperature dependent hydrophobicity of the pNIPAM polymers and screening of the charged surface on which the hairs were grafted.^{23,24} As a result, this system enables us to control the inter-colloid interactions using two variables, namely the temperature and the ionic strength.

5.2. Experimental Section

5.2.1. Materials. Styrene (St, 99%), divinylbenzene (DVB, 55% mixture of isomers, tech. grade), 2-bromoisobutryl bromide (BiBb, 98%), sodium sulfate (Na_2SO_4 , ACS reagent, $\geq 99\%$, anhydrous), *N*-isopropylacrylamide (NIPAM, 97%), copper bromide (Cu(I)Br , 98%), *N,N,N',N',N''*-pentamethyldiethylenetriamine (PMDETA, 99%) and polyethylene glycol sorbitan monolaurate (Tween[®]20) were obtained from Sigma-Aldrich. Potassium persulfate (KPS, $> 99\%$ for analysis), sodium bisulfite (NaHSO_3 , ACS reagent) and pyridine ($> 99\%$) were purchased from Acros Organics. Methanol (MeOH, exceeds ACS specifications) was obtained from J.T. Baker and dichloromethane (DCM, peptide synthesis) from Biosolve. Sodium chloride (NaCl , ACS reagent, $\geq 99.5\%$) was purchased from Merck. All chemicals were used as received. 2-(2-bromoisobutyryloxy) ethyl acrylate (BIEA) was prepared as described in Chapter 4, Section 4.2.2.²⁶ The water used throughout all syntheses was purified using a Milli-Q water purification system.

5.2.2. Preparation of BIEA-polystyrene core-shell colloids. Brominated colloids (CPs-Br) were prepared using the same core-shell approach as described in Chapter 4, Section 4.2.4. Cross-linked polystyrene particles with a radius of 125 nm and a polydispersity of 3.8% as determined with transmission electron microscopy (TEM) were prepared. A cross-linked shell containing styrene, DVB and BIEA was grown on these particles via a seeded emulsion polymerization yielding particles with a hydrodynamic radius of 184 nm and a polydispersity index (PDI) of 0.028. The presence of the bromine moieties was confirmed using IR spectroscopy (1732 cm^{-1}).

An analogous method was used to prepare larger BIEA-p(St) core-shell colloids. These larger particles could be visualized more easily with optical microscopy. To this end, a larger cross-linked seed was used. The seeds were prepared by applying the

same procedure as described above, but by lowering the amount of SDS from 0.25 g to 0.125 g (see Section 2.2.2). This resulted in particles with a radius of 225 nm and a PDI of 0.031 as determined with dynamic light scattering (DLS). The BIEA coated particles based on these seeds were particles with a hydrodynamic radius of 255 nm and a PDI of 0.030.

5.2.3. Atom Transfer Radical Polymerization (ATRP) of NIPAM on the BIEA-colloids: Synthesis of p(St)-g-p(NIPAM). In a typical experiment, NIPAM (0.12 g, 1 mmol) and Cu(I)Br (13 mg, 0.09 mmol) were weighed and transferred directly into an oven-dried Schlenk flask. A MeOH/H₂O mixture (7:3, v/v) (0.5 mL) was added and the solution was stirred for 5 min to dissolve the NIPAM and Cu(I)Br. A light green solution was obtained. After complete dissolution, PMDETA (63 μ L, 0.3 mmol) was added resulting in a blue/green mixture. The monomer/catalyst mixture was degassed by evacuation and refilling with nitrogen (three cycles).

In a separate Schlenk flask, the BIEA-colloids dispersed in a 7:3 (v/v) MeOH/H₂O mixture (0.5 mL, 2 wt %) were degassed by evacuation and refilling with nitrogen (three cycles). After degassing, the dispersion was injected into the monomer/catalyst mixture under inert atmosphere. The resulting reaction mixture was white/green. The ATRP reaction was allowed to run for 4 h at room temperature, after which the reaction was terminated by exposure of the mixture to air, yielding an intense blue color. The resulting particles were washed several times with MeOH, 50 mM NaHSO₃ solution and MilliQ water. The NaHSO₃ solution was used to facilitate the removal of the copper catalyst. Successful grafting was confirmed using IR spectroscopy and DLS measurements.

5.2.4. Characterization. Infrared (IR) spectra were obtained using a PerkinElmer FT-IR/FIR Frontier Spectrometer in attenuated total reflectance (ATR) mode. Measurements were performed on powders obtained by drying the particle dispersion.

Transmission electron microscopy pictures were taken with a Philips Technai10 electron microscope typically operating at 100 kV. Bright field images were recorded using a SIS Megaview II CCD camera. The samples were prepared by drying a drop of diluted, aqueous particle dispersion on top of polymer coated copper grids.

Dynamic light scattering (DLS) and ζ potential measurements were performed using a Malvern Zetasizer Nano using highly diluted aqueous dispersions (20 μ L of a 1 wt% dispersion in 2 mL water). DLS measurements were conducted using glass sample cells. The measurements conducted without the addition of NaCl consisted of 7 runs of 15 individual measurements in backscatter mode (173°) and were run at 20 and 40 °C. An equilibration time of 5 min was applied to ensure that the dispersions were at the set temperature. The DLS experiments performed at elevated ionic strengths (2.5, 5 or 10 mM NaCl) made use of the same settings with the difference that the number of individual runs was adjusted according to the speed at which aggregation

or stabilization occurred. The sizes of the colloids or aggregates are reported as a Z-average diameter and the corresponding polydispersity index (PDI). These values are obtained by using the cumulant method as described in ref. 27. The absolute values obtained for the Z-average diameter and the PDI for the aggregated dispersions are less reliable. Nevertheless, these values can still be used to verify if a colloidal dispersion is randomly aggregating, which results in higher Z-average diameters and PDI values.

For the ζ potential measurements, 7 runs of at least 50 individual measurements were used to obtain a statistically reliable potential. The electrophoretic mobilities were measured in MilliQ-water. Due to the low ionic strength and the relatively small dimensions of the particles, the Hückel limit of the Henry formula was used to convert the electrophoretic mobilities to ζ potentials ($\kappa R \approx 0.04$).^{28,29}

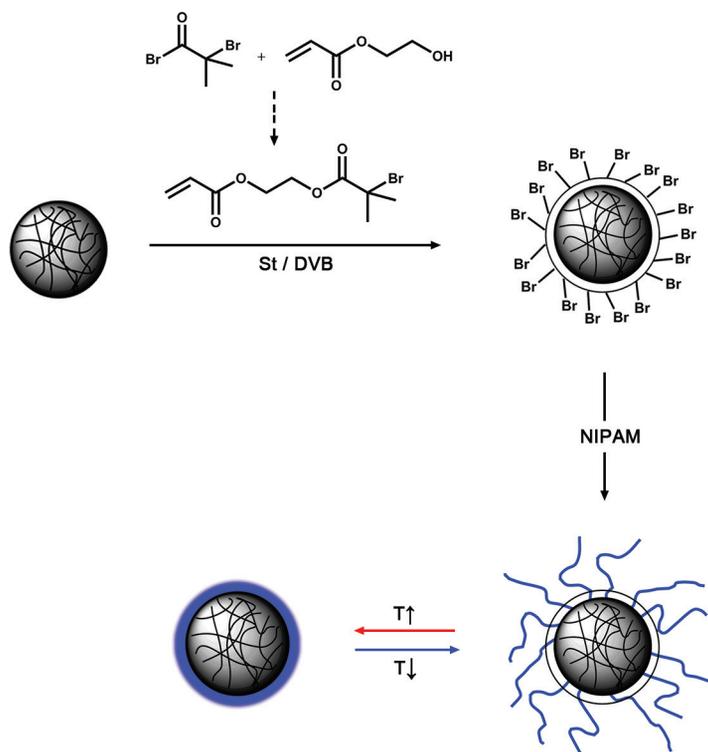
Optical microscopy images of the p(St)-*g*-p(NIPAM) particles and their thermo-reversible aggregation were obtained using a Nikon Eclipse Ti-U inverted microscope equipped with an InfiniX scout camera. A 60 \times magnification objective was used. For the reversible aggregation behavior, capillaries of 0.05 \times 1.00 mm (CM Scientific) were filled with a diluted particle dispersion containing 10 mM NaCl and 1 mM Tween[®]20. Tween[®]20 was added to prevent colloids from sticking to the capillary wall. The capillaries were subsequently flame sealed and directly placed on the heating element of a Linkam THMS 600 heating stage, which was mounted on the table of the optical microscope. The heating stage was connected to a Linkam TP 93 controller which enabled to heat and cool the capillary while the sample was monitored with the optical microscope.

5.3. Results and Discussion

5.3.1. Synthesis of polystyrene colloids equipped with a pNIPAM brush.

The synthetic route towards the pNIPAM grafted polystyrene colloids is shown in Scheme 5.1 and can be divided into three steps. The first step consists of a conventional emulsion polymerization of styrene and divinylbenzene (DVB) using potassium persulfate (KPS) as initiator. The procedure yields uniform, spherical particles which were used as seeds in the second step. A seeded emulsion polymerization with styrene, DVB and 2-(2-bromoisobutyryloxy) ethyl acrylate (BIEA) yielded monodisperse core-shell particles containing tertiary bromine groups on their surface. BIEA was easily prepared by coupling 2-hydroxyethyl acrylate to 2-bromoisobutryl bromide. Shell formation was also initiated using KPS resulting in a negatively charged surface as determined by a ζ potential measurement (-56 ± 6.9 mV). The presence of BIEA on the particles was confirmed using IR spectroscopy, which clearly shows a carbonyl signal (1730 cm^{-1}) originating from the ester moieties in the monomer.

Scheme 5.1. Schematic representation of the synthetic route towards pNIPAM (blue) grafted polystyrene (grey) colloids and its expected thermo-responsive behavior.



In the last step, the surface bromide groups were exploited as initiators for the Atom Transfer Radical Polymerization (ATRP) of *N*-isopropylacrylamide (NIPAM) using Cu(I)Br/PMDETA as catalytic system. The reaction yielded the desired polystyrene particles equipped with a pNIPAM brush. Successful grafting was readily confirmed using IR spectroscopy. Figure 5.1b shows the IR spectrum of the pNIPAM grafted colloids (p(St)-g-p(NIPAM)). pNIPAM related signals at 3300 cm^{-1} (N-H vibration), 1640 cm^{-1} (amide I; carbonyl stretching) and 1536 cm^{-1} (amide II N-H deformation) were clearly visible.³⁰ These signals were absent in the spectrum of the bare, colloidal initiators (Figure 5.1a). Additional evidence for the attachment of the pNIPAM polymers was provided by dynamic light scattering (DLS). A distinct increase of 140 nm in the hydrodynamic radius was measured (see Section 5.3.2). This increase is indicative for the brush thickness.

Dispersion of the hairy particles in a solution with an ionic strength of 500 mM did not result in loss of colloidal stability. This is a clear indication that the grafted

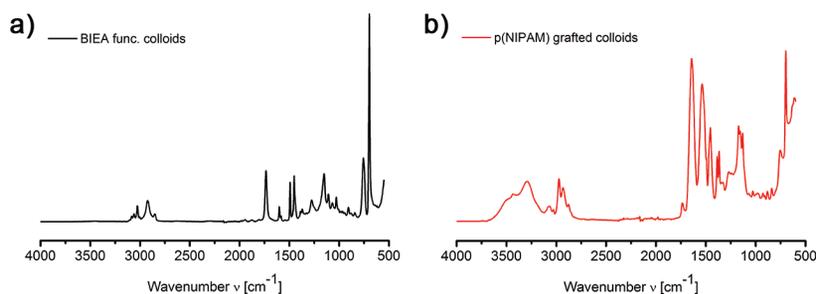


Figure 5.1. (a) Infrared (IR) spectrum of the core-shell particles containing ATRP initiators (black). (b) IR spectrum of the initiator particles grafted with pNIPAM polymers (red).

brush is dense enough to provide steric stabilization of the particles.²⁸ As a reference, introducing the bare, charge stabilized initiator particles in the same salt solution resulted immediately in a highly aggregated system.

The combined results obtained from IR spectroscopy, DLS and the enhanced stability of the polymer grafted colloids at high ionic strengths, showed that the ATRP reaction was successful and suitable for the formation of well-defined pNIPAM brushes on these polystyrene colloids.

5.3.2. Thermo-responsive behavior of p(St)-g-p(NIPAM) particles without addition of salt. Based on pNIPAM's lower critical solution temperature (LCST ≈ 35 °C) as discussed in the Introduction, we expect to measure a temperature-dependent hydrodynamic size of the pNIPAM grafted colloids. At elevated temperatures, the hydrodynamic radius should be significantly smaller than the size measured at temperatures below the LCST. To test this hypothesis, the hydrodynamic size was measured with dynamic light scattering at 20 °C (below the LCST) and 40 °C (above the LCST). During these experiments no salt was added to the system.

Figure 5.2a shows the averaged hydrodynamic diameter and polydispersity index (PDI) measured at each temperature. The measurements performed at 40 °C are highlighted with the red color. In line with our hypothesis, a significantly smaller hydrodynamic radius was measured at 40 °C compared to the sizes obtained at 20 °C. Furthermore, Figure 5.2a clearly shows the high degree of reversibility, here defined to which extent the hydrodynamic diameter of the particles recovers after the heat induced brush collapse. After each heating and cooling cycle, comparable values of the hydrodynamic diameter were obtained (Figure 5.2a). Regardless of the temperature, the PDI of the dispersion remains low. This indicates that the system remained stable throughout all the heating-cooling cycles, in line with previously reported results.^{20,21}

From the obtained values for the particle diameters we deduced that the length of the polymer hairs in the extended case was approximately equal to 140 nm, while the

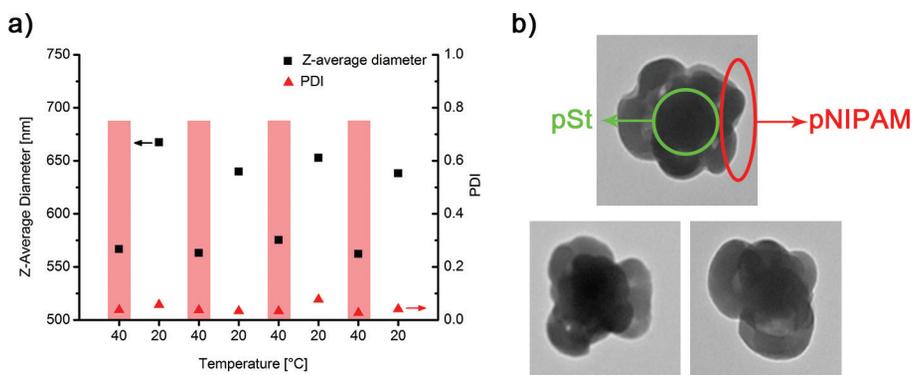


Figure 5.2. (a) Hydrodynamic diameter (black squares) and polydispersity index (PDI; red triangles) of pNIPAM grafted polystyrene colloids (140 nm brush, entry 1, Table 5.1) in deionized water as a function of temperature. The measurements performed at 40 °C are highlighted with the red areas. (b) Transmission electron microscopy (TEM) pictures of dried pNIPAM grafted polystyrene colloids. The polystyrene core is highlighted with the green circle and the collapsed pNIPAM brush with the red ellipsoid.

collapsed pNIPAM brush has a thickness of 100 nm. TEM analysis of the dried particles confirmed these large dimensions of the polymers. Figure 5.2b shows that the dried and therefore collapsed brush indeed has dimensions in the same order of magnitude as the polystyrene core onto which the hairs were grafted.

5.3.3. Thermo-responsive behavior of p(St)-g-p(NIPAM) particles at elevated ionic strength. The measurements performed in the absence of additional salt showed the reversible coil-to-globule transition of the pNIPAM brush without altering the colloidal stability of the dispersion (Section 5.3.2).

The behavior of the colloids at temperatures above the LCST of pNIPAM changes dramatically if salt is added to the dispersions. Figure 5.3a shows the change in the hydrodynamic diameter in a dispersion containing 10 mM NaCl. These low ionic strengths do not affect the solubility of the pNIPAM polymers. Salt induced coil-to-globule transitions of pNIPAM were reported in literature, but the minimal salt concentration required is on the order of 1 M. All the experiments reported here were conducted at least a factor 100 below this critical value.²⁰

Starting the DLS measurements at 20 °C gave similar values for the hydrodynamic radius as obtained for the measurements without the addition of salt (Figure 5.2a). As soon as the temperature was raised to 40 °C, the physical behavior of the colloids changed dramatically compared to the experiments without the addition of salt (Figure 5.2a). A sharp increase in both hydrodynamic diameter as well as PDI was observed (Figure 5.3a and b), clearly indicating particle aggregation. Subsequent cooling of the

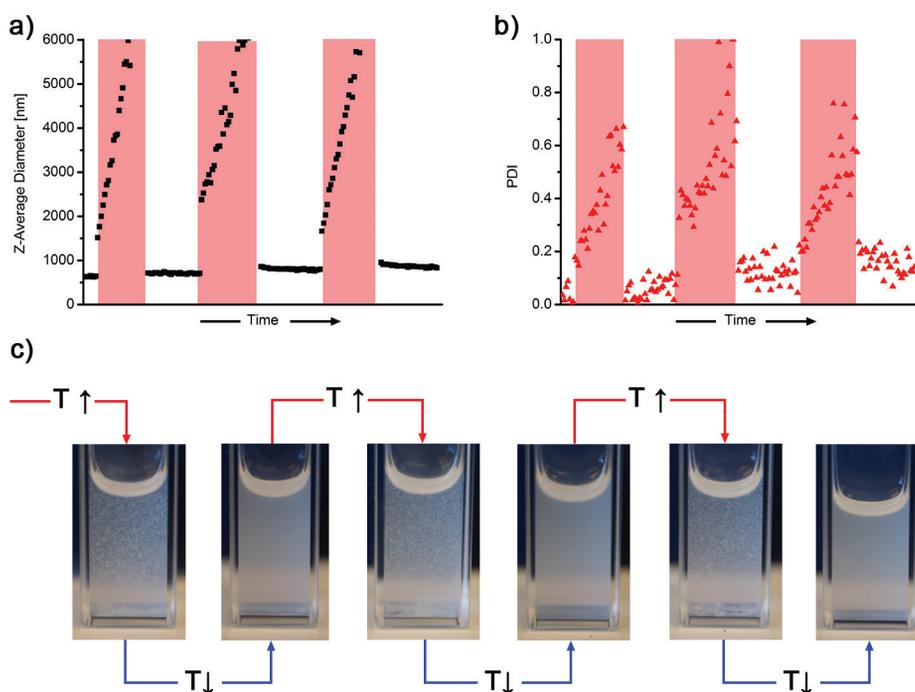


Figure 5.3. (a) Hydrodynamic diameter of pNIPAM grafted polystyrene colloids (entry 1, Table 5.1) dispersed in an aqueous 10 mM NaCl solution as a function of temperature. The measurements performed at 40 °C are highlighted with the red areas. (b) Polydispersity index (PDI) of the pNIPAM grafted polystyrene colloids dispersed in an aqueous 10 mM NaCl solution as a function of temperature. The measurements performed at 40 °C are again highlighted with the red areas. (c) Macroscopic appearance of the DLS samples which were measured to obtain the data depicted in a) and b).

dispersions, showed a decrease in hydrodynamic size and PDI to the initial values again. Repeating the temperature cycle multiple times showed that the process is truly reversible, since the initial values for the hydrodynamic size and the PDI were obtained regardless of the number of cycles that were performed (Figure 5.3a and b).

Reversible aggregation was also observed macroscopically. Figure 5.3c shows the cuvettes used for the DLS measurements of the particles at an ionic strength of 10 mM; at temperatures above the LCST of pNIPAM, flocculates were clearly visible, while a homogenous dispersion was observed at temperatures below the LCST. The homogeneous white appearance is caused by scattering of the individual colloids.

Lastly, optical microscopy was used to visualize the thermo-reversible aggregation of these colloids. To facilitate the visualization, slightly larger colloids were used in this experiment. Besides the addition of NaCl to induce aggregation, the continuous phase

also contained 1 mM of Tween[®]20 to minimize sticking of the colloids to the glass walls of the capillary. Control experiments showed that Tween[®]20 has minor influence on the aggregation behavior of the pNIPAM grafted colloids (Appendix 1, Figure 5.9). Lee et al. also reported no change in the LCST of pNIPAM after the addition of Tween[®]20, which is in agreement with our results.³¹

The formation of colloidal aggregates upon raising the temperature is evidently visible with optical microscopy (Figure 5.4b, d and f). We only allowed the formation of relatively small clusters before the temperature of the heating stage was lowered again to prevent fast sedimentation of large clusters in the small capillary cell. Lowering the temperature yielded highly dispersed colloids again (Figure 5.4a, c and e), illustrating the thermo-reversibility of this system.

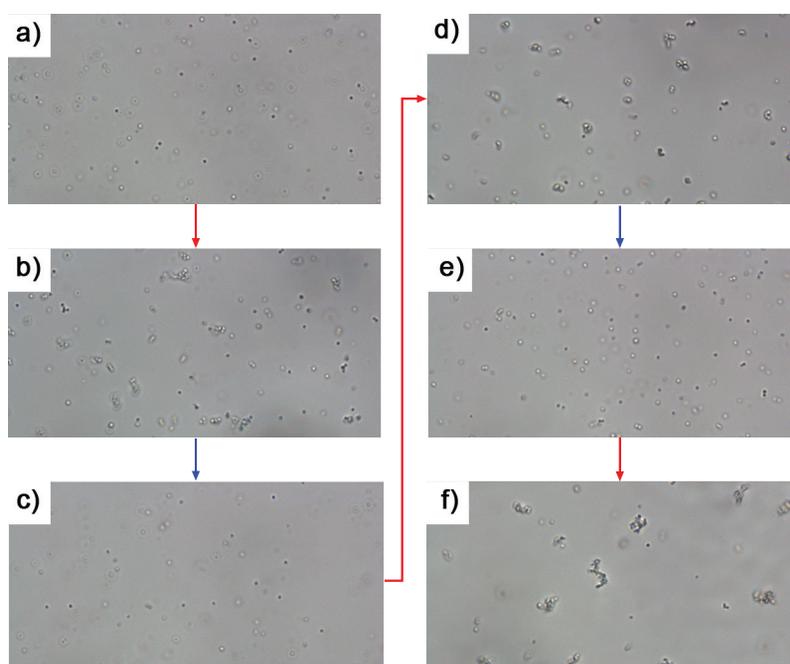


Figure 5.4. Optical microscopy images of polystyrene particles equipped with a pNIPAM brush dispersed in an aqueous 10 mM NaCl solution during cyclic heating and cooling. The pictures depicted in (a), (c) and (e) were taken at temperature below the LCST of pNIPAM, while the pictures shown in (b), (d) and (f) were obtained above the LCST. The red arrows and blue arrows represent heating and cooling, respectively.

Lowering the salt concentration to 2.5 or 5 mM NaCl did not change the physical picture and reversible aggregation was also observed. The use of lower salt

concentrations is in fact preferred over the higher salt concentration (10 mM), since the degree of reversibility, i.e. to which extent the hydrodynamic diameter of the particles recovers after the heat induced aggregation, is slightly higher at lower ionic strengths. This was concluded from the slope of the arrows drawn in Figure 5.5: the steeper slope observed for the measurements performed in an aqueous phase containing 10 mM NaCl (Figure 5.5a) compared to analogous measurements at a salt concentration of 2.5 mM (Figure 5.5b), indicated a larger contribution of irreversible aggregation and therefore a lower degree of reversibility.

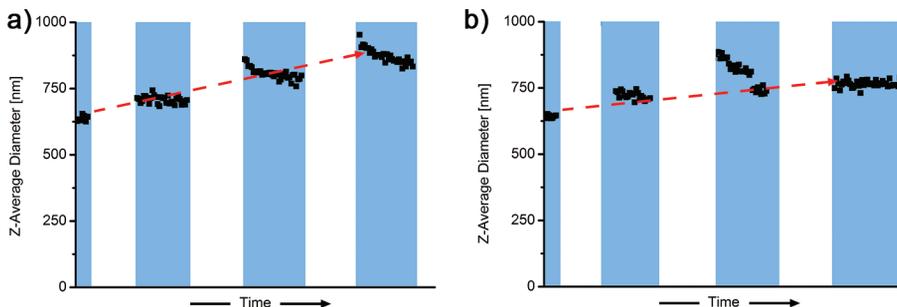


Figure 5.5. (a) The increase of Z-average diameter of the hairy particles grafted with 140 nm pNIPAM hairs (entry 1, Table 5.1) at 10 mM after the heating cycles. (b) The increase of Z-average diameter of the hairy particles grafted with 140 nm pNIPAM hairs (entry 1, Table 5.1) at 2.5 mM after the heating cycles. The highlighted areas represent the measurements conducted at 20 °C.

However, decreasing the salt concentration even further to 1 mM did not result in reversible aggregation. At this ionic strength the particles behave the same as without addition of salt (Section 5.3.2). From these experiments we concluded that there is a critical ionic strength at which reversible aggregation is induced. This can be explained intuitively by the following arguments: the interaction potential between the particles can be roughly described by two main contributions, namely an electrostatic repulsion and a hydrophobic attraction term. The electrostatic repulsion originates from the charges on the polystyrene core, while the hydrophobic interaction term takes the pNIPAM hairs into account. The hydrophobic interaction is expected to be an increasing function of the overlap area of the polymer brushes and interfacial tension (γ) between the brush and the continuous phase. In turn, γ is a function of temperature and can be written as a Taylor expansion around a reference temperature (T_0)³²

$$\begin{aligned} \gamma(T) &= \gamma(T_0) + \left(\frac{\partial \gamma}{\partial T} \right)_{T=T_0} \times (T - T_0) + \dots \\ &\approx \gamma(T_0) - s_0(T - T_0) \end{aligned} \quad (5.1)$$

where s_0 is the surface excess entropy which is negative for many hydrophobic materials and probably also for pNIPAM.³³ If this entropy term is negative, the interfacial tension and therefore the interaction strength increases with increasing temperature. In our system the negative excess entropy drives the coil-to-globule transition of pNIPAM at temperatures above the LCST. At low temperatures, the interfacial tension between the pNIPAM polymers and water is low leading to an extended polymer brush. In this situation the particles are stabilized by means of steric repulsion of the polymer brush as well as a (small) contribution of the electrostatic core-core repulsion. Upon raising the temperature above the LCST, the interfacial tension shoots up leading to a strong hydrophobic attraction between the colloids. If this thermal induced attraction is stronger than the electrostatic repulsion, the effective inter-particles potential will be attractive and particles will aggregate.

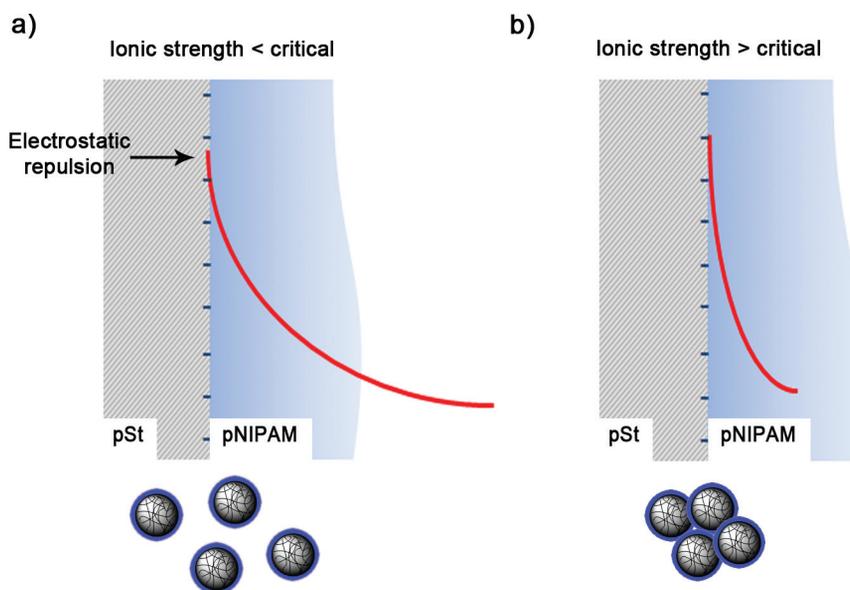


Figure 5.6. Schematic representation of the electrostatic repulsion (red) caused by the charged polystyrene particles. The polystyrene particle is shown in grey and the collapsed pNIPAM brush in blue. At ionic strengths below the critical value a residual repulsion ensures colloidal stability. Above the critical value, the potential is screened within the hydrophobic brush causing aggregation due to hydrophobic forces.

The salt dependence of the interaction follows directly from the electrostatic term. If no salt is added to the system, the negative surface charges are poorly screened resulting in an electrostatic repulsion which is effective over a distance beyond the thickness of the collapsed brush. When two particles then approach each other, the

net repulsive force will prevent the hydrophobic pNIPAM brushes from interacting and therefore, keep the particles separated (Figure 5.6a). On the other hand, if the ionic strength of the continuous phase is high enough such that the electrostatic are completely screened within the collapsed brush, the pNIPAM polymers can come into contact leading to the observed aggregation (Figure 5.6b).

Our proposed explanation implies that there must be a dependence of the critical salt concentration on the thickness of the polymer brush. If the brush is thicker, less salt is required for all the electrostatics to decay within the polymer brush. To verify if this hypothesis is reasonable the next section will treat the synthesis of particles with shorter hairs. Subsequently, their reversible aggregation behavior will be investigated as a function of the ionic strength of the dispersion medium.

5.3.4. Dependence of salt-induced thermo-reversible aggregation on the hair length. Since ATRP is a controlled radical polymerization technique, the resulting hairs are uniform in length. Tuning the hair length is easily achieved by the initial monomer concentration in the reaction mixture. The colloids used in Section 5.3.2 and 5.3.3 were grafted with pNIPAM hairs of 140 nm in the extended situation (below LCST) and 100 nm in the collapsed state (above LCST). Grafting of these hairs required an initial monomer concentration of 1 M during the ATRP reaction. Bringing this concentration down to 0.75 and 0.015 M yielded particles with significantly shorter hairs. Table 5.1 summarizes the DLS data obtained for all the hairy particles that were prepared.

Table 5.1. Hydrodynamic diameters and hair lengths of p(St)-*g*-p(NIPAM) particles at 20 °C and 40 °C as function of the initial NIPAM concentrations.

Entry	[NIPAM] [M]	D _h (20 °C) [nm]	D _h (40 °C) [nm]	Hair length 20 °C [nm]	Hair length 40 °C [nm]
1	1	650	565	142	100
2	0.75	540	500	85	65
3	0.015	387	394	11	14

The DLS results were in agreement with the IR spectra of the particles with different hair lengths. These spectra showed a decrease in the intensity of the pNIPAM related signals (3300, 1640 and 1536 cm⁻¹) if the initial monomer concentration in the reaction mixture was decreased (Figure 5.7). The particles with the shortest hairs (entry 3, Table 5.1) did not show convincing thermo-responsive behavior. Without addition of salt (Fig. 5.2a), the characteristic swelling and shrinking behavior as seen for particles with longer hairs was not observed. This could be caused by the too small difference in brush thickness between the extended and the collapsed state, since this difference seems to be proportional with the thickness of the brush (Table 5.1).

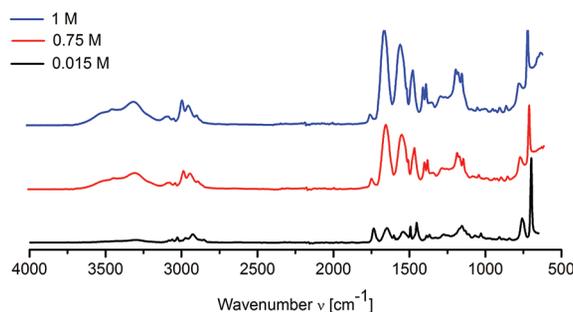


Figure 5.7. Infrared (IR) spectra of polystyrene colloids with grafted with pNIPAM brushes. The thickness of the brush depends on the initial NIPAM concentration in the reaction mixture. The black spectrum (bottom) was obtained in a reaction mixture containing 0.015 M NIPAM, the red spectrum (middle) in a mixture with 0.75 M and the blue spectrum was obtained after a reaction in a mixture with 1 M NIPAM (top).

Increasing the ionic strength up to 15 mM did not change the behavior of the short-haired particles. At even higher ionic strengths the colloidal stability of these particles at room temperature was limited, making temperature dependent measurements unreliable. The observation that the particles do not aggregate, even in the presence of rather high salt concentrations, suggests that the thin collapsed pNIPAM brush is not hydrophobic enough. Plunkett et al. also found that the collapse of end-grafted pNIPAM chains depends on both the grafting density and the molecular weight of the polymer chains.³⁴ If either the grafting density or the molecular weight drops below a critical value, no collapse was observed. With these short-haired particles, it is therefore possible that brush collapse is not induced upon heating. Consequently, no driving force for aggregation will be generated and particles remain dispersed. This feature excluded these particles from testing our hypothesis depicted in Figure 5.6.

Particles with the intermediate hair length (entry 2, Table 5.1) did show the same reversible swelling and shrinking behavior in the absence of salt as the particles with longer hairs (see Appendix 2, Figure 5.10a). Evidently, these brushes are thick enough to induce significant coil-to-globule transitions upon heating.

According to our hypothesis, the onset for reversible aggregation should be located at higher salt concentrations compared to the particles with the 140 nm hairs (entry 1, Table 5.1; see Section 5.3.2 and 5.3.3). To test this hypothesis, temperature dependent DLS measurements were again conducted at different ionic strengths. Salt concentrations of 10 and 5 mM were enough to induce reversible aggregation (see Appendix 2, Figure 5.10b and c).

However, when the same temperature dependent DLS measurements were carried out in a dispersion containing 2.5 mM salt, no aggregation was observed. Analogous

to the situation without salt, swelling/shrinking of the particles was observed without affecting the colloidal stability. In agreement with our hypothesis, the particles with the long hairs already showed aggregation at the same ionic strength (Figure 5.8a). As a control experiment the particles with the shorter hairs (entry 2, Table 5.1) were also measured in a dispersion containing 1 mM of NaCl. Also in this situation no aggregation was observed, which was expected based on the observation that a salt concentration of 2.5 mM was already below the critical salt concentration required to induce aggregation.

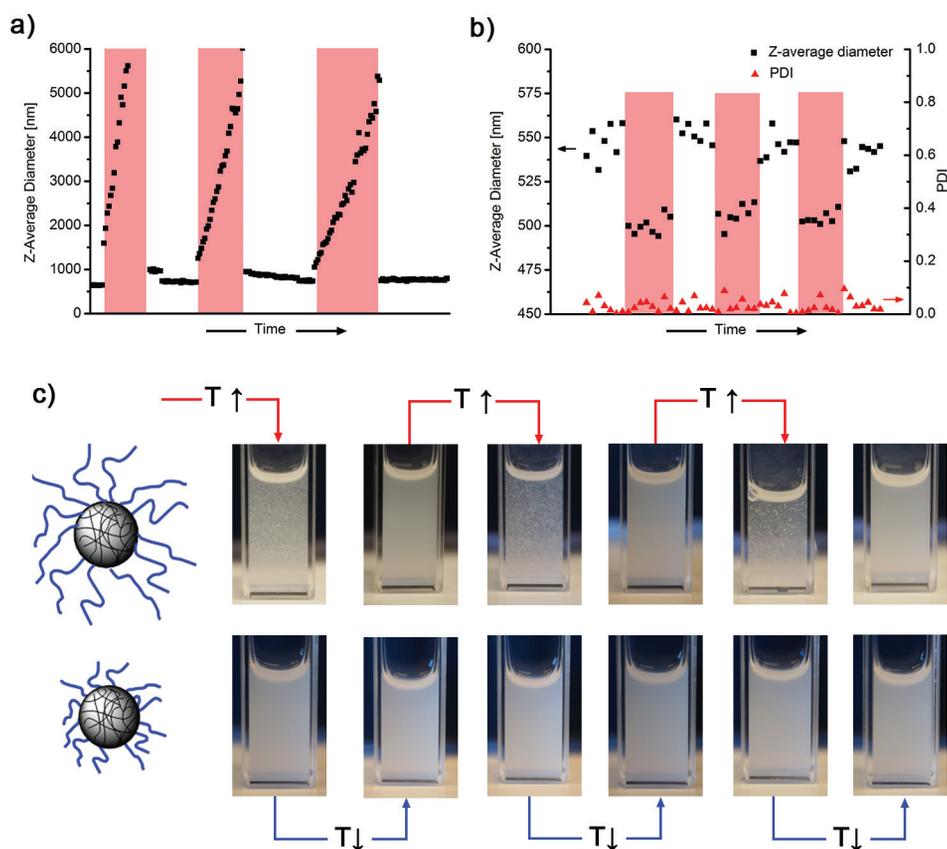


Figure 5.8. (a) The temperature dependence of the Z-average diameter (black squares) of particles grafted with 140 nm long pNIPAM hairs (entry 1, Table 5.1) at an ionic strength of 2.5 mM. (b) The temperature dependence of the Z-average diameter and polydispersity index (PDI; red triangles) of the particles grafted with 85 nm long pNIPAM hairs (entry 2, Table 5.1) at an ionic strength of 2.5 mM. (c) The macroscopic appearance of the dispersion used for the DLS measurements depicted in a) and b). The measurements performed at 40 °C are highlighted with the red areas.

So in principle the physical behavior of the particles equipped with the 85 nm long pNIPAM hairs (entry 2, Table 5.1) is completely analogous to that observed for the particles with the longest pNIPAM hairs (entry 1, Table 5.1). The only difference is the minimal concentration of salt required to shift the system from reversible swelling and shrinking to reversible aggregating.

The critical salt concentrations we find for these hairy particles are in a convenient experimental regime. Addition of low concentrations of salt completely changes the physical behavior of these systems with the restriction that the polymer brush is thick enough. Based on the argument that the interaction potential is a balance between the electrostatic repulsion and a temperature dependent hydrophobic attraction it should be possible to calculate or estimate what salt concentrations are required to let the electrostatics diminish. However, this is not a straightforward exercise. Tu et al. estimated the dielectric constant of a planar pNIPAM brush.³⁵ Values of 48 and 12 in the water swollen and collapsed brushes were found respectively. Consequently, the ionic strength in close proximity of the particles is lower than in the bulk continuous phase and the actual surface potential of the polystyrene cores is not known. The ζ potential of the bare particles is not a good measure, since for these particles the charges are directly in contact with water with a much higher dielectric constant ($\epsilon \approx 80$).

Additionally, the local dielectric constant might also depend on the position inside the polymer brush. From polymer brush theory, it is known that the segment density is not uniform along the height of a brush, especially for long brushes.^{36,37} It is fair to assume that the dielectric constant is proportional to the segment density and therefore the ions will locally feel other environments influencing the actual local salt concentration. There might also be a dependence of the segment density as a function of brush height because the brush is spherical. A simple geometric argument states that the polymer density close to the surface must be much higher and decreases outwards.

This non-uniform polymer density not only has an effect on the electrostatic contribution, but also on the hydrophobic part. Previously it was stated that the hydrophobic contribution is proportional to the surface tension (Section 5.3.3). It is reasonable to assume that the surface tension is also dependent on the polymer density at the point where the polymer brush is facing the continuous aqueous phase. A higher density results in a more hydrophobic environment and therefore in a higher surface tension between the polymer brush and the continuous phase. For particles with different hair lengths, different surface tensions might be found which complicates the comparison between particles with different brush heights even further.

Lastly, there are also practical limitations to this approach. First of all, more data would be required to make a reliable comparison with theory. ATRP enables for tuning

the brush thickness, but too short brushes are not thermo-responsive as was already observed for the particles with the shortest hairs (entry 3, Table 5.1). On the other side of the experimental range, if the brush becomes too thick the polydispersity of the resulting colloids increases, making it difficult to distinguish between initial colloidal instability and temperature induced aggregation. These synthetic limitations result in a small experimental window in which particles with the desired properties can be synthesized. The consequence being that the difference in critical salt concentrations will be very small, i.e. the difference in polymer length of entries 1 and 2 in Table 5.1 is 55 nm, while the difference in critical salt concentration is only on the order of mM.

Furthermore, the determination of the brush height based on an increase in hydrodynamic radius is merely an estimation. DLS effectively measures the slipping plane of the fluid around the colloids when they are moving in solution. For a hard particle this plane is well-defined, but for these hairy particles it is hard to predict where this plane is actually localized. The resulting hydrodynamic radius should therefore be seen as an indication for the brush thickness, rather than a precise value that can be used reliably in calculations. Models to correct for this dynamic behavior are available, although it is beyond the scope of this work to go into the details.^{38,39}

5.4. Conclusions

We have provided a synthetic procedure which yields monodisperse polystyrene particles that act as colloidal initiators in a surface-initiated ATRP reaction. This controlled radical polymerization was used to graft pNIPAM chains on the colloidal surface generating a dense brush of this polymer. Using ATRP as the grafting method, the length of the grafted polymers is easily controlled by the initial concentration of monomer. Without the addition of salt, the hairs undergo reversible swelling and shrinking as the temperature of the dispersion is brought under and above the LCST of pNIPAM, respectively. The cyclic swelling and shrinking did not affect the colloidal stability of the dispersion.

In continuous media containing low salt concentrations to screen the electrostatic repulsion originating from the charged polystyrene core leads to thermo-reversible aggregation of the colloids. This aggregation is driven by hydrophobic attractions between the pNIPAM brushes above the LCST. Reversible aggregation could only be induced if the polymer brush is sufficiently thick. The particles can undergo many aggregation cycles without any significant hysteresis, making this system truly thermo-reversible.

Appendix 1 – Thermo-reversible aggregation of p(St)-g-p(NIPAM) in the presence of Tween®20

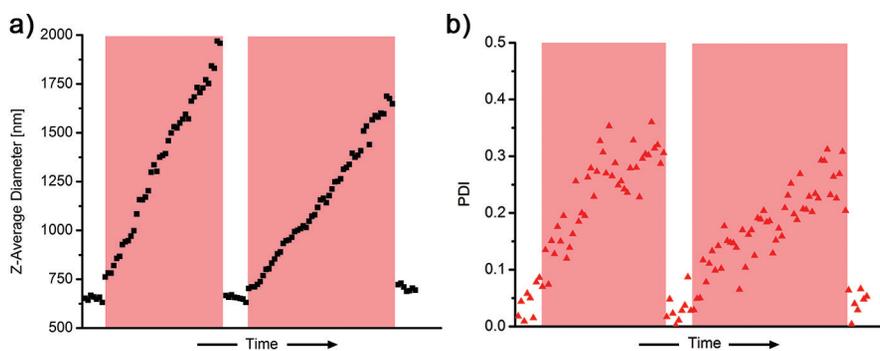


Figure 5.9. (a) The temperature dependence of the Z-average diameter of particles grafted with pNIPAM hairs (entry 1, Table 5.1) at an ionic strength of 10 mM and 1 mM of Tween®20. (b) Polydispersity index (PDI) of pNIPAM grafted polystyrene colloids (entry 1, Table 5.1) dispersed in an aqueous 10 mM NaCl solution containing 1 mM Tween®20 as a function of temperature. The measurements performed at 40 °C are highlighted with the red areas.

Appendix 2 – Thermo-responsive behaviour of polystyrene colloids with shorter pNIPAM hairs (entry 2, Table 5.1) without the addition of salt and dispersed in an aqueous solution containing 10 mM NaCl

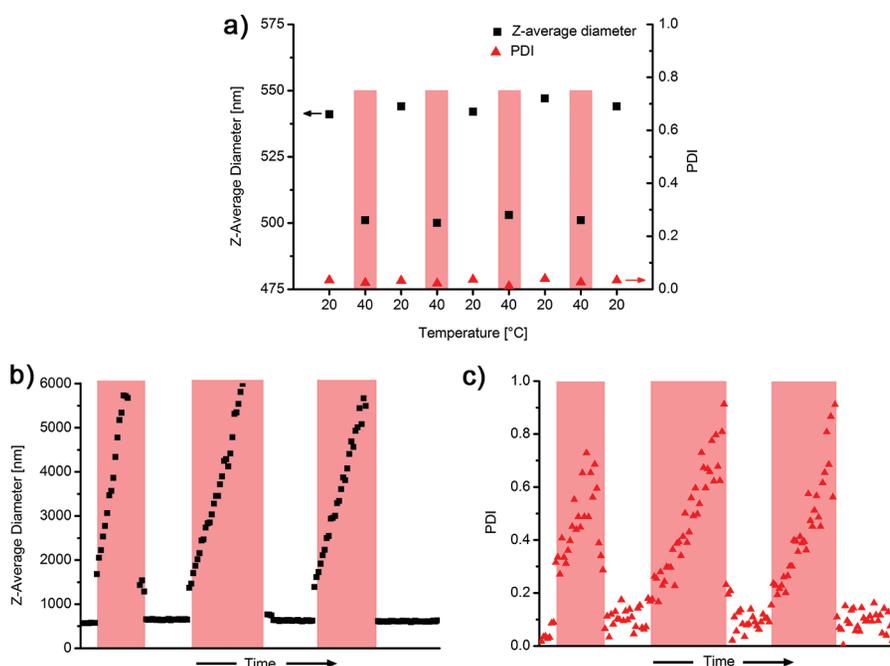


Figure 5.10. (a) Hydrodynamic diameter (black squares) and polydispersity index (PDI; red triangles) of pNIPAM grafted polystyrene colloids (85 nm hairs, entry 2, Table 5.1) dispersed in an aqueous 0 mM NaCl solution as a function of temperature. (b) Hydrodynamic diameter of pNIPAM grafted polystyrene colloids (85 nm hairs, entry 2, Table 5.1) dispersed in an aqueous 10 mM NaCl solution as a function of temperature. (c) Polydispersity index (PDI) of pNIPAM grafted polystyrene colloids (entry 2, Table 5.1) dispersed in an aqueous 10 mM NaCl solution as a function of temperature. The measurements performed at 40 °C are highlighted with the red areas in all panels.

References

- [1] H. Cong, B. Yu, J. Tang, Z. Lia and X. Liu, Current status and future developments in preparation and application of colloidal crystals. *Chem. Soc. Rev.* **2013**, *42*, 7774–7800.
- [2] F. Li, D. P. Josephson, A. Stein, Colloidal assembly: The road from particles to colloidal molecules and crystals. *Angew. Chem., Int. Ed.* **2011**, *50*, 360–388.

-
- [3] S.-M. Yang, S. G. Jang, D.-G. Choi, S. Kim, H. K. Yu, Nanomachining by colloidal lithography. *Small* **2006**, *2*, 458–475.
- [4] O. D. Velev, E. W. Kaler, Structured porous materials via colloidal crystal templating: From inorganic oxides to metals. *Adv. Mater.* **2000**, *12*, 531–534.
- [5] S. C. Glotzer, M. J. Solomon, Anisotropy of building blocks and their assembly into complex structures. *Nat. Mater.* **2007**, *6*, 557–562.
- [6] A. B. Pawar, I. Kretzschmar, Fabrication, Assembly, and application of patchy particles. *Macromol. Rapid Commun.* **2010**, *31*, 150–168.
- [7] G.-R. Yi, D. J. Pine, S. Sacanna, Recent progress on patchy colloids and their self-assembly. *Phys.: Condens. Matter* **2013**, *25*, No. 193101.
- [8] Q. Chen, J. K. Whitmer, S. Jiang, S. C. Bae, E. Luijten, S. Granick, Supracolloidal reaction kinetics of Janus spheres. *Science* **2011**, *331*, 199–202.
- [9] Y. Wang, Y. Wang, D. R. Breed, V. N. Manoharan, L. Feng, A. D. Hollingsworth, M. Weck, D. J. Pine, Colloids with valence and specific directional bonding. *Nature* **2013**, *491*, 51–56.
- [10] D. J. Kraft, R. Ni, F. Smalenburg, M. Hermes, K. Yoon, D. A. Weitz, A. van Blaaderen, J. Groenewold, M. Dijkstra, W. K. Kegel, Surface roughness directed self-assembly of patchy particles into colloidal micelles. *Proc. Natl. Acad. Sci. U.S.A.* **2012**, *109*, 10787–10792.
- [11] J. R. Wolters, G. Avvisati, F. Hagemans, T. Vissers, D. J. Kraft, M. Dijkstra, W. K. Kegel, Self-assembly of “Mickey Mouse” shaped colloids into tube-like structures: experiments and simulations. *Soft Matter* **2015**, *11*, 1067–1077.
- [12] Y. Wang, A. D. Hollingsworth, S. K. Yang, S. Patel, D. J. Pine, M. Weck, Patchy particle self-assembly via metal coordination, *J. Am. Chem. Soc.* **2013**, *135*, 14064–14067.
- [13] Q. Zhang, W.-J. Wang, Y. Lu, B.-G. Li, S. Zhu, Reversibly coagulatable and redispersible polystyrene latex prepared by emulsion polymerization of styrene containing switchable amidine. *Macromolecules* **2011**, *44*, 6539–6545.
- [14] I. de Feijter, L. Albertazzi, A. R. A. Palmans, I. K. Voets, Stimuli-responsive colloidal assembly driven by surface-grafted supramolecular moieties. *Langmuir* **2015**, *31*, 57–64.
- [15] M. Heskins, J. E. Guillet, Solution properties of poly(*N*-isopropylacrylamide). *J. Macromol. Sci., Chem.* **1968**, *2*, 1441–1455.
- [16] H. G. Schild, Poly(*N*-isopropylacrylamide): Experiment, theory and application. *Prog. Polym. Sci.* **1992**, *17*, 163–249.
- [17] P. W. Zhu, D. H. Napper, Studies of aggregation kinetics of polystyrene latices sterically stabilized by poly(*N*-isopropylacrylamide). *Phys. Rev. E* **1994**, *50*, 1360–1366.

- [18] M.-Q. Chen, T. Serizawa, M. Li, C. Wu, M. Akashi, Thermosensitive behavior of poly(*N*-isopropylacrylamide) grafted polystyrene nanoparticles. *Polym. J.* **2003**, *35*, 901–910.
- [19] T. E. Kodger, J. Sprakel, Thermosensitive molecular, colloidal, and bulk interactions using a simple surfactant. *Adv. Funct. Mater.* **2013**, *23*, 475–482.
- [20] J. N. Kizhakkedathu, R. Norris-Jones, D. E. Brooks, Synthesis of well-defined environmentally responsive polymer brushes by aqueous ATRP. *Macromolecules* **2004**, *37*, 734–743.
- [21] K. N. Jayachandran, A. Takacs-Cox, D. E. Brooks, Synthesis and characterization of polymer brushes of poly(*N,N*-dimethylacrylamide) from polystyrene latex by aqueous Atom Transfer Radical Polymerization. *Macromolecules* **2002**, *35*, 4247–4257.
- [22] T. Wu, Y. Zhang, X. Wang, S. Liu, Fabrication of hybrid silica nanoparticles densely grafted with thermoresponsive poly(*N*-isopropylacrylamide) brushes of controlled thickness via surface-initiated Atom Transfer Radical Polymerization. *Chem. Mater.* **2008**, *20*, 101–109.
- [23] S. Yusa, K. Fukuda, T. Yamamoto, Y. Iwasaki, A. Watanabe, K. Akiyoshi, Y. Morishima, Salt effect on the heat-induced association behavior of gold nanoparticles coated with poly(*N*-isopropylacrylamide) prepared via Reversible Addition-Fragmentation chain Transfer (RAFT) radical polymerization. *Langmuir* **2007**, *23*, 12842–12848.
- [24] Z. Zhang, S. Maji, A. Bruno da Fonseca Antunes, R. de Rycke, Q. Zhang, R. Hoogenboom, B. G. de Geest, Salt plays a pivotal role in the temperature-responsive aggregation and layer-by-layer assembly of polymer-decorated gold nanoparticles. *Chem. Mater.* **2013**, *25*, 4297–4303.
- [25] K. Matyjaszewski, S. G. Gaynor, A. Kulfan, M. Podwika, Preparation of hyperbranched polyacrylates by atom transfer radical polymerization. 1. Acrylic AB* monomers in “living” radical polymerizations. *Macromolecules* **1997**, *30*, 5192–5194.
- [26] B. G. P. van Ravensteijn, M. Kamp, A. van Blaaderen, W. K. Kegel, General route toward chemically anisotropic colloids. *Chem. Mater.* **2013**, *25*, 4348–4353.
- [27] J. C. Thomas, The determination of log normal particle size distributions by dynamic light scattering. *J. Colloid Interface Sci.* **1987**, *117*, 187–192.
- [28] H. Ohshima, A simple expression for Henry’s function for the retardation effect in electrophoresis of spherical colloidal particles. *J. Colloid Interface Sci.* **1994**, *168*, 269–271.
- [29] R. J. Hunter, In *Foundations of Colloid Science*, 2nd ed.; Oxford University Press: New York, 2009.

-
- [30] G. Socrates, In *Infrared and Raman Characteristic Groups Frequencies*, 3rd ed.; John Wiley & Sons Ltd: Chichester, England, 2001.
- [31] M. S. Lee, J.-C. Kim, Effects of Surfactants on phase transition of poly(*N*-isopropylacrylamide) and poly(*N*-isopropylacrylamide-*co*-dimethylamino-ethylacrylate). *J. Dispersion Sci. Technol.* **2012**, *33*, 272–277.
- [32] W. K. Kegel, P. van der Schoot, Competing hydrophobic and screened-Coulomb interactions in Hepatitis B virus capsid assembly. *Biophys. J.* **2004**, *86*, 3905–3913.
- [33] P. M. Claesson, R. Kjellander, P. Stenius and H. K. Christenson, Direct measurement of temperature-dependent interactions between nonionic surfactant layers. *J. Chem. Soc. Faraday Trans.* **1986**, *82*, 2735–2746.
- [34] K. N. Plunkett, X. Zhu, J. S. Moore, D. E. Leckband, pNIPAM chain collapse depends on the molecular weight and grafting density. *Langmuir* **2006**, *22*, 4259–4266.
- [35] H. Tu, L. Hong, S. M. Anthony, P. V. Braun, S. Granick, Brush-sheated particles diffusing at brush-coated surfaces in the thermally responsive PNIPAAm system. *Langmuir* **2007**, *23*, 2322–2325.
- [36] B. Zhao, W. J. Brittain, Polymer brushes: Surface-immobilized macromolecules. *Prog. Polym. Sci.* **2000**, *25*, 677–710.
- [37] S. T. Milner, Polymer brushes. *Science* **1991**, *251*, 905–914.
- [38] R. J. Hill, D. A. Saville, ‘Exact’ solutions of the full electrokinetic model for soft spherical colloids: Electrophoretic mobility. *Colloids Surf., A* **2005**, *267*, 31–49.
- [39] I. Berndt, J. S. Pedersen, W. Richtering, Temperature-sensitive core–shell microgel particles with dense shell. *Angew. Chem., Int. Ed.* **2006**, *118*, 1769–1773.

6

Site-specific Surface Modification of Patchy Colloids using Atom Transfer Radical Polymerization

Abstract

In this chapter, chemically anisotropic dumbbells are prepared of which one lobe is functionalized with initiators for Atom Transfer Radical Polymerization (ATRP). These initiators are exploited for site-specific grafting of poly(*N*-isopropylacrylamide) (pNIPAM) brushes on the reactive patches. The geometric ratio between the grafted and non-grafted lobe is tunable by the shape of the initial dumbbell and the pNIPAM grafting time. These partially grafted particles are employed as building blocks for finite-sized colloidal clusters. Two preparation routes are followed. The first route relies on inducing attraction between the non-grafted lobes by increasing the ionic strength of the dispersion medium. The grafted lobes remain non-attractive due to steric stabilization of the grafted polymers. The bonds created to form these clusters are essentially irreversible, thereby limiting the dynamic behavior of these assemblies. Therefore, the second route exploits the temperature responsive properties of the pNIPAM patches to induce thermo-reversible, directional bonds between the particles.

6.1. Introduction

The self-assembly behavior of relatively simple colloidal particles such as spheres, rods and platelets into (liquid) crystals has provided fundamental insight into self-organization mechanisms active on the atomistic and molecular length scales.¹⁻⁵ However, these rather simple colloidal analogues of atoms and molecules clearly fail to capture the assembly processes involved in the formation of more complex (biological) structures such as DNA,^{6,7} virus capsids,^{6,8} and microtubules.⁹ To widen the scope of colloidal self-assembly towards these intriguing examples, colloidal building blocks with anisotropic interactions and/or shape are required.¹⁰⁻¹¹ Especially particles that are able to form directional inter-particle bonds are promising candidates for the formation of new colloidal superstructures. These so-called patchy particles are building blocks that contain one or more specific regions, i.e. patches, that are attractive towards each other. The final assembled structure is in principle determined by the number and distribution of patches over the particle surface. Computer simulations demonstrated the versatility of patchy particles and a wide variety of complex or low-coordination structures were observed as a function of the building block geometry.¹²⁻¹⁸ Experimental realization of these systems remains a challenging task. Despite a few ingenious systems,^{19,20,23,24} most synthetic procedures applied to prepare these particles, such as selective deposition, surface templating, and lithography, are difficult to perform and suffer from low yields, hampering systematic study of these systems.^{21,22}

Applying wet-chemical bulk synthesis methods towards patchy particles will greatly enhance the yield and therefore the availability of these complex building blocks. Recently, patchy systems with directional interactions were prepared via relatively simple emulsion/dispersion based synthesis routes. Colloidal particles with anisotropic shape and one or multiple rough patches were synthesized.^{23,24} Addition of a depletant to dispersions containing these colloids results in a directional depletion interaction and the formation of colloidal micelles²³ or tubular structures.²⁴

In this chapter, we combine the chemically anisotropic colloids with surface modifications via Atom Transfer Radical Polymerization (ATRP). In Chapter 2 and 3 it was shown that functional, chlorinated polystyrene particles can be converted to chemically anisotropic dumbbell-shaped colloids.²⁵ These anisotropic particles consist of two lobes: one chlorinated, functional lobe which originates from the seed particles and a non-functionalized polystyrene protrusion. The functional patch allows for site-specific surface modifications, for example by grafting of (functional) polymers via ATRP (Chapter 4).

The resulting colloidal systems are potentially useful for the formation of well-defined colloidal clusters. We envision two formation routes towards these assemblies (Scheme 6.1, Section 6.3). The first one relies on the partial steric stabilization introduced by the polymers grafted to the reactive patches of the dumbbells. By

dispersing the partially grafted colloids in a high ionic strength medium, a directional attraction between the colloids is established, leading to the formation of colloidal clusters.

The second route pushes the limit of wet-chemical and bulk patchy particle synthesis even further by preparation of a colloidal system containing not only directional, but also reversible interactions. Combining the ability for localized polymer grafting with responsive polymers should enable us to prepare reversible patchy particles assemblies via emulsion-based and conventional polymer chemistry procedures. As demonstrated in Chapter 5, poly(*N*-isopropylacrylamide) (pNIPAM) is a promising candidate as responsive polymer.²⁶ This polymer has hydrophilic properties at low temperatures, while it turns hydrophobic at elevated temperatures. When dispersed in polar media, patches covered with pNIPAM will therefore become attractive upon heating the system. This is expected to trigger the formation directional bonds between the sticky patches eventually leading to the formation of well-defined colloidal clusters. Cooling will lead to a spontaneous disassembly of the clusters, ensuring reversibility.

6.2. Experimental Section

6.2.1. Materials. Styrene (St, 99%), divinylbenzene (DVB, 55% mixture of isomers, tech. grade), vinylbenzyl chloride (VBC, $\geq 90\%$, tech. grade), polyvinylpyrrolidone (PVP, average mol. wt. 40000), 3-butynyl 2-bromoisobutyrate (97%), *N*-isopropylacrylamide (NIPAM, 97%), copper bromide (Cu(I)Br, 98%), polyethylene glycol sorbitan monolaurate (Tween[®]20), dimethylformamide (DMF, $> 99\%$), and vinyl acetate ($\geq 99\%$, contains 3–20 ppm hydroquinone as inhibitor) were obtained from Sigma-Aldrich. Hydroquinone (99%) was purchased from Riedel-de Haën, sodium azide (NaN₃, 99%) from VWR, and sodium dodecyl sulfate (SDS) from BDH. Potassium persulfate (KPS, $> 99\%$ for analysis), sodium bisulfite (NaHSO₃, ACS reagent), azobis(isobutyronitrile) (AIBN, 98%) and dimethyl sulfoxide (DMSO, 99.7%) were purchased from Acros Organics. Sodium chloride (NaCl, ACS reagent, $\geq 99.5\%$) and ethanol (EtOH, absolute, p.a.) were purchased from Merck. Methanol (MeOH, exceeds ACS specifications) was obtained from J.T. Baker. 2-(2-bromoisobutyryloxy) ethyl acrylate (BIEA) was prepared as described in Chapter 4 (Section 4.2.2).²⁷ Micrometer-sized silica colloids were prepared as described in Chapter 9 (Section 9.2.4). All the chemicals were used as received. The water used throughout all of the syntheses was purified using a Milli-Q water purification system.

6.2.2. Synthesis of chlorinated seed particles (CPs-Cl). The chlorinated colloids (CPs-Cl) were prepared using the same core-shell approach as described in Chapter 3, Section 3.2.3.²⁵ This synthesis procedure comprised two steps, namely the synthesis of a cross-linked polystyrene core (CPs) followed by the introduction of a cross-linked chlorinated shell. The shells were grown by using either pure VBC (CPs-

Cl-100) or a mixture of 75 vol% VBC and 25 vol% styrene (CPs-Cl-75). In both cases 3 wt% DVB was added to cross-link the formed shell. The synthetic procedure provided monodisperse particles with a radius of roughly 150 nm as determined using transmission electron microscopy (TEM). The presence of the chlorine groups was confirmed using Fourier transform infrared spectroscopy (FT-IR) (1266 cm^{-1}) and X-ray photoelectron spectroscopy (XPS) [200 and 270 eV (Cl)].

6.2.3. Synthesis of chemically anisotropic dumbbell-shaped colloids containing chlorinated (DB-Cl) patches. The spherical chlorinated seed particles were converted to anisotropic colloids using a method described by Kraft et al.^{28,29} and in Chapter 2 and 3.²⁵ A swelling ratio, here defined as the mass of added monomer divided by the mass of polymer in the seed particles, of 3 was used for CPs-Cl-100, while a swelling ratio of 10 was applied for CPs-Cl-75. The geometric shape of the particles was investigated with TEM. IR spectroscopy was used to probe the presence of the chlorine groups (1266 cm^{-1}).

6.2.4. Synthesis of brominated seed particles (CPs-Br). Brominated colloids (CPs-Br) were prepared using the same core-shell approach as described in Chapter 4, Section 4.2.4. Cross-linked polystyrene particles with a radius of 225 nm and a polydispersity index (PDI) of 0.031 as determined with dynamic light scattering (DLS) were used as seeds. A cross-linked shell containing styrene, DVB and BIEA was grown on these particles via a seeded emulsion polymerization yielding particles with a hydrodynamic radius of 255 nm and a PDI of 0.030. The presence of the bromine moieties was confirmed using IR spectroscopy (1732 cm^{-1}).

6.2.5. Surface-Initiated Atom Transfer Radical Polymerization (SI-ATRP) on CPs-Br. NIPAM (120 mg, 1 mmol) and Cu(I)Br (13 mg, 0.09 mmol) were weighed and transferred directly into an oven-dried Schlenk flask. A MeOH/H₂O mixture (7:3, v/v) (0.5 mL) was added and the solution was stirred for 5 min to dissolve the NIPAM and Cu(I)Br. A light green solution was obtained. After complete dissolution, PMDETA (63 μL , 0.3 mmol) was added resulting in a blue/green mixture. The complete mixture was degassed by evacuation and refilling with nitrogen (three cycles).

In a separate Schlenk flask, the CPs-Br colloids dispersed in a 7:3 (v/v) MeOH/H₂O mixture (0.5 mL, 2 wt%) were degassed by evacuation and refilling with nitrogen (three cycles). After degassing, the dispersion was injected into the monomer/catalyst mixture under inert atmosphere. The resulting reaction mixture was white/green. The ATRP reaction was allowed to run for 4 h at room temperature, after which the reaction was terminated by exposure of the mixture to air, yielding an intense blue color. The particles were washed several times with MeOH, 50 mM NaHSO₃ solution and water. The NaHSO₃ solution was used to facilitate the removal of the copper catalyst. The presence of pNIPAM was probed using IR spectroscopy.

6.2.6. Synthesis of micron-sized non-functionalized polystyrene colloids (MPs). A procedure reported by Kraft et al.²³ and Wolters et al.²⁴ was followed for the preparation of monodisperse linear polystyrene spheres by dispersion polymerization. For this ethanol (126 mL), water (14 mL), styrene (10 mL), AIBN (0.136 g) and PVP (5.0 g) were introduced into a 200 mL round-bottom flask, closed with a rubber septum and sealed with Teflon tape. To initiate polymerization, the flask was immersed in a 75 °C oil bath with its axis of rotation at approximately a 60° angle. Polymerization was conducted for 20 h while rotating the flask at 60 rpm. The resulting particles were washed with ethanol and water. The synthesis yielded colloids with a diameter of 1.2 µm and a polydispersity of 2.9% as determined with TEM.

6.2.7. In situ observation of the aggregation behavior of a dispersion containing spherical pNIPAM grafted particles and non-functionalized polystyrene colloids. MPs colloids were washed several times with concentrated solution of Tween®20 to substitute PVP for Tween®20 as steric stabilizer. A diluted dispersion (total volume 0.5 mL) of pNIPAM grafted colloids (as prepared in Section 6.2.5) and Tween®20-stabilized micron-sized colloids was prepared. The aqueous phase contained 1 mM Tween®20 and 10 mM NaCl. The resulting dispersion was introduced into a capillary, which was subsequently flame sealed. The capillary was directly placed on a heating stage, which was mounted on an optical microscope. Regulating the temperature of the heating stage allowed for in situ observation of the temperature-induced cluster formation.

6.2.8. Introduction of bromine ATRP initiator on DB-Cl using click chemistry (DB-Br). In the first step, the chlorine groups of dumbbell-shaped colloids were substituted for azides. An aqueous dispersion containing chlorinated dumbbells (2.5 mL, solid content = 2%) was centrifuged. The supernatant was replaced with DMSO and colloids were redispersed. NaN₃ (7 mg) was weighed into an elongated, 4 mL reactor tube and the DMSO dispersion was added. Dissolution of NaN₃ was enhanced by sonication of the reaction mixture. After complete dissolution, the mixture was heated to 80 °C for 24 h. After this period, the particles were washed with water to remove all the excess salt. IR spectroscopy was used to verify the presence of the azide functionality which was vital for the next reaction step.

In the second step, the newly introduced azide groups were used to couple the brominated ATRP initiator to the reactive patch of the dumbbells. DMSO was degassed by evacuation and refilling with nitrogen several times. Cu(I)Br (100 mg) was introduced in a separate flask and degassed. Degassed DMSO (2.5 mL) was added. The obtained CuBr/DMSO stock solution was degassed again several times to exclude water and oxygen. A dispersion containing azide functionalized dumbbells (1 mL, solid content = 5%) was transferred to DMSO (0.5 mL) by centrifugation and redispersion. The obtained DMSO dispersion was added into a Schlenk flask together with 3-butynyl

2-bromoisobutyrate (20 μL). The complete mixture was degassed. Finally, CuBr/DMSO stock solution (0.5 mL) was added under inert atmosphere, yielding a slightly green dispersion. The mixture was stirred at room temperature for 12 h. After this period, the particles were washed with ethanol and water. IR spectroscopy revealed successful introduction of the bromine containing ATRP initiator (1732 cm^{-1}).

6.2.9. SI-ATRP of NIPAM on DB-Br. The ATRP reaction was performed as described in Section 6.2.5. All the reported quantities were doubled to yield a 2 mL reaction mixture. This facilitated the withdrawal of samples to monitor the ATRP reaction in time. All samples were directly diluted with a 7:3 (v/v) MeOH/H₂O mixture and rapidly washed to quench the polymerization reaction. After 4 h, the flask was opened and the remaining reaction mixture exposed to air. The mixture became intensely blue. After washing with water, 50 mM NaHSO₃ solution and MeOH, a white stable dispersion was obtained. The presence of pNIPAM was probed using IR spectroscopy.

6.2.10. Formation of (chemically) anisotropic colloidal dimers via aggregation-quenching procedure. Both the micron-sized silica colloids and the polystyrene particles with a radius of approximately 250 nm were dispersed in water. A NaCl solution (500 mM) was added to the obtained dispersion, lowering the ionic strength to 250 mM. The reaction tube containing the dispersion was gently shaken by hand for 60 s. Aggregation was quenched by addition of water to lower the final ionic strength to 3.3 mM. The crude dispersions were analyzed with optical microscopy. To fuse the colloidal doublets, toluene was added (5 vol%). Toluene swells the polystyrene particles and consequently lowers the glass transition temperature (T_g). Subsequent heating to 80 °C for 15 min fused the clusters permanently together. The clusters were analyzed after centrifugation and sonication with optical microscopy and TEM.

6.2.11. Characterization. Infrared (IR) spectra were obtained using a PerkinElmer FT-IR/FIR Frontier Spectrometer in attenuated total reflectance (ATR) mode. Measurements were performed on powders obtained by drying the particle dispersion.

Transmission electron microscopy (TEM) pictures were taken with a Philips Technai10 electron microscope typically operating at 100 kV. Bright field images were recorded using a SIS Megaview II CCD camera. The samples were prepared by drying a drop of diluted aqueous particle dispersion on top of polymer coated copper grids.

Dynamic light scattering (DLS) measurements were performed using a Malvern Zetasizer Nano using highly diluted aqueous dispersions (20 μL of a 1 wt% dispersion in 2 mL water). DLS measurements were conducted using glass sample cells. The measurements performed without the addition of NaCl consisted of 7 runs of 15 individual measurements in backscatter mode (173°) and were run at 20 and 40 °C. An equilibration time of 5 min was applied to ensure that the dispersions were at the set

temperature. The DLS experiments conducted at higher ionic strengths made use of the same settings with the difference that the number of individual runs was adjusted according to the speed at which aggregation or stabilization occurred. The sizes of the colloids or aggregates are reported as *Z*-average diameters and the corresponding polydispersity index (PDI). These values were obtained by using the cumulant method as described in ref. 30. The absolute values obtained for the *Z*-average diameter and the PDI for the aggregated dispersions are less reliable. Nevertheless, these values can still be used to verify if a colloidal dispersion is randomly aggregating, which results in higher *Z*-average diameters and PDI values.

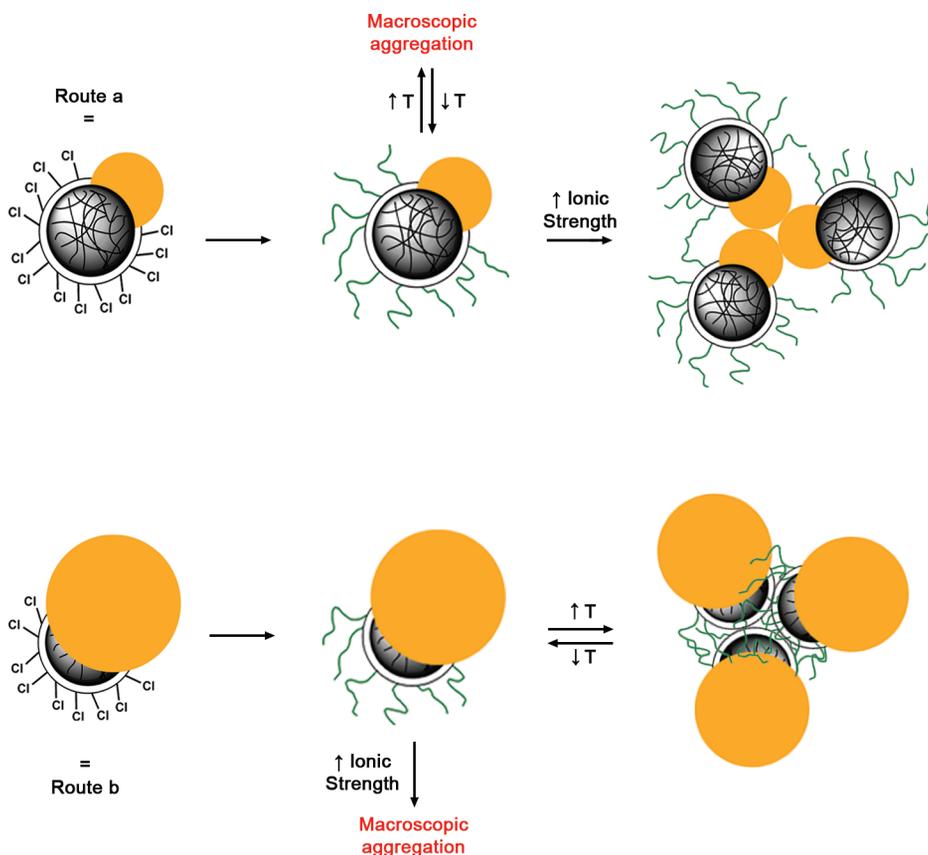
Optical microscopy images of the p(St)-*g*-p(NIPAM) particles and their thermo-reversible aggregation were obtained using a Nikon Eclipse Ti-U inverted microscope equipped with an InfinityX scout camera. A 60 \times or 100 \times magnification objective was used. For the reversible aggregation behavior, capillaries of 0.05 \times 1.00 mm (CM Scientific) were filled with a diluted particle dispersion containing 10 mM NaCl and 1 mM Tween[®]20. Tween[®]20 was added to prevent colloids from sticking to the capillary wall. The capillaries were subsequently flame sealed and directly placed on the heating element of a Linkam THMS 600 heating stage, which was mounted on the table of the optical microscope. The heating stage was linked to a Linkam TP 93 controller which enabled heating and cooling of the capillary while the sample was monitored with the optical microscope.

6.3. Results and Discussion

The envisioned formation routes towards finite-sized colloidal clusters based on partially grafted colloids are schematically depicted in Scheme 6.1. Cluster formation is triggered either by an increase in temperature or ionic strength. For both routes, *N*-isopropylacrylamide (NIPAM) was the grafting monomer of choice. ATRP of this monomer leads to the formation of thermo-responsive patches on the chemically anisotropic particles. Thermo-reversible attractions are therefore accessible between the polymer grafted patches, in a similar fashion as described in Chapter 5, where the aggregation behavior of isotropic spherical pNIPAM grafted particles was studied. At room temperature, the grafted pNIPAM hairs are hydrophilic and extend into the aqueous solution. However, heating above the lower critical solution temperature (LCST) turns the pNIPAM polymers hydrophobic. Particles containing these hydrophobic brushes attract each other. In theory, the pNIPAM in this colloidal design is now confined to a single patch per particle, leading to a directional interaction. If the system is cooled down below the LCST again, the effective attraction between the particles vanishes and the formed clusters/aggregates disassemble spontaneously.

Alternatively, the salt-induced directional attractions are induced between the bald lobes of the dumbbells, since these patches are not sterically stabilized. The polymers

Scheme 6.1. Routes towards finite-sized colloidal clusters built up from partially grafted dumbbell-shaped particles.^a



^aRoute (a): starting from dumbbell-shaped particles with protrusions (yellow) smaller than the reactive chlorinated patch, dumbbells with large pNIPAM (green hairs) domains are prepared via Surface-Initiated Atom Transfer Radical Polymerization (SI-ATRP). The protrusions become sticky by an increase in the ionic strength. The polymers grafted on the large patch provide steric stabilization, leading to directionality in the aggregation process. Route (b): starting from dumbbells with protrusions larger (yellow) than the reactive patch, dumbbells with small pNIPAM patches are accessible. These small pNIPAM lobes can induce thermo-reversible directional bonding between the colloids. For both routes, the small patches are made attractive to prevent macroscopic aggregation.

grafted on the reactive patch of the dumbbell provide steric stabilization and guarantee colloidal stability of this part of the colloids after an increase in ionic strength. In this situation, the thermo-responsive properties of pNIPAM are not exploited. The aggregation experiments were performed below the LCST, where pNIPAM behaves

as an ordinary hydrophilic polymer that extends into the continuous phase providing the necessary steric stabilization.

Having site-specific interactions is, however, not enough to prepare well-defined clusters. The second design constraint for successful formation of finite-sized clusters is that the attractive patch should be relatively small compared to the dimensions of the whole particle.^{31,32} Localizing the temperature- or salt-induced attractions on small patches ensures that only a low number of bonds per particle can be formed. Only in this way the aggregation is self-limiting and is macroscopic aggregation prevented (Scheme 6.1). This geometric constraint can be met by the strategies to tune the geometric balance between the reactive and non-reactive lobes for chemically anisotropic dumbbells presented in Chapter 3. The colloids which are used throughout this chapter, together with the geometric ratio between the chlorinated seed and protrusion, are (schematically) depicted in Figure 6.1. The particles containing a larger chlorinated patch are suitable for studying the salt-induced aggregation, since these particles will eventually lead to colloids polymer grafted patches which are larger than the bald protrusions (Figure 6.1a and b).

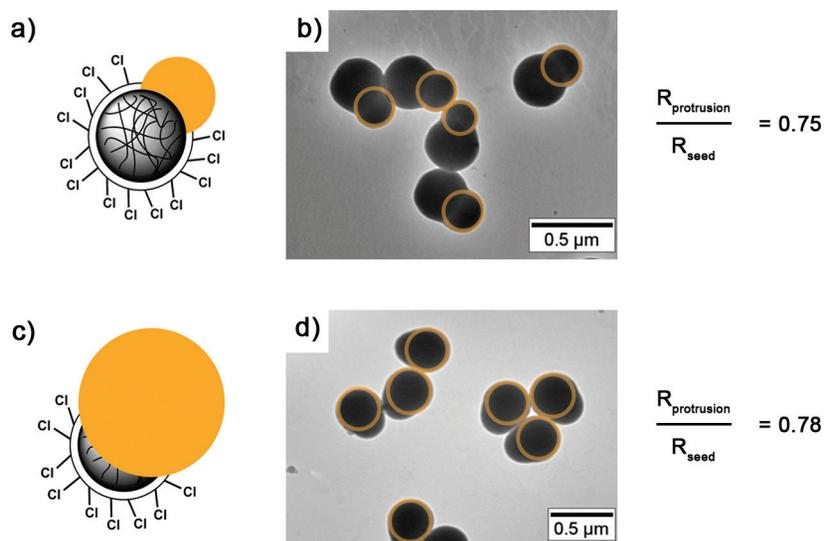


Figure 6.1. (a) Schematic representation of dumbbell-shaped colloids containing non-functionalized protrusions (yellow) which are smaller than the chlorinated lobes. (b) Transmission electron microscopy (TEM) image of the particles schematically shown in a). (c) Schematic representation of dumbbell-shaped colloids containing non-functionalized protrusions (yellow) which are larger than the chlorinated lobes. (d) TEM image of the particles schematically shown in c). The protrusions are highlighted with yellow circles in both TEM images. For both types of particles, the ratio between the radius of the protrusion and chlorinated seed are shown on the right.

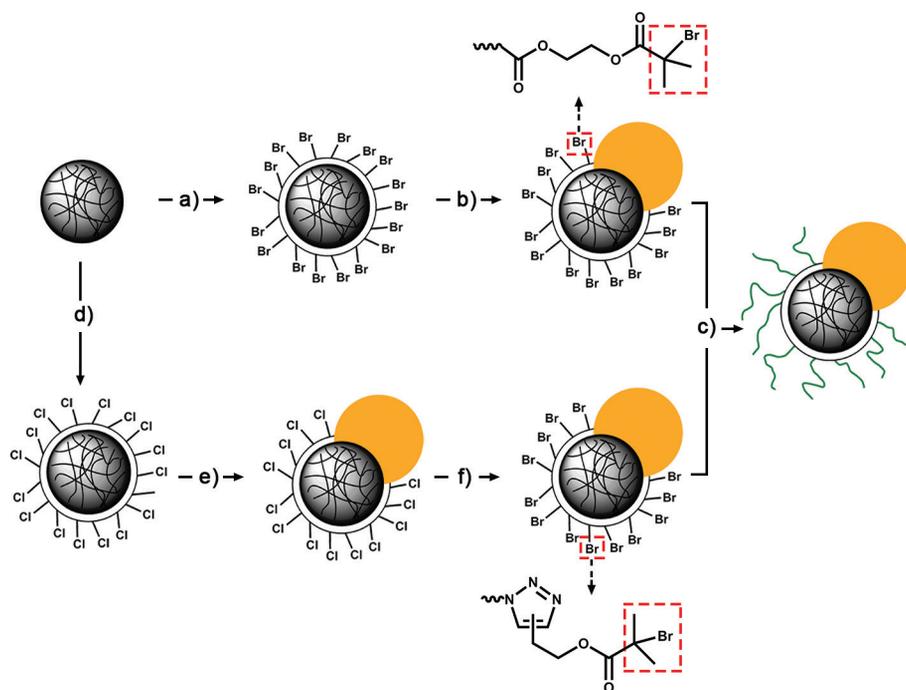
In contrast, the dumbbells with the smaller chlorinated patch should in principle yield finite size clusters after introducing some stickiness to the reactive patches (Figure 6.1c and d). The geometric ratios between attractive and non-attractive lobes for both assembly routes (Scheme 6.1) are close to the value of the colloidal dumbbells used by Kraft et al., which assembled into finite-size colloidal micelles.²⁴

6.3.1. Partial polymer grafting of chemically anisotropic dumbbells. The first prerequisite for either of the two routes towards finite-sized colloidal clusters (Scheme 6.1) is the capability of pNIPAM grafting onto the reactive patches of the chemically anisotropic dumbbell. The benzyl chloride functionalities present on the reactive patches could be exploited directly as ATRP initiators (Chapter 4). However, the initiator efficiency for pNIPAM grafting proved to be poor (see Appendix 1) and no convincing polymer brushes could be tethered onto the chlorinated patches. Instead of the benzyl chloride moieties, tertiary bromine based ATRP initiators were required. The bromoisobutyryloxy functionalized colloids employed in Chapter 5 were capable of initiating the grafting of pNIPAM efficiently under ambient reaction conditions. The most straightforward route towards dumbbells which contain these active bromine initiators on the reactive patches relies on protrusion formation using brominated colloids as seeds (step a and b, Scheme 6.2). Although protrusions were successfully introduced, subsequent ATRP grafting experiments revealed that pNIPAM brushes could not be grown from the brominated patches. Details of the dumbbell formation reactions and attempts to maintain initiator activity after protrusion formation can be found in Appendix 2.

Since we could not use the dumbbells prepared starting from brominated seed particles and the chlorine groups are not efficient initiators, an alternative synthesis route was devised. In Chapter 2 it was shown that the chlorinated patches are still reactive towards surface modification reactions via click chemistry. The orthogonal character of click chemistry allows for site-specific introduction of ATRP initiators which are chemically equivalent to those present on the brominated seeds used in Chapter 5 (step d–f, Scheme 6.2). This click chemistry route should yield dumbbells with the desired active brominated initiator patches.

Introduction of the active bromine initiator was conducted for both types of dumbbells that are shown in Figure 6.1. Since the applied surface chemistry is analogous for both systems and similar results were obtained, only the data for dumbbells with a smaller protrusion (Figure 6.1a and b) will be presented here. To make the chlorinated dumbbells suitable for modification via click chemistry, the surface chlorines were firstly replaced by azides via a simple nucleophilic substitution reaction with sodium azide. The presence of the azides was readily confirmed using IR spectroscopy. The characteristic azide vibration (2100 cm^{-1} , red middle spectrum, Figure 6.2) clearly appears while the $-\text{CH}_2\text{-Cl}$ signal (1266 cm^{-1} , black bottom spectrum, Figure 6.2)

Scheme 6.2. Synthetic routes towards dumbbell-shaped colloids with a pNIPAM patch.^a



^a Step (a): introducing bromoisobutyryloxy ATRP initiators on cross-linked polystyrene colloids (top left) by seeded emulsion polymerization of styrene, DVB and 2-(2-bromoisobutyryloxy) ethyl acrylate (BIEA). Step (b): protrusion formation on brominated seeds to create dumbbell-shaped colloids containing a reactive brominated patch, which is able to participate in an ATRP reaction, and a non-reactive protrusion (yellow). The chemical linkage of the brominated ATRP initiator to the colloidal surface is shown on top. Step (c): Surface-Initiated ATRP reaction of NIPAM from the brominated patch of the dumbbells to give partially pNIPAM grafted particles. Step (d): seeded emulsion polymerization of vinylbenzyl chloride (VBC) to introduce chlorines on the surface of cross-linked polystyrene colloids. Step (e): synthesis of dumbbell-shaped colloids with a chlorinated patch by protrusion formation. Step (f): converting surface chlorines of the chemically anisotropic dumbbells to azides and subsequently linking the active bromine containing ATRP initiator using click chemistry. The chemical linkage of the initiator is shown at the bottom of the figure.

disappears after the substitution reaction. The newly introduced azides were reacted with 3-butylnyl 2-bromoisobutyrate. Besides the tertiary bromine moiety that can act as ATRP initiator, this molecule contains an alkyne functionality which reacts with the surface immobilized azides in a similar fashion as described in Chapter 2. Proof for

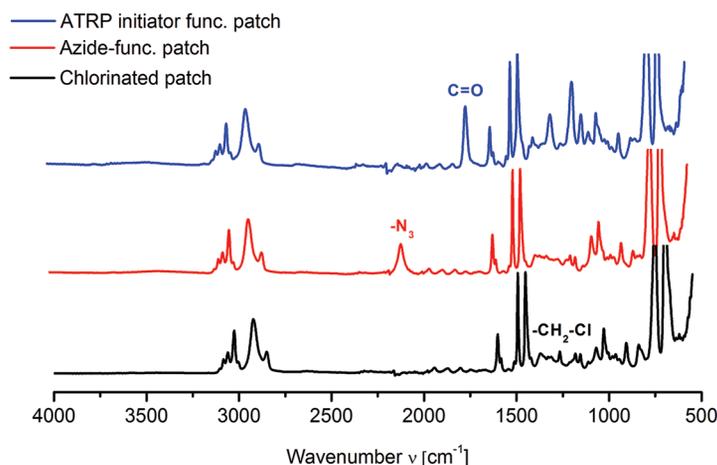


Figure 6.2. Infrared (IR) spectra of dumbbell-shaped colloids with chlorinated patches (black, bottom), azide-functionalized patches (red, middle) and patches containing bromine initiators after click reaction with 3-butynyl 2-bromoisobutyrate (blue, top).

successful immobilization of the ATRP initiators via click chemistry was again provided by IR spectroscopy. After coupling of 3-butynyl 2-bromoisobutyrate, the azide vibration disappeared, while a carbonyl signal (1732 cm^{-1} , blue top spectrum, Figure 6.3) originating from the ester moiety in 3-butynyl 2-bromoisobutyrate was gained. To highlight the chemical equivalence of the ATRP initiators immobilized via the click chemistry route (step d–f, Scheme 6.2) and direct protrusion formation of brominated seeds (step a and b, Scheme 6.2), the chemical structures of both initiators are drawn in Scheme 6.2. Control grafting experiments on spherical colloids confirmed that the minor differences in the tethering details of the ATRP initiators did not influence the thermo-responsive behavior of the resulting particles.

With the ATRP initiators immobilized on the functionalized patch, subsequent grafting of pNIPAM was attempted. In agreement with the previously observed reactivity of the chlorine groups, ATRP was effective on these colloids. Samples were withdrawn during the polymerization to monitor the brush formation using IR spectroscopy and DLS. The IR spectra show a gradual increase in intensity of the pNIPAM related signals (3300 cm^{-1} : N-H vibration, 1640 cm^{-1} : amide I; carbonyl stretching and 1536 cm^{-1} : amide II N-H deformation) over time (Figure 6.3a). The signal intensities at 1640 cm^{-1} were used to estimate monomer conversions (black dot, Figure 6.3b) and to construct a semi-logarithmic kinetic plot (see Chapter 4, Section 4.1.2 and 4.3.2). Maximum conversion was reached after approximately 90 min. Up to this point, the kinetic plot fits reasonable well to a straight line, indicating a controlled polymerization (Figure 6.3b, red triangles). The IR data were in agreement with the

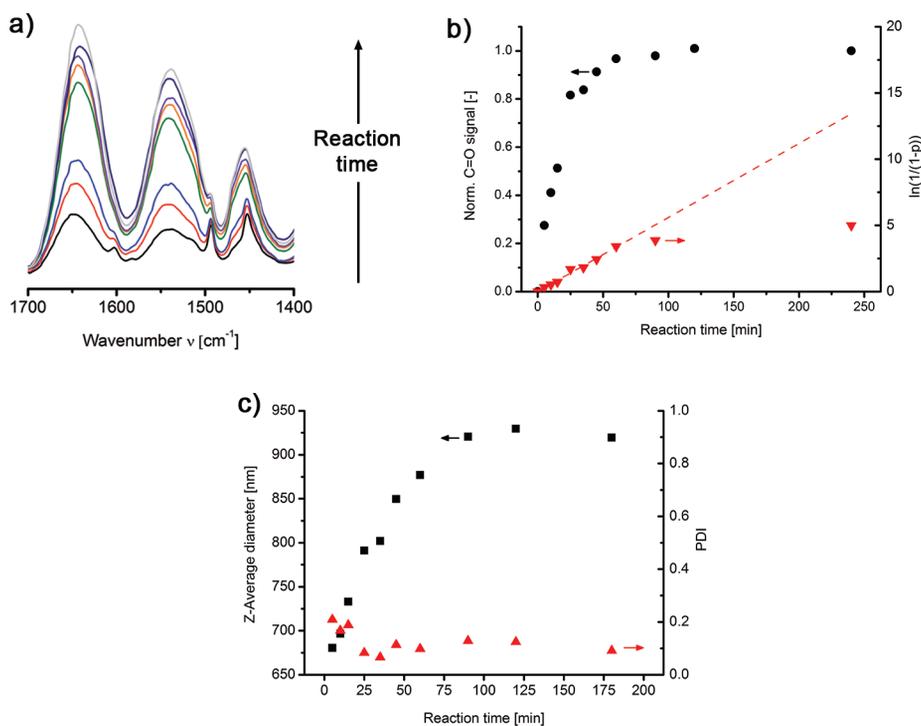


Figure 6.3. (a) Overlay of the amide vibrations (1640 cm^{-1} and 1536 cm^{-1}) observed in infrared (IR) spectra during the grafting of pNIPAM on dumbbell-shaped colloids with brominated initiator patches. (b) Black circles: plot of the normalized intensity of the amide vibration (1640 cm^{-1}) (shown in a)) versus reaction time. Red triangles: semi-logarithmic kinetic plot based on monomer conversions determined from the carbonyl vibrations. The straight line indicates the theoretical curve for a controlled radical polymerization. (c) Dynamic light scattering (DLS) results of the dumbbell-shaped colloidal initiators during the grafting of pNIPAM. The size of the colloids is reported as the Z-average diameter (black squares). The polydispersity index (PDI) of particles is depicted by the red triangles. All data were obtained using colloids with protrusions smaller than the reactive patch (Figure 6.1a). Similar data were obtained for colloids with larger protrusions (Figure 6.1c).

DLS results. The Z-average diameter (Figure 6.3c, black squares) of the colloids increases from 670 to approximately 900 nm after 100 min of reaction. The measured values are only indicative for the particle size, since the raw DLS data were converted to sizes by applying a model which assumes a spherical particle geometry. The polydispersity index (PDI, red triangles, Figure 6.3c) is rather high (≈ 0.2) at the beginning of the reaction. As the grafting reaction proceeds, the PDI drops and colloidal stability increased. This effect was probably caused by the increase in steric repulsion between the pNIPAM grafted colloids with increasing length of the immobilized polymers.

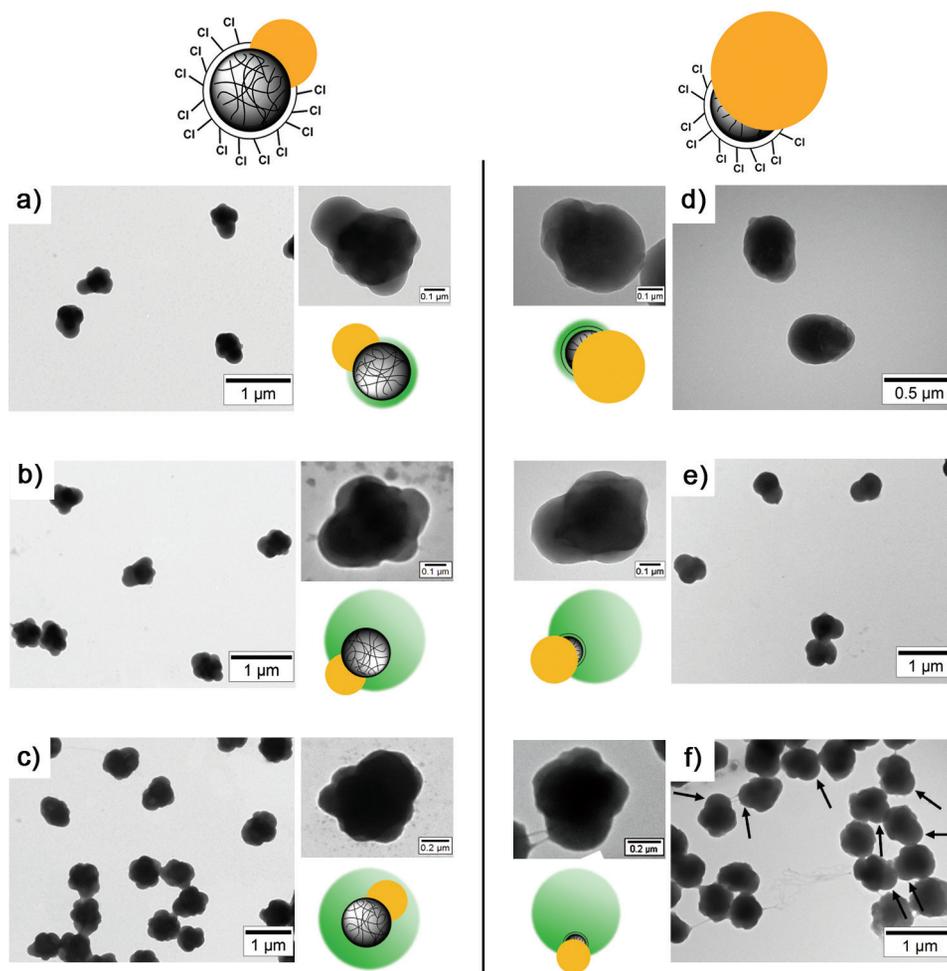


Figure 6.4. Transmission electron microscopy (TEM) images of colloidal dumbbells during grafting of pNIPAM on the reactive patch. Figure a), b) and c) show the evolution of the particle shape using dumbbells with a protrusion smaller than the reactive patch onto which pNIPAM was grafted. Figure d), e) and f) show the same shape-evolution, but for colloids with a reactive patch smaller than the protrusion. The black arrows in f) highlight the bald protrusions. The grafting time increases from top to bottom. For each figure, a higher magnification image is shown together with a schematic representation to highlight the structure of the observed colloids. In the schematic representation, the pNIPAM brush is depicted as a fuzzy green corona.

As a final analysis technique, TEM was used to obtain visual evidence for successful polymer grafting. TEM images of dried pNIPAM grafted colloids as a function of the grafting time are shown in Figure 6.4. Results are shown for both colloids with larger

and smaller reactive patches compared to the protrusion. To facilitate understanding of the observed particle structure, schematic representations are included in the figure.

Before grafting, smooth particles were observed as shown in Figure 6.1. Shortly after the start of the ATRP reaction we clearly observed enhanced surface roughness on the reactive lobes of the dumbbells (Figure 6.4a and d). This extra structure is most probably caused by the presence of the pNIPAM brush on this lobe of the dumbbells. For particles with a large reactive patch, we observed that prolonged grafting times resulted in complete wrapping of the dumbbell in pNIPAM (Figure 6.4b and c). Based on these TEM results it seems that both chemical and geometric anisotropy is completely lost. However, extracting information about the patchiness of these particles based on TEM results is unreliable. The TEM images were all recorded after drying the particles which unavoidably induced collapse of the polymer brushes. In the dispersed state we expect the polymers to extend into the continuous phase, since the pNIPAM polymers are end-tethered and hydrophilic. The anisotropy of the particles should therefore be more evident than these TEM images might suggest.

For the dumbbells with smaller reactive patches we observed a slightly different evolution of the particle morphology. Instead of losing shape-anisotropy, the pNIPAM hairs stayed confined on one side of the dumbbell regardless of the grafting time (Figure 6.5d–f). After sufficient reaction time, the size of the pNIPAM lobe exceeds the dimensions of the non-functionalized protrusion (Figure 6.4e and f). After complete grafting, the Janus character is more difficult to observe. However, smooth lobes originating from the large protrusion were still visible (highlighted with arrows, Figure 6.4f), in contrast to the completely shapeless particles observed in Figure 6.4c. Therefore, the site-specific grafting of polymers onto these particles provides a synthesis pathway for preparation of colloids with tunable Janus balance, i.e. geometric ratio between both lobes of the colloids. Combining the tunability of the size of the lobe with the chemical versatility of ATRP allows for extension of the presented synthesis procedure and the preparation of a wide variety of polymer functionalized anisotropic colloids.

With these partially pNIPAM grafted dumbbells in hand we proceeded to investigate the triggered assembly of these particles into colloidal clusters.

6.3.2. Salt-induced cluster formation of hairy dumbbells. As mentioned in the Introduction and at the beginning of this section, we hypothesized that the colloidal particles with a larger pNIPAM grafted patch compared to the bald protrusion are suitable building blocks for the formation of finite-sized cluster if attractions are introduced between the smaller non-grafted patch (Scheme 6.1, route a). This attraction was easily introduced by dispersing the hairy dumbbells (Figure 6.4b) in a high ionic strength aqueous solution. At room temperature, pNIPAM is an ordinary hydrophilic polymer that will extend into the solution ensuring local steric stabilization.

The bare protrusions do not have this extra stabilizing polymer brush and become attractive if the few surface charges that are present on the protrusions are screened. It is reasonable to assume that some charges were present on the protrusions, since this explains the observed colloidal stability of the dumbbell-shaped particles. These charges probably originated from the adsorption of surfactants during formation of the liquid protrusions. The phenomenon was previously reported by Zukoski et al. who prepared dumbbells with positively charged protrusions by adsorption of a positively charged surfactant.³³

The presence of charges on the protrusions was confirmed using ζ potential measurements as a function of the pNIPAM grafting time (Figure 6.5). For a charged spherical particle grafted with neutral polymers one expects the ζ potential to decrease with increasing brush thickness due to an outwards shift of the hydrodynamic shear plane (see Chapter 4, Section 4.3.5). Based on this argument, the potential should vanish if the polymer brush becomes sufficiently long. Figure 6.5 shows that even before reaching the maximum hydrodynamic radius after 100 min (see Figure 6.3c), a steady potential of approximately -12 mV was measured. This indicated that before the polymer hairs reach their maximum length, the charges present on the functional seed particle do not contribute any more to the measured charge. This implied that the observed ζ potential originated from charges on the protrusions.

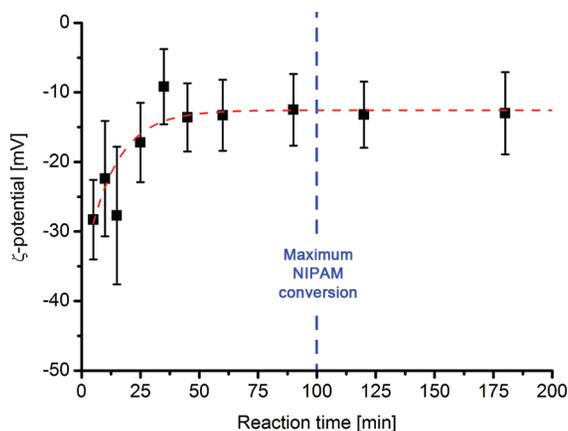


Figure 6.5. ζ potential of dumbbell-shaped colloids as function of the pNIPAM grafting time. Dumbbells with protrusions smaller than the reactive seed were used.

To investigate if the formation of small colloidal assemblies upon increasing the salt concentration was indeed feasible, partially pNIPAM grafted colloids (shown in Figure 6.4b) were dispersed in a 100 mM NaCl solution and subsequently analyzed with

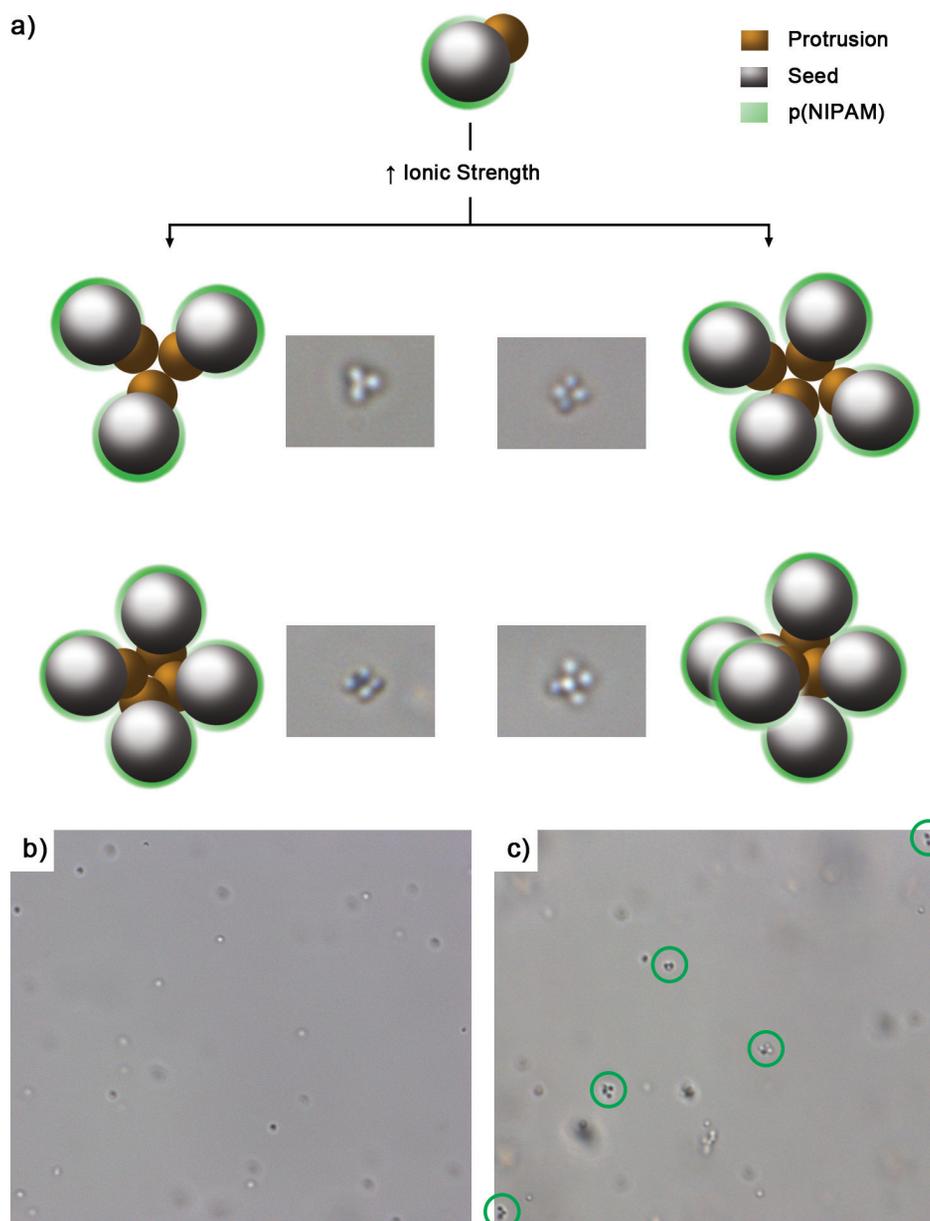


Figure 6.6. (a) Finite-size colloidal clusters observed with optical microscopy after introducing dumbbell-shaped colloids with pNIPAM grafted patches (grey sphere with green corona) larger than the protrusion (yellow lobe) in a high ionic strength medium. The speculated internal structure of the clusters is illustrated by schematic representations. (b) Overview of the dumbbell-shaped colloids with large pNIPAM grafted patches without the addition of salt to the reaction medium. (c) Overview of clusters, highlighted by the green circles, formed in a 100 mM NaCl solution.

optical microscopy. This analysis revealed the presence of single particles as well as small colloidal clusters. Figure 6.6 shows a few typical examples of observed clusters together with a schematic representation of dumbbell positions inside these assemblies. These clusters were absent in aqueous solution containing no additional salt (Figure 6.6b), indicating that the stickiness of the colloids is indeed salt-induced. The precise structure of the clusters is obviously speculative. The dumbbells are relatively small, which made it impossible to extract any reliable structural information of the clusters from these microscopy images. The formation of finite-size clusters is in agreement with the assumption that the patchiness of the colloids in solution is more pronounced than observed in TEM. Although the protrusion is hardly visible on TEM images of the particles (Figure 6.4b), in solution the protrusions were apparently not covered by pNIPAM. If the colloids would be covered completely in pNIPAM, an isotropic steric stabilization would be provided to the particles and therefore no salt-induced clustering should occur.

Furthermore, the fact that we observed the formation of finite-sized colloidal clusters is strong evidence that these assemblies are formed by attraction between the smaller, smooth protrusions. Additional confirmation of this directional bonding was provided from the images depicted in Figure 6.7a and b. These images show the resulting ill-defined clusters obtained if dumbbells with larger bald lobes (Figure 6.4d) were introduced in a high ionic strength continuous phase. Since the attractive domains are too big in this situation, the aggregation was not self-limiting.

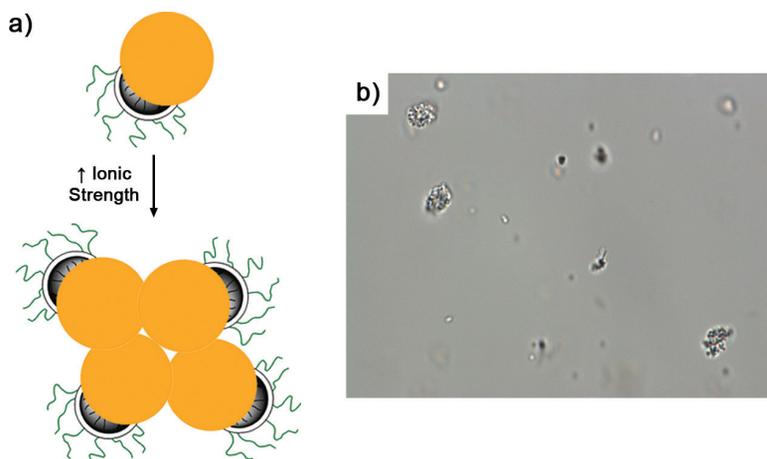


Figure 6.7. (a) Schematic representation of salt-induced clustering of dumbbells with small pNIPAM covered patches. Addition of salt results in an attraction between the large, bald protrusions (yellow). (b) Light microscopy image of the ill-defined clusters observed after introducing the partially pNIPAM grafted dumbbells with a large protrusion in a 100 mM NaCl solution.

To fully confirm the directional bonding in the clusters shown in Figure 6.6, larger colloidal analogues should be synthesized to facilitate the analysis of particle orientations.

Based on classical DLVO theory³⁴ one would expect that this clustering is not reversible. Combination of the relatively low charge density on the protrusions and the high ionic strength of the continuous phase, the protrusions are expected to be forced into the primary minimum of the interaction potential. Fabrication of the clusters followed by dilution to decrease the ionic strength did indeed not lead to a disintegration of the clusters. Typical light microscopy images of the diluted cluster dispersions are shown in Figure 6.8a and b. The presented route therefore yields irreversible, finite-sized colloidal clusters.

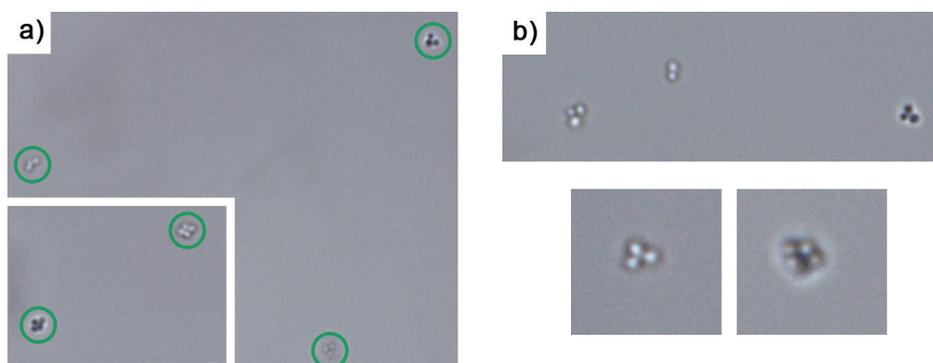


Figure 6.8. Finite-sized colloidal clusters consisting of dumbbell-shaped colloids with large pNIPAM grafted patches prepared by raising the ionic strength (see Figure 6.6). Subsequent dilution of the continuous phase with pure water to lower the ionic strength does not lead to disassembly of the clusters. (a) Set of trimers and tetramers of dumbbells and (b) enlarged view of the clusters present after lowering the ionic strength.

6.3.3. Verification of specificity of attractions between pNIPAM. In the upcoming sections, the thermo-reversible assembly of colloidal clusters will be investigated (Scheme 6.1, route b) by exploiting the thermo-responsiveness of the pNIPAM patches.

Before we employ the partially pNIPAM grafted dumbbells for the temperature-induced aggregation study, we would like to confirm that the interactions between the pNIPAM grafted patches were specific. Besides the requirement that the attractive patch should be small compared to the non-attractive lobe of the colloids, an even more important feature for the successful self-assembly into finite-size clusters is a strictly specific interaction between the pNIPAM patches upon heating the dispersion

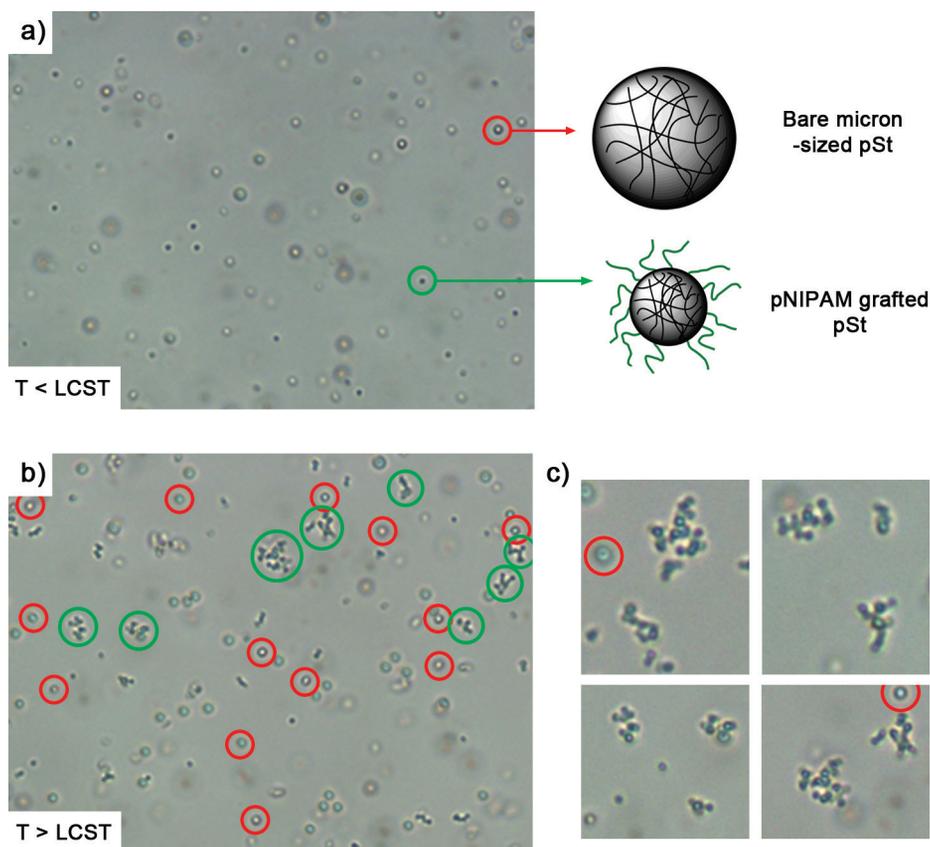


Figure 6.9. (a) Optical microscopy image of a dispersion containing pNIPAM grafted polystyrene colloids and non-functionalized micron-sized polystyrene colloids. The pNIPAM grafted particles are smaller than the micron-sized colloids which makes differentiating between the two types of particles possible. The image was recorded below the lower critical solution temperature (LCST) of pNIPAM. (b) Optical microscopy image of the same dispersion as shown in a), but now above the LCST of pNIPAM. The non-functionalized particles are highlighted with the red circle. The formed clusters, which consist of purely pNIPAM grafted colloids, are labelled with green circles. (c) Enlargement of the colloidal clusters formed above the LCST of pNIPAM to confirm that the non-functionalized colloids (red circles) do not participate in the aggregation process.

above the LCST of this polymer. The pNIPAM patches should not be attracted to the non-functionalized lobes of the dumbbells, since in that case, the directionality and therefore specificity of the attractions is lost. At first sight, this specificity might not be apparent. Above the LCST, pNIPAM turns hydrophobic. The non-grafted protrusions consist of polystyrene and are therefore also hydrophobic, implying that protrusion-

pNIPAM interactions cannot be ruled out.

To investigate if patches with pNIPAM brushes would specifically bind to each other above the LCST, the following experiment was designed. Spherical polystyrene colloids grafted with a pNIPAM brush were mixed with non-functionalized polystyrene particles. These bare colloids were significantly larger than the pNIPAM grafted particles (diameters of 1.2 μm versus 500 nm), which enabled us to distinguish both types of colloids with optical microscopy. Using the size of the particles to distinguish them does not require the use of dye molecules or other markers, which could influence the inter-particle interactions. By using this set of particles we effectively separated the pNIPAM patch and bare polystyrene protrusion of one dumbbell-shaped particle. The non-functional particles were sterically stabilized with Tween[®]20. The choice for sterically, and not charged, stabilized particles is justified by the very low ζ potentials measured for the partially grafted dumbbells (Figure 6.5). Tween[®]20 was chosen, because it does not interfere with the thermo-responsive behavior of pNIPAM (see Chapter 5, Appendix 1).

Heating a capillary containing both types of particles using a heating stage mounted on an optical microscope allowed us to monitor the aggregation process in situ. Figure 6.9a shows the mixed dispersion at a temperature below the LCST of pNIPAM. The size difference of the colloids makes it indeed possible to distinguish between both types. As expected, a well-dispersed system was obtained at room temperature. Upon heating, small clusters started to appear (Figure 6.9b). Examining the clusters in more detail reveals that these aggregates consisted of only the smaller, pNIPAM grafted colloids (Figure 6.9c). The non-functionalized particles were still well-dispersed and did not participate in cluster formation. This result indicated that above the LCST, the formation of pNIPAM-pNIPAM contacts is more favorable than pNIPAM-polystyrene bonds. Extrapolating this to dumbbell-shaped colloids which are partially grafted with pNIPAM, it should be possible to induce site-specific, directional interactions between these particles.

6.3.4. Temperature-induced response of pNIPAM grafted dumbbells.

Based on geometric arguments presented in the beginning of Section 6.3, we expect all dumbbells with a pNIPAM patch larger than the non-functionalized protrusion will result in macroscopic aggregation when a dispersion containing these colloids is heated above the LCST of pNIPAM. This was verified by conducting DLS measurements which allowed probing the hydrodynamic size of the colloids as a function of temperature. For these experiments, we were limited by the use of particles with longer polymer hairs (> 80 nm, estimated using DLS/TEM data), since the clearly anisotropic colloids (Figure 6.4a) showed hardly any thermo-response due to the limited length of the grafted polymers.³⁵ The colloidal dumbbells shown in Figure 6.4b,c,e,f all have pNIPAM patches larger than the non-attractive protrusion. Diluted

dispersions of these particles in aqueous Tween[®]20 solutions were prepared and the aggregation process was followed with DLS as a function of temperature. As observed in the previous section, addition of Tween[®]20 ensures a specific pNIPAM-pNIPAM interaction. This stabilizer adsorbs onto the bald protrusion providing extra colloidal stability to these parts of the dumbbells. As mentioned before, addition of Tween[®]20 does not influence pNIPAM mediated thermo-reversible aggregation. DLS confirmed that, regardless of the exact particle geometry, a tremendous increase in both size and PDI was measured, which is obviously indicative for colloidal aggregation (Figure 6.10a). The aggregation was also macroscopically evident, since large flocculates were observed by eye (Figure 6.10c). Finally, optical microscopy images of typical clusters revealed no directionality in the bonding of these particles. The formation mechanism of the clusters is therefore probably diffusion-controlled.

The ill-defined clusters formed upon raising the temperature are in sharp contrast to the small clusters observed after the addition of salt (Figure 6.6). Again, this underlines the importance of an attractive patch which is smaller than the non-attractive lobe.

Geometrically, only the particles shown in Figure 6.4d potentially form well-defined thermo-reversible clusters. However, DLS measurements at elevated temperatures of these particles suspended in aqueous Tween[®]20 solutions showed again severe aggregation (Figure 6.10b). Analogous to the results obtained for the colloids with the larger pNIPAM brush (Figure 6.4c), macroscopic aggregation was visible by eye and ill-defined clusters were observed with optical microscopy (Figure 6.10d). Apparently, the attractive pNIPAM patches on these particles were already too big to induce self-limiting aggregation.

From these experiments we concluded that the well-defined geometric ratio between attractive and non-attractive patches of the original chlorinated colloidal dumbbells was lost during or after the grafting of pNIPAM. The size of the attractive patch grows to such an extent that particles with relatively large attractive areas were always obtained even if dumbbells with a smaller reactive patch were exploited as colloidal initiators. Going to very short grafting times, i.e. short polymer hairs, will result in better confinement of the polymer brush. However, these short hairs do not show any thermo-responsive behavior.³⁵

The only way to circumvent this problem is to start with dumbbells that have functional patches much smaller compared to the size of the non-functionalized lobes. Unfortunately, particles with such large protrusions could not be prepared (Chapter 3). In the upcoming section, preliminary results of an alternative synthesis procedure towards partially grafted pNIPAM colloids are presented. This alternative allows for much more control over the geometric shape of the resulting anisotropic colloids.

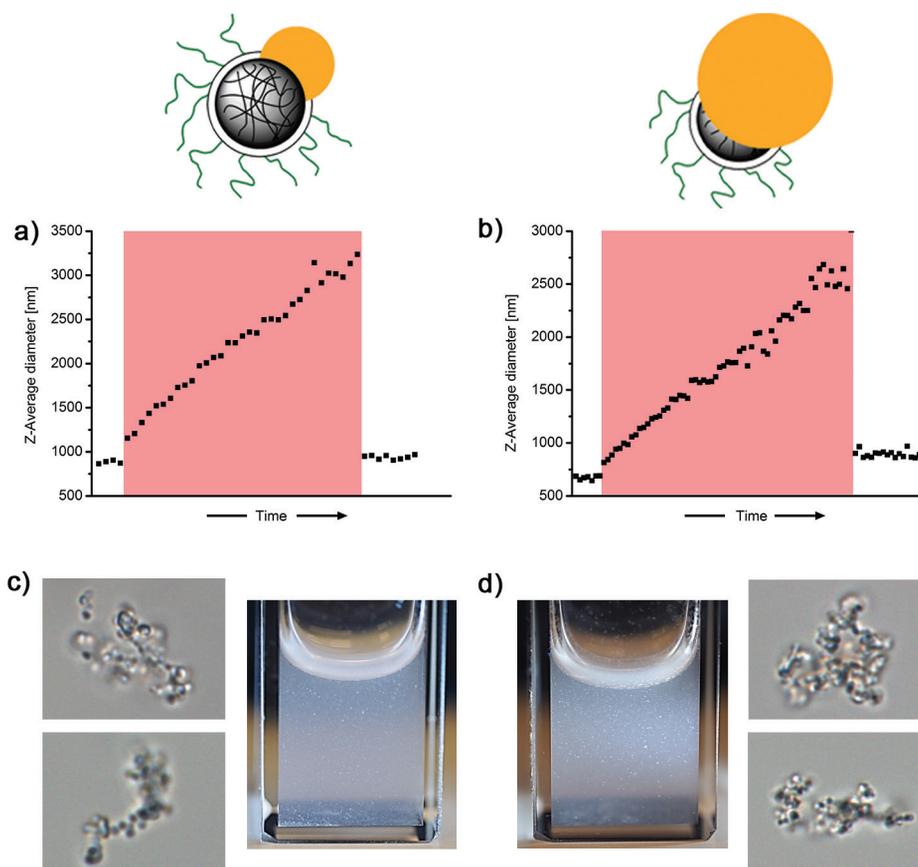


Figure 6.10. (a) The temperature dependence of the Z-average diameter of colloidal dumbbells grafted with pNIPAM measured with dynamic light scattering (DLS). Dumbbells with initiator patches larger than the protrusion were used (top left). Transmission electron microscopy (TEM) images of the used particles are shown in Figure 6.4c. (b) The temperature dependence of the Z-average diameter of colloidal dumbbells grafted with pNIPAM hairs measured with DLS. Dumbbells with initiator patches smaller than the protrusion were used (top right). TEM images of the used particles are shown in Figure 6.4d. The DLS measurements were carried out in aqueous solution containing 10 mM NaCl. The measurements conducted at 40 °C are highlighted with the red areas. Clusters observed with optical microscopy and macroscopic appearance of a dispersion containing dumbbell-shaped colloids with (c) pNIPAM grafted patches larger than the protrusion and (d) grafted patches smaller than the protrusion after heating above the lower critical solution temperature (LCST) of pNIPAM.

6.3.5. Alternative synthesis route towards chemically anisotropic dumbbells: Salting-out–Quenching–Fusing (SQF) technique. The emulsion-based synthesis routes used so far for the preparation of anisotropic colloids allows for preparation of large quantities of these particles. However, the tunability of the particle geometry proved to be limited. An interesting alternative to the synthesis procedures treated so far is the so-called Salting-out–Quenching–Fusing (SQF) technique developed by Yake et al. (Figure 6.11a).³⁶ In this method, charge stabilized colloids are introduced in a high ionic strength mixture for a short period. During this period, the surface charges are heavily screened and the particles start to aggregate. The duration of the optimal aggregation period is estimated by the Smoluchowski (rapid flocculation) time

$$\tau = \frac{\pi\eta a^3 W}{2k_B T \phi} \quad (6.1)$$

where η represents the viscosity of the continuous phase, a the radius of the particles, W the stability ratio (equal to 1 for fast flocculation), k_B the Boltzmann constant, T the temperature, and ϕ the volume fraction of colloids in the dispersion. After the flocculation time, typically a few seconds, the dispersion is diluted to lower the ionic strength to such an extent that colloidal stability is restored and aggregation is quenched. Aggregation times cannot be too long, since undefined clusters will be formed.

The last step of this procedure is a heat treatment to fuse the particles that formed a cluster together permanently. This treatment increases the mechanical stability of the whole entity. Without fusion the doublets cannot withstand sonication or centrifugation. The fusing strategy relies on heating the cluster dispersion above the glass transition temperature (T_g) of the applied polymer colloids. The T_g of polystyrene is approximately 105 °C, which makes fusing in water not feasible.³⁷ However, swelling the polystyrene colloids with toluene after cluster formation decreases the T_g to below the boiling point of water, enabling fusion in an aqueous environment.

The advantage of this procedure is that only spherical colloidal particles are required. These spherical particles are prepared in separate syntheses which ensures easy control over the size ratio between the lobes of the resulting doublets. Yake et al.³⁶ showed that this procedure is applicable for the preparation of homo-doublets of colloidal spheres and even hetero-doublets consisting of two different colloidal particles. This last feature is of interest in the context of this chapter; we can apply the SQF-technique to prepare colloidal doublets consisting of two different lobes: one lobe containing the ATRP initiators required for the introduction of the pNIPAM and one non-functionalized lobe which fulfils the role of the protrusion.

To investigate if this method would indeed be useful for our purposes, the fabrication of colloidal doublets was investigated by using micron-sized silica particles

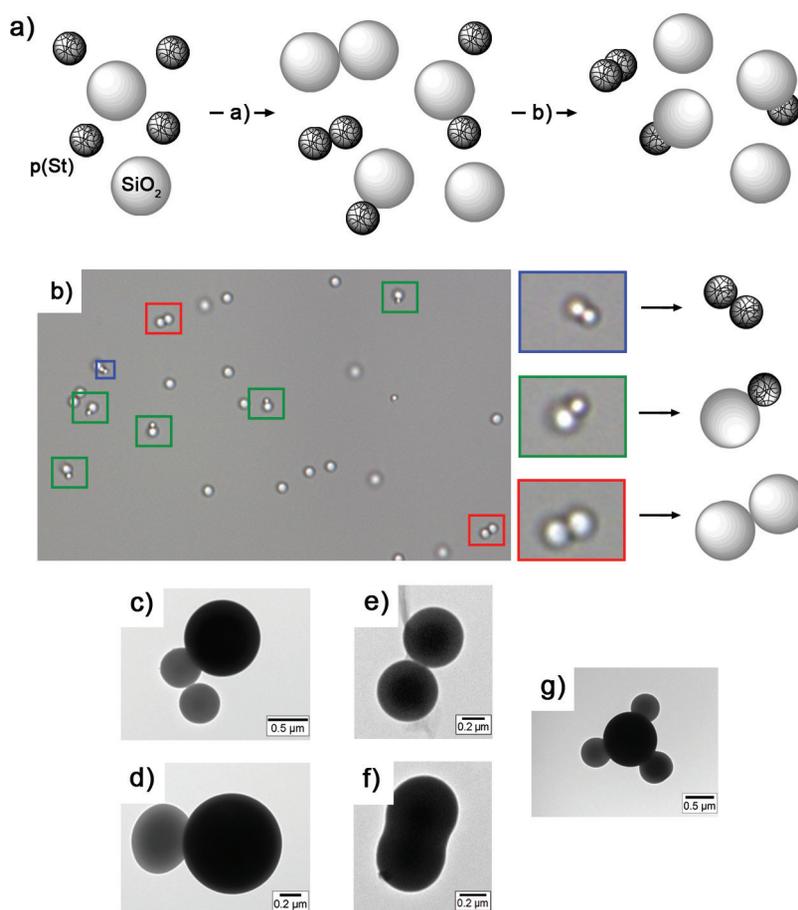


Figure 6.11. (a) Schematic representation of the Salting-out–Quenching–Fusing (SQF) technique to fabricate colloidal doublets.³⁶ A dispersion containing micron-sized silica (SiO₂) and charge stabilized polystyrene colloids are introduced in a high ionic strength medium. This induces aggregation and therefore cluster formation. After a short period, the aggregation is quenched by diluting the dispersion, leading to small clusters (step a). The obtained clusters can be fused together by heating above the glass transition of (toluene swollen) polystyrene colloids. Sonication will break up clusters containing exclusively silica, since fusion of these particles requires much higher temperatures (step b). (b) Optical microscopy image obtained after salting-out and quenching the aggregation of a dispersion containing SiO₂ and polystyrene colloids. The formed doublets are highlighted with a square: red = homo-doublet of silica particles, green = hetero-doublet of silica and polystyrene particles, and blue = homo-doublet of polystyrene colloids. Enlarged pictures of the clusters are shown on the right. (c) and (d) Transmission electron microscopy (TEM) images of hetero-doublets observed after fusion and sonication. (e) TEM image of two polystyrene colloids which are not fused. (f) TEM image of fused polystyrene homo-doublet. (g) TEM image of a typical hybrid cluster consisting of one central silica colloid surrounded by three fused polystyrene particles.

in combination with (brominated) polystyrene colloids with radii of approximately 250 nm. Silica particles were selected for this purpose, because the colloids are both large and charge stabilized. The synthesis of micron-sized, charged polystyrene colloids is challenging, since the upper limit for monodisperse charged polystyrene particles is roughly 500 nm in diameter.³⁸ Larger polymer colloids are usually prepared via dispersion polymerization and are therefore sterically stabilized.³⁸ The absence of charge on these particles makes them not suitable for the SQF-technique.

After salt-induced aggregation of a dispersion containing both the polystyrene and the silica particles and subsequent quenching of the aggregation process by dilution, formation of colloidal dimers was confirmed with optical microscopy (Figure 6.11b). Besides the formation of hetero-doublets, a small fraction of homo-doublets (two silica particles or two polystyrene colloids) was observed. With the confirmation that the doublets were formed, attempts were conducted to fuse the doublets permanently together by using the previously mentioned heat treatment. In this step, the use of silica colloids offered a second advantage. Silica particles cannot be fused together under the applied conditions. Sonication after fusion will therefore also break up silica homo-doublets, making polystyrene doublets and single particles the only impurities in the mixture. TEM was used to probe if fusing was successful. TEM samples were prepared from highly diluted dispersions to minimize the chance that single particles aggregate during the drying process and appear as a cluster. Representative images of clusters are shown in Figure 6.1c and d. The polystyrene particles are not completely spherical anymore (grey, smaller objects in Figure 6.11c–g), indicating that the heat treatment caused the polymer particles to partially merge with silica colloids (larger black colloids in Figure 6.11c–g). The effectiveness of the fusion process is neatly illustrated in Figure 6.11e and f, which shows the clear difference between two polystyrene colloids that are just lying next to each other (Figure 6.11e) and two fused particles (Figure 6.11f). Finally, Figure 6.11g shows the formation of a cluster containing one central silica particle surrounded by three fused polystyrene colloids. The presence of these atypical clusters illustrated that aggregation of spherical particles does not lead to very good control over the formed cluster distribution.

Overall, the SQF process produced the desired hetero-doublets. However, the yield was very low ($\approx 5\%$), even after optimizing the procedure in terms of aggregation time, volume fraction of colloids, and the salt concentration. On top of this, the colloids are dispersed in a large volume caused by dilution to quench the aggregation process. This hampers isolation and limits further processing of the colloidal doublets.

6.4. Conclusions

We showed that combining chemically anisotropic colloids with Surface-Initiated ATRP enables for site-specific tethering of pNIPAM brushes. The resulting

dumbbells consist of one bald lobe and one lobe covered by pNIPAM hairs. The geometric ratio between the grafted lobe and the bald lobe is tunable by both the shape of the starting dumbbell and the grafting time. The current system provides an alternative route towards the formation of colloidal clusters by exploiting the partial steric stabilization of the grafted dumbbells. Dispersing these particles in high ionic strength media induces attractions between the non-sterically stabilized lobes. Since these lobes are smaller than the pNIPAM lobes, finite colloidal clusters were formed. The disadvantage of this strategy is the irreversible nature of the formed inter-particle bonds.

Exploiting the thermo-responsive characteristics of pNIPAM to assemble these particles with pNIPAM patches into finite-sized clusters in a reversible fashion remains challenging. Self-limiting aggregation or formation of well-defined clusters was not observed upon heating. Instead, the dispersions displayed macroscopic aggregation, regardless of the geometry of the starting dumbbells or grafting time. This uncontrolled aggregation was attributed to the fact that the attractive pNIPAM patch was too large compared to the non-attractive lobe to prevent a limited number of bonds per particle.

To prevent macroscopic aggregation, dumbbells with much smaller reactive patches are required. The current emulsion-based synthesis procedure to prepare these dumbbells does not allow for such extreme particles shapes (Chapter 3). Formation of colloidal doublets via the Salting-out–Quenching–Fusing (SQF) technique allows for the preparation of highly anisotropic dumbbells. However, the particle yield is unacceptably low, hampering further synthesis and self-assembly experiments.

Acknowledgments

I would like to thank Dominique Thies-Weesie for kindly providing the micrometer-sized silica colloids.

Appendix 1 – Comparison between chlorinated and brominated particles as colloidal initiators for the surface initiated ATRP of NIPAM: IR spectroscopy

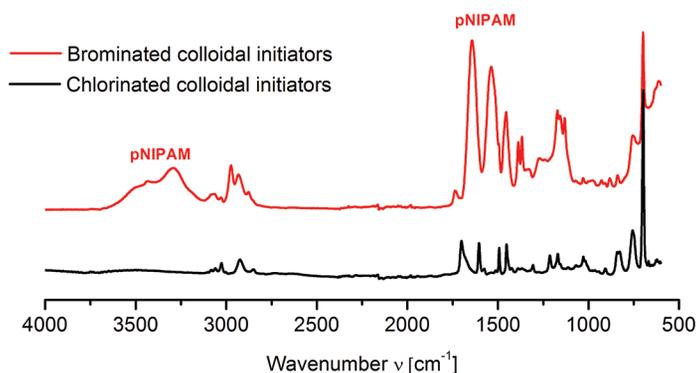


Figure 6.12. Infrared (IR) spectra of particles obtained after surface-initiated ATRP of NIPAM using spherical chlorinated particles (CPs-Cl, black, bottom spectrum) or brominated particles (CPs-Br, red, top spectrum) as colloidal initiators. ATRP using the chlorinated seeds as initiator was performed as described in Section 4.2.5. Clearly, no pNIPAM related signals (3300 cm^{-1} , 1640 cm^{-1} and 1536 cm^{-1}) were present after the attempted grafting reaction if chlorinated seeds are used. This illustrates the incapability of these particles to initiate the NIPAM polymerization. Exploiting the brominated particles as initiators yields colloids with significant pNIPAM content.

Appendix 2 – Protrusion formation of brominated seeds

A2.1. Experimental

A2.1.1. Synthesis of brominated seed particles. Brominated seed particles were prepared as described in Section 6.2.4. Cross-linked polystyrene particles with a radius of 145 nm and a polydispersity 3.5% as determined with TEM were used as seeds. The seed dispersion (16 mL, solid content = 7%) was diluted with water (16 mL). The mixture was purged with nitrogen for 30 min and subsequently heated to 70 °C. A mixture containing styrene (0.64 mL) and DVB (12.8 μL) was added. The dispersion was stirred for 10 min and BIEA was injected. The mixture was stirred for another 5 min after which the polymerization was initiated by injection of a degassed KPS solution (20.5 mg in 3.2 mL water). The polymerization was allowed to run for 6 h. After this period, the particles were washed repeatedly with water. After washing, the solid content of the dispersion was adjusted to 5%. The presence of the bromine moieties was confirmed using IR spectroscopy (1732 cm^{-1}).

Variations on the above procedure to enhance the surface hydrophilicity of the

surface were the following. Using a KPS/NaHSO₃ solution (25 mg KPS and 20 mg NaHSO₃ in 2.5 mL water) to initiate the shell formation. The second strategy relied on using a premixed solution of BIEA and vinyl acetate instead of pure BIEA (molar ratio BIEA:vinyl acetate = 1:1 or 3:1).

A2.1.2. Synthesis of chemically anisotropic dumbbell-shaped colloids based on brominated colloids. The spherical chlorinated seed particles were converted to anisotropic colloids using a method described by Kraft et al.^{28,29} and in Chapter 2 and 3.²⁵ A swelling ratio, here defined as the mass of added monomer divided by the mass of polymer in the seed particles, of 6 was used for all seed particles. The resulting particles were washed and analyzed with TEM to reveal the obtained particle shape.

A2.1.3. ATRP on chemically anisotropic dumbbells with brominated patches. The ATRP reactions to graft pNIPAM brushes on the brominated patches were conducted as described in Section 6.2.5. The same procedure was used for all the variations of brominated seeds. IR spectroscopy was used to probe if the grafting procedures were effective.

A2.2. Results and Discussion

As a starting point for the preparation of colloids which contain pNIPAM patches, brominated colloidal particles (as prepared in Chapter 5) were selected as seeds. These colloidal particles are functionalized with tertiary bromine moieties on the surface, which proved to be efficient ATRP initiators that allow for grafting pNIPAM polymers onto the surface. Converting the brominated seeds to dumbbells should yield dumbbells that carry ATRP initiators localized on one patch only, analogous to the chlorinated particles used in Chapter 2 and 3. Subsequent grafting of pNIPAM from these reactive patches should directly yield the desired thermo-responsive patchy colloids (route a, Scheme 6.2).

Figure 6.13a shows a TEM image confirming that the brominated particles could be used as seeds for the preparation of dumbbell-shaped colloids. One lobe of the dumbbells possesses some surface roughness. Since the brominated seeds were also rough, this surface texture was used to distinguish between functional and non-functional lobes of the dumbbells. The shape of the dumbbells was not optimized, since we first investigated if grafting of pNIPAM from the reactive patches was still possible after protrusion formation.

IR spectroscopy was used to probe if the ATRP initiators were still attached to the resulting colloids. As described in Chapter 5, the carbonyl vibration at 1732 cm⁻¹ is characteristic for the bromine containing initiator moieties. This vibration was still clearly visible (Figure 6.13b, black bottom spectrum), suggesting that the ATRP initiators

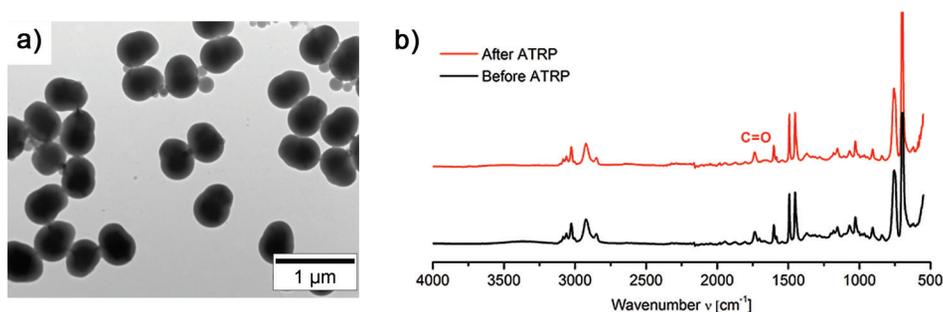


Figure 6.13. (a) Transmission electron microscopy (TEM) image of dumbbell-shaped colloids obtained after protrusion formation using brominated colloidal initiator particles as seeds. The smooth larger lobe is the introduced protrusion, while the bumpy patch of these dumbbells is the functional lobe containing ATRP initiators. (b) Infrared (IR) spectra of brominated dumbbells shown in a) before (bottom black spectrum) and after (red top spectrum) attempted grafting of pNIPAM via ATRP.

were still attached. However, employing the obtained dumbbells as colloidal initiators for grafting of pNIPAM was not successful. Analyzing the obtained colloids with IR spectroscopy showed complete absence of pNIPAM related vibrations (3300 cm^{-1} , 1640 cm^{-1} and 1536 cm^{-1}) (Figure 6.13b, red top spectrum).

Failure of the ATRP reaction was possibly caused by either the absence of active initiators or complete inaccessibility of the brominated moieties. To verify if the ATRP initiators might deactivate during protrusion formation, spherical brominated particles, which proved to be active ATRP initiators for pNIPAM grafting, were subjected to the same experimental conditions required for introduction of protrusions (heating at $80\text{ }^{\circ}\text{C}$ for 72 h). After this heat treatment, the colloids were again employed as colloidal ATRP initiators for the formation of a pNIPAM brush. The spectrum of the resulting colloids did not show significant differences compared to the spectrum obtained after grafting pNIPAM on the colloids which were not subjected to the heat treatment (Figure 6.14). This result clearly illustrated that the brominated moieties survive heating and should not disintegrate or deactivate during protrusion formation.

This result implies that the initiators attached to the brominated dumbbells are unreachable for monomer and/or the ATRP catalytic system. A possible explanation might be that the initiators are buried under a thin layer of polystyrene. As discussed in Chapter 2 and 3, dumbbell formation occurs via the formation of a liquid protrusion which is expelled upon heating a monomer swollen seed. It is possible that the surface of the brominated seeds is slightly wetted with monomer in this step. Polymerizing the wetted particles results in colloids where the ATRP initiators are no longer at the surface and therefore unreachable for any subsequent grafting reaction.

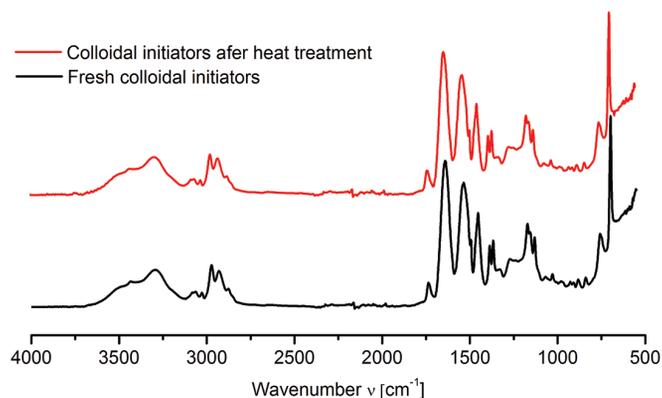


Figure 6.14. Infrared (IR) spectra obtained after grafting pNIPAM via ATRP on the surface of brominated spherical colloids. The applied colloidal initiators were either freshly prepared (bottom black spectrum) or subjected to a heat treatment (red top spectrum, 80 °C for 72 h) to test the thermal stability of the ATRP initiators.

Attempts to decrease the wetting by increasing the hydrophilicity of the outer BIEA-containing layer of the colloids by incorporating vinyl acetate in the brominated shell, proved to be futile (route a, Figure 6.15a). Incorporation of vinyl acetate did not affect the seeded emulsion polymerization. Monodisperse and stable particles were formed, regardless of the ratio between BIEA and vinyl acetate. However, subsequent protrusion formation reactions of these particles resulted in completely aggregated systems. After the initial swelling step in the protrusion formation procedure a significant amount of free styrene was still observed. Apparently, the poly(vinyl acetate) in the shell of these colloids hampers monomer uptake. The free monomer caused the whole system to aggregate during polymerization. Since protrusion formation was not successful, no ATRP reactions were performed using these colloids as initiators.

The second strategy to increase the surface hydrophilicity of the outer BIEA-shell entailed the use of an initiator mixture of KPS and sodium bisulfite (NaHSO_3) for the seeded emulsion polymerization (route b, Figure 6.15a). By applying this mix of initiator salts one could speculate that the charge density and therefore surface hydrophilicity increases during the shell formation. Also in this case, monodisperse and stable brominated seed particles were obtained. Subsequent protrusion formation was also successful and resulted in dumbbell-shaped colloids (Figure 6.15b). IR spectroscopy confirmed the presence of the ester moieties (1732 cm^{-1}) originating from BIEA (Figure 6.15c, bottom black spectrum). Unfortunately, the incorporated initiators were again not active, since no pNIPAM could be grafted on these particles as was concluded from the IR spectroscopy results (Figure 6.15c, top red spectrum).

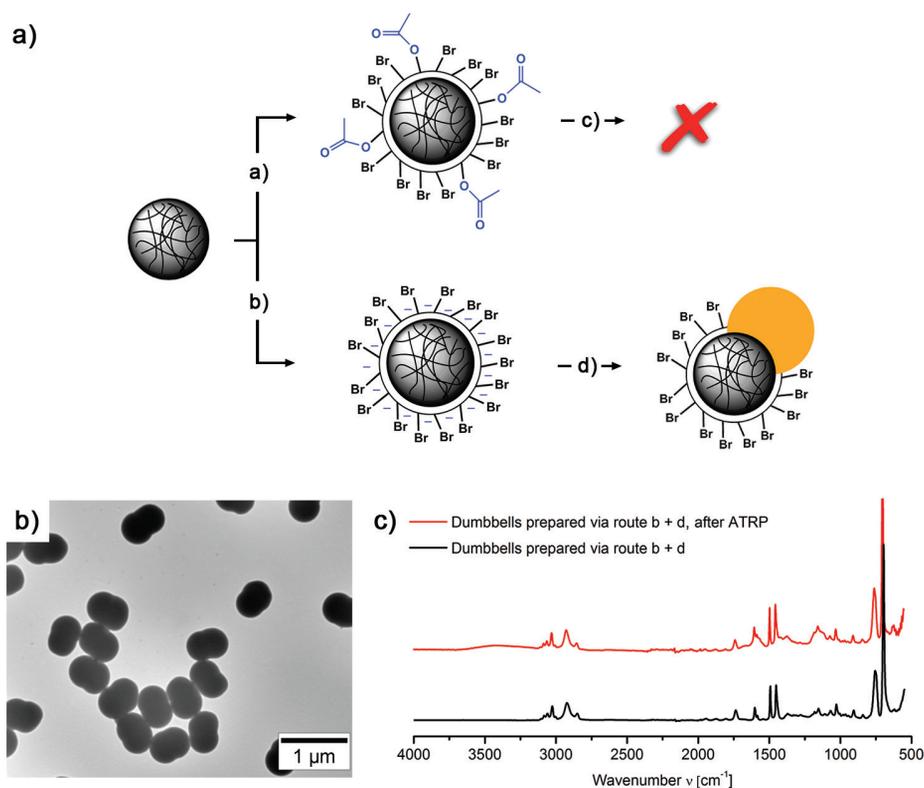


Figure 6.15. (a) Schematic representation of strategies to increase the surface hydrophilicity of the brominated seed particles. Route a) relies on the incorporation of vinyl acetate, while route b) uses a mixture of two ionic radical initiators to increase the charge density on the surface. Both seed particles were used in dumbbell formation reactions. Only the particles with the enhanced surface charge density resulted in well-defined dumbbells (step d). (b) Transmission electron microscopy (TEM) image of dumbbell-shaped colloids obtained using particles with enhanced surface charge density as seeds. (c) Infrared (IR) spectra obtained before (bottom black spectrum) and after (red top spectrum) attempted grafting of pNIPAM via ATRP using the dumbbells shown in b).

Inverting the synthesis procedure shown in Scheme 6.1, route a–c, by first growing pNIPAM brushes on spherical brominated colloids followed by protrusion formation was also unsuccessful, since highly aggregated dispersions were obtained upon swelling the hairy colloids with styrene.

From these experiments we concluded that the brominated seed particles were not suitable for the preparation of active chemically anisotropic colloids. The brominated patch of the particles is no longer able to initiate brush formation reactions, making these seeds not useful for site-specific polymer grafting.

References

- [1] P. N. Pusey, W. van Meegen, Phase behaviour of concentrated suspensions of nearly hard colloidal spheres. *Nature* **1986**, *320*, 340–342.
- [2] M. E. Leunissen, C. G. Christova, A.-P. Hynninen, C. P. Royall, A. I. Campbell, A. Imhof, M. Dijkstra, R. van Roij, A. van Blaaderen, Ionic colloidal crystals of oppositely charged particles. *Nature* **2005**, *437*, 235–240.
- [3] G. J. Vroege, H. N. W. Lekkerkerker, Phase transitions in lyotropic colloidal and polymer liquid crystals. *Rep. Prog. Phys.* **1992**, *55*, 1241–1309.
- [4] G. J. Vroege, H. N. W. Lekkerkerker, Liquid crystal phase transitions in suspensions of mineral colloids: New life from old roots. *Philos. Trans. R. Soc. A* **2013**, *371*, 20120263.
- [5] G. A. Vliegenthart, A. van Blaaderen, H. N. W. Lekkerkerker, Phase transitions, aggregation and crystallization in mixed suspensions of colloidal spheres and rods. *Faraday Discuss.* **1999**, *112*, 173–181.
- [6] D. Philp, J. F. Stoddart, Self-assembly in natural and unnatural systems. *Angew. Chem., Int. Ed.* **1996**, *35*, 1154–1196.
- [7] J. D. Watson, F. H. Crick, A structure for deoxyribose nucleic acid. *Nature* **1953**, *171*, 737–738.
- [8] J. J. McManus, A. Lomakin, O. Ogun, A. Pande, M. Basan, J. Pande, and G. B. Benedek, *Proc. Nat. Ac. Sci. U.S.A.* **2007**, *104*, 16856–16861.
- [9] A. Desai, T. J. Mitchison, Microtubule polymerization dynamics. *Annu. Rev. Cell Dev. Biol.* **1997**, *13*, 83–117.
- [10] S. C. Glotzer, M. J. Solomon, Anisotropy of building blocks and their assembly into complex structures. *Nat. Mater.* **2007**, *6*, 557–562.
- [11] A. van Blaaderen, Materials science: Colloids get complex. *Nature* **2006**, *439*, 545–546.
- [12] Z. Zhang, S. C. Glotzer, Self-assembly of patchy particles. *Nano Lett.* **2004**, *4*, 1407–1413.
- [13] S. C. Glotzer, M. J. Solomon, N. A. Kotov, Self-assembly: From nanoscale to microscale colloids. *AIChE J.* **2004**, *50*, 2978–2985.
- [14] E. Bianchi, J. Largo, P. Tartaglia, E. Zaccarelli, F. Sciortino, Phase diagram of patchy colloids: Towards empty liquids, *Phys. Rev. Lett.* **2006**, *97*, 168301.
- [15] F. Sciortino, A. Giacometti, G. Pastore, Numerical study of one-patch colloidal particles: From square-well to Janus. *Phys. Chem. Chem. Phys.* **2010**, *12*, 11869–11877.
- [16] E. Bianchi, P. Tartaglia, E. Zaccarelli, F. Sciortino, Theoretical and numerical study of the phase diagram of patchy colloids: Ordered and disordered patch arrangements, *J. Chem. Phys.* **2008**, *128*, 144504.

- [17] G. Doppelbauer, E. Bianchi, G. Kahl, Self-assembly scenarios of patchy colloidal particles in two dimensions, *J. Phys.: Condens. Matter* **2010**, *22*, 1–12.
- [18] E. Mani, E. Sanz, S. Roy, M. Dijkstra, J. Groenewold, W. K. Kegel, Sheet-like assemblies of spherical particles with point-symmetrical patches. *J. Chem. Phys.* **2012**, *136*, 144706.
- [19] Y. Wang, Y. Wang, D. R. Breed, V. N. Manoharan, L. Feng, A. D. Hollingsworth, M. Weck, D. J. Pine, Colloids with valence and specific directional bonding. *Nature* **2013**, *491*, 51–56.
- [20] Q. Chen, J. K. Whitmer, S. Jiang, S. C. Bae, E. Luijten, S. Granick, Supracolloidal reaction kinetics of Janus spheres. *Science* **2011**, *331*, 199–202.
- [21] G.-R. Yi, D. J. Pine, S. Sacanna, Recent progress on patchy colloids and their self-assembly. *Phys.: Condens. Matter* **2013**, *25*, 193101.
- [22] A. B. Pawar, I. Kretzschmar, Fabrication, assembly, and application of patchy particles. *Macromol. Rapid Commun.* **2010**, *31*, 150–168.
- [23] D. J. Kraft, R. Ni, F. Smalenburg, M. Hermes, K. Yoon, D. A. Weitz, A. van Blaaderen, J. Groenewold, M. Dijkstra, W. K. Kegel, Surface roughness directed self-assembly of patchy particles into colloidal micelles. *Proc. Natl. Acad. Sci. U.S.A.* **2012**, *109*, 10787–10792.
- [24] J. R. Wolters, G. Avvisati, F. Hagemans, T. Vissers, D. J. Kraft, M. Dijkstra, W. K. Kegel, Self-assembly of “Mickey Mouse” shaped colloids into tube-like structures: Experiments and simulations. *Soft Matter* **2015**, *11*, 1067–1077.
- [25] B. G. P. van Ravensteijn, M. Kamp, A. van Blaaderen, W. K. Kegel, General route toward chemically anisotropic colloids. *Chem. Mater.* **2013**, *25*, 4348–4353.
- [26] M. Heskins, J. E. Guillet, Solution properties of poly(*N*-isopropylacrylamide). *J. Macromol. Sci., Chem.* **1968**, *2*, 1441–1455.
- [27] K. Matyjaszewski, S. G. Gaynor, A. Kulfan, M. Podwika, Preparation of hyperbranched polyacrylates by Atom Transfer Radical Polymerization. 1. Acrylic AB* monomers in “living” radical polymerizations. *Macromolecules* **1997**, *30*, 5192–5194.
- [28] D. J. Kraft, W. S. Vlug, C. M. van Kats, A. van Blaaderen, A. Imhof, W. K. Kegel, Self-assembly of colloids with liquid protrusions. *J. Am. Chem. Soc.* **2009**, *131*, 1182–1186.
- [29] D. J. Kraft, J. Groenewold, W. K. Kegel, Colloidal molecules with well-controlled bond angles. *Soft Matter* **2009**, *5*, 3823–3826.
- [30] J. C. Thomas, The determination of log normal particle size distributions by dynamic light scattering. *J. Colloid Interface Sci.* **1987**, *117*, 187–192.
- [31] F. Romano, F. Sciortino, Colloidal self-assembly: Patchy from the bottom up. *Nat. Mater.* **2011**, *10*, 171–173.

-
- [32] A. Giacometti, F. Lado, J. Largo, G. Pastore, F. Sciortino, Effects of patch size and number within a simple model of patchy colloids. *J. Chem. Phys.* **2010**, *132*, 174110.
- [33] E. B. Mock, C. F. Zukoski, Emulsion polymerization routes to chemically anisotropic particles. *Langmuir* **2010**, *26*, 13747–13750.
- [34] E. J. W. Verwey, J. T. G. Overbeek, In *Theory of the stability of lyophobic colloids*, 2nd ed.; Dover Publications: Mineola, NY, 1999.
- [35] K. N. Plunkett, X. Zhu, J. S. Moore, D. E. Leckband, pNIPAM chain collapse depends on the molecular weight and grafting density. *Langmuir* **2006**, *22*, 4259–4266.
- [36] A. M. Yake, R. A. Panella, C. E. Snyder, D. Velegol, Fabrication of colloidal doublets by a salting out-quenching-fusing technique. *Langmuir* **2006**, *22*, 9135–9141.
- [37] D. R. Lide, H. P. R. Frederikse, *CRC Handbook of Chemistry and Physics*, 76th ed.; CRC Press: Boca Raton, FL, 1995.
- [38] R. Arshady, Suspension, emulsion, and dispersion polymerization: A methodological survey. *Colloid Polym. Sci.* **1992**, *270*, 717–732.

7

Out-of-equilibrium Aggregation of Colloidal Building Blocks

Abstract

Dissipative assembly operates under the continuous influx of energy resulting in superstructures which exist far from equilibrium. Although perfected in biological systems like microtubules, this class of assembly is sparsely used in synthetic/colloidal systems. Since non-equilibrium structures can be formed, dissipative processes provide a route towards structures unreachable by conventional equilibrium self-assembly. Here, we present a novel colloidal system which shows dissipative aggregation driven by reaction with a chemical fuel. The system consists of polystyrene particles grafted with block-copolymers with charged carboxylic acid end-segments. The chemical fuel removes these charges and increases the hydrophobicity of the polymer brush by methylation of the carboxylic acids, inducing an effective attraction between them. Depletion of the fuel leads to spontaneous disassembly of the formed clusters by reintroducing the charged moieties on the grafted polymer hairs via base-catalyzed hydrolysis reactions. This reassures that the system returns to an equilibrium state. The colloidal system presented serves as model for further development of dissipative and out-of-equilibrium assembly systems based on biological design principles.

7.1. Introduction

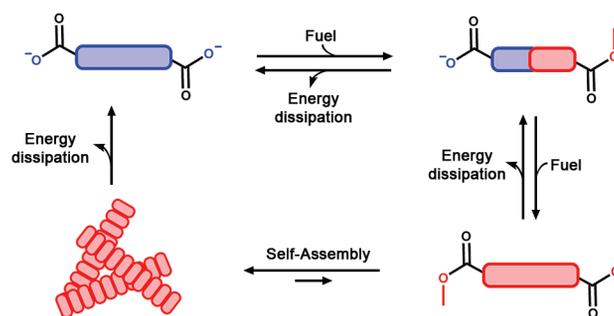
Self-assembly of (colloidal) building blocks has proven to be a powerful strategy for the preparation of superstructures.^{1–6} This ‘bottom-up’ strategy relies on designing building blocks with geometries and inter-particle interactions such that the desired assemblies are formed spontaneously and autonomously. Recently, numerous designs of building blocks were reported.^{7–11} These systems vary in the chemistries used to tune and induce the interactions and rely on for example hydrogen bonding, site-specific depletion interactions and metal-coordination.^{7–11} Furthermore, the synthetic procedures to control the number of attractive patches enables to access a wider variety of assembled structures.^{2,3} Regardless of the details, the previously mentioned building blocks are designed such that the desired assemblies exist in (local) thermodynamic minimum. Despite the dynamics that these structures display, i.e. exchange of building blocks, the formed assemblies are stable and will not change significantly over time.

Equilibrium self-assembly is in sharp contrast to many biological self-assembly processes which are dissipative in nature. In these systems, the assembly is driven by the continuous input of energy, resulting in assemblies which can only exist far from equilibrium.^{12,13} The moment the energy supply is stopped, assemblies will spontaneously start to disintegrate and the system returns to its equilibrium configuration. The supplied energy offers an additional degree of freedom to tune the driving force for assembly compared to conventional equilibrium self-assembly, allowing for spatio-temporal control over the assembly process. A striking example is the formation of microtubules.^{14,15} Microtubules are supra-molecular polymers which are built up from α/β -tubulin dimers which polymerize in an end-to-end fashion. These dimers are bound to energy-rich guanosin-5'-triphosphate (GTP) molecules. After addition of the GTP-subunits to the growing microtubule, the connected GTP is hydrolyzed to the corresponding guanosine diphosphate (GDP)-subunit. The GDP-tubulin dimer has the tendency to detach from the tubule if it is exposed to chain-ends. However, the rate of GTP hydrolysis is slower than the rate of GTP-subunit incorporation. In contrast to the GDP-tubulin, the GTP-building blocks are strongly bound to the chain-ends of microtubules and therefore provide chain-end stability. The polymerization occurs until the concentration of GTP-tubulin in the continuous phase is so low, that hydrolysis prevails. GDP-subunits will be exposed at the chain-ends and rapid depolymerization of the microtubules will occur, since the majority of the incorporated tubulin dimers are hydrolyzed during the life-time of the microtubulus. Polymerization may be re-induced by raising the concentration of energy-rich GTP(-tubulin) units that attach to the shrinking chain-end. Therefore, GTP serves as chemical fuel in this system.

The complete process is even more sophisticated by the interplay with microtubule-associated proteins (MAPs), which further regulate microtubules stability and increases the dynamic behavior of these systems.^{14,15}

Synthetic examples of systems capable of assembling in a dissipative fashion are only sparsely found in literature. Most examples deal with large mesoscopic objects, for example magnetic droplets on super-hydrophobic surfaces and magnetic spinners at air-water interfaces which are driven by the input of external energy by moving magnetic fields.^{16–18} Recently, a molecular synthetic system which resembles biological systems more was developed by Boekhoven et al.¹⁹ A molecular gel was formed by converting a carboxylated gelator precursor into its active gelating form by removing the charge on the carboxylate by reaction with a methylating agent, which then acts as the fuel. After depletion of the chemical fuel, the gel disintegrated by energy dissipation by base-catalyzed hydrolysis of the active gelator back to the precursor. To successfully employ this dissipative cycle, the rate of energy consumption (the fuel driven reaction), must be faster than the rate of energy dissipation (hydrolysis). The complete dissipative cycle is schematically depicted in Scheme 7.1.¹⁹

Scheme 7.1. Dissipative, cyclic formation of a molecular gel.^a



^a The gelator precursor (left top in blue) is methylated by a chemical fuel yielding the active gelator (right bottom in red). The diester assembles into fibers or a gel. The created structure is maintained in the presence of fuel. After depletion of the fuel, ester hydrolysis (energy dissipation) takes over completely and the gel disintegrates into the original gelator precursors.

Here, we extend the system developed by Boekhoven et al.¹⁹ to the colloidal regime. By immobilizing carboxylic acids on the surface of colloidal particles in a suitable way, the outer surface of the colloids can be switched between a charged and a neutral methylated state upon reaction with a chemical fuel. In the charged state, electrostatic repulsion keeps the colloids dispersed in the aqueous medium, while aggregation is favored if the charges are replaced by hydrophobic methyl esters. As for the molecular gelator analogue, the reactions are performed in a continuous phase containing a buffer to ensure a basic reaction environment. This promotes the energy

dissipation step in which the charges on the colloids are reintroduced by means of base-catalyzed hydrolysis of the methyl esters.

The design principles presented in this chapter provide a guideline for future 'bottom-up' designed dissipative systems allowing for the introduction of more sophisticated features, such as feed-back loops as observed in many biological systems, like the microtubules discussed before. Ultimately, these dissipative systems will lead to dynamic formation of colloidal structures which are simply unreachable by equilibrium self-assembly. The basic principles behind the formation of these out-of-equilibrium structures might lead to more understanding of the assembly dynamics observed in biology.

7.2. Experimental Section

7.2.1. Materials. Styrene (St, 99%), divinylbenzene (DVB, 55% mixture of isomers, tech. grade), methyl methacrylate (MMA, 99%), *N*-isopropylacrylamide (NIPAM, 97%), 2-bromoisobutyryl bromide (BiBb, 98%), sodium sulfate (Na_2SO_4 , ACS reagent, $\geq 99\%$, anhydrous), copper bromide (Cu(I)Br , 98%), *N,N,N',N',N''*-pentamethyldiethylenetriamine (PMDTA, 99%) and dimethyl sulfate (DMS, $\geq 99.8\%$) were obtained from Sigma-Aldrich. Potassium persulfate (KPS, $> 99\%$ for analysis), sodium bisulfite (NaHSO_3 , ACS reagent) and pyridine ($> 99\%$) were purchased from Acros Organics. Disodium tetraborate decahydrate ($\text{Na}_2\text{B}_4\text{O}_7 \cdot 10 \text{H}_2\text{O}$, for analysis), sodium hydroxide (NaOH , $\geq 99\%$) and hydrochloric acid (HCl , 37% fuming, for analysis) were obtained from Merck. Methanol (MeOH , Exceeds ACS specifications) was obtained from J.T. Baker and dichloromethane (DCM , Peptide synthesis) from Biosolve. 2-(2-bromoisobutyryloxy) ethyl acrylate (BIEA) was prepared as described in Chapter 4, Section 4.2.2.²⁰ The water used throughout all syntheses was purified using a Milli-Q water purification system.

7.2.2. Synthesis of brominated colloidal initiators (CPs-Br). The colloidal particles functionalized with Atom Transfer Radical Polymerization (ATRP) initiators were prepared as described in Chapter 4, Section 4.2.4. The two-step procedure can be summarized in the following way. In the first step, cross-linked polystyrene colloids (CPs) were prepared using conventional emulsion polymerization. These particles were used in a seeded emulsion polymerization in which a shell of styrene, DVB and BIEA was grown around the core particles. The tertiary bromide group in BIEA will act as ATRP initiator. After washing, the presence of BIEA on the colloidal particles was confirmed using infrared (IR) spectroscopy (1732 cm^{-1} ; corresponding to the two ester moieties in this molecule). Particles with a hydrodynamic radius of 184 nm and a polydispersity index (PDI) of 0.028 were obtained.

7.2.3. Atom Transfer Radical Polymerization (ATRP) on CPs-Br: Synthesis of p(St)-g-p(NIPAM-co-MMA). NIPAM (0.1 g, 0.88 mmol) and Cu(I)Br (13 mg,

0.09 mmol) were weighed and transferred directly into an oven-dried Schlenk flask. A MeOH/H₂O mixture (7:3, v/v) (0.5 mL) was added and the solution was stirred for 5 min to dissolve the NIPAM and Cu(I)Br. A light green solution was obtained. After complete dissolution, PMDETA (63 μ L, 0.3 mmol) was added, resulting in a blue/green mixture. The monomer/catalyst mixture was degassed by evacuation and refilling with nitrogen (three cycles).

In a separate Schlenk flask, the CPs-Br dispersed in a 7:3 (v/v) MeOH/H₂O mixture (0.5 mL, 2 wt%) were degassed by evacuation and refilling with nitrogen (three cycles). After degassing, the dispersion was injected into the monomer/catalyst mixture under inert atmosphere. The resulting reaction mixture was white/green. After 2 h, 0.1 mL of a degassed solution of MMA (0.1 mL) dissolved in the MeOH/H₂O mixture (7:3, v/v) (1 mL) was injected under inert atmosphere. The ATRP reaction was allowed to run for 12 more hours at room temperature. After this period, the reaction was terminated by exposure of the mixture to air yielding an intense blue color. The particles were washed several times with MeOH, 50 mM aqueous NaHSO₃ solution and MilliQ water. The NaHSO₃ solution was used to facilitate the removal of the copper catalyst. Successful grafting was confirmed using IR spectroscopy and dynamic light scattering (DLS) measurements.

7.2.4. Dissipative aggregation of p(St)-g-p(NIPAM-co-MMA) colloids. A dispersion containing p(St)-g-p(NIPAM-co-MMA) colloids (10 μ L, solid content based on polystyrene core particles = 1 wt%) was diluted in disodium tetraborate decahydrate buffer (1.5 mL, 75–250 mM based on boron). The resulting dispersion was slightly sonicated. Finally, DMS was added. The concentration of fuel in the sample was varied between 0 and 10 mM. The samples were stirred for 2 h, after which the dispersion was probed for aggregation using optical microscopy and DLS. These analyses were repeated after 24 h to investigate the reversibility of the aggregation. The pH was monitored during the process to ensure a basic reaction environment. If colloidal stability was regained, a second dissipative cycle could be conducted by addition of fresh DMS. This process was repeated until the pH of the mixture dropped below 7.

7.2.5. Characterization. Infrared (IR) spectra were obtained using a PerkinElmer FT-IR/FIR Frontier Spectrometer in attenuated total reflectance (ATR) mode. Measurements were performed on powders obtained by drying the particle dispersion.

Dynamic light scattering (DLS) and ζ potential measurements were performed using a Malvern Zetasizer Nano using highly diluted aqueous dispersions (20 μ L of a 1 wt% dispersion in 2 mL water). DLS measurements were conducted using glass sample cells. The measurements consisted of 7 runs of 15 individual measurements in backscatter mode (173°) and were run at 20 °C. An equilibration time of 5 min was applied to ensure that the dispersion was at the set temperature. The sizes of the colloids or aggregates are reported as a Z-average diameter and the corresponding

polydispersity index (PDI). These values were obtained by using the cumulant method as described in ref. 21. The absolute values obtained for the *Z*-average diameter and the PDI for the aggregated dispersions are less reliable. Nevertheless, these values can still be used to verify if a colloidal dispersion is randomly aggregating, which results in higher *Z*-average diameters and PDI values.

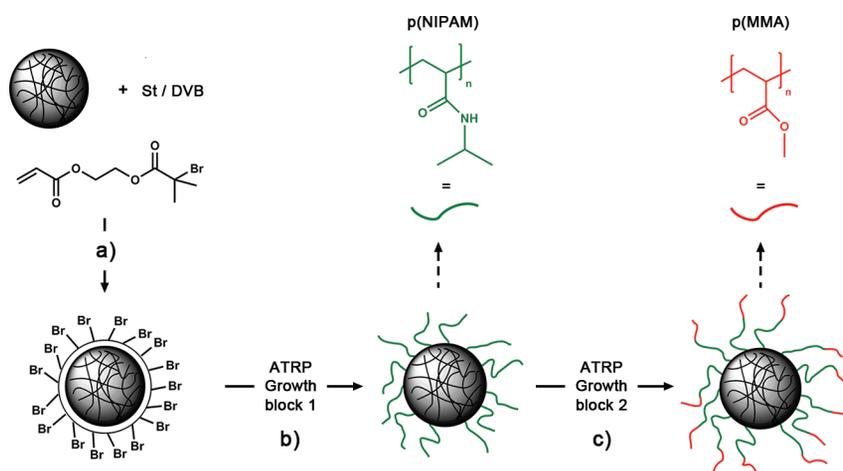
For the ζ potential measurements, 7 runs of at least 50 individual measurements were used to obtain a statistically reliable potential. The electrophoretic mobilities and DLS measurements were performed in aqueous solutions of pH 3, 7 and 11. Alternations of the pH were achieved by the addition of HCl or NaOH.

Optical microscopy images of the particles throughout this study were obtained using a Nikon Eclipse Ti-U inverted microscope equipped with an InfiniX scout camera. A 60 \times magnification objective was used.

7.3. Results and Discussion

7.3.1. Design and synthesis of dissipative colloids. To convert the dissipative molecular system reported by Boekhoven et al.¹⁹ (Scheme 7.1) to the colloidal domain, the particles should meet the following requirements. Firstly, the particles should contain carboxylic acids that can undergo the fuel driven ester formation which reduces repulsion and introduces attraction between the colloids. Secondly, the colloids should be stable at high ionic strengths. The chemical fuel which was used throughout this chapter, dimethyl sulfate (DMS), forms methyl sulfate (CH_3SO_4^-) as byproduct of the methylation reaction and competing auto-hydrolysis.²² This leads to a decrease in the pH of the reaction mixture with the consequence that the base-catalyzed hydrolysis reaction of the formed esters slows down significantly, eventually causing the formation of practically irreversible aggregates. Furthermore, low pH conditions should be prevented, since the carboxylic acids will be protonated and uncharged, promoting aggregation which is not fuel mediated. To counteract the drop in pH, the dissipative process is conducted in borate buffer (disodium tetraborate decahydrate ($\text{Na}_2\text{B}_4\text{O}_7 \cdot 10 \text{H}_2\text{O}$)). In the molecular dissipative system high buffer concentrations were required. Dissolving the borate results in formation of multivalent ions, giving rise to a high ionic strength reaction mixture. Lastly, the attraction generated after the fuel mediated methylation of the carboxylic acids should not be too strong. If the colloids are trapped in their primary minimum, the aggregation will be irreversible.

We hypothesized that the colloidal design depicted in Scheme 7.2 satisfies these criteria. Colloids are equipped with a block-copolymer brush consisting of a hydrophilic inner segment and a terminal block containing carboxylic acids/methyl esters. The function of the terminal block is evident; it provides carboxylic acids which participate in the dissipative methylation reaction. The hydrophilic inner segment acts as a spacer between the colloidal surface and the terminal block. The spacer provides steric

Scheme 7.2. Synthetic strategy towards dissipative colloids.^a

^a Step (a): seeded emulsion polymerization to grow a layer consisting of styrene (St), divinylbenzene (DVB) and 2-(2-bromoisobutyryloxy) ethyl acrylate (BIEA) onto cross-linked polystyrene particles to prepared colloidal ATRP initiators. Step (b): grafting a hydrophilic poly(*N*-isopropylacrylamide) (pNIPAM) brush (in green) onto the brominated colloidal initiators. Step (c): chain extension reaction of the grafted pNIPAM brush with methyl methacrylate (MMA, red) to yield colloids functionalized with a block-copolymer of pNIPAM and pMMA (p(St)-*g*-p(NIPAM-*co*-MMA)).

stabilization to retain colloidal stability when dispersed in high ionic strength media. Furthermore, the spacer ensures that the outer segments are separated from the colloidal surface. Consequently, the fuel induced attraction will only be present at the outer rim of the polymer brush. Therefore, after formation of colloidal clusters, the colloidal core particles are still separated preventing strong core-core Van der Waals interactions, thereby promoting reversibility.

The described colloidal design is easily accessible via Surface-Initiated Atom Transfer Radical Polymerization (SI-ATRP). This controlled polymerization technique enables the growth of (block-co)polymers from the surface of particles that are functionalized with ATRP-initiators. These ATRP-initiators act as grafting points for the polymer hairs. Polystyrene particles containing 2-(2-bromoisobutyryloxy) ethyl acrylate (BIEA, bromine containing molecule on the left in Scheme 7.2) on their surface were used throughout this chapter as colloidal initiators. Since block-copolymers are required, the hairs were introduced in a two-step process. In the first step, the hydrophilic inner segment was grown (green polymers in Scheme 7.2). After consumption of the first monomer, the grafted hairs were extended by addition of a

second monomer (red polymer segments in Scheme 7.2). Synthetic and mechanistic details can be found in Chapter 4. The total synthetic pathway towards the dissipative colloids is summarized in Scheme 7.2.

As the hydrophilic spacer, poly(*N*-isopropylacrylamide) (pNIPAM, green in Scheme 7.2) was selected. pNIPAM is a hydrophilic polymer at temperatures below 37 °C.²³ pNIPAM contains side groups with amide bonds which are stable towards (base-catalyzed) hydrolysis. Therefore, the introduction of charged groups onto these polymer segments is prevented (see Chapter 4, Section 4.3.5).²³ A neutral hydrophilic spacer is of importance, since the dissipative attraction will only be generated between the outer segments of the block-copolymer hairs. If the spacer contains too many charges, the attractive outer segments cannot reach each other due to electrostatic repulsion between the approaching colloids.

Poly(methyl methacrylate) (pMMA, red in Scheme 7.2) was used as the terminal block. Poly(acrylic acid) might seem a more obvious choice, since this polymer contains the pending carboxylic acid groups which are the starting point for the dissipative process. However, monomers containing carboxylic acids cannot be polymerized using ATRP.²⁴ Instead, we synthesized a terminal pMMA block containing pending methyl esters. These esters can be subsequently hydrolyzed to form the desired carboxylic acids.

Polymer grafting was monitored using IR spectroscopy. The spectrum of the colloidal initiators clearly showed a carbonyl signal at 1732 cm⁻¹ originating from the two ester moieties in BIEA (black, bottom spectrum, Figure 7.1).

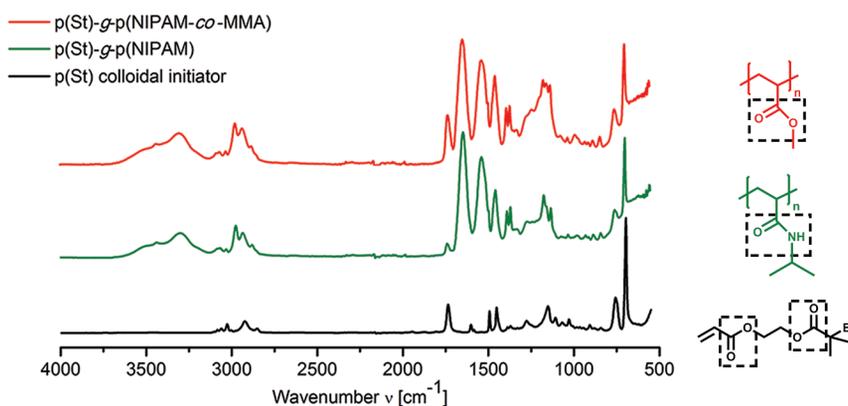


Figure 7.1. Infrared (IR) spectra of the brominated colloidal initiators (black, bottom spectrum), of colloidal particles grafted with a hydrophilic poly(*N*-isopropylacrylamide) (pNIPAM) brush (green, middle spectrum), and of the particles obtained after chain extension of the pNIPAM brush with methyl methacrylate (MMA) to yield colloids functionalized with a block-copolymer of pNIPAM and pMMA (red, top spectrum).

Compared to the spectrum of the colloidal initiators, the spectrum obtained after introduction of the hydrophilic pNIPAM brush (green, middle spectrum, Figure 7.1) shows the appearance of pNIPAM related signals at 3300 cm^{-1} (N-H vibration), 1640 cm^{-1} (amide I; carbonyl stretching) and 1536 cm^{-1} (amide II N-H deformation). The BIEA related carbonyl vibration is still visible in this spectrum. The intensity of the carbonyl vibration increases significantly after chain extension with MMA (red, top spectrum, Figure 7.1). This is in line with the formation of a terminal pMMA block, since these polymers contains pending ester groups. These IR results indicate that p(NIPAM-*co*-MMA) hairs were successfully grafted onto the colloidal particles.

DLS also confirmed successful grafting of a polymer brush onto the colloidal surface. After introduction of the pNIPAM brush, the hydrodynamic diameter increased approximately 300 nm which is equivalent to polymer hairs of 150 nm (Figure 7.2). No significant difference in hydrodynamic size was measured between the particles with a pNIPAM homopolymer brush and particles with a brush consisting of p(NIPAM-*co*-MMA) hairs (p(St)-*g*-p(NIPAM-*co*-MMA)). This can be explained based on the small number of MMA repeating units compared to the number of repeating units of pNIPAM, since a significantly lower monomer concentration was used during the chain extension reaction of the grafted pNIPAM with MMA. Furthermore, a geometric argument dictates that increasingly more monomer is required to increase the diameter of a spherical polymer brush. The relatively short pMMA blocks will therefore not contribute significantly to the final diameter of the block-copolymer grafted particles.

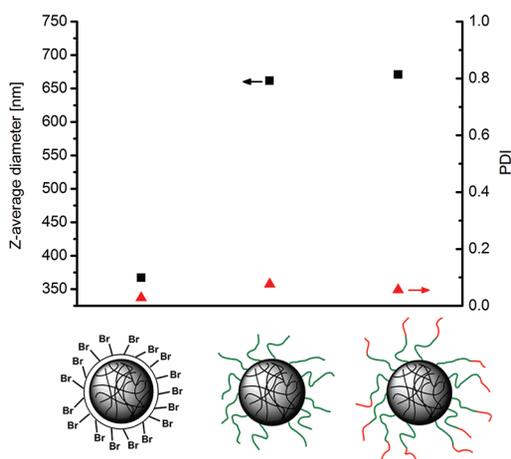


Figure 7.2. Hydrodynamic sizes (black squares) and corresponding polydispersity indices (PDI's, red triangles) obtained with dynamic light scattering (DLS) for the brominated colloidal initiators (left), colloids grafted with a poly(*N*-isopropylacrylamide) (pNIPAM) brush (middle), and colloids grafted with a block-copolymer of pNIPAM and poly(methyl methacrylate) (pMMA) (right).

The introduction of both the pNIPAM homopolymer brush and the p(NIPAM-*co*-MMA) brush did not affect the colloidal stability. For both hairy colloids low values for the polydispersity index (PDI) were measured, comparable to that of the bare colloidal initiators (red triangles, Figure 7.2). This observed stability for the pNIPAM brush was expected, since the introduction of these hydrophilic polymers enhances the colloidal stability due to steric stabilization. The observation that the p(NIPAM-*co*-MMA) grafted colloids were still stable is more surprising, since a hydrophobic pMMA block was introduced. According to our proposed colloidal design, the particles should aggregate in this situation and these colloids should only be stable after hydrolysis of the pending esters in the terminal pMMA segment. However, from results presented in Chapter 4, Section 4.3.7, we know that a part of the pending ester groups are already hydrolyzed during the ATRP reaction. This hydrolysis reaction generates carboxylic acids which are charged at neutral pH. These charged moieties at the outer rim of the polymer brush provide charge stabilization of the hairy colloids resulting in the observed colloidal stability.

To verify the presence of carboxylic acids on the p(St)-*g*-p(NIPAM-*co*-MMA) colloids, ζ potential measurement as function of pH were performed. The expected chemical structure of the terminal pMMA blocks as function of the pH is schematically shown in Figure 7.3a. Based on this picture, we should measure more negative ζ potentials with increasing pH. Dispersing the colloids in acidic media should result in protonation of the carboxylic acids with the consequence that the ζ potential approaches zero.

Figure 7.3b shows the measured ζ potentials at pH 3, pH 7 and pH 11. In agreement with the schematic representation in Figure 7.3a, the ζ potential becomes more negative as the pH increases. In the acidic medium no measurable charge is left. Apparently, the grafted polymers have such lengths that the charges present on the polystyrene core, originating from the initiators used in the emulsion polymerization to prepare the colloidal initiators, no longer contribute to the measured charge. In this situation, the particles were expected to aggregate, because electrostatic repulsion does not occur between the outer segments of the polymer brushes. A significant part of the pending functional groups in the pMMA block still contains the methyl ester, since hydrolysis of methyl esters under the applied mild ATRP conditions is expected to be a slow process.^{25,26} Furthermore, the particles were directly measured after being dispersed in the low pH mixture, to prevent acid mediated hydrolysis of esters. The outer corona of the particles is therefore hydrophobic, generating an attraction between the colloidal particles. DLS measurements as function of the pH confirmed this aggregation behavior (Figure 7.3c). If the pH is equal to 3, the measured hydrodynamic diameter is significantly larger than the values obtained at neutral or basic pH. Optical microscopy analysis (Figure 7.3a) was consistent with this observation: aggregates were clearly

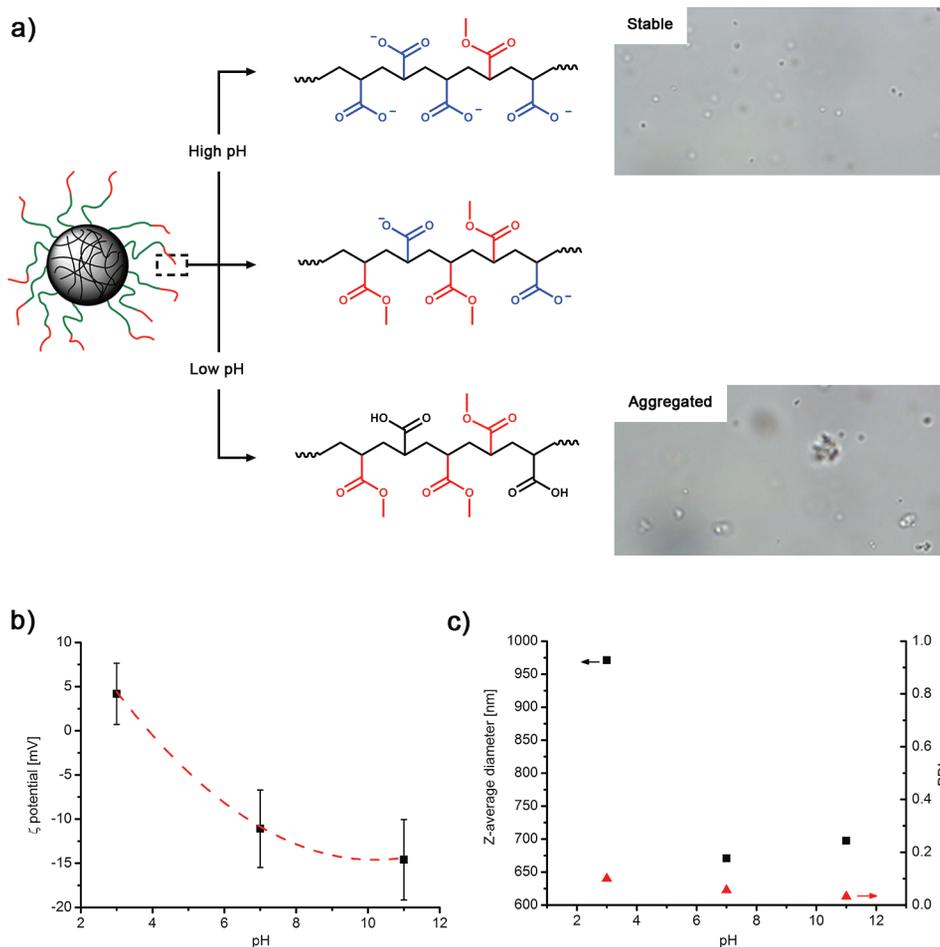


Figure 7.3. (a) Schematic representation of the molecular structure of poly(methyl methacrylate) (pMMA) segments on the grafted polymer as a function of pH. Optical microscopy pictures of particles functionalized with a block-copolymer poly(*N*-isopropylacrylamide) (pNIPAM) and pMMA (p(St)-*g*-p(NIPAM-*co*-MMA)) at pH 11 and 3 are shown on the right. (b) ζ potential as function of pH for p(St)-*g*-p(NIPAM-*co*-MMA) colloids. (c) Hydrodynamic diameter (black squares) and polydispersity index (PDI, red triangles) as function of pH for p(St)-*g*-p(NIPAM-*co*-MMA) particles.

present if the particles were dispersed in an acidic medium. In contrast, exclusively single particles were observed at pH 11, which is a clear sign of colloidal stability.

The pH dependent aggregation provides a promising starting point for the dissipative aggregation of this system. Addition of the chemical fuel does not only remove charges from the pMMA end-blocks, it also enhances the hydrophobicity by

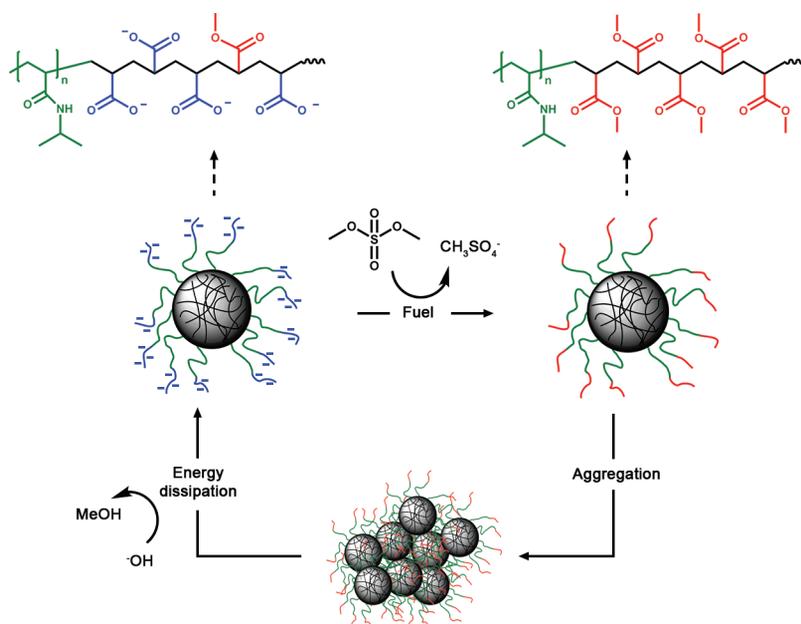
the formation of methyl esters. This enhancement in hydrophobicity is absent if the charges are removed by protonation only. Therefore, we expect the fuel mediated aggregation to be more pronounced compared to the situation where only charge density is altered by pH.

For the dissipative cycle to work, not only aggregation, but also spontaneous disintegration of the colloidal clusters should take place after depletion of the fuel. As mentioned in the beginning of Section 7.3.1, spontaneous redispersion requires high pH conditions, which can be achieved by the addition of buffer. This will inevitably lead to an increase in the ionic strength. To this end, the colloidal stability of p(St)-*g*-p(NIPAM-*co*-MMA) grafted colloids was measured in an aqueous solution containing 200 mM NaCl. The measured values for the hydrodynamic size (717 nm) and the PDI (0.082) are comparable to those obtained in pure water (Figure 7.2), indicating colloidal stability even at high ionic strengths. This observation shows that the introduced polymer brush indeed provides steric stabilization, since purely charge stabilized colloids aggregated under these high ionic strength conditions.

7.3.2. Dissipative aggregation of colloids. The aggregation process is schematically depicted in Scheme 7.3, which is basically the colloidal analogue of Scheme 7.1. The dissipative aggregation of colloidal particles requires a three-component system: the colloidal particles with the p(NIPAM-*co*-MMA) brush that can undergo the dissipative process, the chemical fuel (dimethyl sulfate, DMS) that induces hydrophobicity to the colloids via methylation, and the borate buffer which ensures high pH conditions enabling disintegration of the formed aggregates returning to equilibrium. Obviously, dispersion of the colloids in the buffer solution without any fuel should result in a stable dispersion. Only in this way, aggregation induced by elevated ionic strength can be neglected. Dispersing of p(St)-*g*-p(NIPAM-*co*-MMA) in aqueous buffer solution with different concentrations revealed a maximum allowable buffer concentration of 75 mM (based on boron). The pH of 75 mM borate buffer was 9 in agreement with the reported pK_a of 9.23.²⁷

Based on this buffer concentration, we optimized the fuel concentration. As mentioned before, consumption of the fuel leads to the formation of methyl sulfate (CH_3SO_4^-) and the consumption of hydroxide. If too much hydroxide is consumed, the buffering capacity of the mixture is lost and the system becomes acidic. To find the concentration range of fuel where the system remains basic, a concentration series was prepared in samples containing 75 mM borate buffer. The mixtures were left to stir for 24 h after which the pH was measured. Fuel concentration equal to or larger than 30 mM gave strongly acidic mixtures of pH 3 or even lower. Lowering the fuel concentration to 20 mM resulted in neutral solutions, setting the limit to the experimentally allowable fuel concentration.

With both the buffer and the fuel concentration optimized, dissipative aggregation

Scheme 7.3. Dissipative aggregation of colloidal particles.^a

^a In the initial situation, the colloidal particles are dispersed in a high pH solution. This causes the outer poly(methyl methacrylate) (pMMA) of the grafted hairs to be negatively charged due to formation of carboxylic acids (top left situation). The negative charges provide colloidal stability through electrostatic repulsion. Addition of chemical fuel (dimethyl sulfate, DMS) removes these charges by methylation and thereby increases the hydrophobicity of the outer corona of the polymer brush (top right situation). The increased hydrophobicity induces aggregation between the colloidal particles (bottom cluster). After depletion of the fuel, the hydrolysis reaction of the formed methyl esters becomes dominant. The charges are re-introduced on the grafted polymers, leading to the disintegration of the formed clusters and returning to the initial equilibrium situation.

experiments were conducted. Samples containing 75 mM buffer, p(St)-*g*-p(NIPAM-*co*-MMA) and fuel concentrations ranging between 0 and 10 mM were prepared. The mixtures were stirred for 2 h after which the dispersions were measured with DLS and visualized using optical microscopy to probe the colloidal stability. After 2 h the chemical fuel is expected to be completely converted to methyl sulfate (CH_3SO_4^-), either by methylation of carboxylic acids present on the particles or by hydrolysis.²² After this period, fuel is therefore effectively depleted and an aggregated system should be obtained. The DLS results are shown in Figure 7.4a and b. The Z-average diameter obtained after 2 h (Figure 7.4a, black filled squares) increased significantly for all

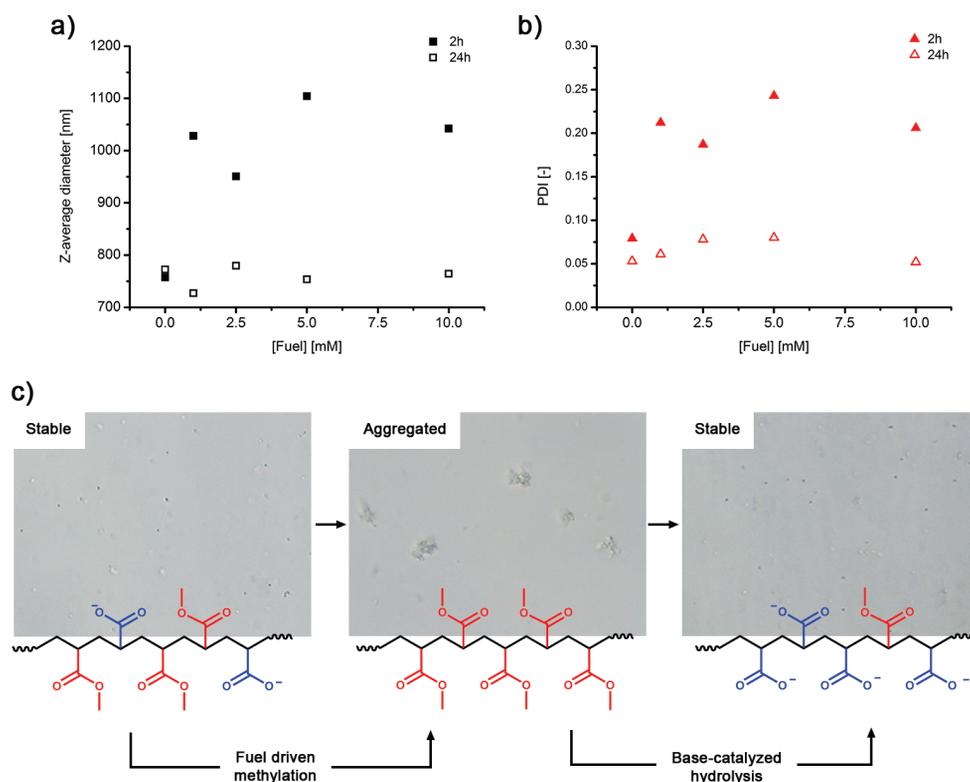


Figure 7.4. (a) Hydrodynamic diameters of colloidal particles grafted with a block-copolymer of poly(*N*-isopropylacrylamide) (pNIPAM) and poly(methyl methacrylate) (pMMA) (p(St)-*g*-p(NIPAM-*co*-MMA)) measured with dynamic light scattering (DLS) 2 h after addition of chemical fuel (filled squares). The open squares represent hydrodynamic sizes measured using the same samples after stirring for an additional 24 h. (b) Polydispersity indices (PDI's) of p(St)-*g*-p(NIPAM-*co*-MMA) measured with DLS 2 h after addition of chemical fuel (filled triangles). The open triangles represent PDI's measured using the same samples after stirring for an additional 24 h. (c) Representative optical microscopy images of p(St)-*g*-p(NIPAM-*co*-MMA) colloids during a dissipative cycle. From left to right: the colloidal dispersion before addition of fuel, 2 h after injection of fuel, the dispersion after an additional stirring period of 24 h.

fuel concentrations compared to the sample containing no fuel. This strong indication for aggregation is supported by the increase in PDI (Figure 7.4b, red filled triangles). The aggregation process is purely based on random collisions between the particles. Collision probabilities are proportional to the number density of colloids and the aggregation time. Therefore, the low particle concentration and the short period that the colloids are attractive limit the size of the formed clusters. No trend was observed

in the hydrodynamic sizes measured versus the fuel concentration, suggesting that 1 mM of fuel is sufficient to induce a significant attraction between the particles.

The DLS data were consistent with the optical microscopy images. Representative images for the samples are shown in Figure 7.4c. Before the injection of fuel, well-dispersed colloids were observed (left picture, Figure 7.4c), while aggregates were formed after the introduction of the fuel (middle picture, Figure 7.4c). The first half of the dissipative cycle was therefore successful.

The samples were stirred for an additional 24 h and the DLS and microscopy analyses were then repeated. During this period, the base-catalyzed hydrolysis reaction should take over to break up the formed clusters. From the DLS results we concluded that this process indeed occurs. Both the hydrodynamic radius (Figure 7.4a, black open squares) and the PDI (Figure 7.4b, red open triangles) decreased significantly compared to the values measured after 2 h. The obtained values for the size and the PDI are comparable to those of the sample in which no fuel was added. This indicated that the system indeed goes back to its initial, equilibrium situation. Microscopy images reveal a similar picture. In contrast to the aggregates observed after 2 h (Figure 7.4c, middle picture), the dispersion after 24 h consisted of only well-dispersed colloidal particles (Figure 7.4c, right picture) indicating colloidal stability. These results underline that also the second part of the dissipative cycle was successfully completed.

7.3.3. Repetitive aggregation by multiple dissipative cycles. From the results obtained in Section 7.3.2, we concluded that the dissipative aggregation cycle was successful for this colloidal system. Since this process is cyclic it must be possible to repeat the dissipative aggregation multiple times. The only limitation would be the amount of fuel which can be added before an acidic mixture is obtained, leading to irreversible aggregation. Fuel concentrations of 1 mM were already sufficient to aggregate the system as was shown with DLS measurements (Figure 7.4a and b). Fuel concentrations of 10 mM were accessible without acidifying the mixture too much. This implies that multiple cycles should indeed be possible. A completely similar experimental set-up was used as described before, however, additional chemical fuel was added to start a new cycle. The process was monitored with optical microscopy and the results are shown in Figure 7.5. Evidently, two consecutive cycles could be carried out without any problems. Aggregation was induced directly after fuel addition, while stable dispersions were obtained after fuel depletion and hydrolysis. However, we noted that more fuel was required in the second cycle. The third cycle required even more fuel to induce aggregation. Unfortunately, in the third cycle the aggregation proved to be not completely reversible, since small clusters were still present after 24 h. This can be explained by the acidic pH of the mixture 24 h after injection of the fuel. The p(St)-*g*-p(NIPAM-*co*-MMA) colloids are not stable in acidic media (Figure 7.3c), promoting aggregation which is not fuel induced and therefore not reversible.

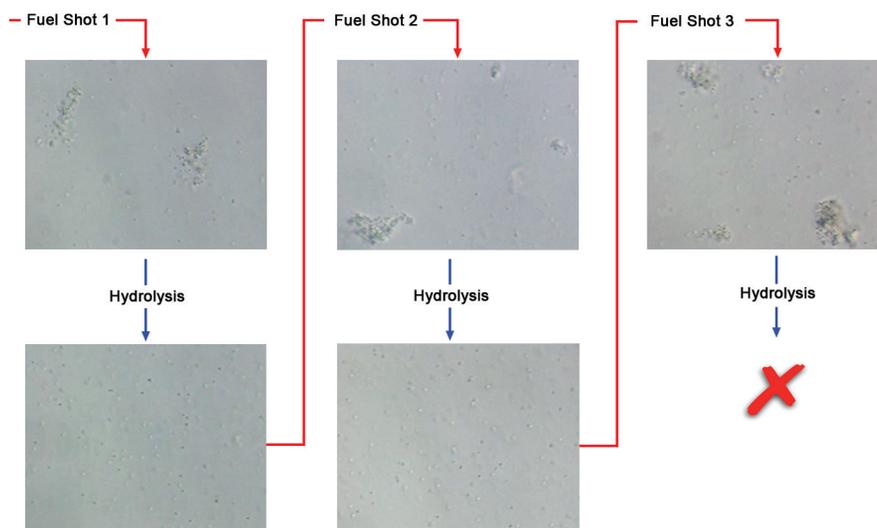


Figure 7.5. Optical microscopy images obtained from multiple dissipative cycles with colloidal particles grafted with a block-copolymer of poly(*N*-isopropylacrylamide) (pNIPAM) and pMMA (p(St)-*g*-p(NIPAM-*co*-MMA)). Images obtained 2 h after injection of chemical fuel (dimethyl sulfate, DMS) are depicted in the top row. Pictures taken after stirring for additional 24 h are shown in the bottom row.

The observation that more fuel was required in each addition step clearly limits the number of cycles. A possible explanation for this behavior is that in the 24 h after addition of fuel more carboxylic acids were formed than there were methylated. Before the addition of fuel, only a small fraction of the repeating units in the pMMA end-segment was present as charged carboxylic acids. For the first cycle, only this small fraction needs to be methylated to induce aggregation, hence low fuel concentrations were sufficient. After fuel depletion, ester hydrolysis becomes the dominant reaction and it is possible that more carboxylic acids were formed in the period between fuel depletion and addition of new fuel. To methylate this increasing number of acid groups, more fuel is required each cycle. This problem can be solved if the kinetics of the process are followed in more detail. The minimal time and hence number of charged carboxylic acids required for the entire cluster to disintegrate can be determined. If the number of charged groups is kept at a minimal level, so will be the fuel required to induce aggregation in a consecutive cycle, resulting in a system that can undergo more dissipative turns.

7.3.4. Blank experiments to verify necessity of components in colloidal system. The dissipative mechanism depicted in Scheme 7.1 and 7.3 relies on the presence of carboxylic acids/methyl esters. Although the results presented in

the previous sections show the expected behavior, we have no evidence that this methylation/demethylation reaction cycle is actually occurring. To strengthen our claim of a dissipative colloidal system, we conducted two essential blank experiments.

Firstly, the necessity of the pMMA segment in p(St)-*g*-p(NIPAM-*co*-MMA) colloids for dissipative aggregation was verified. Colloids functionalized with a homopolymer brush of pNIPAM were used. These particles were dispersed in the borate buffer and

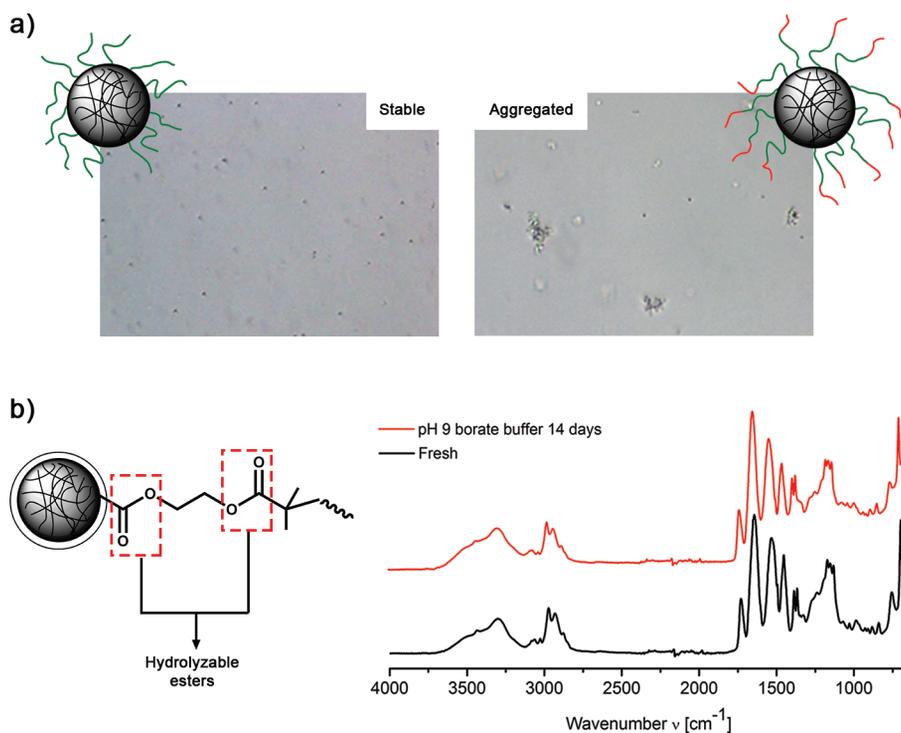


Figure 7.6. (a) Optical microscopy images obtained 2 h after addition of 10 mM chemical fuel (dimethyl sulfate, DMS) to colloids grafted with a poly(*N*-isopropylacrylamide) (pNIPAM) homopolymer brush (left) and colloids functionalized with a block-copolymer of pNIPAM and poly(methyl methacrylate) (pMMA). (b) Chemical structure of the polymer tethering points. Two hydrolyzable ester moieties are highlighted. On the right, infrared (IR) spectra of colloids grafted with a block-copolymer of pNIPAM and pMMA (p(St)-*g*-p(NIPAM-*co*-MMA)) are depicted. The black, bottom spectrum was obtained directly after synthesis. The red, top spectrum was obtained after the particles were dispersed in 75 mM borate buffer (pH = 9) for 14 days.

fuel was added. According to the proposed mechanism, no aggregation should occur, since the polymer hairs on these particles cannot be hydrophobized by methylation. In

agreement with this expectation, no aggregation was observed with optical microscopy (Figure 7.6a, left picture) for the particles with a p(NIPAM) brush after addition of chemical fuel. Aggregates are clearly visible if the same particles are used, but now the polymer hairs are extended with pMMA segments (Figure 7.6a, right picture). This result underlines the indispensability of the pending esters/carboxylic acids.

A second blank experiment that was performed was inspired on results reported in Chapter 4, Section 4.3.6, where cleavage of polymer hairs was observed. Figure 7.6b shows the chemical structure of the polymer tethering points. Two ester moieties are present, which could be hydrolyzed in basic media (as used throughout the dissipative cycle) resulting in cleavage of the polymer hairs. If the polymer cleavage occurs after fuel induced aggregation, the hydrophobic hairs are removed leading to a dispersion of stable, charge stabilized bare polystyrene cores. To investigate if polymer cleavage plays a role in this system, p(St)-*g*-p(NIPAM-*co*-MMA) colloids were dispersed in the borate buffer (75 mM, pH 9) for 2 weeks. After this period, the resulting particles were analyzed using IR spectroscopy (Figure 7.6b, top red spectrum). The obtained spectrum was compared with the spectrum of the freshly synthesized particles (Figure 7.6b, bottom black spectrum). To compare the spectra fairly, they were normalized to the polystyrene related signal at 698 cm^{-1} . The ratio between a pNIPAM signal (1644 cm^{-1}) and the polystyrene signal (698 cm^{-1}) proved to be unchanged after dispersion in the borate buffer. This strongly suggests that polymer hair cleavage can be neglected in the dissipative cycles presented here. The ester moieties of the polymer tethering points are most probably inaccessible for cleavage, because they are buried deep inside the polymer brush. An additional effect limiting the degree of chain cleavage might be that the polystyrene surface is negatively charged, hampering the reaction with likely charged hydroxyl ions required for the hydrolysis reaction.

7.4. Conclusions

To our knowledge, we presented the first experimental example of a colloidal dissipative system which is chemically fueled. Polystyrene particles were functionalized with a polymer brush consisting of an inner pNIPAM segment and a terminal pMMA block. A small fraction of the methyl esters in the pMMA block were hydrolyzed providing carboxylic acids on the outer rim of the polymer hairs. These charged moieties provided colloidal stability. Methylation of the carboxylic acids to remove the charges and increase the hydrophobicity of the terminal polymer segments by the addition of a methylation agent (fuel) induces colloidal aggregation. Since the reactions were conducted in high pH mixtures, hydrolysis of the esters took over after fuel depletion. Hydrolysis reactions led to re-introduction of charged carboxylic acids which in turn resulted in the disintegration of the formed clusters due to electrostatic repulsion. Eventually the system returned to its initial, stable state completing the

full dissipative cycle. We showed that more cycles are in principle possible, although experimental optimization is required to increase the number of accessible cycles.

The results presented here are a proof of principle for dissipative colloidal systems. Extension of the current system to, for example, patchy particles opens the way to directional, non-equilibrium structures. The fuel concentration provides a new degree of freedom to tune the attraction between the building blocks and force the system to assembly into out-of-equilibrium structures. Spatially controlled formation of assemblies is in principle within reach by applying gradients or patterns in the fuel concentration.

Acknowledgments

I would like to thank my coauthor Wouter Hendriksen and Dr. Rienk Eelkema from Delft University of Technology for introducing us to the field of dissipative assembly and the fruitful collaboration which led to the results presented in this chapter.

References

- [1] S. C. Glotzer, M. J. Solomon, N. A. Kotov, Self-assembly: From nanoscale to microscale colloids. *AIChE J.* **2004**, *50*, 2978–2985.
- [2] B. A. Grzybowski, C. E. Wilmer, J. Kim, K. P. Browne, K. J. M. Bishop, Self-assembly: From crystals to cells. *Soft Matter* **2009**, *5*, 1110–1128.
- [3] S. C. Glotzer, M. J. Solomon, Anisotropy of building blocks and their assembly into complex structures. *Nat. Mater.* **2007**, *6*, 557–562.
- [4] A. B. Pawar, I. Kretzschmar, Fabrication, assembly, and application of patchy particles. *Macromol. Rapid Commun.* **2010**, *31*, 150–168.
- [5] S. Sacanna, D. J. Pine, G.-R. Yi, Engineering shape: The novel geometries of colloidal self-assembly. *Soft Matter* **2013**, *9*, 8096–8106.
- [6] G.-R. Yi, D. J. Pine, S. Sacanna, Recent progress on patchy colloids and their self-assembly. *Phys.: Condens. Matter* **2013**, *25*, 193101.
- [7] Y. Wang, Y. Wang, D. R. Breed, V. N. Manoharan, L. Feng, A. D. Hollingsworth, M. Weck, D. J. Pine, Colloids with valence and specific directional bonding. *Nature* **2013**, *491*, 51–56.
- [8] D. J. Kraft, R. Ni, F. Smalenburg, M. Hermes, K. Yoon, D. A. Weitz, A. van Blaaderen, J. Groenewold, M. Dijkstra, W. K. Kegel, Surface roughness directed self-assembly of patchy particles into colloidal micelles. *Proc. Natl. Acad. Sci. U.S.A.* **2012**, *109*, 10787–10792.

- [9] J. R. Wolters, G. Avvisati, F. Hagemans, T. Vissers, D. J. Kraft, M. Dijkstra, W. K. Kegel, Self-assembly of “Mickey Mouse” shaped colloids into tube-like structures: Experiments and simulations. *Soft Matter* **2015**, *11*, 1067–1077.
- [10] Y. Wang, A. D. Hollingsworth, S. K. Yang, S. Patel, D. J. Pine, M. Weck, Patchy particle self-assembly via metal coordination. *J. Am. Chem. Soc.* **2013**, *135*, 14064–14067.
- [11] I. de Feijter, L. Albertazzi, A. R. A. Palmans, I. K. Voets, Stimuli-responsive colloidal assembly driven by surface-grafted supramolecular moieties. *Langmuir* **2015**, *31*, 57–64.
- [12] B. Alberts, A. Johnson, J. Lewis, M. Raff, K. Roberts, P. Walter, In *Molecular Biology of the Cell*, 4th ed.; Garland Science, New York, 2002.
- [13] R. Phillips, J. Kondev, J. Theriot, H. Garcia, In *Physical Biology of the Cell*, 2nd ed.; Garland Science, New York, 2012.
- [14] A. Desai, T. J. Mitchison, Microtubule polymerization dynamics. *Annu. Rev. Cell Dev. Biol.* **1997**, *13*, 83–117.
- [15] T. Mitchison, M. Kirschner, Dynamic instability of microtubule growth. *Nature* **1984**, *312*, 237–242.
- [16] B. A. Grzybowski, H. A. Stone, G. M. Whitesides, Dynamic self-assembly of magnetized, millimeter-sized objects rotating at a liquid-air interface. *Nature* **2000**, *405*, 1033–1036.
- [17] M. Fialkowski, K. J. M. Bishop, R. Klajn, S. K. Smoukov, C. J. Campbell, B. A. Grzybowski, Principles and implementations of dissipative (dynamic) self-assembly. *J. Phys. Chem. B* **2006**, *110*, 2482–2496.
- [18] J. V. I. Timonen, M. Latikka, L. Leibler, R. H. A. Ras, O. Ikkala, Switchable static and dynamic self-assembly of magnetic droplets on superhydrophobic surfaces. *Science* **2013**, *341*, 235–240.
- [19] J. Boekhoven, A. M. Brizard, K. N. K. Kowlgi, G. J. M. Koper, R. Eelkema, J. H. van Esch, Dissipative self-assembly of a molecular gelator using a chemical fuel. *Angew. Chem., Int. Ed.* **2010**, *49*, 4825–4828.
- [20] K. Matyjaszewski, S. G. Gaynor, A. Kulfan, M. Podwika, Preparation of hyperbranched polyacrylates by Atom Transfer Radical Polymerization. 1. Acrylic AB* monomers in “living” radical polymerizations. *Macromolecules* **1997**, *30*, 5192–5194.
- [21] J. C. Thomas, The determination of log normal particle size distributions by dynamic light scattering. *J. Colloid Interface Sci.* **1987**, *117*, 187–192.
- [22] R. E. Robertson, S. E. Sugamori, The hydrolysis of dimethyl sulfate and diethyl sulfate in water. *Can. J. Chem.* **1966**, *44*, 1728–1730.
- [23] M. Heskins, J. E. Guillet, Solution properties of poly(*N*-isopropylacrylamide). *J. Macromol. Sci., Chem.* **1968**, *2*, 1441–1455.

-
- [24] K. Matyjaszewski, J. Xia, Atom Transfer Radical Polymerization. *Chem. Rev.* **2001**, *101*, 2921–2990.
- [25] C. Speyerer, K. Borchers, T. Hirth, G. E. M. Tovar, A. Weber, Surface etching of methacrylic microparticles via basic hydrolysis and introduction of functional groups for click chemistry. *J. Colloid Interface Sci.* **2013**, *397*, 185–191.
- [26] L. S. Connell, J. R. Jones, J. V. M. Weaver, Transesterification of functional methacrylate monomers during alcoholic copper-catalyzed Atom Transfer Radical Polymerization: Formation of compositional and architectural side products. *Polym. Chem.* **2012**, *3*, 2735–2738.
- [27] D. R. Lide, H. P. R. Frederikse, *CRC Handbook of Chemistry and Physics*, 76th ed.; CRC Press: Boca Raton, FL, 1995.

Part 3

Colloids with Tunable Surface Charge

8

Charge Inversion of Chlorinated Colloids in Dimethylformamide

Abstract

In this chapter we report the observation that cross-linked chlorinated polystyrene colloids invert the sign of their surface potential while being dispersed in dimethylformamide (DMF). The particles are initially negatively charged due to the presence of sulfonate and sulfate groups on the surface which originate from the initiators used for the preparation of the chlorinated particles. However, storing the particles in DMF without the addition of any other reactants leads to significant positive values of the ζ potential. We believe that this charge inversion is the result of a reaction between DMF and the surface chlorine groups resulting in formation of tertiary and permanently charged quaternary amines. Surprisingly, the dispersions show colloidal stability after charge reversal, which is not expected based on standard DLVO theory. This reaction could therefore be used to control the surface charge of these colloids. Unfortunately, it turns out that the reaction cannot be quenched efficiently at a desired potential due to residual DMF which swells the particles and a two-step reaction mechanism responsible for the formation of the permanent positive charges.

8.1. Introduction

Surface modification of particles is of great interest in the field of colloid and material science. The physical properties of colloids heavily depend on their surface characteristics. Besides the use of charged moieties or polymers for stabilizing colloids against aggregation,^{1,2} the introduction of engineered molecules to the surface is of interest in, for example, solid phase synthesis,^{3,4} immobilization of (bio)catalysts,^{5,6} and tuning of interactions between particles.⁷⁻¹⁰ Direct attachment of complex molecules during particle synthesis is usually not possible due to instability of the emulsion or dispersion. However, particles equipped with small, but reactive chemical handles, e.g. OH, COOH and Cl can be easily synthesized by choosing appropriate (co)monomers.¹¹ Numerous post-functionalization methods based on straightforward organic chemistry are known to convert these groups into the desired functional moieties. Examples can be found throughout this thesis.¹²

Since the intermediate particles carry reactive groups on their surface, side reactions can (easily) occur leading to unwanted changes of the colloidal surface with dramatic alternations in their physical properties. Many of the chemical post-functionalization procedures referred to in the previous paragraph are conducted in dimethylformamide (DMF). DMF is a well-known and widely used solvent in organic and polymer chemistry due to its great solvation power for hydrophobic as well as hydrophilic compounds. DMF is a-protic, which makes this liquid one of the solvents of choice for S_N2 substitution reactions.¹³ Especially reactions involving negatively charged reactants are effective, because DMF is incapable of efficient solvation of these species; in contrast, cations are stabilized through interaction with the oxygen atoms.¹³ An advantage which is especially useful in the field of colloid chemistry is that DMF is very polar. Therefore, it is possible to disperse charge stabilized particles in this solvent without losing colloidal stability and allowing for homogenous surface reactions.

However, the use of DMF is not completely without risk, especially in the absence of other, more reactive species. Here we present an example of an unanticipated side reaction of chlorinated colloids with DMF leading to the formation of tertiary and quaternary amines on the surface.¹⁴ The chlorinated particles are charge stabilized by the presence of sulfonate and sulfate groups on their surface and have therefore a negative surface potential. Since quaternary amines have a permanent positive charge, the surface charge becomes more positive when the reaction proceeds, eventually leading to a complete reversal of the sign of the ζ potential. Interestingly, we found that the colloids only temporarily lose their colloidal stability near the iso-electric point. Continuing the reaction and therefore increasing the number of positive charges on the colloids resulted in regaining colloidal stability. Using this reaction to our advantage to tune and control the surface potential of the particles proved to be difficult since

the quaternary amines are introduced via a multi-step reaction mechanism.^{14–16} Additionally, DMF swells the polystyrene colloids which makes it difficult to quickly quench the increase in surface potential.

Our example shows that one has to take care in the choice of solvent and should realize that seemingly inert chemicals can still react up to such levels that the whole colloidal system is altered.

8.2. Experimental Section

8.2.1. Materials. Styrene (St, 99%), divinylbenzene (DVB, 55% mixture of isomers, tech. grade), vinylbenzyl chloride (VBC, $\geq 90\%$, tech. grade) and dimethylformamide (DMF, $> 99\%$) were purchased from Sigma-Aldrich. Potassium persulfate (KPS, $> 99\%$ for analysis), sodium bisulfite (reagent ACS) and dimethyl sulfoxide (DMSO, 99.7%) were obtained from Acros Organics. All chemicals were used as received. The water used throughout all syntheses was purified using a Milli-Q water purification system

8.2.2. Surface reaction of chlorinated colloids (CPs-Cl) with DMF. Chlorinated colloids (CPs-Cl) were prepared using the same core-shell approach described in Chapter 2.¹² This synthesis consisted of two steps, namely the synthesis of a cross-linked polystyrene core (CPs) followed by the introduction of a cross-linked chlorinated shell. The synthetic procedure provided particles with a radius of 155 nm and a polydispersity of 4.4% as determined using transmission electron microscopy (TEM). The presence of the chlorine groups was confirmed using Fourier transform infrared spectroscopy (FT-IR) (1266 cm^{-1}) and X-ray photoelectron spectroscopy (XPS) [200 and 270 eV (Cl)].

After washing, the CPs-Cl particles were transferred from water to DMF by centrifugation and redispersion (three times). During this process the solid content was adjusted to 1%. A total of 5 mL DMF dispersion was obtained which was heated at 90 °C for 24 h. During the reaction, aliquots of 100 μL were withdrawn from the dispersion. The samples were washed directly with water (three times) and ethanol (two times) by centrifugation and redispersion cycles. After the last washing step the particles were transferred back to water. The resulting dispersions were characterized in terms of hydrodynamic size (and its distribution) and the ζ potential. A similar reaction was conducted with DMSO as solvent.

8.2.3. Synthesis of non-chlorinated particles (CPs-St). The same core-shell approach as described in Section 8.2.2 was applied to prepare non-chlorinated particles. The crude CPs dispersion (25 mL) and water (10 mL) were introduced in a 50 mL three-neck flask equipped with a magnetic stir bar and submerged in a thermostated oil bath. This dispersion was bubbled with nitrogen for 30 min at room temperature (needle through a septum). After this 30 min, a mixture of styrene (1 mL) and DVB

(20 μL) was injected under inert atmosphere. After 1 h of swelling, the temperature was increased to 60 $^{\circ}\text{C}$. When this temperature was reached, the initiator solution (0.04 g KPS; 0.03 g sodium bisulfite dissolved in 2.5 mL water) was injected. After 4 h, the reaction was stopped and the particles were washed with water. The particles were analyzed by measuring their ζ potential.

8.2.4. Characterization. Infrared (IR) spectra were obtained using a PerkinElmer FT-IR/FIR Frontier Spectrometer in attenuated total reflectance (ATR) mode. Measurements were taken on powders obtained by drying the particle dispersion.

Dynamic light scattering (DLS) and ζ potential measurements were performed using a Malvern Zetasizer Nano using highly diluted aqueous dispersions at a temperature of 25 $^{\circ}\text{C}$. The DLS measurements were performed in 7 runs of 15 individual measurements in backscatter mode (173°). The sizes of the colloids or aggregates are reported as the Z-average diameter and the corresponding polydispersity index (PDI). These values were obtained by using the cumulant method as described in ref. 17. The absolute values obtained for the Z-average diameter and the PDI for the aggregated dispersions are less reliable. Nevertheless, these values can still be used to verify if a colloidal dispersion is randomly aggregating, which results in higher Z-average diameters and PDI values. For the ζ potential measurements, 7 runs of at least 50 individual measurements were performed to obtain a statistically reliable potential. Electrophoretic mobilities were measured in Milli-Q water (ionic strength $\approx 10^{-5}$). Given this ionic strength and the size of our particles we used an analytical expression developed by Ohshima to calculate the value of the Henry function ($f(\kappa R)$), which turned out to be 1.05.¹⁸ For simplicity, the Hückel limit ($f(\kappa R) = 1$) of the Henry equation was used to convert the electrophoretic mobilities to ζ potentials.¹

8.3. Results and Discussion

8.3.1. Experimental observation of charge inversion of chlorinated colloids dispersed in DMF. As discussed in the Introduction, DMF is a perfect solvent for conducting reactions that follow a polar mechanism, such as $\text{S}_{\text{N}}2$ displacements. Due to the high polarity, this solvent can also be used for surface reactions on charge stabilized colloids as shown in Chapter 2, where surface chlorine groups were replaced by azides in DMF. Since in this type of reactions, the present nucleophile (azide anion) is very reactive, usually no side reaction with DMF occur.¹²

However, we found that storing the chlorinated particles in DMF for a long time at room temperature in the absence of any other reactants resulted in a reversal of the ζ potential from negative to positive while remaining colloidally stable. Based on this observation, we did a controlled experiment where we dispersed the chlorinated particles in DMF and monitored the ζ potential during the process. The reaction was conducted at 90 $^{\circ}\text{C}$ to speed up the process. The progression of the ζ potential

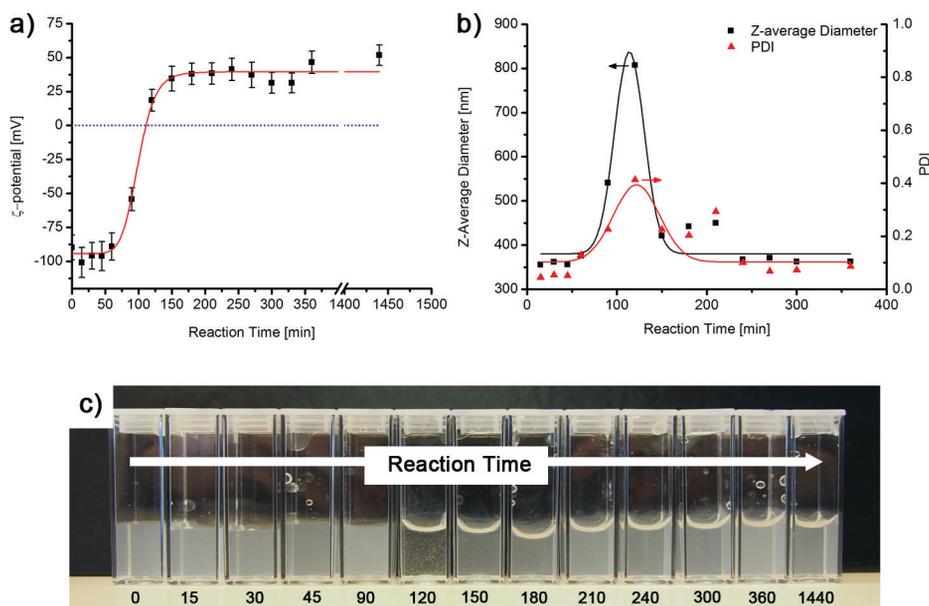
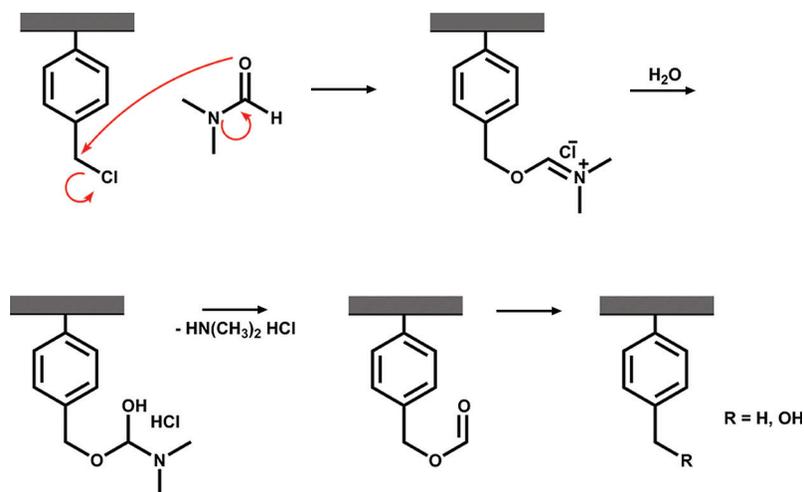


Figure 8.1. (a) The evolution of the ζ potential in time of the chlorinated particles dispersed in DMF at 90 °C. (b) The evolution of the Z-average diameter and the polydispersity index (PDI) of the chlorinated particles during the reaction with DMF. (c) Macroscopic picture of the colloidal stability of the chlorinated particles during the reaction with DMF. The numbers in the bottom of the figure correspond to the reaction time in minutes.

in time is plotted in Figure 8.1a. The ζ potential remained rather constant during the first hour. After this period, the potential increased very rapidly to a final potential of approximately +45 mV. After 110 min, the particles had a ζ potential of 0 mV. At this point no net electrostatic repulsion was present to stabilize the colloids against aggregation via Van der Waals attraction. The Z-average size and the polydispersity index (PDI) of the particles shot up around 110 min, corresponding to uncontrolled aggregation (Figure 8.1b). The aggregation was also observed macroscopically as shown in Figure 8.1c, where the cuvettes used for the DLS measurements are depicted. The aggregated colloids appear as large white flocculates in a clear dispersion medium, while the colloidally stable dispersion showed a homogenous white dispersion caused by scattering of light by the individual colloids.

Purely based on DLVO theory, the particles should be trapped in their primary minimum and therefore irreversibly aggregated at the point where the ζ potential equals zero.^{1,2} However, when the surface reaction with DMF proceeded the Z-average size and the PDI decreased again to values similar to that of the initial chlorinated colloids. In other words, the particles regained their colloidal stability. The details of

Scheme 8.1. The formation of hydroxyl and methyl moieties at the surface after reaction of DMF with the benzyl chloride functional groups present at the colloidal surface.¹⁴

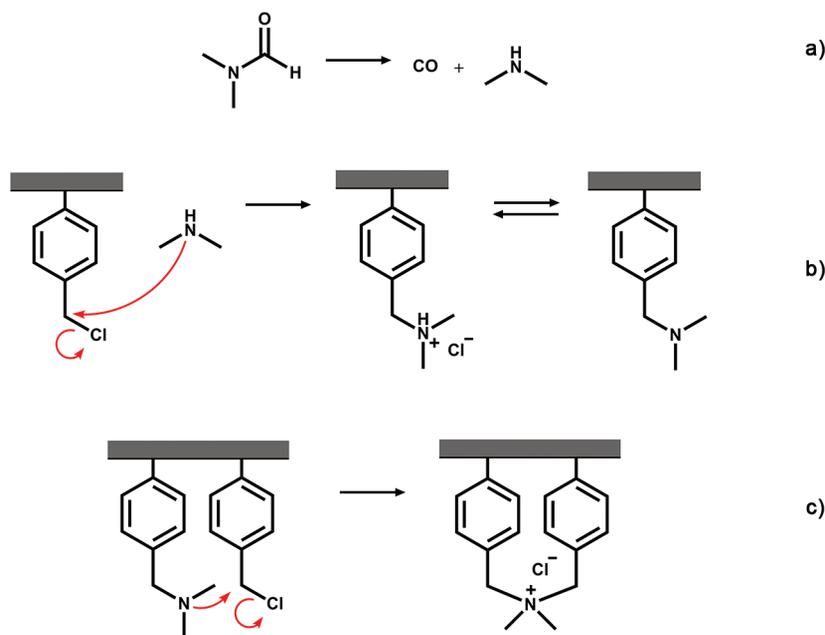


this behavior will be treated in Chapter 9, which deals with a more controlled and robust way of inverting the charge of these colloids.

8.3.2. Mechanistic insight into the surface modification reactions. Particles without chlorine functionalities did not show any increase in the ζ potential, even after 48 h of heating in DMF. This observation is in line with the work of Alexandratos et al., who reported that the use of DMF in combination with chlorinated beads at elevated temperatures leads to the replacement of the chlorine groups by dimethylamines, $-CH_2OH$ or methyl groups (Scheme 8.1).¹⁴ The formation of the hydroxyl and methyl moieties proceeds via the formation of a formate ester using a Vilsmeier-type reaction mechanism. Decomposition of the formate ester with water results in the hydroxyl group, while the methyl group is formed if no water is involved. The tertiary amines are formed after amination of the chlorine group with dimethylamine. Dimethylamine is formed during the decomposition of DMF (a) in Scheme 8.2). The tertiary amines can be protonated resulting in a positive charge. This would imply that the particles are only positively charged in (slightly) acidic media. The reactions by Alexandratos et al. were performed on poly(VBC) beads of 250–450 μm which are not colloidal and the effect of the reaction on the ζ potential was therefore not addressed.

The previous ζ potential measurements (Figure 8.1) were conducted at a pH of 6 to 7. At this pH, we expected that a fraction of the tertiary amines, if present, were

Scheme 8.2. Thermal degradation of DMF into dimethylamine and CO (a) and subsequent formation of tertiary (b) and quaternary (c) amines on the surface of chlorinated particles.¹⁴



protonated. To test if the positive charges were indeed pH dependent, we measured the potential of the sample obtained after 24 h of reaction at pH 2 (5 mM HCl) and pH 12 (5 mM NaOH). The ζ potential was also measured at neutral pH, but at the same ionic strength (5 mM NaCl) to be able to compare the obtained potentials fairly. As indicated in Figure 8.2a, the ζ potential did not change due to the higher ionic strength by introducing sodium chloride into the solution. Therefore, the obtained potentials could be measured accurately at this slightly elevated ionic strength. Changing the pH did also not affect the measured potential (Figure 8.2a), which showed that the charge on the particles is not regulated by protonation of the colloidal surface. Instead, there must be a chemical entity with a permanent, pH independent positive charge. These entities could in principle be generated when the formed tertiary amines react with a second surface benzyl chloride group, resulting in quaternary amines (Scheme 8.2). This type of reactions were observed in literature where benzyl chloride was reacted with DMF.^{15,16}

The time series presented in Figure 8.1 suggested that this synthesis gives us a protocol to tune the ζ potential as function of the reaction time. By extracting a sample from the reaction mixture and removing the DMF, one could stop the surface reaction

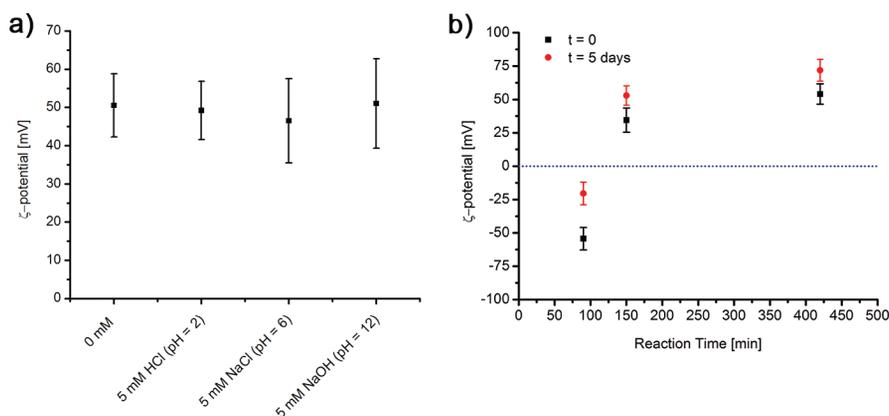


Figure 8.2. (a) The ζ potential of the chlorinated particles measured after 24 h of reaction with DMF as function of the pH and the ionic strength. (b) Change in the ζ potential of the chlorinated particles reacted with DMF after storing the particles in water for 5 days.

and stop the charging of the particles, leading to the desired ζ potential. To test if this was indeed possible, samples taken after 90, 150 and 420 min were kept in water for 5 days. After this period the ζ potential was measured again. In all three cases the potential increased significantly compared to the ζ potential measurement performed directly after the reaction (Figure 8.2b).

Two possible explanations can be given for this behavior. Firstly, DMF is able to swell the cross-linked polystyrene particles. When the particles are dispersed in DMF, the solvent penetrates into the core of the particle. After withdrawing samples from the mixture and the standard washing procedure via centrifugation and redispersion with water it is possible that some residual DMF remains inside the particles. The DMF diffuses slowly out of the particles and reacts with the chlorine groups when it reaches the surface of the particles.

The second explanation might come from the reaction mechanism shown in Scheme 8.2. The formation of quaternary amines is a two-step process in which only the first step, the formation of the tertiary amine, requires the presence of DMF. After removal of DMF, the formed tertiary amines can still react with the pending benzyl chloride moieties, ultimately leading to an increase in the ζ potential. Data dealing with the reaction rate of these coupling reactions are not known, so it could be that this reaction is rather slow and proceeds for a long time after removal of the DMF.

8.3.3. DMSO versus DMF. Finally, we would like to have an alternative for DMF. An obvious candidate for this is dimethyl sulfoxide (DMSO). Similar to DMF, DMSO is a polar a-protic solvent. To investigate if no side reactions occur that alter the surface charge of the colloids, the chlorinated particles were dispersed in DMSO

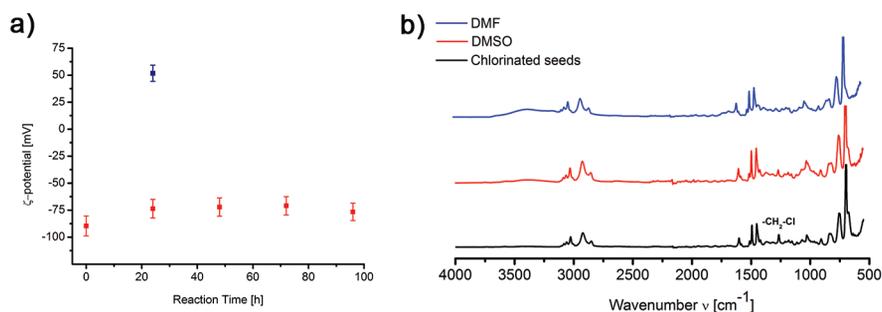


Figure 8.3. (a) Change in the ζ potential of the chlorinated particles reacted with DMSO (red symbols) and with DMF (blue symbol) at 90 °C. (b) Infrared (IR) spectra of the chlorinated seed particles (black) and the resulting particles after heating for 24 h at 90 °C in DMSO (red) or DMF (blue).

and heated at 90 °C for 24 h (analogous to the controlled reaction performed with DMF). Figure 8.3a shows the resulting ζ potential as function of reaction time. Clearly, no difference in potential was measured. Additionally, Figure 8.3b shows the IR spectra obtained before heating (black) and after heating the particles at 90 °C for 24 h in DMF (blue) and DMSO (red). The spectrum of the particles dispersed in DMF show complete disappearance of the $-\text{CH}_2\text{-Cl}$ signal at 1266 cm^{-1} , while this signal is still prominently present in the spectrum obtained from the colloids dispersed in DMSO. Therefore, the chemical handle was preserved on the surface. The slight decrease in intensity of this signal can be explained by hydrolysis of the chlorine groups by water which is inevitably present in DMSO (DMSO is very hygroscopic). This also explains the weak signal observed around 3200 cm^{-1} .

An additional advantage of DMSO over DMF is the limited solubility of polystyrene in DMSO.^{19,20} Even without high degrees of cross-linking, polystyrene particles can be dispersed in this solvent without significant dissolution and disintegration of the colloidal particles.

8.4. Conclusions

We showed that the surface charge of the chlorinated particles inverted by reaction with DMF. During this charge reversal, the colloids aggregated reversibly around the point of zero surface charge. Proceeding the surface reaction with DMF resulted in regaining of the colloidal stability and stable dispersion of colloids with a positive ζ potential were obtained.

The reaction mechanism is debatable and involves several reaction steps which most probably results in the formation of a colloidal surface with several different chemical moieties ($-\text{CH}_3$, $-\text{CH}_2\text{OH}$, $\text{CH}_2\text{N}(\text{CH}_3)_2$, $(\text{CH}_2)\text{N}^+(\text{CH}_3)_2$). Furthermore,

DMF swells the particles, which hampers removal of all DMF upon washing. These features make it difficult to quench and control the potential at a certain desired value. Nevertheless, the fact that charge inversion takes place without the loss of colloidal stability is remarkable.

The surface reaction with DMF was unexpected and shows that surface modification reactions need to be performed with great caution. Seemingly unlikely or unimportant side reactions might have a huge effect on the physical behavior of the resulting particles. For the chlorinated particles the side reactions could be easily circumvented by substituting DMF for DMSO, which has no measurable effect on the surface potential of these particles.

References

- [1] R. J. Hunter, In *Foundations of Colloid Science*, 2nd ed.; Oxford University Press: New York, 2009.
- [2] J. N. Israelachvili, In *Intermolecular & Surface Forces*, 3rd ed.; Academic Press, Amsterdam, The Netherlands, 2011.
- [3] P. H. H. Hermkens, H. C. J. Ottenheijm, D. Rees, Solid-phase organic reactions: A review of the recent literature. *Tetrahedron* **1996**, *52*, 4527–4554.
- [4] R. C. D. Brown, Recent developments in solid-phase organic synthesis. *J. Chem. Soc., Perkin Trans.* **1998**, *1*, 3293–3320.
- [5] E. M. Claesson, N. C. Mehendale, R. J. M. Klein Gebbink, G. van Koten, A. P. Philipse, Magnetic silica colloids for catalysis. *J. Magn. Magn. Mater.* **2007**, *11*, 41–45.
- [6] S. Shylesh, V. Schnemann, W. R. Thiel, Magnetically separable nanocatalysts: Bridges between homogeneous and heterogeneous Catalysis. *Angew. Chem., Int. Ed.* **2010**, *49*, 3428–3459.
- [7] X. Y. Ling, I. Y. Phang, C. Acikgoz, M. D. Yilmaz, M. A. Hampenius, G. J. Vansco, J. Huskens, Janus particles with controllable patchiness and their chemical functionalization and supramolecular assembly. *Angew. Chem., Int. Ed.* **2009**, *121*, 7813–7818.
- [8] N. Geerts, E. Eiser, DNA-functionalized colloids: Physical properties and applications. *Soft Matter* **2010**, *6*, 4647–4660.
- [9] Y. Wang, Y. Wang, D. R. Breed, V. N. Manoharan, L. Feng, A. D. Hollingsworth, M. Weck, D. J. Pine, Colloids with valence and specific directional bonding. *Nature* **2013**, *491*, 51–56.
- [10] Y. Wang, A. D. Hollingsworth, S. K. Yang, S. Patel, D. J. Pine, M. Weck, Patchy particle self-assembly via metal coordination. *J. Am. Chem. Soc.* **2013**, *135*, 14064–14067.

-
- [11] A. M. van Herk, In *Chemistry and technology of emulsion polymerisation*, Blackwell Publishing, 2005.
- [12] B. G. P. van Ravensteijn, M. Kamp, A. van Blaaderen, W. K. Kegel, General route toward chemically anisotropic colloids. *Chem. Mater.* **2013**, *25*, 4348–4353.
- [13] M. A. Fox, J. K. Whitesell, In *Organic Chemistry*, 3rd ed.; Jones and Bartlett Publishers: Sudbury, MA, 2003; pp 373–375.
- [14] S. D. Alexandratos, X. Zhu, Amination of poly(vinylbenzyl chloride) with *N,N*-dimethylformamide. *Macromolecules* **2003**, *36*, 3436–3439.
- [15] G. M. Coppinger, Preparations of *N,N*-dimethylamides. *J. Am. Chem. Soc.* **1954**, *76*, 1372–1373.
- [16] N. Kornblum, R. K. Blackwood, The interaction of alkyl halides with dimethyl formamide. *J. Am. Chem. Soc.* **1956**, *78*, 4037–4039.
- [17] J. C. Thomas, The determination of log normal particle size distributions by dynamic light scattering. *J. Colloid Interface Sci.* **1987**, *117*, 187–192.
- [18] H. Ohshima, A simple expression for Henry's function for the retardation effect in electrophoresis of spherical colloidal particles. *J. Colloid Interface Sci.* **1994**, *168*, 269–271.
- [19] A. Rudin, In *The elements of polymer science and engineering*, 2nd ed.; Academic Press: San Diego, 1999.
- [20] A. F. M. Barton, In *CRC handbook of solubility parameters and other cohesion parameters*, 2nd ed.; CRC Press: Boca Raton, FL, 1991.

9

Colloids with Continuously Tunable Surface Charge

Abstract

In this chapter, we present a robust way to tune the surface potential of polystyrene colloids without changing the pH, ionic strength or solvent. The colloids are composed of a cross-linked polystyrene core and a cross-linked vinylbenzyl chloride layer. Besides the chlorine groups, the particle surface contains sulfate/sulfonate groups arising from the polymerization initiators which provide a negative surface potential. Performing a Menshutkin reaction on the surface chlorine groups with tertiary amines allows us to introduce quaternary, positively charged amines. The overall charge on the particles is then determined by the ratio between the sulfate/sulfonate moieties and the quaternary amines. Using this process, we were able to invert the charge in a continuous manner without losing colloidal stability upon passing the isoelectric point. The straightforward reaction mechanism together with fast quenching of the reaction results in a colloidal system in which the ζ potential can be tuned between -80 and $+45$ mV. As proof of principle, the positively charged particles are used in heterocoagulation experiments with nanometer and micrometer-sized negatively charged silica particles to create geometrically well-defined colloidal (nano-)clusters.

9.1. Introduction

Control over the surface charge of colloids is a priori a versatile way to tune interactions between particles.^{1,2} Examples of systems in which this strategy has been used are capsules as delivery systems,³ colloidal clusters,⁴ and colloidal ionic crystals.⁵ To achieve control over the surface charge, various methods have been described, e.g. the addition of pH-sensitive functionalities to the surface (carboxylic acid, amines, and hydroxyl groups) usually in a covalent fashion by using functional monomers^{6–8} and initiators^{8–11} or the adsorption of (poly)electrolytes.^{12–14}

Here we present a new method for tuning the surface potential of particles, namely via chemical reactions that covalently link charged species to the colloidal surface. We will focus on the charge reversal of particles that are initially negatively charged because of the presence of sulfate/sulfonate groups on the surface. Besides these negatively charged groups, the particles are decorated with chlorine groups that we can convert to permanently positively charged quaternary amines via the Menshutkin reaction using tertiary amines (see Scheme 9.1). The overall charge of the particle is then determined by the ratio between the sulfate/sulfonate groups and quaternary amines. Because the surface potential is determined by covalently attached moieties, they provide a means of controlling the number of charges on the particles without changing other variables in the system such as the ionic strength or the type of solvent.

To show the synthetic utility of these particles, a few examples are shown of electrostatically driven self-assembly for the formation of organic–inorganic hybrid colloidal clusters.

9.2. Experimental Section

9.2.1. Materials. Styrene (St, 99%), divinylbenzene (DVB, 55% mixture of isomers, technical grade), vinylbenzyl chloride (VBC, $\geq 90\%$, technical grade), dimethylformamide (DMF, $> 99\%$), trimethylamine (TMA, ~ 45 wt% aqueous solution), tetraethoxysilane (TEOS, $\geq 99\%$, GC), and LUDOX TMA colloidal silica (34 wt% aqueous dispersion, particle diameter of ≈ 17 nm, Sigma-Aldrich data sheet) were purchased from Sigma-Aldrich. Potassium persulfate (KPS, $> 99\%$ for analysis) and sodium bisulfite (NaHSO_3 , ACS reagent grade) were obtained from Acros Organics. Triethylamine (TEA, puriss. p.a.; $\geq 99.5\%$) was obtained from Fluka. Ethanol (absolute, p.a.) was purchased from Merck. Ammonia (analytical reagent grade, 25% aqueous solution) from Fischer was used. All chemicals were used as received. The water used throughout all syntheses was purified using a Milli-Q water purification system.

9.2.2. Synthesis of chlorinated particles (CPs-Cl). The chlorinated colloids (CPs-Cl) were prepared using the same core-shell approach as described in Chapter 2.¹⁵ This synthesis consisted of two steps, namely the synthesis of a cross-linked

polystyrene core (CPs) followed by the introduction of a cross-linked chlorinated shell. The synthetic procedure yielded particles with a radius of 155 nm and a polydispersity of 4.4% as determined by transmission electron microscopy (TEM). The presence of the chlorine groups was confirmed by Fourier transform infrared spectroscopy (FT-IR) (1266 cm^{-1}) and X-ray photoelectron spectroscopy (XPS) [200 and 270 eV (Cl)].

9.2.3. Surface reaction of CPs-Cl with TEA. A CPs-Cl dispersion (0.5 mL) was diluted with water to a solid content of 1%. To this mixture, triethylamine (TEA, 35 μL) was added while the dispersion was vigorously stirred. The reaction was conducted at 20, 25, 35, 50, and 80 $^{\circ}\text{C}$ in a thermostated oil bath. During the reaction, aliquots (100 μL) were withdrawn from the mixture. The Menschutkin reaction was quenched by rapid centrifugation (several seconds at 11000g) and replacement of the TEA-containing supernatant with water. Additional washing steps with water (two times) and ethanol (two times) by centrifugation and redispersion were conducted. After the last washing step, the particles were transferred back to water and characterized in terms of hydrodynamic size (and its distribution) and their ζ potential. The particle morphology was probed via TEM.

9.2.4. Synthesis of micrometer-sized silica colloids. For preparation of large silica spheres, the method of Zhang et al.¹⁶ was used. This method is based on the standard Stöber synthesis¹⁷ and on the seeded growth method developed by Philipse et al.¹⁸ To a mixture of ethanol (48.4 mL) and ammonia (11.6 mL), a solution of TEOS (0.5 mL) in ethanol (2.0 mL) was added. The resulting mixture was stirred for 2 h. Within a few min, the dispersion turned opaque, indicating the formation of the core particles. These particles were grown by addition of TEOS (5 mL) diluted with ethanol (20 mL) over an period of approximately 2 h. The dispersion was stirred overnight and subsequently washed repeatedly by centrifugation and redispersion in ethanol. A particle radius of 465 nm and a polydispersity of 2.6% were measured using TEM.

9.2.5. Heterocoagulation between positively charged polystyrene colloids and negatively charged silica nanoparticles (LUDOX). A LUDOX dispersion (25 μL) was diluted to 0.5 mL and sonicated 10 min before use. The diluted silica dispersion was slowly dropped into a flask containing the positively charged polystyrene dispersion (25 μL , particles prepared as described in Section 9.2.3 at 20 $^{\circ}\text{C}$) and water (0.5 mL) while the mixture was sonicated. The mixture was sonicated for an additional 10 min after which the aggregates were washed by centrifugation and redispersion cycles in water. The washed aggregates were analyzed with TEM.

9.2.6. Heterocoagulation between positively charged polystyrene colloids and negatively charged micrometer-sized silica colloids. The crude silica dispersion (0.3 mL, particles prepared as described in Section 9.2.4) was washed and transferred from ethanol (in which the particles were prepared) to water (0.3 mL) by

two centrifugation and redispersion cycles. The dispersion containing the positively charged polystyrene particles (2 μL , see Section 9.2.3. Reaction with TEA was performed at 20 $^{\circ}\text{C}$) was diluted with water to 1 mL. The silica dispersion was added dropwise while the mixture was sonicated. The resulting dispersion was analyzed using light microscopy without any further purification.

A similar heterocoagulation experiment was performed DMF instead of water. After formation of the clusters, the dispersion was heated at 110 $^{\circ}\text{C}$ for 30 min. The resulting clusters were washed by centrifugation and redispersion via sonication and analyzed with TEM.

9.2.7. Characterization. Transmission electron microscopy (TEM) pictures were taken with a Philips Technai10 electron microscope typically operating at 100 kV. Bright field images were recorded using a SIS Megaview II CCD camera. The samples were prepared by drying a drop of a diluted, aqueous particle dispersion on top of polymer coated copper grids.

The XPS measurements were taken with a Thermo Scientific K-Alpha instrument, equipped with a monochromatic small-spot X-ray source and a 180 $^{\circ}$ double-focusing hemispherical analyzer with a 128-channel detector. Spectra were recorded using an aluminum anode (Al K α = 1486.6 eV) operating at 72 W and a spot size of 400 μm . Survey scans were measured at a constant pass energy of 200 eV and region scans at 50 eV. The background pressure was 2×10^{-9} mbar and during measurement 3×10^{-7} mbar of argon because of the charge compensation dual-beam source.

IR spectra were obtained using a PerkinElmer FT-IR/FIR Frontier Spectrometer in attenuated total reflectance (ATR) mode. Measurements were taken on powders obtained by drying the particle dispersion.

Dynamic light scattering (DLS) and ζ potential measurements were performed using a Malvern Zetasizer Nano instrument using highly diluted aqueous dispersions at 25 $^{\circ}\text{C}$. The DLS measurements were taken in seven runs of 15 individual measurements in backscatter mode (173 $^{\circ}$). The sizes of the colloids or aggregates are reported as Z-average diameters and the corresponding polydispersity index (PDI). These values were obtained by using the cumulant method as described in ref. 19. The absolute values obtained for the Z-average diameter and the PDI for the aggregated dispersions are less reliable. Nevertheless, these values can still be used to verify if a colloidal dispersion is randomly aggregating, which results in higher Z-average diameters and PDI values. For the ζ potential measurements, seven runs of at least 50 individual measurements were conducted to obtain a statistically reliable potential. Electrophoretic mobilities were measured in Milli-Q water (ionic strength of $\approx 10^{-5}$). Given this ionic strength and the size of our particles, we used an analytical expression developed by Ohshima to calculate the value of the Henry function $[f(\zeta R)]$, which turned out to be 1.05.²⁰ For the sake of simplicity, the Hückel limit $[f(\zeta R) = 1]$ of the

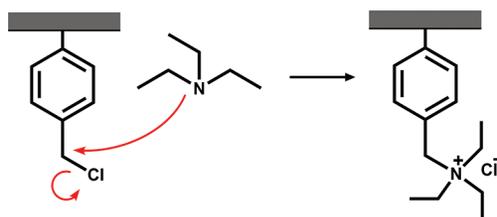
Henry formula was used to convert the electrophoretic mobilities to ζ potentials.²¹

Light microscopy was performed using a Zeiss Axioplan microscope equipped with an oil immersion lens (NA = 1.4, 100 \times magnification). The pictures were captured with a Basler scout camera. Samples were prepared by placing a drop of the diluted dispersion on a microscopy slide.

9.3. Results and Discussion

9.3.1. Synthesis of chlorinated colloids and their charge inversion using the Menshutkin reaction. We synthesized polystyrene particles that contained a chlorinated outer layer via a previously published method.¹⁵ The presence of the benzyl chloride functionalities was confirmed using both IR and XPS measurements. The particles were charge-stabilized by the presence of sulfate/sulfonate groups at the colloidal surface originating from potassium persulfate and sodium bisulfite that acted as an initiator system. As pointed out in Chapter 2, a combination of KPS and sodium bisulfite was used as initiator system to shift the mechanism for radical formation from a purely thermal process by decomposition of persulfate to a redox process in which the bisulfite ion acts as a reductor.²² In this way, polymerization could be conducted at a lower temperature, suppressing the undesired hydrolysis of the relatively labile chlorine functionality of VBC. The chlorine groups on the surface provide a chemical handle that can be easily converted to a variety of functionalities.²³ The introduction of charged moieties and therefore, regulation of the surface potential, should also be possible. To investigate this, we made use of the Menshutkin reaction (Scheme 9.1).²⁴ This choice was based on previous observations in which chlorinated particles reversed their charge without losing colloidal stability upon a surface reaction with dimethylformamide (Chapter 8). The Menshutkin reaction converts the chlorine functionalities of the particles to quaternary amines with permanent positive charges in a one-step reaction with tertiary amines, in this case triethylamine. The final charge of the colloids is expected to be determined by the ratio between the negative sulfate/sulfonate groups and the newly introduced quaternary amines.

Scheme 9.1. Menshutkin reaction between surface benzyl chloride groups and triethylamine (TEA) leading to the formation of a permanently positively charged quaternary amine at the colloidal surface.



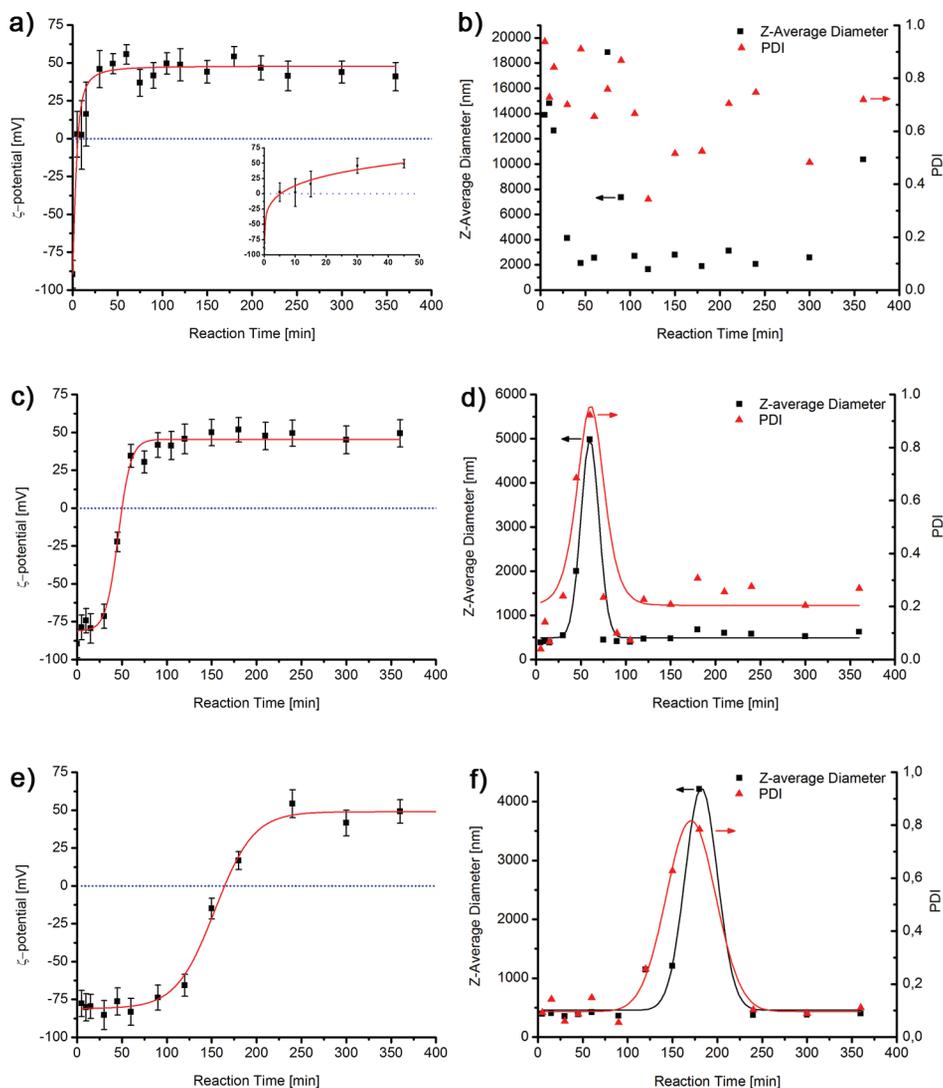


Figure 9.1. (a) Evolution of the ζ potential of the chlorinated particles over time during the reaction with triethylamine (TEA) at 80 °C. (b) Evolution of the Z-average diameter and the polydispersity index (PDI) of the chlorinated particles during the reaction with TEA at 80 °C. (c) Evolution of the ζ potential of the chlorinated particles during the reaction with TEA at 35 °C. (d) Z-average diameter and PDI of the chlorinated particles during the reaction with TEA at 35 °C. (e) Evolution of the ζ potential at a reaction temperature of 20 °C. (f) Z-average diameter and PDI over time at a reaction temperature of 20 °C.

The surface reaction was conducted at 20, 25, 35, 50, and 80 °C. The ζ potential as well as the Z-average diameter and its polydispersity index (PDI) as a function of time for the reactions conducted at 20, 35, and 80 °C are plotted in Figure 9.1. The plots for the other reaction temperatures can be found in Appendix 1 (Figure 9.11).

In all cases, a final potential of approximately +45 mV was found (Figure 9.1a, c and e). The reaction rate (k) increases significantly with an increase in temperature as reflected in the reaction times required to pass the point of zero charge: less than 1 min for 80 °C and 180 min for 20 °C. For the highest reaction temperatures, the particles remained aggregated and colloidal stability was not restored, as was observed from the macroscopic appearance of the dispersions shown in Figure 9.2a and the large values measured for both the Z-average diameter and the PDI (Figure 9.1a and b). Interestingly, when the reaction temperature was decreased, we found that colloidal stability could be restored (Figure 9.1c–f). The return of colloidal stability becomes more significant with decreasing reaction temperature. At a temperature of 20 °C, the PDIs and size distributions were identical to those obtained for the chlorinated particles, indicating fully restored stability. The restored stability is also reflected in the macroscopic picture of the dispersion (Figure 9.2b). Compared to Figure 9.2a, it is evident that these particles were much more stable. The samples that reacted at

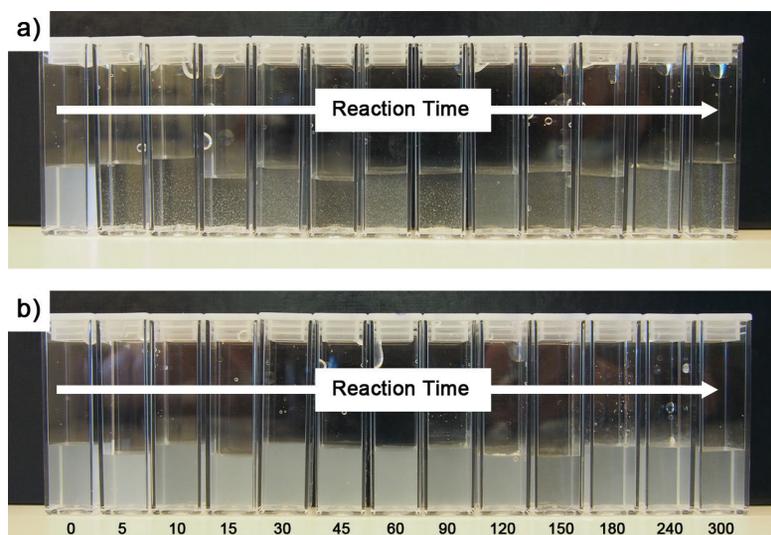


Figure 9.2. (a) Picture of the macroscopic colloidal stability during the surface reaction with triethylamine (TEA) at 80 °C. Large aggregates of colloids are formed after crossing the isoelectric point (< 5 min). Fast sedimentation causes the clear appearance of the samples. (b) Picture of the macroscopic colloidal stability at a reaction temperature of 20 °C. The numbers at the bottom correspond to the reaction times in minutes for both panels a and b.

20 °C were turbid because of scattering of the freely moving particles suspended in solution, while the macroscopic picture in Figure 9.2a shows large aggregates that sediment quickly to the bottom of the sample vial, causing the clear appearance of these samples. The fact that the curves of Z-average diameter versus time and PDI versus time have a common maximum indicates that the observed clusters were formed due to random aggregation. Detailed analysis of the shapes of the curves of ζ potential versus time and the mechanism for regaining colloidal stability will be discussed in Sections 9.3.2 and 9.3.3.

The presented method provides a straightforward and reproducible way to control the ζ potential of the polystyrene colloids. To verify the robustness and permanent character of the obtained potentials, we extracted four samples (45, 90, 240, and 360 min) during a charge reversal reaction conducted at 20 °C. These samples were washed and the ζ potentials measured directly afterwards. After three days, the potentials were measured again. The results are summarized in Figure 9.3.

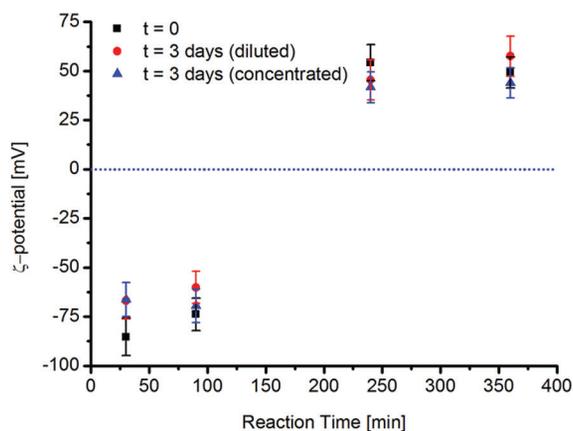


Figure 9.3. Change in ζ potential of the chlorinated particles reacted with triethylamine (TEA) after being stored in water as concentrated or diluted dispersion for three days.

It is immediately clear that the potentials that were measured after three days were comparable to the ζ potentials obtained directly after the surface reaction within experimental error. Storing the particles as a highly diluted (red dots) or concentrated (blue triangles) dispersion did not influence the measured potential, which is an indication that the species that are responsible for the positive charges were strongly bound to the colloids (no diffusion), which is in agreement with the mechanism of the Menshutkin reaction (Scheme 9.1). Quenching the reaction at a certain moment in time therefore provides an easy method for tuning the overall surface charge of these particles.

9.3.2. Theoretical considerations for regaining stability after charge inversion. To gain more insight into the process of charge reversal, attempts were made to explain the observations depicted in Figures 9.1 and 9.2. Restoring colloidal stability implies that the particles were not trapped in a deep attractive (Van der Waals) potential well close to the isoelectric point, as would be expected in the case of polystyrene particles in water according to DLVO theory. In other words, a cut-off distance that provides a limit to the minimal inter-particle distance and therefore, to the magnitude of the attractive Van der Waals force, must exist. This limit can be caused by the presence of a ‘hairy’ soft (polyelectrolyte) layer on the colloidal surface or a minimal possible inter-particle distance. Vigil et al. described a similar observation for the interaction potentials between silica surfaces.²⁵ At small separations ($< 20 \text{ \AA}$), a repulsive force was measured instead of a strong attraction predicted by DLVO theory. This repulsion was assigned to protruding silanol and silicilic acid groups causing a strong steric repulsion. If we extrapolate these findings to our system, it is possible that the tertiary amines introduced to the surface of the polystyrene colloids fulfill the same steric stabilization as the silanol and silicilic groups. However, direct experimental evidence of this is very hard to obtain.

TEM analysis revealed that the particles possess a rough surface with a typical length scale on the order of a few nanometers (Figure 9.4). As a crude approximation, this rough surface can be modeled as a smooth surface on which the minimal possible inter-particle distance is set by the magnitude of the roughness. The steric bulk of the introduced quaternary amines is much smaller than the roughness, so we assume that the steric layer on the particles does not influence the interaction potential between the colloids and conventional DLVO theory can be applied. The roughness was observed regardless of the reaction temperature used for the charge reversal reaction.

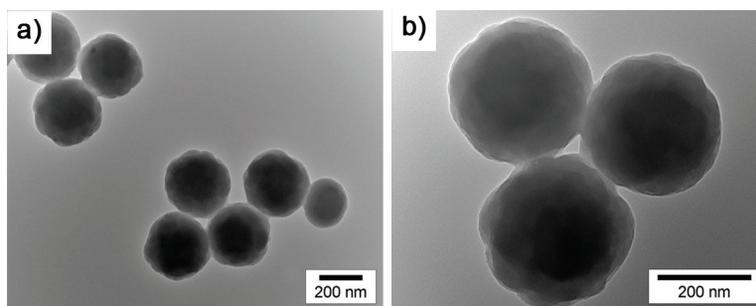


Figure 9.4. Transmission electron microscope (TEM) images of the positively charged particles, obtained after charge reversal using the Menshutkin reaction.

Using Eq. 9.1,¹ we calculated the DLVO potential in units of $k_B T$ for smooth spheres ($U_{DLVO}/k_B T$) by

$$\frac{U_{DLVO}}{k_B T} = -\frac{A_H R}{12d} + \left(\frac{e\zeta}{k_B T}\right)^2 \frac{R^2}{\lambda_B (2R + d)} e^{-\kappa d} \quad (9.1)$$

where A_H represents the dimensionless Hamaker constant of two polystyrene surfaces across water, R the radius of the particles, d the inter-particle distance, e the elemental charge, ζ the ζ potential, k_B the Boltzmann constant, T the temperature, λ_B the Bjerrum length, and κ the inverse screening length. κ was estimated based on the concentration of TEA. TEA is a weak base and via the base dissociation constant ($pK_b = 3.25$ at 25 °C),²⁶ we calculated the pH and therefore the ionic strength of the continuous phase. We assumed a constant ionic strength during the whole charge inversion, because TEA was present in a large excess compared to surface chlorine groups. In addition, we generate chlorine ions during the amination reaction that partially compensate for the loss of ions due to covalent coupling of TEA.

Calculation of the DLVO potentials assuming smooth surfaces (see Appendix 2) showed that inter-particle distances of < 1 nm should result in irreversible aggregation, while a distance larger than this critical value results in restoring of the colloidal stability upon charging the colloids via introduction of additional quaternary amines. The roughness observed on the particles (Figure 9.4) is clearly larger than this critical value, suggesting that based on this crude approximation, the stability of the dispersion should indeed be regained.

This finding explained the results obtained at reaction temperatures of 20 °C. However, it does not explain the complete lack of colloidal stability after charge reversal at higher reaction temperatures (Figures 9.1 and 9.2). The surface of the colloids should be chemically equivalent, regardless of the temperature used to introduce the quaternary amines. The final ζ potential was independent of the reaction temperature, so the electrostatic repulsion between the particles after charge reversal must also be of similar magnitude. Calculation of DLVO barriers with Debye screening lengths corrected for the temperature and the temperature dependence of the pK_b of TEA (Appendix 3) could not explain the enormous differences in colloidal stability. In fact, the screening lengths increase with increasing temperature, suggesting more efficient charge stabilization at higher reaction temperatures, which contradicts our results.

From experiments conducted with a larger excess of TEA and trimethylamine (TMA), which is more reactive in these types of reactions,²⁷ we concluded that the final stability was determined by the rate of charge reversal and was not directly related to the temperature (see Appendix 4). In both reactions, fast rates were achieved at 20 °C. Despite this low temperature, colloidal stability could not be regained.

An explanation for this rate dependence might be the formation of an inhomogeneous surface charge distribution bearing positively charged ‘patches’ at high reaction rates. This idea is inspired by the formation of charged patches due to the adsorption of an oppositely charged polyelectrolyte on colloidal particles.²⁸ These patches strongly interact with the originally negatively charged surface of the colloids. The extra electrostatic attraction forces the particles into a deeper potential well causing irreversible aggregation. The formation of patches might be dominant at faster reaction rates because there is simply no time for the amines to explore the colloidal surface and probe the energetically most favourable reaction sites, leading to situations in which positive charges are placed in close proximity of each other on the particles. At lower temperatures, the reaction is slower and the TEA molecules now have time to sample the colloidal surface and find the most favourable reaction sites. This results in a more uniform charge distribution. Although this is merely a hypothesis, experimental techniques based on atomic force microscopy (AFM) could be used to probe the charge distribution as a function of time and position. At this point, these experiments are beyond the scope of this work.

9.3.3. Explaining the curves of ζ potential versus time. We will now focus on the shape of the curves of ζ potential versus reaction time in more detail. All these curves possess a significant lag time before there is a measurable change in the ζ potential (Figure 9.1). This lag time is probably caused by ion condensation to the surface of the colloid.^{29,30} Ion condensation is caused by a high charge density on the colloids, resulting in ions that are strongly bound to the surface. When the ζ potential of such a system is measured, one measures an effective charge of the colloid due to shielding by the condensed ions. The presence of a lag time does therefore not imply that there is no reaction occurring, but rather that the effect of the reaction is not reflected in a change in the ζ potential. At a certain point, the surface charge becomes sufficiently low that ion condensation can be neglected, with the consequence that increasing potentials could be measured (Figure 9.1). It is not likely that the reaction mechanism itself causes the observed lag time, because it is a straightforward one-step reaction and not, for example, a two-step mechanism involving a slow initial reaction step or uncharged intermediates.

To verify this hypothesis, we set up the following experiment. TEA was allowed to react with the chlorinated particles at 20 °C for 90 min, after which the reaction was quenched by quickly washing the particles. The 90 min period corresponds to the length of the lag time (Figure 9.1e). In the second step, TEA was again added to the resulting particles and the change in ζ potential over time was monitored (Figure 9.5). We observed that the potential immediately started to increase, without any lag time. From this, we conclude that the lag time is indeed not caused by the surface reaction itself; if this was the case, we would also observe a lag time the second time we add

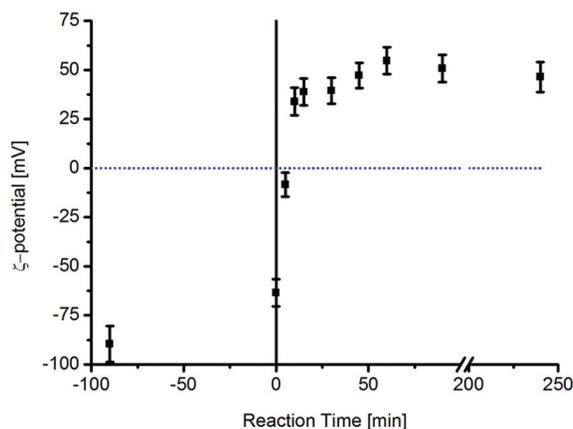


Figure 9.5. Curve of the ζ potential versus reaction time for a two-step reaction to investigate if the observed lag time was intrinsically linked to the reaction mechanism. At $t = 0$ a second addition of triethylamine (TEA) was done.

TEA. The rate at which the point of zero potential was crossed was higher than in the one-step reaction conducted at 20 °C (Figure 9.1e). This can be attributed to the larger excess of TEA that was present after the second addition.

As mentioned before, increasing the reaction temperature caused a significant increase in the reaction rate. The slope of the ζ potential versus time around zero potential is a measure of reaction rate k . In Figure 9.6a, the rates for the lower reaction temperatures were estimated by fitting a tangent to the linear part of the curve. This procedure was experimentally not possible for the higher reaction temperatures because of the high reaction rates. Extrapolation of the tangents revealed that the lines cross at one single point located on the y -axis at approximately -175 mV. The physical meaning of this extrapolation is quite straightforward: at time zero, no TEA has been added to the colloids, which must imply that the colloids bear their full negative charge. The extrapolation to zero time is phenomenological and based on the observation that potential varies linearly with time over a small time interval. The constant extrapolated values point to an internally consistent procedure that provides a plausible estimate of the bare charge densities.

As discussed before, the bare charge cannot be measured because of ion condensation. Therefore, Eq. 9.2 was used to determine if these potentials were physically reasonable.^{30,31}

$$Z = \frac{R(1 + \kappa R)}{\lambda_B} \frac{e\zeta}{k_B T} \quad (9.2)$$

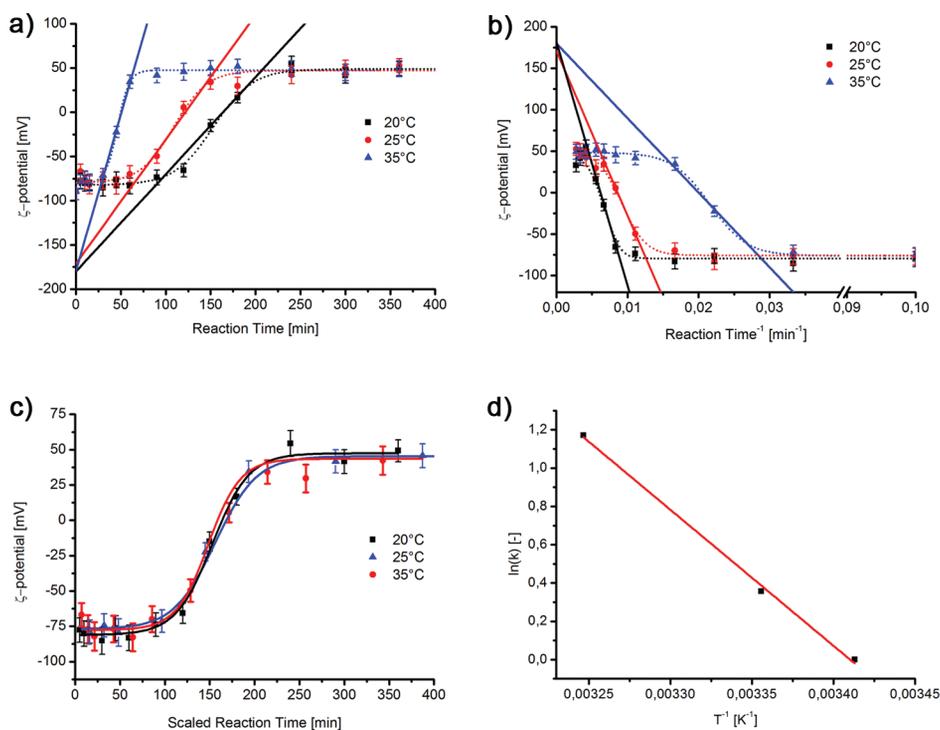


Figure 9.6. (a) Overlay of the curves of ζ potential versus time for reactions conducted at 20, 25, and 35 °C and extrapolation of the tangents around the point of zero potential to determine reaction rates and bare surface charges. (b) Overlay of the curves of ζ potential versus reciprocal time for reactions conducted at 20, 25, and 35 °C and extrapolation of the tangents to obtain the full positive potential of the colloids after charge reversal. (c) Master curve obtained after the plots of ζ potential versus time have been scaled (panel a) to their reaction rates (k). (d) Arrhenius plot of the rates obtained from the scaling factors of the ζ potential versus time curves (panel c).

where Z is the apparent number of charges. Dividing Z by the surface area of the particles leads to a charge density of ~ 0.22 negative charge/nm² (1 charge per 4.6 nm²). This value is reasonable if we keep in mind that the negative charges originate from relatively small sulfate/sulfonate entities.

Regardless of the reaction temperature, a limiting value of $\sim +45$ mV was measured. Naively, one might explain this by crowding of the colloidal surface with the rather bulky reaction product of TEA. To verify if this is the case, we applied the same strategy that was used to estimate the number of negative charges on the colloid. However, in this case, the ζ potential was plotted against the reciprocal time. Constructing a tangent to the linear part of the curves and performing the same phenomenological

extrapolation to time zero leads to the potential obtained after infinite reaction time or the true value of the surface potential without ion condensation. Also in this limit, the three curves show a common intersect at the y -axis at a potential of ~ 178 mV (Figure 9.6b). Overcharging to a potential of $+178$ mV requires a total of 352 mV worth of positive charges. Plugging this potential into Eq. 9.2 and dividing by the surface area of a particle, we find 0.43 positive charges/nm² (or 1 charge per 2.3 nm²). The area covered by the reaction product of TEA (equivalent to one positive charge) was estimated to be 0.7 nm² (see Appendix 5). Comparing both numbers shows that it is possible to accommodate all the charges on the surface and that the surface is indeed quite packed with quaternary amines. The remaining surface area is probably occupied by the negative charges, yielding a fully covered surface.

The fact that the tangents drawn in Figure 9.6a intersect at one particular point suggests that the obtained curves are scalable to a single master curve that describes the kinetics and the influence of temperature on these reactions. The length of the lag time scales inversely proportionally with the reaction rate, because it is solely caused by ion condensation as discussed before. To determine if a master curve could be generated, an attempt was made to collapse the raw experimental data by multiplying the x -axis with a certain factor. Overlaying factors of 1, 0.81, and 0.3 were required for reaction temperatures of 20, 25, and 35 °C, respectively (Figure 9.6c). The inverses of these factors were indeed in good agreement with the values of the tangents of each corresponding curve and therefore to the reaction rate k . Constructing an Arrhenius plot based on the inverse of the overlaying factors showed that plotting $\ln(k)$ versus T^{-1} yielded a straight line (Figure 9.6d). This indicates that the surface reaction follows classical behaviour of a single-step thermally activated reaction, which is in agreement with the hypothesis that the lag time is caused by ion condensation and is not an intrinsic property of the reaction mechanism.

9.3.4. Preparation of hybrid colloidal clusters via heterocoagulation. With the method of tuning the charge at hand, we briefly explored the potential of this system in electrostatically mediated assembly of colloids. As proof of principle, we prepared organic–inorganic hybrid clusters by the addition of negatively charged silica particles to the polystyrene colloids obtained after charge reversal reactions.

The first example deals with negatively charged nanometer-sized silica particles (LUDOX). A large excess of these particles was mixed with the positively charged polystyrene particles to prevent bridging of the positive polystyrene particles by the negative silica which could possibly lead to macroscopic aggregation. The resulting, stable dispersions were washed by centrifugation to remove free silica particles. TEM analysis yielded the pictures depicted in panels a and b of Figure 9.7. As can clearly be seen, the polystyrene particles are fully covered with silica particles yielding raspberry-like colloidal aggregates.^{32–35} The uniform distribution of silica colloids over the polystyrene

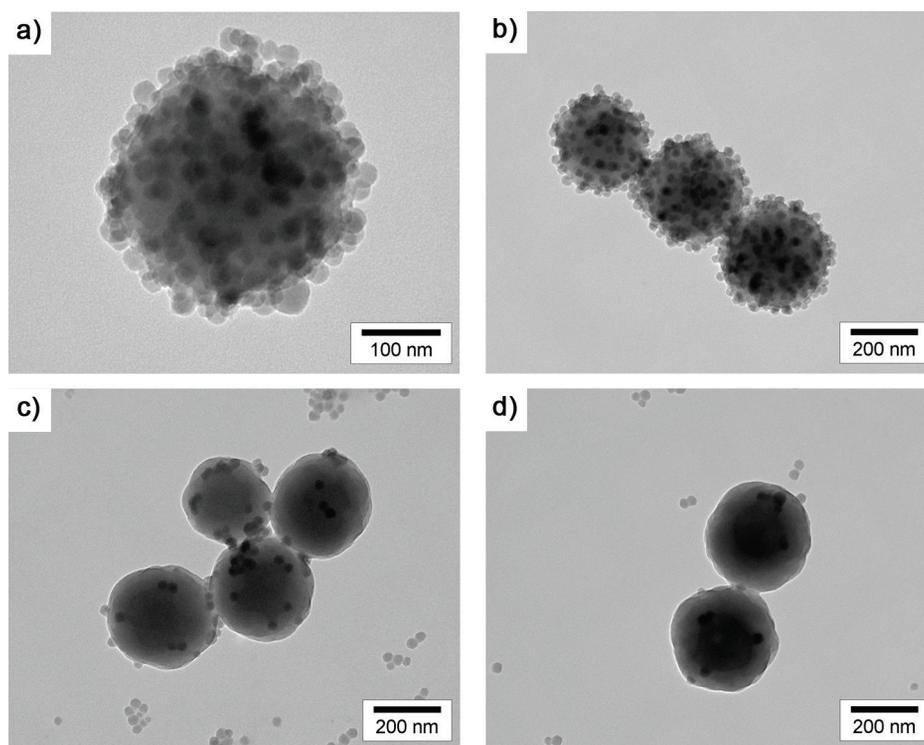


Figure 9.7. (a and b) Transmission electron microscopy (TEM) images of the clusters formed after electrostatically driven self-assembly of negatively nanometer-sized silica particles and positively charged polystyrene particles obtained after amination with TEA. (c and d) TEM pictures of a blank experiment in which negatively charged silica particles were added to negatively charged chlorinated polystyrene colloids.

core is a good indication of a uniform charge distribution of the particles. Measuring the ζ potential of these aggregates yielded a value of -41 mV, indicating that the surface is now overcharged with negative species, resulting in the observed colloidal stability. This phenomenon is also observed in the overcharging with polymeric polyelectrolytes that adsorb onto an oppositely charged surface or colloid.^{28,36,37}

To verify that the assembly of the negatively charged particles was electrostatically driven, the same silica particles were also added to the original negatively charged chlorinated colloids (Figure 9.7c and d). In this case, hardly any silica particles adsorbed onto the polystyrene surface. The incidental aggregation of the two particles was attributed to a drying effect during sample preparation.

Besides using nanometer-sized silica, the other extreme was also explored in which micrometer-sized negatively charged silica colloids were added to the positively charged

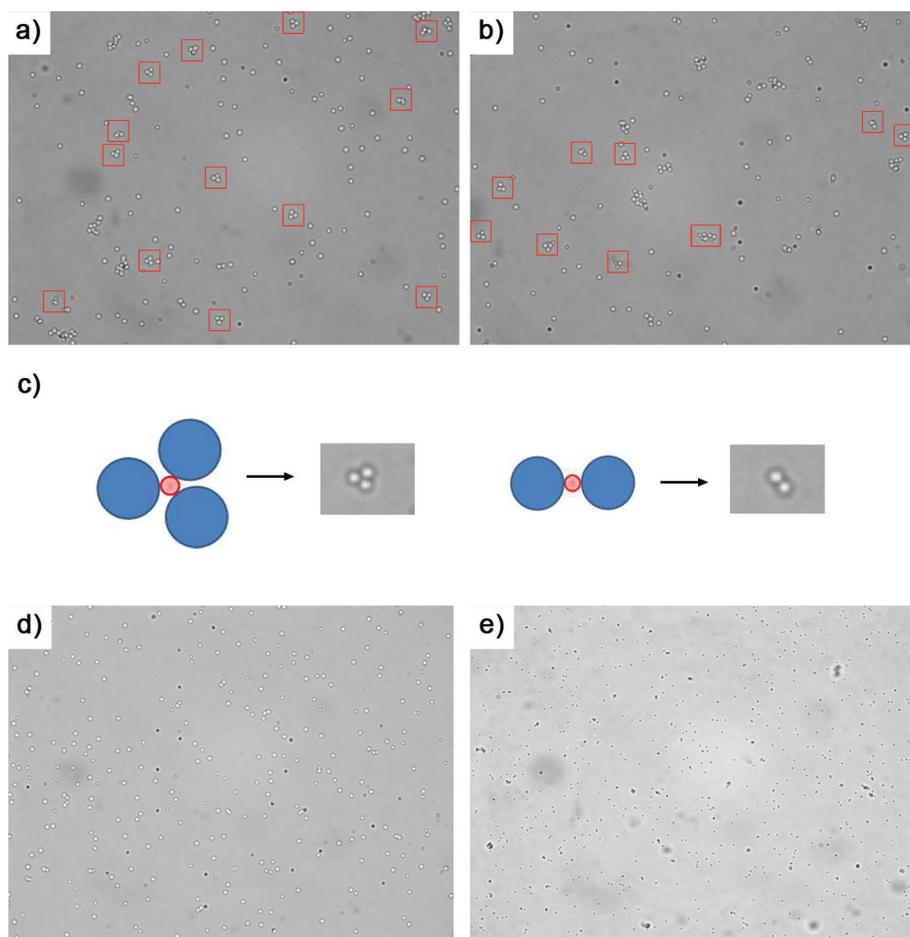


Figure 9.8. (a and b) Light microscopy images of clusters formed after mixing positively charged polystyrene particles with micrometer-sized negatively charged silica colloids. (c) Schematic representation of the tetramers (left) and trimers (right) of silica colloids (blue) formed after heterocoagulation with the positively charged polystyrene colloids (red). (d) Light microscopy image of solely the silica colloids. (e) Light microscopy image of solely the polystyrene particles. All pictures were taken at a magnification of 100 \times .

polystyrene particles.^{38,39} Again, a large excess of negatively charged silica particles was added. The resulting unwashed dispersions were analyzed using optical microscopy. Representative images are shown in panels a and b of Figure 9.8. In the obtained images, only the micrometer-sized silica particles are visible. The smaller polystyrene particles (Figure 9.8e) appear as dots in the picture due to the limited resolution of the optical microscope.

Compared to the image of solely the silica colloids (Figure 9.8d), the images of the mixed system showed the presence of a considerable amount of small clusters (Figure 9.8a and b). Evidently, the number of single silica particles was high, because of the large excess of these colloids that was added. When all the clusters, i.e. excluding the single particles of a large number of pictures were counted, we found that 43% of all clusters were tetramers, consisting of one polystyrene center particle and three silica spheres; 34% of all the clusters were trimers (one polystyrene particle with two silica particles), while the remaining clusters were built up with five or more colloids. Geometrically, no more than three large silica spheres can fit around the central positive colloid, explaining the observed preference for tetramers and trimers (Figure 9.8c). (The ratio of the radii of the red and blue circles is equivalent to that of the polystyrene and silica colloids used in these experiments.). Figure 9.9 shows snap shots of a movie recorded with the optical microscope to show that the clusters remain intact and move as single entities through the solution.

To verify if the clusters indeed consisted of polystyrene particles surrounded with silica colloids, the same heterocoagulation experiments were conducted in dimethylformamide (DMF).

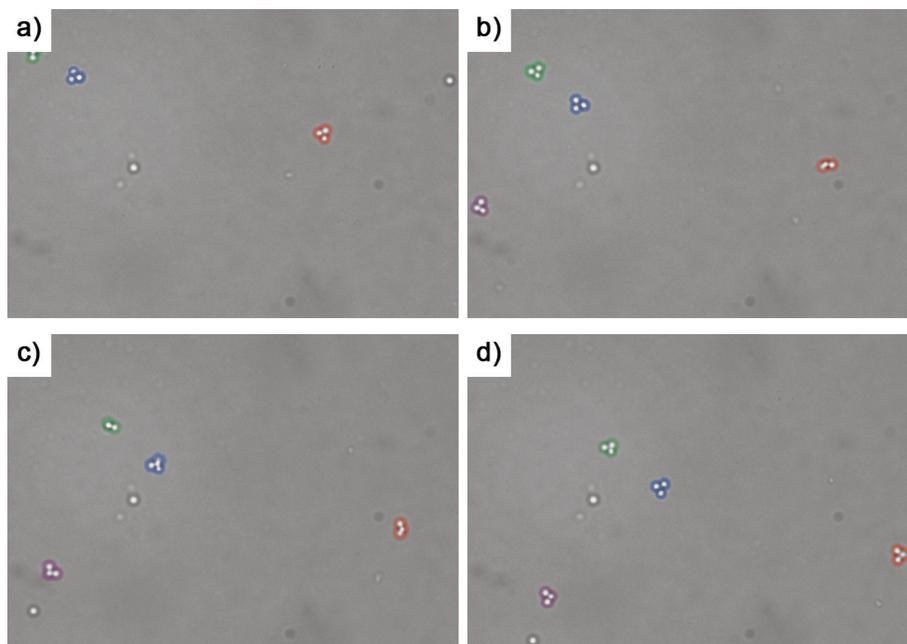


Figure 9.9. Snap shots of colloidal tetramers freely moving in solution. Time proceeds from a)–d). The clusters were followed for 10 s in total. The clusters are colored to follow their trajectories more easily. All pictures were taken at a magnification of 100 \times .

Since DMF is a high boiling solvent it was possible to form the clusters and subsequently heat the whole mixture above the glass transition temperature of polystyrene ($T_g = 110\text{ }^\circ\text{C}$).²⁶ This heat treatment softens the polystyrene, which then fuses to the silica particles to create mechanically stable colloidal clusters.⁴¹ Since the particles were now connected to each other it was possible to purify the clusters via centrifugation and redispersion using sonication. This procedure was not possible for the unfused clusters which disintegrated during sonication.

The purified colloids were analyzed with TEM, since drying of the clusters without disrupting them should also be possible after the heat treatment. Low particle concentrations were used to prepare the TEM samples to minimize the chance that single particles aggregate during the drying process and appear as a cluster. Figure 9.10 shows representative images of the clusters which were found.

The actual clusters are built up like schematically shown in Figure 9.8c with the big silica particles surrounding a small polystyrene particle. Unlike in the light

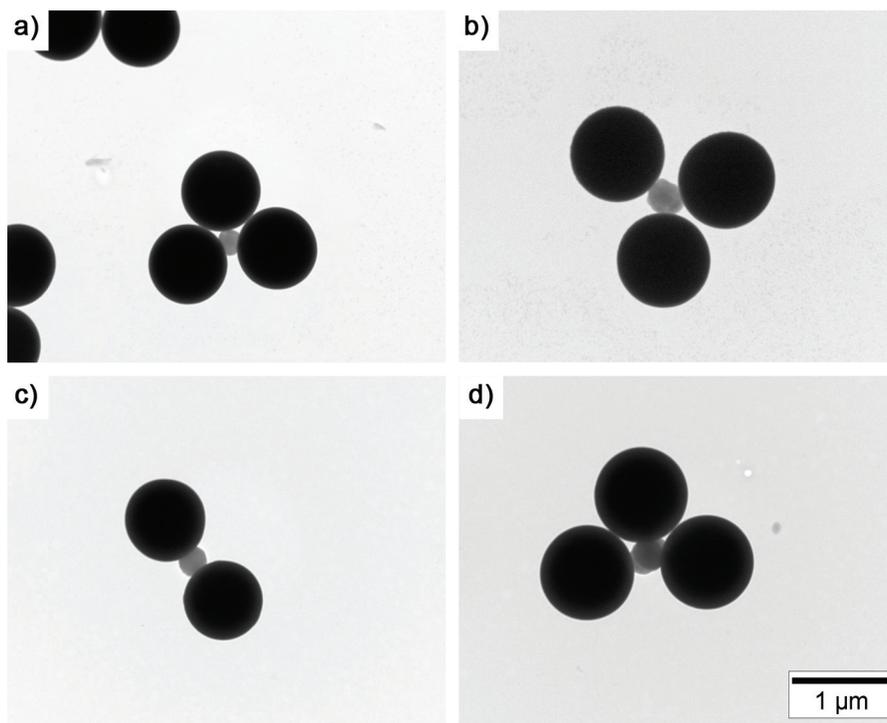


Figure 9.10. (a,b and d) Transmission electron microscopy (TEM) pictures of colloidal tetramers obtained via heterocoagulation followed by fusion of the polystyrene core to the surrounding silica particles. (c) TEM picture of colloidal trimer obtained via the same route as the tetramers.

microscopy images (Figure 9.8 and 9.9), where the silica colloids seem to touch each other, we observed some free space around a polystyrene core after formation of a tetramer, which was expected based on purely geometric arguments. Since the docking of three silica spheres around one central polystyrene colloid is not completely space filling we observed some fluctuations in the docking angle. The polystyrene core is a bit deformed, probably caused by the heat treatment which was employed to fuse the clusters together. As mentioned in literature before, the type of cluster that is most dominant can in principle be tuned by the changing the size and concentration ratio between both species.^{38,39}

9.4. Conclusions

We have developed a straightforward method for controlling and even reversing the overall surface charge of polystyrene colloids. The colloidal surface was initially covered with sulfate/sulfonate moieties providing negative charge for stabilization and benzyl chloride groups as a chemical handle for further modification. Positive charges in the form of quaternary amines were introduced via the Menshutkin reaction between the surface chlorines and tertiary amines. The overall charge was then determined by the ratio between positive quaternary amines and negative sulfate/ sulfonate groups on the surface. Despite that the charge reversal is a continuous process and the colloids pass through the point of zero overall charge, colloidal stability could be maintained under appropriate conditions. Crucial for maintaining the stability was to conduct the charge reversal reaction at sufficiently low reaction rates. Increasing the temperature and therefore, the reaction rate, resulted in irreversible aggregation. This behavior is possibly related to the formation of positively charged patches on the surface of the particles that induce an extra electrostatic contribution to the attractive forces between the colloids. The time evolution of the ζ potential was explained in terms of ion condensation and a classical Arrhenius type reaction mechanism.

As an example of an application of the adjustable ζ potential of the colloids, we demonstrated the formation of organic–inorganic hybrid clusters via heterocoagulation with both nanometer- and micrometer-sized silica particles yielding raspberry-like particles and colloidal tetramers and trimers, respectively.

Acknowledgments

I would like to thank Jan Groenewold for useful discussions regarding the physical understanding of the charge reversal reactions, Sonja Castillo for the idea to use nanometer-sized silica for the heterocoagulation experiments, and Dominique Thies-Weesie for kindly providing the micrometer-sized silica colloids. This chapter is reprinted with kind permission from reference [42]. Copyright 2014 American Chemical Society.

Appendix 1 – Evolution of ζ potential and size distributions at 25/50 °C

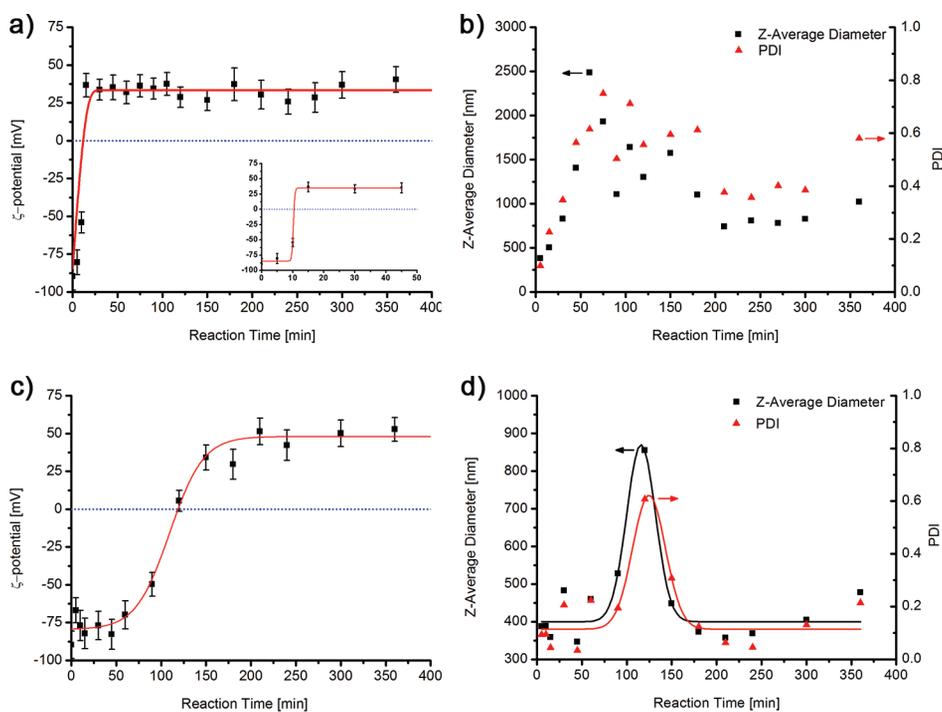


Figure 9.11. a) The evolution of the ζ potential in time of the chlorinated particles during the reaction with triethylamine (TEA) at 50 °C. b) The evolution of the Z-average diameter and the polydispersity index (PDI) of the chlorinated particles during the reaction with TEA at 50 °C. c) The ζ potential evolution of the chlorinated particles during the reaction with TEA at 25 °C. d) The Z-average diameter and the PDI of the chlorinated particles during the reaction with TEA at 25 °C.

Appendix 2 – Plots of DLVO potential as function of ζ potential and inter-particle distance

Eq. 9.1 of the main chapter was used to calculate the DLVO potential (at room temperature).

$$\frac{U_{DLVO}}{k_B T} = -\frac{A_H R}{12d} + \left(\frac{e\zeta}{k_B T} \right)^2 \frac{R^2}{\lambda_B (2R + d)} e^{-\kappa d}$$

Plotting the DLVO potential as function of the inter-particle separation for different

ζ potentials yields classical pictures for charge stabilized colloids (Figure 9.12). For low surface potentials ($0, \pm 10$ mV) the particles are attractive for all inter-particle distances due to dominating Van der Waals forces. Increasing the charge on the particles leads to the formation of a barrier against aggregation.

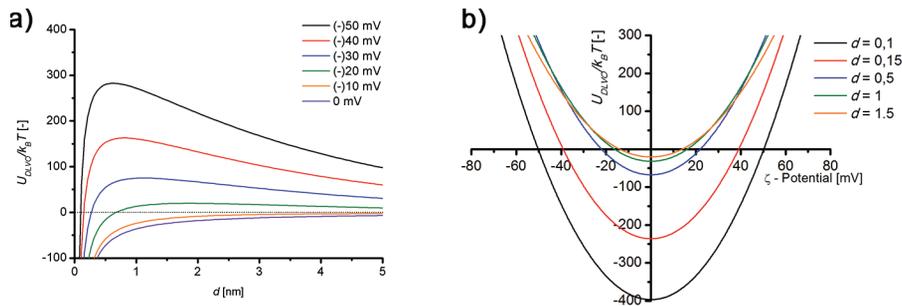


Figure 9.12. a) Plot of the DLVO potential against the inter-particle distance d in nanometers for different ζ potentials. b) Plot of the DLVO potential as function of the ζ potential at fixed inter-particle distances.

For very small particle separations ($d < 0.1$ nm) the Van der Waals attraction is very large and particles are highly attractive. Charging up these particles to the final potential of 50 mV leads to a decrease in attraction, but the electrostatic repulsion cannot prevent the particles from attracting each other. In other words, the overall DLVO potential can turn repulsive, but the system remains at the left side of the barrier against aggregation. Therefore, the particles are expected to fall back into the potential minimum. The situation becomes different if we take an inter-particle distance of 0.5 nm. The attraction at the point of zero potential is on the order of $75 k_B T$. Charging to 50 mV leads to a net repulsive potential of $280 k_B T$ which belongs to the maximum of the red curve in Figure 9.12. When the particles are in this situation they either fall into the potential well left from the barrier or increase the distance between each other; hence, this is the minimum particle separation required to regain some of the colloidal stability. If the separation is larger than this minimal distance, the particles need to overcome a barrier to fall into an attractive potential well. For example, if the particle distance is 1.5 nm, already a barrier of approximately $35 k_B T$ prevents the colloids from coagulation. The roughness on the colloids is most probably significantly larger which ensures that there will be a sufficiently high barrier to prevent (irreversible) aggregation.

Appendix 3 – Debye screening length as function of temperature

The Debye screening length (κ^{-1}) was calculated using Eq. 9.3²

$$\kappa^{-1} = \sqrt{\frac{\varepsilon_r \varepsilon_0 k_B T}{2 N_A e^2 I}} \quad (9.3)$$

where I is the ionic strength of the electrolyte in $\text{mol} \cdot \text{m}^{-3}$, ε_0 the permittivity of vacuum, ε_r the dielectric constant, k_B the Boltzmann constant, T the absolute temperature in Kelvin, N_A the number of Avogadro and e the elementary charge. Obviously, κ^{-1} has a square root dependence on the temperature. In this particular case an extra contribution of the temperature comes in via the ionic strength due to the temperature dependence of the $\text{p}K_b$ of TEA. The standard molar enthalpy and entropy for the conjugated acid are known from literature and are equal to $43.13 \text{ kJ mol}^{-1}$ and $0.06 \text{ kJ mol}^{-1} \cdot \text{K}^{-1}$, respectively.⁴⁰ Using Eq. 9.4 enables us to calculate the molar Gibbs free energy at different temperatures and relate this to the corresponding acid dissociation constant (K_a).

$$\begin{aligned} \Delta G &= \Delta H - T \Delta S \\ \Delta G &= -RT \ln K_a \end{aligned} \quad (9.4)$$

From the obtained constants it is straightforward to obtain base association constants at the various temperatures. The ionic strength was subsequently determined by using the definition of the base association constant (Eq. 9.5).

$$K_a = \frac{[\text{OH}^-] [\text{HN}^+ \text{Et}_3]}{[\text{NEt}_3]} \approx \frac{[\text{OH}^-]^2}{[\text{NEt}_3]} \quad (9.5)$$

Plugging the obtained ionic strength and the temperature in Eq. 9.3 yields the values listed in Table 9.1 for the screening length as function of the temperature.

Table 9.1. Variation of the Debye screening length with temperature.

T [K]	κ^{-1} [nm]
298	3.59
303	3.89
323	5.23
343	6.82
353	7.70

Appendix 4 – Menshutkin reaction with TMA and larger excess of TEA

A4.1. Experimental

A4.1.1. Surface reaction of chlorinated particles (CPs-Cl) with TMA. CPs-Cl dispersion (0.5 mL) was diluted with water to a solid content of 1%. To this dispersion, trimethylamine (TMA) solution (39 μL) was added. The mixture was stirred at room temperature for 24 h. During the reaction samples were withdrawn from the mixture. The samples were washed directly with water (three times) and ethanol (two times) by centrifugation and redispersion cycles. After the last washing step, the particles were transferred back to water and the particles were characterized in terms of hydrodynamic size (and its distribution) and their ζ potential.

A4.1.2. Surface reaction of CPs-Cl with larger excess of TEA. The same procedure as described in the main text was applied (Section 9.2.3). Instead of the addition of 35 μL , 87 μL TEA was used.

A4.2. Results and Discussion

The goal of these experiments was to find an explanation for the large differences observed in the final colloidal stability as function of the reaction temperature (Figure 9.1). The most straightforward explanation which we could envision was softening of the polystyrene colloids at elevated temperatures. Even though the particles were cross-linked, heating causes the polymer network to soften. If the particles have the chance to come close to each other due to the lack of electrostatic stabilization, they can slightly fuse. A flattened contact between the particles can be formed, which increases the Van der Waals interaction tremendously. As lower estimate of the glass transition temperature of the colloids, we can take the glass transition temperature of linear polystyrene which is located around 110 $^{\circ}\text{C}$.²⁶ Heating to 80 $^{\circ}\text{C}$ might therefore result in some softening of the particles. The effect of softening decreases of course if the temperature of the system is lowered and should be negligible at temperatures at or slightly above room temperature.

To investigate if the observed irreversible aggregation was solely caused by the higher reaction temperature, two experiments were performed: the first one was a Menshutkin reaction with triemethylamine (TMA) instead of TEA and the second one was a reaction with a larger excess of TEA compared to the previous experiments. TMA is more reactive than TEA due to less steric crowding of alkyl chains around the central nitrogen atom, which results in a faster reaction at the same reaction temperature.²⁷ In the second experiment, the larger excess of TEA should also cause an increased reaction rate. Effectively we decouple the rate and the temperature with these two experiments. Both reactions were performed at 20 $^{\circ}\text{C}$, so based on the hypothesis we expect that colloidal stability should be regained.

The results of the amination reaction with TMA are shown in Figure 9.13a and b. The charge reversal reaction was indeed much faster and the point of zero charge was reached within approximately 15 min compared to 180 min for the reaction with TEA (Figure 9.1). The value of the final ζ potential was approximately the same as in the charge reversal reactions with TEA. Contradictory to our hypothesis, this system still showed a significantly higher PDI and Z-average diameter after complete charge reversal compared to the amination with TEA at the same temperature.

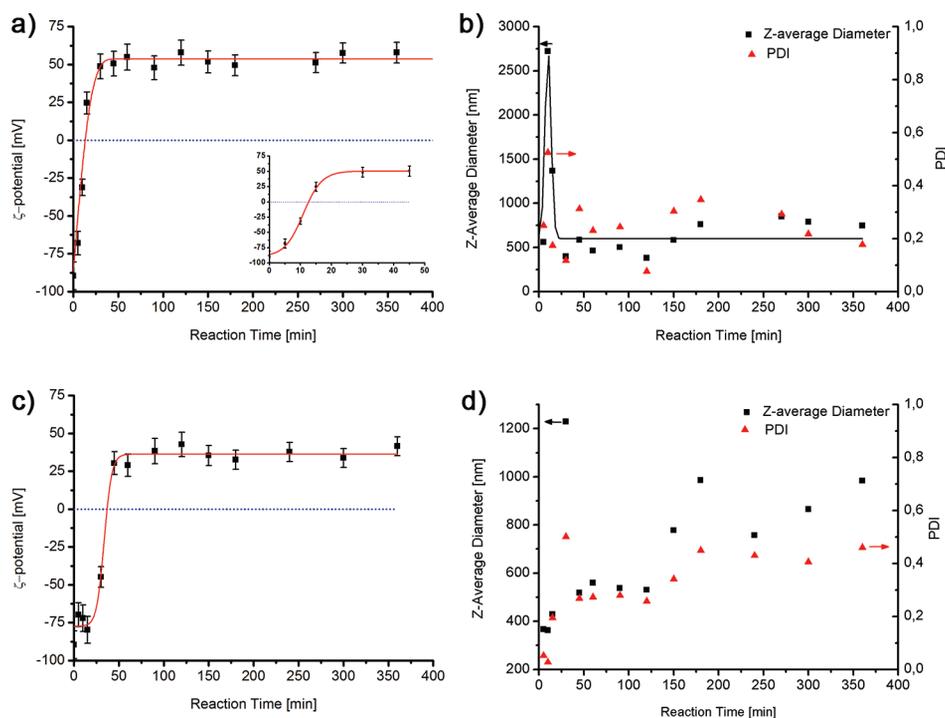


Figure 9.13. a) The evolution of the ζ potential in time of the chlorinated particles during the reaction with trimethylamine (TMA) at 20 °C. The inset shows a magnification of the first 50 min. b) The evolution of the Z-average diameter and the polydispersity index (PDI) of the chlorinated particles during the reaction with TMA at 20 °C. c) The evolution of the ζ potential in time of the chlorinated particles during the reaction with a larger excess of TEA at 20 °C. d) The evolution of the Z-average diameter and the PDI of the chlorinated particles during the reaction mentioned under c).

Increasing the concentration of TEA in the reaction mixture also caused a significantly faster charge reversal. Compared to the results depicted in Figure 9.1e and f, 2.5 times more TEA was added. The extra TEA does not cause a dramatic increase in ionic strength which enabled us to fairly compare both amination reactions performed

at 20 °C. As in the surface reaction with TMA, a large PDI and high Z-average size of the colloids was observed after charge reversal as shown in Figure 9.13c and d.

From these two experiments we concluded that the final stability is determined by the rate of charge reversal and is not directly related to the temperature. In both reactions, fast rates were achieved at 20 °C. Despite this low temperature, colloidal stability was not regained.

Appendix 5 – Estimation of surface occupied per quaternary amine after reaction of TEA

The surface area covered by one generated quaternary amine after reaction between TEA and the surface chlorine groups was approximated as follows.

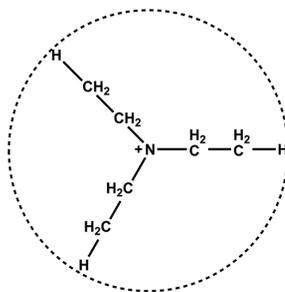


Figure 9.14. Schematic representation of a quaternary amine obtained after reaction of TEA with the surface chlorines. The circle represents the surface occupied by one charged moiety (0.7 nm²).

We take the nitrogen of the formed quaternary amine and attach the three ethyl groups to it (Figure 9.14). To get an upper limit for the surface area we fully stretch these ethyl arms (binding angles of 180°). The length of one arm is simply equal to the sum of all bond lengths: 150 pm + 151 pm + 106 pm = 470 pm = 0.47 nm ([C-N] + [C-C] + [C-H]).²⁶ A circle with the radius equal to the stretched ethyl moiety was drawn around the central nitrogen atom. The surface occupied by one positive charge is then equal to the area of a circle with a radius of 0.47 nm. Calculation reveals a surface area of 0.7 nm² per positive charge.

References

- [1] E. J. W. Verwey, J. T. G. Overbeek, In *Theory of the stability of lyophobic colloids*, 2nd ed.; Dover Publications: Mineola, NY, 1999.

-
- [2] J. N. Israelachvili, In *Intermolecular & Surface Forces*, 3rd ed.; Academic Press: Amsterdam, 2011.
- [3] Y. Wang, A. S. Angelatos, F. Caruso, Template synthesis of nanostructured materials via layer-by-layer assembly. *Chem. Mater.* **2008**, *20*, 848–858.
- [4] E. Spruijt, H. E. Bakker, T. E. Kodger, J. Sprakel, M. A. Cohen Stuart, J. van der Gucht, Reversible assembly of oppositely charged hairy colloids in water. *Soft Matter* **2011**, *7*, 8281–8290.
- [5] M. E. Leunissen, C. G. Christove, A.-P. Hynninen, C. P. Royall, A. I. Campbell, A. Imhof, M. Dijkstra, R. van Roij, A. van Blaaderen, Ionic colloidal crystals of oppositely charged particles. *Nature* **2005**, *437*, 235–240.
- [6] I. H. Harding, Amphoteric polystyrene latex colloids: Polymerization pathway and the control of particle size and potential. *Colloid Polym. Sci.* **1985**, *263*, 58–66.
- [7] I. H. Harding, T. W. Healy, Electrical double layer properties of amphoteric polymer latex colloids. *J. Colloid Interface Sci.* **1985**, *107*, 382–297.
- [8] J. Ramos, J. Forcada, R. Hidalgo-Alvarez, Cationic polymer nanoparticles and nanogels: From synthesis to biotechnological applications. *Chem. Rev.* **2014**, *114*, 367–428.
- [9] K. Sakota, T. Okaya, Preparation of cationic polystyrene latexes in the absence of emulsifiers. *J. Appl. Polym. Sci.* **1976**, *20*, 1725–1733.
- [10] J. Blaakmeer, G. J. Fleer, Synthesis of a polystyrene latex with a positive, pH independent, surface charge. *Colloids Surf.* **1989**, *36*, 439–447.
- [11] J. W. Goodwin, R. H. Ottewill, R. Pelton, Studies on the preparation and characterization of monodisperse polystyrene lattices. V: The preparation of cationic lattices. *Colloid Polym. Sci.* **1979**, *257*, 61–69.
- [12] N. Kato, P. Schuetz, A. Fery, F. Caruso, Thin multilayer films of weak polyelectrolytes on colloid particles. *Macromolecules* **2002**, *35*, 9780–9787.
- [13] R. Messina, C. Holm, K. Kremer, Polyelectrolyte multilayering on a charged sphere. *Langmuir* **2003**, *19*, 4473–4482.
- [14] J. Lyklema, Overcharging, charge reversal: Chemistry or physics? *Colloids Surf., A* **2006**, *291*, 3–12.
- [15] B. G. P. van Ravensteijn, M. Kamp, A. van Blaaderen, W. K. Kegel, General route toward chemically anisotropic colloids. *Chem. Mater.* **2013**, *25*, 4348–4353.
- [16] J. H. Zhang, P. Zhan, Z. L. Wang, W. Y. Zhang, N. B. Ming, Preparation of monodisperse silica particles with controllable size and shape. *J. Mater. Res.* **2003**, *18*, 649–653.
- [17] W. Stöber, A. Fink, E. Bohn, Controlled growth of monodispersed spheres in the micron size range. *J. Colloid Interface Sci.* **1968**, *26*, 62–69.

- [18] A. P. Philipse, A. Vrij, Polydispersity probed by light scattering of secondary particles in controlled growth experiments of silica spheres. *J. Chem. Phys.* **1987**, *87*, 5634–5643.
- [19] J. C. Thomas, The determination of log normal particle size distributions by dynamic light scattering. *J. Colloid Interface Sci.* **1987**, *117*, 187–192.
- [20] H. Ohshima, A simple expression for Henry's function for the retardation effect in electrophoresis of spherical colloidal particles. *J. Colloid Interface Sci.* **1994**, *168*, 269–271.
- [21] R. J. Hunter, In *Foundations of Colloid Science*, 2nd ed.; Oxford University Press: New York, 2009.
- [22] J. R. Ebdon, T. N. Huckerby, T. C. Hunter, Free-radical aqueous slurry polymerizations of acrylonitrile: 2. End-groups and other minor structures in polyacrylonitriles initiated by potassium persulfate/sodium bisulfite. *Polymer* **1994**, *35*, 4659–4664.
- [23] J. P. Monthéard, C. Jegat, M. Camps, Vinylbenzyl chloride (chloromethylstyrene), polymers, and copolymers. Recent reactions and applications. *J. Macromol. Sci., Polym. Rev.* **1999**, *39*, 135–174.
- [24] N. Menschutkin, Beiträgen zur Kenntnis der Affinitätskoeffizienten der Alkylhaloide und der organischen Amine. *Z. Phys. Chem.* **1890**, *6*, 41–57.
- [25] G. Vigil, Z. Xu, S. Steinberg, J. Israelachvili, Interaction of silica surfaces. *J. Colloid Interface Sci.* **1994**, *165*, 367–385.
- [26] D. R. Lide, H. P. R. Frederikse, *CRC Handbook of Chemistry and Physics*, 76th ed.; CRC Press: Boca Raton, FL, 1995.
- [27] D. P. Evans, The influence of alkyl groups upon reaction velocities in solution. Part V. The formation of phenyltrialkylammonium iodides in methyl alcohol. *J. Chem. Soc.* **1944**, 422–425.
- [28] I. Popa, G. Gillies, G. Papastavrou, M. Borkovec, Attractive electrostatic forces between identical colloidal particles induced by adsorbed polyelectrolytes. *Langmuir* **2012**, *28*, 6211–6215.
- [29] L. Belloni, Ionic condensation and charge renormalization in colloidal suspensions. *Colloids Surf., A* **1998**, *140*, 227–243.
- [30] S. Alexander, P. M. Chaikin, P. Grant, G. J. Morales, P. Pincus, Charge renormalization, osmotic pressure, and bulk modulus of colloidal crystals: Theory. *J. Chem. Phys.* **1984**, *80*, 5776–5781.
- [31] M. F. Hsu, E. R. Dufresne, D. A. Weitz, Charge stabilization in nonpolar solvents. *Langmuir* **2005**, *21*, 4881–4887.
- [32] S. Harley, D. W. Thompson, B. Vincent, The adsorption of small particles onto larger particles of opposite charge: Direct electron microscope studies. *Colloids Surf.* **1992**, *62*, 163–176.

-
- [33] K. Furusawa, C. Anzai, Heterocoagulation behaviour of polymer latices with spherical silica. *Colloids Surf.* **1992**, *63*, 103–111.
- [34] A. M. Islam, B. Z. Chowdhry, M. J. Snowden, Heteroaggregation in colloidal dispersions. *Adv. Colloid Interface Sci.* **1995**, *62*, 109–136.
- [35] M. Chen, S. Zhou, B. You, L. Wu, L. Novel preparation method of raspberry-like PMMA/SiO₂ hybrid microspheres. *Macromolecules* **2005**, *38*, 6411–6417.
- [36] I. Szilagy, A. Sadeghpour, M. Borkovec, M. Destabilization of colloidal suspensions by multivalent ions and polyelectrolytes: From screening to overcharging. *Langmuir* **2012**, *28*, 6211–6215.
- [37] I. Szilagy, G. Trefalt, A. Tiraferri, P. Maroni, M. Borkovec, Polyelectrolyte adsorption, interparticle forces, and colloidal aggregation. *Soft Matter* **2014**, *10*, 2479–2502.
- [38] C. L. Phillips, E. Jankowski, M. Marval, S. C. Glotzer, Self-assembled clusters of spheres related to spherical codes. *Phys. Rev. E* **2012**, *86*, 041124.
- [39] N. B. Schade, M. C. Holmes-Cerfon, E. R. Chen, D. Aronzon, J. W. Collins, J. A. Fan, J. F. Capasso, V. N. Manoharan, Tetrahedral colloidal clusters from random parking of bidisperse spheres. *Phys. Rev. Lett.* **2013**, *110*, 148303.
- [40] R. N. Goldberg, N. Kishore, R. M. Lennen, Thermodynamic quantities for the ionization reactions of buffers. *J. Phys. Chem. Ref. Data* **2002**, *31*, 231–370.
- [41] A. M. Yake, R. A. Panella, C. E. Snyder, D. Velegol, Fabrication of colloidal doublets by a salting-out–quenching–fusing. *Langmuir* **2006**, *22*, 9135–9141.
- [42] B. G. P. van Ravensteijn, W. K. Kegel, Colloids with continuously tunable surface charge. *Langmuir* **2014**, *30*, 10590–10599.

Part 4

Colloids for Catalysis

10

The Immobilization of a Transfer Hydrogenation Catalyst

Abstract

In this chapter we report a synthetic procedure to immobilize a transfer hydrogenation catalyst on the surface of colloidal polystyrene particles. The synthesis relies on covalent attachment of terpyridine moieties on the particle surface. These immobilized terpyridines are subsequently employed as colloidal ligands for the preparation of a ruthenium based transfer hydrogenation catalyst. The resulting colloidal catalysts prove to be active in the catalytic transfer hydrogenation of acetophenone with 2-propanol as hydrogen donor.

To investigate the influence of the colloidal particles as solid support, the activity of the catalytic particles is compared to the homogeneous analogue of the immobilized catalyst. Despite a slight decrease in catalytic activity, full conversion is still reached within 24 h. The main advantage of the immobilization is easy recovery of the catalyst from the reaction medium by simple centrifugation. Preliminary experiments show that the catalytic colloids are recyclable without significant loss of transfer hydrogenation activity.

10.1. Introduction

The use of catalysts to promote the formation of a desired material or molecule is nowadays common practice in both the laboratory and on an industrial scale.¹ Addition of a catalyst offers an alternative pathway for the reaction, which is energetically more favorable due to lowering of the activation energy barrier(s). This decrease in activation energy results in higher reaction rates under milder conditions. In general, catalytic processes consist of three elementary steps: coordination of the reactant(s) to the catalyst, reaction on the catalyst, and finally the release of product(s) from the active center. From this simplified picture it becomes clear that the catalyst is not consumed during the process, which has the consequence that low catalyst concentrations are sufficient to speed up the reaction significantly.¹

Roughly all catalysts can be divided into two categories, namely heterogeneous and homogeneous.¹ As the names suggest, this classification is made based on the phase in which the catalyst is present during the reaction. While homogeneous catalysts reside in the same phase as the reactants, heterogeneous catalysts are present in a different phase, for example, a solid catalyst active in a gas phase reaction. The latter category has the advantage that the catalytic species are easy to separate from the reaction mixture, which facilitates recycling of the expensive catalytic material. For homogeneous catalysts, e.g. organo-metallic complexes or enzymes, recycling is much more difficult since these compounds are molecularly dissolved in the reaction mixture. However, this drawback is compensated by superior activity and selectivity of homogeneous catalysts. The active (metal) center is well-defined and for all catalytic species exactly the same, leading to the formation of single, pure products. Additionally, it is possible to extensively tune the properties of the active center by changing the local environment through the use of coordinating ligands. A striking example is the preparation of stereospecific products when the active metal center is surrounded by chiral ligands. In heterogeneous systems this level of control is practically unreachable. Surfaces of catalysts are usually ill-defined, making it impossible to define one type of catalytic center. This spread in catalytic species translates to the formation of a variety of products instead of the synthesis of a pure product.

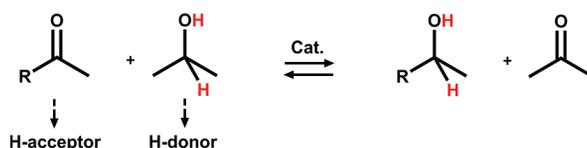
To combine the advantages of both homogeneous and heterogeneous catalytic systems, a vast amount of research was and is conducted on procedures for the efficient immobilization of molecular catalysts onto a (solid) support.² Activity and selectivity of the resulting hybrid catalytic systems are determined by the well-defined structure of the molecular species, while recycling is promoted by attachment of these homogeneous complexes onto solid surfaces.²⁻⁶ Bonding between catalyst and support can be achieved by covalent attachment as well as non-covalent interactions, i.e. electrostatics, Van der Waals interactions, and hydrogen bonding.^{2,6} Obviously, covalent bonds result in the most stable hybrid systems, since the active species are irreversibly bound to the support.

The vast majority of the literature dealing with immobilization strategies report on the attachment of catalysts onto macroscopic surfaces, i.e. beads well beyond the colloidal regime, (porous) silica structures, metallic nanoparticles (< 50 nm) and dendrimers.² Compared to a purely homogeneous system all strategies are already a significant improvement with regard to the recyclability of the catalyst. However, these immobilization strategies are not optimal: if large beads or non-porous immobilization media are used, the available surface area for tethering of the catalyst is relatively low. The lack of catalyst mobility and low catalyst loading inevitable leads to a decrease in catalytic activity compared to the truly homogeneous analogue. In this respect, nanoparticles or dendrimers as immobilization platforms are more beneficial. These catalyst carriers have an enormous surface area available for catalyst immobilization and move freely through the solution due to Brownian motion. The small dimensions of these platforms are also their drawback, since it is still relatively difficult to extract them from the reaction mixture. Magnetic carrier particles are an exception, since they can be separated from the medium by applying an external magnetic field.^{7,8}

As a compromise between macroscopic surfaces and nanoparticles, colloidal particles can be used as catalyst carriers. The intermediate size regime (100 nm–1 μm) of colloidal particles ensures reasonable surface area and catalyst mobility as well as facile recovery of the catalyst from the reaction mixture by sedimentation or centrifugation.

To exploit the benefits of a colloid as a catalyst carrier, we used polystyrene particles with a diameter of roughly 350 nm. A ruthenium-based transfer hydrogenation catalyst was covalently attached to the colloidal surface. Transfer hydrogenation reactions are synthetically attractive reactions in which unsaturated compounds, for example ketones, are reduced without the use of highly flammable and explosive hydrogen gas or hazardous reducing agents.^{9–13} Instead, transfer hydrogenation processes rely on the use of secondary alcohols as hydrogen donors (see Scheme 10.1). The O-H and C-H hydrogens (highlighted in red in Scheme 10.1) are donated to the ketone present in the system, resulting in the formation of the desired alcoholic product. Most reported systems use 2-propanol as hydrogen donor, since acetone is formed as byproduct.

Scheme 10.1. Schematic representation of the transfer hydrogenation of a ketone (hydrogen acceptor) yielding the corresponding alcohol. 2-propanol acts as hydrogen donor.



Conducting the transfer hydrogenation reactions at (slightly) elevated temperatures ensures evaporation of acetone, which shifts the transfer hydrogenation equilibrium (Scheme 10.1) towards the right, promoting high yield of the desired alcohol.

A large number of organo-metallic complexes that catalyze (enantio-selective) transfer hydrogenations are reported in literature.⁹⁻¹⁴ During this study, we selected a ruthenium-based catalyst reported by Kelson et al., which consists of a fully saturated coordination environment of only hard donor ligands.¹⁵ These features circumvents in situ preparation of the active catalyst and allows for easy synthesis and characterization.¹⁵ Immobilization of the catalyst was achieved by covalently tethering one of the ligands required for the formation of the ruthenium catalyst (terpyridine) to the surface of the polystyrene particles. The immobilized ligands were subsequently used to form the complete and active catalyst in a similar procedure as described for the homogeneous counterpart.

As a model reaction, the transfer hydrogenation of acetophenone (Scheme 10.1, $R = C_6H_5$) to 1-phenylethanol with 2-propanol as hydrogen donor was studied. We show that upon immobilization, catalytic activity was preserved. Recycling of the catalytic species was easily realized by centrifugation of the carrier colloids.

10.2. Experimental Section

10.2.1. Materials. Styrene (St, 99%), divinylbenzene (DVB, 55% mixture of isomers, tech. grade), vinylbenzyl chloride (VBC, $\geq 90\%$, tech. grade), 4'-chloro-2,2':6',2''-terpyridine (99%), 2,2':6',2''-terpyridine (98%), ruthenium(III)chloride hydrate ($RuCl_3 \cdot xH_2O$, 40.00–49.00% ruthenium), 2-hydroxypyridine (97%), dimethylformamide (DMF, $> 99\%$), acetophenone (98%), 1,10-phenanthroline ($> 99\%$), hydroxylamine hydrochloride (puriss p.a.), iron(II)chloride tetrahydrate ($FeCl_2 \cdot 4H_2O$, puriss p.a. $> 99\%$), and acetone-d₆ (99.9 atom% D) were purchased from Sigma-Aldrich. Powdered potassium hydroxide (KOH), sodium hydroxide (NaOH) pellets and absolute ethanol (EtOH) were purchased from Merck. 2-propanol was purchased from Carl Roth and sodium dodecylsulfate (SDS) from BDH. Finally, potassium persulfate (KPS, $> 99\%$ for analysis) was obtained from Acros Organics. All chemicals were used as received. The water used throughout all syntheses was purified using a Milli-Q water purification system.

Transfer hydrogenation reactions were performed in deoxygenated Schlenk flasks under nitrogen atmosphere. Samples withdrawn from the transfer hydrogenation reactions were stored in the freezer ($-8\text{ }^\circ\text{C}$).

10.2.2. Synthesis of chlorinated seed particles (CPs-Cl). The chlorinated colloids (CPs-Cl) were prepared using the same core-shell approach as described in Chapter 2.¹⁶ This synthesis consisted of two steps, namely the synthesis of a cross-linked polystyrene core (CPs) followed by the introduction of a cross-linked chlorinated

shell. The shell was grown by the addition of VBC and DVB. The synthetic procedure yielded particles with a radius of 155 nm and a polydispersity of 4.4% as determined using transmission electron microscopy (TEM). The presence of the chlorine groups was confirmed using Fourier transform infrared spectroscopy (FT-IR) (1266 cm^{-1}) and X-ray photoelectron spectroscopy (XPS): E_b [eV]: 200 (Cl), 270 (Cl).

10.2.3. Synthesis of homogeneous catalyst (*trans*-[(terpy)Ru(NC₅H₄O- κ N)₂(OH₂)] (TPR)). The complexation of ruthenium chloride with 2,2':6',2''-terpyridine was performed as described by Sullivan et al.¹⁷ An excess of RuCl₃·xH₂O (275 mg) was dissolved in ethanol (125 mL). 2,2':6',2''-terpyridine (225 mg, 0.97 mmol) was added and the resulting mixture was refluxed for 3 h. Ru(III) terpyCl₃ was formed as a brownish/black solid which was isolated via filtration and washed three times with ethanol. Yield: 68.8%. FT-IR: $\nu_{\text{max}}\text{ cm}^{-1}$: 1595s, 1564m, 1537m, 1444s, 774s, 729s.

Ru(III)terpyCl₃ obtained from the previous step was used to synthesize the homogeneous catalyst as described by Kelson et al.¹⁵ Ru(III)terpyCl₃ (0.14 gram, 0.28 mmol) was dissolved in ethanol (50 mL). 2-Hydroxypyridine (0.125 gram, 1.31 mmol) was added and the mixture was refluxed for 1 h. After refluxing, an aqueous NaOH solution (25 mL, 300 mM) was added and refluxing was continued for two additional hours. After refluxing, the mixture was cooled down to room temperature. Ethanol was evaporated under reduced pressure. During this process, purple crystals formed. The crystals were filtered and washed twice with water (10 mL). Yield: 93%. The product was analyzed with FT-IR: $\nu_{\text{max}}\text{ cm}^{-1}$: 1604s, 1539s, 1470s, 1443s, 1375s, 1274s, 1009s, 965w, 845m, 762m, 738m and ¹H-NMR: 400 MHz (acetone-d₆) δ : 9.24(2H, m); 8.43 (4H, m); 7.90 (2H, t); 7.70 (1H, t); 7.56 (2H, m); 6.78 (2H, t); 5.74 (4H, m); 5.50 (2H, m).

10.2.4. Synthesis of terpyridine functionalized particles. Powdered KOH (20 mg, 0.35 mmol) was added to a dispersion containing chlorinated polystyrene particles (CPs-Cl) in dimethylformamide (DMF) (10 mL, solid content = 1%). The mixture was heated to 60 °C for 48 h. After hydrolysis, the colloids were washed with DMF (three times) and water (three times). The chemical composition was monitored with FT-IR: $\nu_{\text{max}}\text{ cm}^{-1}$: 3400br appears and 1266s disappears.

Attachment of 4'-chloro-2,2':6',2''-terpyridine to the obtained hydrolyzed polystyrene colloids was performed as described in references 18–20. The particles containing surface hydroxyl moieties were redispersed in DMF (10 mL, solid content = 1%) and subsequently mixed with KOH (25 mg, 0.44 mmol) and 4'-chloro-2,2':6',2''-terpyridine (60 mg, 225 μ mol). The resulting reaction mixture was heated to 70 °C for 48 h. A green/yellow mixture was obtained. This mixture was washed with DMF (three times) and water (three times). The presence of terpyridine on the surface of the particles was verified by addition of FeCl₂ to an aqueous dispersion of the obtained

particles. After addition, a bright pink dispersion was obtained, which indicated the formation of a coordination complex between Fe^{2+} and the terpyridine moieties.¹⁸ Centrifugation of the pink dispersion yielded a colorless supernatant and an intensely pink sediment, confirming that the iron-terpyridine complex was indeed bound to the colloids. The presence of iron ions was confirmed using energy dispersive X-ray (EDX) spectroscopy (6.4 and 7.1 keV). The chemical composition of the terpyridine functionalized particles was probed with FT-IR and XPS. FT-IR: ν_{max} cm^{-1} : 1600s, 1581s, 1561s, 1493s, 752m, 697s. XPS: E_b [eV]: 543 (O), 398 (N), 284 (C).

10.2.5. Estimation of terpyridine surface density. The surface coverage of terpyrides was estimated by the following titration experiment. An aqueous solution of $\text{FeCl}_2 \cdot 4\text{H}_2\text{O}$ (14 μM) was added in steps of 2 mL to a dispersion containing terpyridine functionalized particles (2 mL, solid content = 1%). After each step, the dispersion was sonicated for 5 min to ensure complete complex formation between the Fe^{2+} ions and the terpyridines. After sonication, the dispersion was centrifuged and 2 mL of the supernatant was collected and used to determine the concentration of free Fe^{2+} . To measure the concentration of iron ions, first a UV-Vis spectrum of the supernatant was recorded which was used as blank. After measuring the blank, a 1,10-phenanthroline solution (0.1 mL, 5.5 mM) and hydroxylamine·HCl solution (20 μL , 1.4 M) were added to the supernatant according to ref. 21. 1,10-phenanthroline forms complexes with the Fe^{2+} ions which are highly UV active. This enabled us to measure very low quantities of Fe^{2+} . Hydroxylamine was added to ensure that all the present iron ions had oxidation state 2+. The resulting solution was measured again using UV-Vis spectroscopy. After subtraction of the blank spectrum, the absorbance at 508 nm was indicative for the Fe^{2+} concentration. The relation between iron concentration and absorbance was previously determined by measuring a concentration series of the iron-1,10-phenanthroline complex.

This procedure was repeated until free Fe^{2+} ions were measured. Based on the total amount of ions added to the particles minus the free ions which were measured in the last titration step, the total iron uptake per particle could be calculated. The resulting terpyridine surface density turned out to be roughly one terpyridine moiety per 4 nm^2 .

10.2.6. Synthesis of immobilized catalyst (TPRC). The synthetic route for preparation of the immobilized catalyst was analogous to the one used for preparation of the homogeneous catalyst (Section 10.2.3), with the only difference that the terpyridine ligands were covalently bound to the polystyrene colloids. An excess $\text{RuCl}_3 \cdot x\text{H}_2\text{O}$ (20 mg) was added to a dispersion containing the terpyridine functionalized colloids as prepared in Section 10.2.4 (10 mL, solid content 1% = 0,094 μmol terpyridine/mL) in ethanol. The obtained mixture was refluxed for 3 h, after which it was washed with water (two times) and ethanol (two times). The colloids were analyzed with FT-IR and XPS. FT-

IR: ν_{\max} cm^{-1} : 1600s, 1493s, 752m, 697s. XPS: E_b [eV]: 543 (O), 461 (Ru), 398 (N), 284 (C), 270 (Cl), 200 (Cl).

The particles containing ruthenium coordinated terpyridine ligands were redispersed in ethanol (10 mL) and 2-hydroxypyridine (0.42 mg, 4.4 μmol) was added. The mixture was refluxed for 1 h, after which an aqueous NaOH solution (5 mL, 300 mM) was added. Refluxing was continued for two additional hours. The colloids were washed once with water, ethanol and 2-propanol. The chemical composition was probed with IR spectroscopy and XPS. FT-IR: ν_{\max} cm^{-1} : 1607s, 1550br, 1382br. XPS: E_b [eV]: 543 (O), 461 (Ru), 398 (N), 284 (C).

10.2.7. General procedure for transfer hydrogenation reaction with TPR.

A TPR solution in 2-propanol (1 mL, concentration of catalyst was varied. See Table 10.1, Section 10.3.4) was degassed by careful evacuation and refilling with nitrogen. NaOH stock solutions in 2-propanol with varying concentrations were prepared (Table 10.1, Section 10.3.4), degassed and added to the catalyst solution. The resulting mixture was refluxed for 30 min under nitrogen atmosphere. A color change from purple to yellow was observed. Finally, a degassed acetophenone stock solution in 2-propanol (2 mL, 20 mM) was added. Conversions of acetophenone were measured with gas chromatography-mass spectrometry (GC-MS). If necessary, the samples were diluted with 2-propanol before measuring.

10.2.8. General procedure for transfer hydrogenation reaction with TPRC.

A similar approach as described for the reactions with the homogenous catalyst was followed (Section 10.2.7). TPRC dispersed in 2-propanol (1 mL, solid content 2% \approx 0.188 μmol catalytic moieties) was degassed. A degassed NaOH solution in 2-propanol (2 mL) was added. NaOH concentrations were varied (Table 10.2, Section 10.3.5). The resulting mixture was refluxed for 30 min under nitrogen atmosphere. A color change from purple to yellow was observed. Finally, a degassed acetophenone stock solution in 2-propanol (2 mL, 20 mM) was injected. Conversions were determined with GC-MS using the supernatant obtained after centrifugation of the samples that were withdrawn from the reaction mixture. Only the top part of the supernatant was used for GC-MS measurements to avoid the presence of particles in the samples.

10.2.9. Transfer hydrogenation under normal atmosphere. TPR (8.13 mg, 15 μmol) and a NaOH solution in 2-propanol (3 mL, 66 mM) were refluxed for 30 min. Acetophenone stock solution in 2-propanol (2 mL, 1050 mM) was subsequently added. Refluxing was continued for an additional 20 h. Samples were withdrawn from the reaction mixture and diluted 50 times before acetophenone conversion was measured using GC-MS.

10.2.10. Recycling of TPRC. TPRC colloids which were previously used in a catalytic reaction (Section 10.2.8) were separated from the reaction mixture by

centrifugation. The colloids were then redispersed in 2-propanol and a new catalytic reaction was performed as described in Section 10.2.8. The conversion of acetophenone was measured with GC-MS and compared with the conversion obtained after the first catalytic reaction performed with these particles.

10.2.11. Measuring adsorption of TPR on polystyrene colloids. Non-functionalized colloids (CPs, 1 mL, solid content = 1%) were centrifuged. The supernatant was removed and the particles were subsequently redispersed in a solution of TPR in 2-propanol (1 mL, 0.188 mM). The resulting dispersion was stirred for 1 h to provide sufficient time for possible TPR adsorption. After this period, the dispersion was centrifuged. Adsorption of purple complex to the white polystyrene particles should result in a color change of the sediment. This color change was probed by eye.

10.2.12. Characterization. Transmission electron microscopy (TEM) pictures were recorded with a Philips Technai10 electron microscopy typically operating at 100 kV. Bright field images were recorded using a SIS Megaview II CCD camera. The samples were prepared by drying a drop of diluted, aqueous particle dispersion on top of polymer coated copper grids.

Energy dispersive X-ray (EDX) spectra were recorded on a TechnaiF20 from FEI with an acceleration voltage of 200 kV. The microscope was equipped with an EDX system from EDAX using Emispec software in STEM mode.

X-ray photoelectron spectroscopy (XPS) was performed using a Thermo Scientific K-Alpha, equipped with a monochromatic small-spot X-ray source and a 180° double focusing hemispherical analyzer with a 128-channel detector. Spectra were obtained using an aluminum anode (Al K α = 1486.6 eV) operating at 72 W and a spot size of 400 μ m. Survey scans were measured at a constant pass energy of 200 eV and region scans at 50 eV. The background pressure was 2×10^{-9} mbar and during measurement 3×10^{-7} mbar argon because of the charge compensation dual beam source.

Infrared (IR) spectra were obtained using a Perkin Elmer FT-IR /FIR Frontier Spectrometer. The attenuated total reflectance (ATR) mode was used. Measurements were performed on powders obtained by drying the particle dispersion. UV-Vis spectra were recorded on a Perkin-Elmer Lambda-35 spectrophotometer.

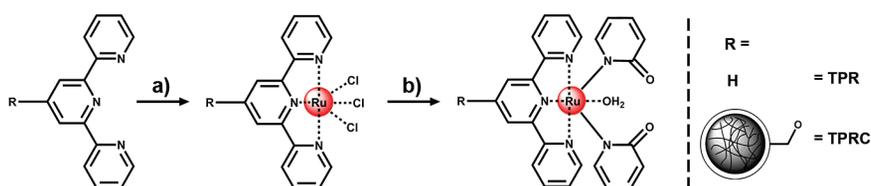
$^1\text{H-NMR}$ spectra were recorded using a Varian MRF400 400MHz NMR machine. Acetone- d_6 was used as solvent.

Gas chromatography-mass spectrometry (GC-MS) measurements were conducted using a Perkin Elmer Austosystem XL Gas Chromatograph equipped with a PE-17 column (50% phenyl, 50% methylpolysiloxane; 30 m \times 0.23 \times 0.5 μ m). In all measured traces, only signals corresponding to acetophenone and the product (1-phenylethanol) were observed, indicating the absence of side-products and high selectivity of the (immobilized) catalyst. The obtained conversions were therefore indicative for the yield.

10.3. Results and Discussion

10.3.1. Synthesis of the homogeneous transfer hydrogenation catalyst (TPR). The ruthenium complex depicted in Scheme 10.2 was selected as transfer hydrogenation catalyst. This choice was based on a paper published by Kelson et al. who showed that the catalyst can be easily obtained by a two-step reaction (Scheme 10.2).^{15,17}

Scheme 10.2. Schematic representation of the synthesis route towards the transfer hydrogenation catalyst starting from terpyridine.^a



^a Step (a): coordination of Ru₃Cl to terpyridine. Step (b): addition of 2-hydroxypyridine in combination with a base, leading to the coordination of the auxiliary pyridonate ligands. This completes the formation of the catalyst. R represents either a proton (= homogeneous catalyst TPR) or a polystyrene colloidal particle (= immobilized catalyst TPRC). The terpyridine moieties are attached to the surface of the colloids via an ether bond.

The first step comprised the coordination of RuCl₃ to terpyridine by addition of terpyridine to a solution of RuCl₃·x H₂O in ethanol (step a, Scheme 10.2). In the second step, two auxiliary pyridonate ligands were introduced by addition of 2-hydroxypyridine and a base (NaOH). Formation of the complete catalyst was accompanied by the appearance of a purple color and the pure catalyst was isolated as dark purple/black crystals. The resulting crystals were analyzed using infrared (IR) spectroscopy (Figure 10.1a) and ¹H-NMR (Figure 10.1b). The signals observed in both spectra were in good agreement with the spectra reported in literature, which proved that the complex was successfully prepared.¹⁵ To emphasize the similarity between the literature spectra and the spectra we obtained, the reported signals are highlighted with a red star (Figure 10.1).

Both reaction steps did not require demanding reaction condition, e.g. complete exclusion of water or oxygen, and the final catalyst was stable under normal atmosphere. These features make the synthesis easily adaptable towards immobilization on colloidal particles, as will be described in the next section.

10.3.2. Covalent immobilization of terpyridine ligands to a colloidal surface. The immobilization of the homogeneous catalyst (TPR) was achieved by using

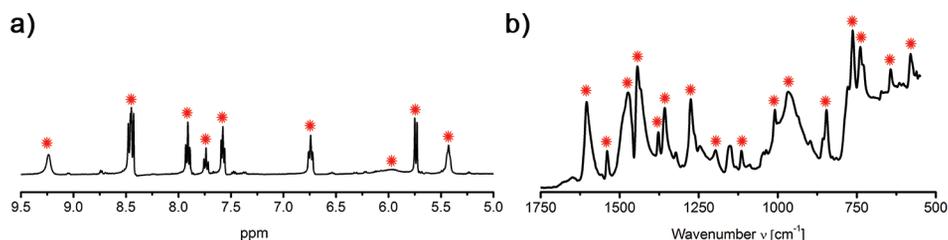
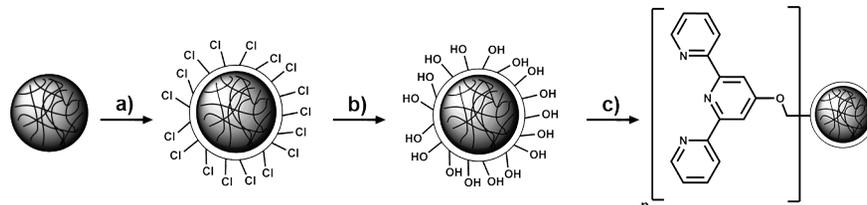


Figure 10.1. (a) Proton Nuclear Magnetic Resonance (¹H-NMR) spectrum and (b) Infrared (IR) spectrum of the homogeneous transfer hydrogenation catalyst (TPR). The signals reported in literature are highlighted with the red stars.¹⁴

polystyrene colloids that were functionalized with covalently attached terpyridine moieties. These terpyridines were subsequently employed as colloidal ligands which participated in the formation of the catalytic complex in a similar fashion as described for the homogenous complex (Section 10.3.1).

Scheme 10.3. Schematic representation of the synthetic route towards colloidal particles equipped with terpyridine moieties at their surface.^a



^a Step (a): seeded emulsion polymerization of vinylbenzyl chloride (VBC) and divinylbenzene (DVB) in the presence of polystyrene seeds. Step (b): hydrolysis of the surface chlorine groups by reaction of KOH in DMF. Step (c): attachment of 4'-chloro-2,2':6,2''-terpyridine to the hydrolyzed particles by reaction in DMF in the presence of KOH.

Firstly, terpyridine functionalized colloids were successfully synthesized in four steps, which are schematically depicted in Scheme 10.3. The first step was a straightforward emulsion polymerization of styrene and divinylbenzene to yield monodisperse, cross-linked seed particles.¹⁶ These seed particles were used to grow a chlorinated shell around these particles by means of a seeded emulsion polymerization (step a, Scheme 10.3).¹⁶ Proof of successful incorporation of the chlorine functionality was provided by both IR spectroscopy (Figure 10.2, blue spectrum) and X-ray photoelectron spectroscopy (XPS) (Figure 10.3, red spectrum). Comparing the IR

spectra of the bare polystyrene seeds (Figure 10.2, red spectrum) and the chlorinated particles showed the clear appearance of a new signal at 1266 cm^{-1} , which corresponds to the $-\text{CH}_2\text{-Cl}$ vibration of the incorporated vinylbenzyl chloride. Binding energies of 200 and 270 eV in the XPS spectrum corresponding to chlorine were detected, providing additional proof that the groups were present at the particle surface; XPS is a surface elemental analysis technique with a penetration depth of only 1–10 nm. The detected carbon signal (284 eV) obviously originated from the polystyrene core of the colloids. Oxygen was measured due to the presence of sulfate and sulfonate groups at the surface of the colloids. These moieties originated from the initiator system employed in the emulsion polymerization steps to form the particles (KPS and NaHSO_3).²²

The introduction of chlorine groups to the surface of the particles ensured the presence of a chemical handle for further modification. Since the chlorine groups resided at the surface of the synthesized particles, all subsequent chemistry will take place at the surface. This is a major advantage, because it will ensure good accessibility of the catalyst in the final transfer hydrogenation reactions (Section 10.3.5).

The surface chlorine groups were hydrolyzed by addition of KOH (step b, Scheme 10.3), yielding OH modified polystyrene particles. After hydrolysis, IR spectroscopy revealed the disappearance of the characteristic $-\text{CH}_2\text{-Cl}$ (1266 cm^{-1}) vibration and the appearance of a broad OH signal at 3400 cm^{-1} (green spectrum in Figure 10.2), indicating successful hydrolysis.

In the final step, the surface hydroxyl groups were used to covalently attach 4'-chloro-2,2':6',2''-terpyridine via a nucleophilic aromatic substitution reaction (step c, Scheme 10.3). The presence of the terpyridine moieties on the surface was confirmed with IR spectroscopy (orange spectrum in Figure 10.2). The spectrum of the terpyridine functionalized particles showed lowering of the OH signal and the appearance of a characteristic terpyridine signal at 1562 cm^{-1} corresponding to C=N vibrations of the pyridine rings.²² XPS analysis provided additional proof for successful attachment of the terpyridine. A sharp decrease of the chlorine signals (200 and 270 eV) was accompanied by the appearance of a nitrogen signal at 398 eV (Figure 10.3, blue spectrum). The signals around 490 eV represent Sn impurities.

Final proof of successful immobilization of the terpyridine ligands was provided by the addition of FeCl_2 to a dispersion of terpyridine containing particles. Before addition, the dispersion was white in appearance (vial I, Figure 10.4a). Upon addition of FeCl_2 an intense pink color was formed (vial III, Figure 10.4a). The pink color is characteristic for the terpyridine- Fe^{2+} complex.¹⁸ Centrifugation yielded a pink sediment and a colorless supernatant, indicating that the iron-terpyridine complex was indeed bound to the colloids. Addition of FeCl_2 to a dispersion containing non-functionalized polystyrene particles did not induce a color change (vial II, Figure 10.4a).

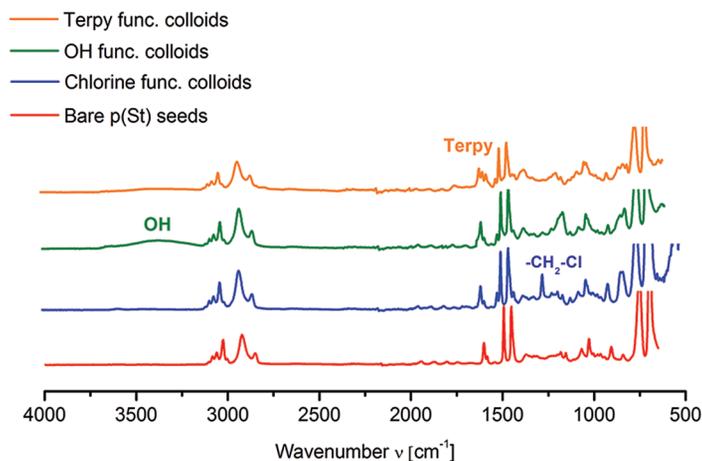


Figure 10.2. Infrared (IR) spectra of the bare polystyrene seeds (red), chlorinated core-shell particles (blue), the particles obtained after hydrolysis of the surface chlorine groups (green) and the terpyridine functionalized polystyrene colloids (orange). Characteristic signals are labelled with the corresponding chemical entity causing the vibration.

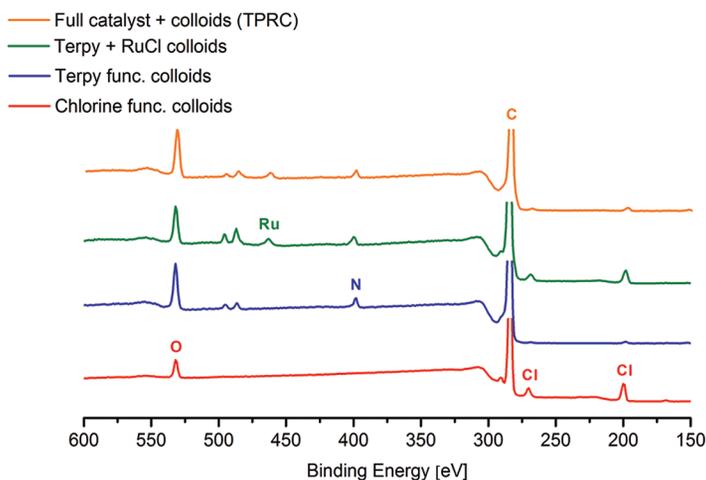


Figure 10.3. X-ray photoelectron spectroscopy (XPS) spectra of chlorinated core-shell particles (red), the terpyridine functionalized polystyrene colloids (blue), the terpyridine containing colloids after the complexation reaction with RuCl_3 (green) and the spectrum obtained of the particles equipped with the complete transfer hydrogenation catalyst on their surface (orange). Characteristic signals are labelled with the corresponding element appearing at that binding energy.

The complexation capability of the terpyridine groups on the surface was further confirmed using energy dispersive X-ray spectroscopy (EDX). The particles containing iron saturated terpyridine ligands were measured using this elemental analysis technique, which resulted in a clear iron signal located at 6.4 and 7.1 keV as shown in Figure 10.4b. The copper and silicon signals originated from the grid on which the sample was placed and detector impurities, respectively.

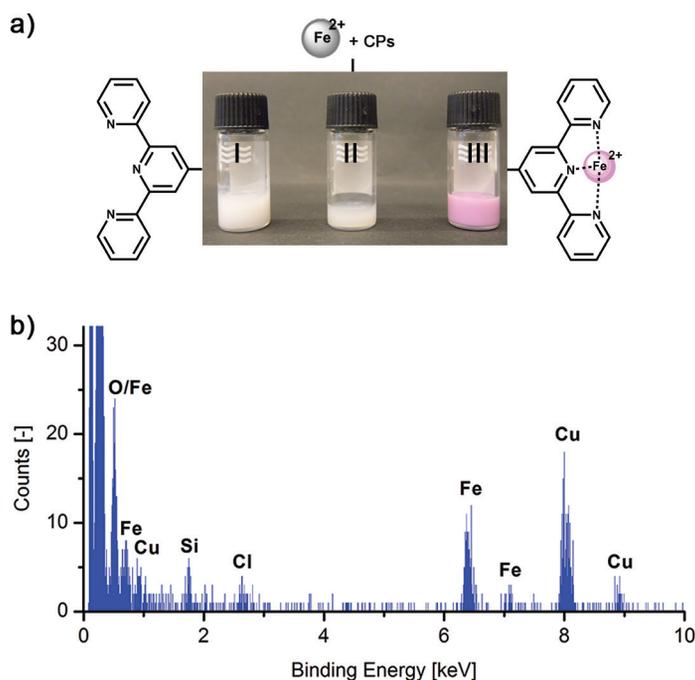


Figure 10.4. (a) Macroscopic appearance of the terpyridine functionalized particles without the addition of FeCl_2 (I), non-functionalized particles in the presence of FeCl_2 (II), and the pink dispersion obtained after adding FeCl_2 to a dispersion containing terpyridine functionalized particles (III). The pink color is characteristic for the Fe^{2+} -terpyridine complex. (b) Energy dispersive X-ray (EDX) spectrum of the iron-loaded terpyridine functionalized polystyrene particles.

Before proceeding to the formation of the immobilized catalyst, it would be convenient to have an indication of the terpyridine surface density on these particles. An estimation for the terpyridine surface density is useful for determining the quantities of reactants required for catalyst formation. Furthermore, knowledge of the terpyridine density provides an upper limit for the catalyst loading per colloidal particle. The estimated maximal catalyst loading allows for fair comparison of the catalytic activity of the homogeneous and immobilized catalyst, since catalytic transfer hydrogenation

reactions with equal concentrations of catalytic species can be conducted (Section 10.3.4 and 10.3.5).

To estimate the terpyridine surface density, a titration experiment was conducted in which FeCl_2 was added stepwise to a dispersion containing terpyridine functionalized particles. After each addition step, the dispersion was stirred to allow for the iron ions to coordinate to terpyridine. After complex formation, the dispersions were centrifuged and the supernatants were tested for residual iron ions by means of UV-Vis spectroscopy. Detection of Fe^{2+} ions was possible after addition of 1,10-phenanthroline. The resulting Fe-phenanthroline complex is highly UV-active, allowing for the detection of iron ions down to the ppm level.²¹ This procedure was repeated until a certain concentration of free ions was measured. Based on the total amount of ions added to the particles minus the free ions which were measured in the last titration step, the total iron uptake per particle could be determined. The surface density of terpyridines was subsequently calculated by assuming that each iron center was coordinated to one terpyridine moiety. A surface density of 1 terpyridine unit per 4 nm^2 was obtained. Although this density is probably a slight overestimation due to, for example, non-specific ion adsorption, it indicates that the colloidal surface was densely packed with terpyridines.

10.3.3. Synthesis of the immobilized transfer hydrogenation catalyst (TPRC). With successful introduction of terpyridine ligands to the colloidal surface and an estimation of the surface density, we proceeded to the formation of the actual transfer hydrogenation catalyst. Analogous to the synthesis of the homogenous complex, the first synthetic step was coordination of RuCl_3 to the surface bound terpyridine ligands (step a, Scheme 10.2). Indications for successful coordination of the ruthenium were provided by XPS measurements. The spectrum obtained after mixing the terpyridine containing particles with RuCl_3 (Figure 10.3, green spectrum) showed both the appearance of a ruthenium signal (461 eV) and an increase in the chlorine content caused by auxiliary chlorines coordinated to the ruthenium. Addition of 2-hydroxypyridine and NaOH to complete the formation of the catalyst, resulted in a decrease of the chlorine content as observed with XPS (Figure 10.3, orange spectrum). This is in agreement with replacement of the chlorine ligands by two pyridonate ligands (Scheme 10.2). The nitrogen and ruthenium signals remained visible, suggesting that the complete catalyst was indeed formed.

Although the XPS results provide compositional information, no structural details could be extracted. Therefore, it was not possible to prove that the true transfer hydrogenation catalyst was formed. However, the color of particles with the immobilized catalyst was purple, resembling the color observed for the homogeneous catalyst. The match in color was a strong indication that ruthenium was present in oxidation state 2+ and that the observed elemental composition indeed corresponds

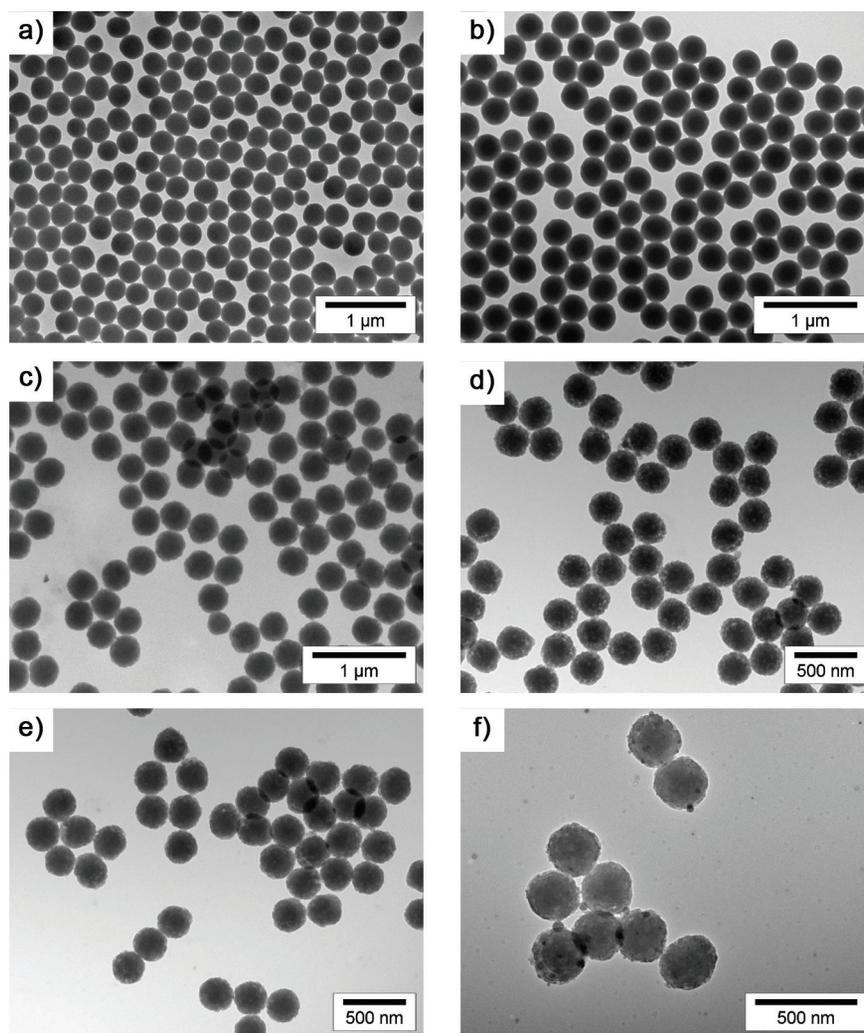


Figure 10.5. Transmission electron microscopy (TEM) pictures of (a) bare polystyrene seeds, (b) the chlorinated core-shell particles, (c) particles obtained after the hydrolysis of the surface chlorines, (d) terpyridine functionalized particles, (e) terpyridine functionalized particles after complexation with RuCl_3 , and (f) colloids equipped with the full transfer hydrogenation catalyst.

to the formation of the active catalytic complex. Indisputable evidence for formation of the aimed complex will be provided by measuring the transfer hydrogenation activity of these colloids (Section 10.3.5).

From a molecular point of view, catalyst immobilization appeared successful. However, to exploit the colloids as immobilization platform, the particles should still

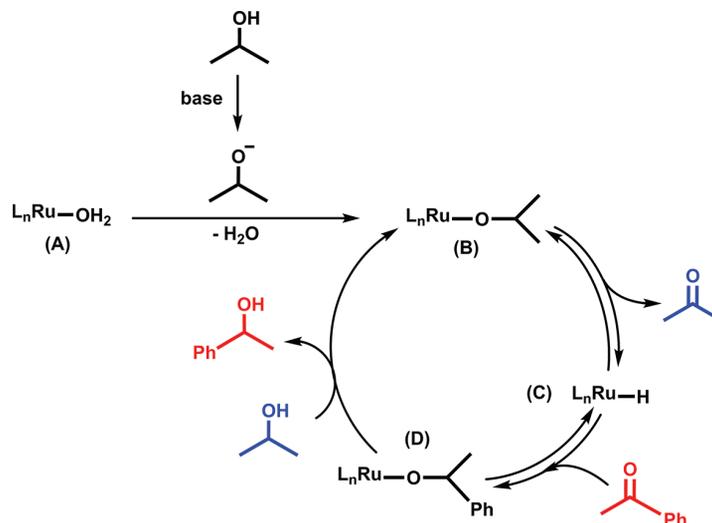
be intact after the chemical treatments required for catalyst formation. To verify the robustness of the particles, TEM was used to image the particles after each reaction step. The results are summarized in Figure 10.5. The bare polystyrene particles (Figure 10.5a), as well as the chlorinated particles (Figure 10.5b) were spherical and had a smooth surface. After hydrolysis of the surface chlorine groups (Figure 10.5c) and introduction of the terpyridine ligands (Figure 10.5d), the colloidal surface became much rougher. This was probably caused by dissolution of non-cross-linked polystyrene from the colloids in DMF. The complexation of ruthenium (Figure 10.5e) and addition of the pyridonate ligands (Figure 10.5f) did not lead to a change in the particle morphology.

From these TEM images we concluded that the bulk of the polystyrene carrier colloids survived the catalyst immobilization procedure. The catalytic moieties were therefore still tethered to a relatively heavy carrier which allows for easy separation of the catalyst from the reaction mixture by centrifugation. The introduced surface roughness was not expected to have any negative influence on the catalytic transfer hydrogenation reactions.

10.3.4. Transfer hydrogenation of acetophenone with TPR. The catalytic transfer hydrogenation of acetophenone (hydrogen acceptor, $R = C_6H_5$ in Scheme 10.1) was first conducted with the homogenous complex (TPR) to compare the catalytic activity of the immobilized catalyst, to test our experimental set-up and to probe the importance of the various experimental parameters. Acetophenone was chosen as substrate for the transfer hydrogenation, since it readily reacts in this type of reactions and is commonly used as model hydrogen acceptor.^{14,24} 2-propanol was used both as the hydrogen donor and the solvent. After donation of the hydrogen atoms (Scheme 10.1, highlighted in red) to acetophenone, the product (1-phenylethanol) and acetone are formed. The reactions will be performed at 80 °C, which ensures the removal of acetone from the reaction mixture. As explained in the Introduction, acetone evaporation forces the equilibrium of the reaction continuously to the product side, eventually leading to high conversions of acetophenone.

Although the precise mechanism for this specific catalyst is not reported in literature, it is fair to assume that the hydrogen transfer occurs via the formation of a metal hydride.^{14,24–26} The expected catalytic cycle is depicted in Scheme 10.4. The metal hydride (**C**) is formed after β -H-elimination from species (**B**). Acetone is formed as byproduct in this step. The metal hydride (**C**) can subsequently coordinate a ketone that is present in the reaction mixture. In this migratory insertion step, the hydride is transferred to the carbonyl carbon of the incoming ketone. The ketone is therefore effectively reduced. The migratory insertion is basically the reverse reaction of the β -H-elimination responsible for the formation of (**C**) from (**B**). Since acetone is continuously removed, there is a strong preference for the reduction of acetophenone, resulting in the

Scheme 10.4. Schematic representation of the proposed catalytic cycle for the transfer hydrogenation of acetophenone.^a



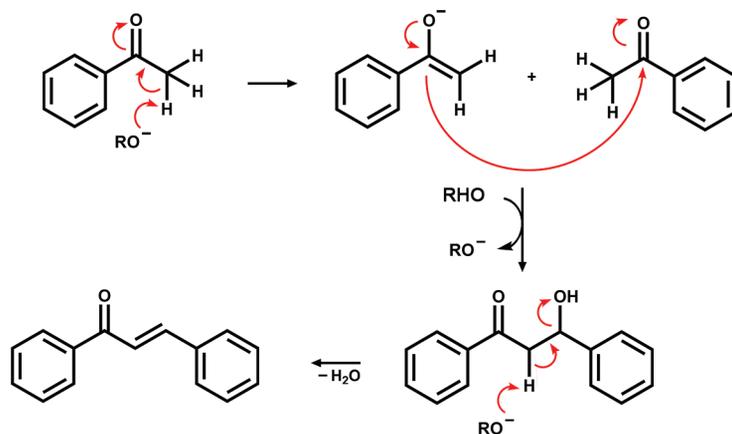
^a L_n represents the terpyridine and pyridonate ligands coordinated to the ruthenium center (see Scheme 10.2). The weakly coordinated water molecule in the pre-catalyst (**A**) is substituted by an isopropoxide ion to yield complex (**B**). The isopropoxide ions are formed by deprotonation of 2-propanol. Complex (**B**) undergoes β -H-elimination yielding acetone and the ruthenium hydride (**C**). Compound (**C**) reduces acetophenone via a migratory insertion, forming complex (**D**). Finally, (**D**) reacts quickly with 2-propanol resulting in 1-phenylethanol as product and the regeneration of complex (**B**). Coordination of ketones to the ruthenium center is an equilibrium process. The formation of complex (**D**) is enhanced by the continuous removal of acetone through evaporation.

formation of the ruthenium alkoxide complex (**D**). In the final step of the cycle, the ruthenium alkoxide (**D**) reacts with 2-propanol to yield 1-phenylethanol and the initial isopropoxide complex (**B**).

As commonly observed for these transfer hydrogenations, the addition of base enhances the reaction rate tremendously. Baratta et al. reported that the rate of acetophenone reduction follows second-order kinetics and depends on both the catalyst concentration and the concentration of base.²⁶ By increasing the base concentration, the formation rate of the active isopropoxide complex (**B**) is sped up. Deprotonation of 2-propanol yields isopropoxide ions, which readily coordinate to the pre-catalyst (**A**). This coordination is typically accompanied by the elimination of a labile ligand, e.g. H_2O .

With these mechanistic considerations in mind, transfer hydrogenation

Scheme 10.5. Aldol condensation of acetophenone leading to the formation of the corresponding β -hydroxyketone and α,β -unsaturated ketone.



experiments were conducted. Table 10.1 gives an overview of the reactions performed with the homogeneous catalyst. The molar ratios between catalyst, NaOH and ketone were varied to find the optimal reaction conditions.

Entry 1 represents a reproduction of the transfer hydrogenation reaction conducted by Kelson et al.¹⁵ Nearly full conversion was reached within one hour, in agreement with the reported results. Although not mentioned by Kelson et al,¹⁵ it was key that acetophenone and the NaOH solution were degassed separately before mixing these components. If these components are degassed together, hardly any product formation was observed. This observation might be attributed to aldol condensations taking place in the acetophenone/NaOH mixture before addition to the catalyst (Scheme 10.5). This condensation results in the formation of the corresponding α,β -unsaturated ketone through the intermediate β -hydroxyketone and therefore depletion of acetophenone before the catalyst is introduced into the mixture.²⁷

A second prerequisite for successful transfer hydrogenation was exclusion of oxygen from the reaction mixture. Entry 2 represents the same reaction as entry 1, however no measures were performed to exclude oxygen from the reaction mixture. The catalytic activity decreased dramatically, indicating that the catalyst did not function properly under normal atmospheric conditions.

For further experiments, the catalyst loading was lowered from 10 μmol to 0.2 μmol . The motivation behind this decrease in catalyst concentration was that it allows us to directly compare the reaction rate measured with the homogeneous complex and the immobilized catalyst (Section 10.3.5), since the catalyst concentration was kept constant. Due to the relatively low number of catalysts per particle (Section 10.3.2),

Table 10.1. Summary of transfer hydrogenations conducted with acetophenone as substrate, 2-propanol as hydrogen donor (+ solvent) and the homogeneous catalyst (TPR). Conversions were determined with gas chromatography-mass spectrometry GC-MS. (n.d. = not determined).

Entry	[TPR] [μmol]	NaOH [μmol]	Acetophenone [μmol]	Ratio TPR : NaOH : ketone	Conversion after 2 h [%]	Conversion after 24 h [%]
1	10^{*2}	200	2100	1 : 20 : 210	100 ^{*4}	n.d.
2	$10^{*2,3}$	200	2100	1 : 20 : 210	19	n.d.
3	0.2	0	40	1 : 0 : 200	0	0
4	0.2	4	40	1 : 20 : 200	7	46
5	0.2	100	40	1 : 500 : 200	27	100
6	0.2	200	40	1 : 1000 : 200	62	100 ^{*4}

^{*1} All reaction were conducted in 2-propanol; total volume was 5 mL. ^{*2} Degassed as solid.

^{*3} No measures were taken to exclude oxygen form the reaction mixture. ^{*4} Full conversion was reached before measuring.

it is not feasible to work at high catalyst loading, since this would require high solid content dispersions. Entry 4 was conducted with similar ratios between the reactants as described by Kelson et al.,¹⁵ resulting in a reaction mixture with concentrations that were a factor 50 lower compared to the standard reaction conditions (entry 1, Table 10.1). Obviously lower reaction rates were measured under these conditions. However, 46% acetophenone conversion was still reached after 24 h with these low catalyst concentrations.

Since Baratta et al. showed that the reaction rate is proportional to the base concentration,²⁶ transfer hydrogenation reactions were performed at elevated base concentrations (entry 5 and 6, Table 10.1) in an attempt to enhance the reaction rate. Indeed, significantly higher conversions were measured upon an increase of the base concentration and full conversion could be reached within 24 h. Finally, a transfer hydrogenation reaction was conducted in the absence of base (entry 3, Table 10.1). No catalytic activity was measured under these conditions, which is agreement with the proposed mechanism (Scheme 10.4).

From the transfer hydrogenation catalyzed with the homogeneous complex we concluded that the complex we prepared showed similar activity as reported in literature. Key aspects for successful transfer hydrogenations were the exclusion of oxygen from the reaction mixture and separate degassing of the base and acetophenone solutions. The decrease in reaction rate upon lowering the catalyst loading was counteracted by increasing the base concentration. This allowed for conducting the transfer hydrogenation of acetophenone at low catalyst loadings, which is beneficial for the

catalytic reactions that will be conducted with the immobilized variant of the catalyst in the next section.

10.3.5. Transfer hydrogenation of acetophenone with TPRC. In this section the transfer hydrogenation reaction of acetophenone performed in the presence of the immobilized catalyst (TPRC) is described. The catalytic activity will be compared with its homogeneous analogue (Section 10.3.4). The reactions were conducted under similar conditions to directly probe the influence of the immobilization on the catalytic activity.

Table 10.2 lists the catalytic transfer hydrogenation reactions conducted with the immobilized catalyst. For all transfer hydrogenations, a maximal catalyst loading based on the surface density of terpyridine was assumed. This translates into one catalytic species per 4 nm² (or 0.094 μmol/mL dispersion with a solid content of 1 wt%).

Analogous to the catalytic reactions with the homogeneous complex (entry 3, Table 10.1), the addition of base was required to obtain any hydrogenation activity. (entry 1, Table 10.2). Entries 1–4 in Table 10.2 showed that catalytic activity was preserved after catalyst immobilization. However, the activity decreased compared to the homogeneous counterpart (entries 3–6, Table 10.1) as was deduced from the measured conversions after 2 and 24 h. The true nature of the decrease in catalytic activity is difficult to assess and different explanations have been reported for a variety of immobilized catalysts.^{2,3,5,6} Factors that are commonly proposed in literature include the relatively slow diffusion of the particles compared to the molecular catalyst. This causes less efficient transport of reactants towards the catalytic species. Another feature that possibly decreases catalyst activity is related to the large dimensions of the particles compared to the molecular scale of the catalyst. Naively, the colloid can be regarded as an extremely bulky ligand providing steric hindrance for incoming or eliminated species.^{2,3,5,6} Finally, the colloidal surface has an effect on the local environment of the catalyst. An important factor in this respect is the negative surface charge of the colloidal particles. This negative charge, originating from the initiator moieties and required for colloidal stability, may result in a locally lower hydroxyl concentration around the colloids due to simple electrostatic repulsion.^{22,28,29} Since the reaction rate for transfer hydrogenation is dependent on the base concentration, the local suppression in the concentration of hydroxyl ions slows down the reaction. This reasoning might also explain why higher NaOH concentrations were required to significantly speed up the transfer hydrogenations catalyzed with the immobilized catalysts (entry 3 and 4, Table 10.2) compared to hydrogenation reactions catalyzed with the homogeneous complex (entry 5 and 6, Table 10.1).

Nevertheless, the decrease in reaction rate upon immobilization was not dramatic and full conversion of acetophenone was still reached relatively fast in the presence of high base concentrations. However, the increase in base concentration was limited

Table 10.2. Summary of transfer hydrogenations conducted with acetophenone as substrate, 2-propanol as hydrogen donor (+ solvent) and the immobilized catalyst (TPRC). Conversions were determined with gas chromatography-mass spectrometry GC-MS after centrifugation to remove the catalytic colloids. (n.d. = not determined).

Entry ^{*1}	[TPR] [μmol]	NaOH [μmol]	Acetophenone [μmol]	Ratio TPR : NaOH : ketone	Conversion after 2 h [%]	Conversion after 24 h [%]
1	0.2	0	40	1 : 0 : 210	0	0
2	0.2	4	40	1 : 20 : 200	n.d.	21
3	0.2	100	40	1 : 500 : 200	5	40
4	0.2	200	40	1 : 1000 : 200	18	100
5	0.2 ^{*2}	200	40	1 : 1000 : 200	n.d.	83

^{*1} All reaction were conducted in 2-propanol; total volume was 5 mL. ^{*2} TRP was reused from entry 4.

by the colloidal stability of the catalytic colloids. Upon addition of more NaOH, the ionic strength of the reaction medium increases, consequently resulting in more efficient screening of surface charges. The decreased electrostatic repulsion between the particles eventually leads to the formation of colloidal aggregates.^{28,29} A fraction of the catalytic species present on the particles will therefore be trapped inside the particle clusters, lowering the effective catalyst concentration. Therefore, optimization of the NaOH concentration seems crucial to exploit this system to its full capacity.

10.3.6. Immobilization of TPR by adsorption on colloidal surface.

The previously discussed immobilization strategy to covalently bind the catalyst to the colloidal surface required a significant number of synthesis steps. To verify the necessity of the covalent bond between the colloids and the catalyst, immobilization of the homogeneous catalyst by simple adsorption was investigated. One could argue that the hydrophobic surface of the polystyrene colloids could be used to adsorb the catalyst. If the binding energy is sufficiently high, immobilization will be achieved without any particle modification reactions, making this procedure synthetically less demanding.

To probe the feasibility of the adsorption approach, TPR was added to a dispersion of non-functionalized polystyrene seeds (CPs as prepared in Section 10.2.2) in 2-propanol. After complete mixing, a homogenous pink dispersion was obtained. This color was caused by the intense purple color of TPR. The resulting dispersion was stirred for a long period to facilitate TPR adsorption. Subsequent centrifugation to separate the particles from the continuous phase yielded a white sediment and a purple supernatant. This visual observation already strongly suggests that the catalyst did not

adsorb (significantly) to the colloidal surface. The resulting particles were not employed in subsequent transfer hydrogenation reactions, due to the insignificant concentration of immobilized catalyst. Furthermore, the unmodified particles were marginally stable under the reaction conditions required for the transfer hydrogenation reaction (2-propanol and NaOH), which further hampers transfer hydrogenation experiments. These findings prove that the immobilization strategy based on covalent attachment of the catalyst was indeed necessary to keep the catalyst bound to the colloids.

10.3.7. Recycling of catalytic particles. As mentioned in the Introduction, the ability to recover the catalyst from the reaction medium is the main advantage of immobilized catalysts in general. To investigate if our system was indeed recyclable, we took the crude reaction mixture of the transfer hydrogenation reaction labelled with entry 4 in Table 10.2. The particles were separated by centrifugation and redispersed in pure 2-propanol. The same transfer hydrogenation reaction was performed again with these particles (entry 5, Table 10.2). For both reactions the conversion was measured after 24 h. The recycled catalyst reached a conversion of 83%, while the same reaction with fresh particles yielded 100% conversion. The catalytic activity was clearly still present. This was rather remarkable, because the particles were exposed to air during the centrifugation steps after the first catalytic reaction. Catalytic transfer hydrogenations with the homogeneous complex performed under normal atmosphere yielded significantly lower conversions than the same reaction under inert atmosphere (entries 1 and 2, Table 10.1), indicating that exclusion of oxygen is crucial if the catalyst was dissolved in the reaction mixture. Furthermore, loss of particles due to centrifugation is inevitable leading to an apparent decrease in catalytic activity. To correct for this loss, the catalytic activity should be measured as function of the mass of catalytic colloids added to each transfer hydrogenation reaction.

This preliminary recycling experiment showed that recovery and reuse of these catalytic particles is feasible. Probably a large part of the (apparent) activity loss is caused by either oxygen-mediated catalyst deactivation or simple loss of catalytic material due to centrifugation. Both problems are experimentally solvable. Conducting more recycle experiments are definitely required to claim full recyclability of this catalytic system and to investigate the true loss in catalytic activity per transfer hydrogenation cycle.

10.4. Conclusions

The immobilization of terpyridine ligands on colloidal polystyrene particles was achieved. Subsequent complexation of ruthenium and auxiliary ligands onto this metal center resulted in the formation of an active transfer hydrogenation catalyst. The activity of the catalyst was demonstrated by transforming acetophenone into 1-phenylethanol using 2-propanol as hydrogen donor. The catalytic activity

decreased upon immobilization. Nevertheless, a significant transfer hydrogenation rate was measured resulting in high conversions after workable reaction times. Initial experiments show that these particles could be used again in a subsequent transfer hydrogenation reaction after extracting the catalyst from the reaction mixture via simple centrifugation. Exploiting colloids as mobile catalyst carriers promotes facile recyclability while catalytic activity is retained.

Acknowledgments

I would like to thank Dirk-Jan Schild for performing a major part of the experimental work described in this chapter, prof. Bert Klein Gebbink from the Organic Chemistry and Catalysis Group for useful discussions and reviewing of the manuscript. Hans Meeldijk is thanked for performing the EDX measurements. Finally, Judith van Wijk is acknowledged for the XPS analysis at the Eindhoven University of Technology.

References

- [1] I. Chorkendorff, J. W. Niemantsverdriet, In *Concepts of modern catalysis and kinetics*, 1st ed.; Wiley-VCH Verlag GmbH & Co. KgaA, Weinheim, 2003.
- [2] P. Barbaro and F. Liguori, In *Heterogenized homogeneous catalysts for fine chemicals production*, 1st ed.; Springer, Dordrecht, 2010.
- [3] A. Choplin, F. Quignard, From supported homogeneous catalysts to heterogeneous molecular catalysts. *Coord. Chem. Rev.* **1998**, *178–180*, 1679–1702.
- [4] J. M. Brown, H. Molinari, Supported rhodium-phosphine hydrogenation catalysts of high mobility and reactivity. *Tetrahedron Lett.* **1979**, *31*, 2933–2936.
- [5] F. R. Hartley, P. N. Vezey, Supported transition metal complexes as catalysts. *Adv. Organomet. Chem.* **1977**, *15*, 189–234.
- [6] X. S. Zhao, X. Y. Bao, W. Guo, F. Y. Lee, Immobilizing catalysts on porous materials. *Mater. Today* **2006**, *9*, 32–39.
- [7] E. M. Claesson, N. C. Mehendale, R. J. M. Klein Gebbink, G. van Koten, A. P. Philipse, *J. Magn. Magn. Mater.* **2007**, *11*, 41–45.
- [8] A. Hu, G. T. Yee, W. Lin, Magnetically recoverable chiral catalysts immobilized on magnetite nanoparticles for asymmetric hydrogenation of aromatic ketones. *J. Am. Chem. Soc.* **2005**, *127*, 12486–12487.
- [9] S. Gladiali, E. Alberico, Asymmetric transfer hydrogenation: Chiral ligands and applications. *Chem. Soc. Rev.* **2006**, *35*, 226–236.
- [10] R. Noyori, S. Hashiguchi, Asymmetric transfer hydrogenation catalyzed by chiral ruthenium complexes. *Acc. Chem. Res.* **1997**, *30*, 97–102.

- [11] R. A. W. Johnstone, A. H. Wilby, Heterogeneous catalytic transfer hydrogenation and its relation to other methods for reduction of organic compounds. *Chem. Rev.* **1985**, *85*, 129–170.
- [12] T. Naota, H. Takaya, S.-I. Murahashi, Ruthenium-catalyzed reactions for organic synthesis. *Chem. Rev.* **1998**, *98*, 2599–2660.
- [13] G. Brieger, T. J. Nestruck, Catalytic transfer hydrogenation. *Chem. Rev.* **1974**, *74*, 567–580.
- [14] O. Pàmies, J.-E. Bäckvall, Studies on the mechanism of metal-catalyzed hydrogen transfer from alcohols to ketones. *Chem. Eur. J.* **2001**, *7*, 5052–5058.
- [15] E. P. Kelson, P. P. Phengsy, Synthesis and structure of a ruthenium(II) complex incorporating π N bound 2-pyridonato ligands; a new catalytic system for transfer hydrogenation of ketones. *J. Chem. Soc., Dalton Trans.* **2000**, *22*, 4023–4024.
- [16] B. G. P. van Ravensteijn, M. Kamp, A. van Blaaderen, W. K. Kegel, General route toward chemically anisotropic colloids. *Chem. Mater.* **2013**, *25*, 4348–4353.
- [17] B. P. Sullivan, J. M. Calvert, T. J. Meyer, Cis-Trans isomerism in (trpy)(PPh₃)RuCl₂. Comparisons between the chemical and physical properties of a cis-trans isomeric pair. *Inorg. Chem.* **1980**, *19*, 1404–1407.
- [18] U. S. Schubert, A. Alexeev, P. R. Andres, Terpyridine-functionalized TentaGel microbeads: Synthesis, metal chelation and first sequential complexation. *Macromol. Mater. Eng.* **2003**, *288*, 852–860.
- [19] D.-W. Yoo, S.-K. Yoo, C. Kim, J.-K. Lee, A novel mononuclear Fe(III) mono(terpyridine) complex having labile solvent ligands and its catalytic activity. *J. Chem. Soc., Dalton Trans.* **2002**, *21*, 3931–3932.
- [20] U. Sampath, W. C. Putnam, T. A. Osiek, S. Touami, J. Xie, D. Cohen, A. Cagnolini, P. Droege, D. Klug, C. L. Barnes, A. Modak, J. K. Bashkin, S. S. Jurisson, Terpyridyl derivatives as bifunctional chelates: Synthesis and crystal structures of 4'-[2-(1,3-dioxolan-2-yl)ethylsulfanyl]-2,2':6',2''-terpyridine and chloro(4'-methylsulfanyl-2,2':6',2''-terpyridine)gold(III) bis(trifluoromethanesulfonate). *J. Chem. Soc., Dalton Trans.* **1999**, *12*, 2049–2058.
- [21] W. B. Fortune, M. G. Mellon, Determination of iron with *o*-phenanthroline: A spectrophotometric study. *Ind. Eng. Chem. Anal. Ed.* **1938**, *10*, 60–64.
- [22] J. R. Ebdon, T. N. Huckerby, T. C. Hunter, Free-radical aqueous slurry polymerizations of acrylonitrile: 2. End-groups and other minor structures in polyacrylonitriles initiated by potassium persulfate/sodium bisulfite. *Polymer* **1994**, *35*, 4659–4664.
- [23] G. Socrates, In *Infrared and Raman Characteristic Groups Frequencies*, 3rd ed.; John Wiley & Sons Ltd: Chichester, England, 2001.

-
- [24] J. S. M. Samec, J.-E. Bäckvall, P. G. Andersson, P. Brandt, Mechanistic aspects of transition metal-catalyzed hydrogen transfer reactions. *Chem. Soc. Rev.* **2006**, *35*, 237–248.
- [25] S. E. Clapham, A. Hadzovic, R. H. Morris, Mechanisms of the H₂-hydrogenation and transfer hydrogenation of polar bonds catalyzed by ruthenium hydride complexes. *Coord. Chem. Rev.* **2004**, *248*, 2201–2237.
- [26] W. Baratta, K. Siwga, P. Rigo, Catalytic transfer hydrogenation with terdentate CNN ruthenium complexes: The influence of the base. *Chem. Eur. J.* **2007**, *13*, 7479–7486.
- [27] M. A. Fox, J. K. Whitesell, In *Organic Chemistry*, 3rd ed.; Jones and Bartlett Publishers: Sudbury, MA, 2003.
- [28] E. J. W. Verwey, J. T. G. Overbeek, In *Theory of the stability of lyophobic colloids*, 2nd ed.; Dover Publications: Mineola, NY, 1999.
- [29] J. N. Israelachvili, In *Intermolecular & Surface Forces*, 3rd ed.; Academic Press: Amsterdam, 2011.

Summary

The main focus of this thesis is the synthesis of well-defined colloidal particles which can be used as building blocks for larger structures. Through careful design of the colloid surface properties one gains control over the strength and directionality of the inter-particle interactions between individual building blocks. Manipulation of interactions between colloids allows for formation of predetermined, well-defined assemblies. The main motivation behind the desire to synthesize these self-assembling colloidal systems can be found in biology. From the formation of virus capsids to the folding of proteins and cell motility, a wide variety of processes are driven by a spontaneous assembly (and disassembly) of the corresponding building blocks. To understand the underlying mechanisms of these complex molecular systems, colloidal analogues are employed to facilitate both systematic tunability and visualization of the relatively large building blocks.

In **Part 1** the synthesis of chemically anisotropic colloidal particles is described. With the reported synthesis procedure we are able to prepare dumbbell-shaped colloids which consist of two chemically different lobes. The procedure starts from cross-linked, chlorinated polystyrene particles. To an aqueous dispersion of these seeds additional monomer (styrene) is added. Since the monomer is hydrophobic it diffuses into the chlorinated particles, thereby swelling the seeds. Swelling induces stress onto the cross-linked polymer network inside the seeds. This stress is relieved by heating the monomer-swollen seed dispersion. Relaxation of the network is accompanied by expulsion of the monomer present inside the seed particle. The chlorinated outer layer of the seed particles provides hydrophilicity to the particle surface ensuring that the expelled monomer does not fully wet the surface, but instead forms a liquid droplet on the surface of the seed. Polymerization of this monomer protrusion yields solid dumbbell-shaped particles. Since the chlorine functionalities are covalently attached to the seeds, they remain localized on one lobe. The lobe originating from the protrusion does not contain the functional chlorine moieties and therefore these particles can be modified in a site-specific way. As proof of principle, site-specific surface modifications were conducted using click chemistry as orthogonal functionalization method (**Chapter 2**).

By changing the properties of the seed particles or the experimental conditions during protrusion formation, the geometric shape of the resulting chemically anisotropic

dumbbells is tunable (**Chapter 3**). This allows for the preparation of a collection of anisotropic particles which vary in relative size of the functional patch. These particles are interesting as starting point for self-assembly studies, since directional interactions are within reach upon introduction of the proper surface chemistries on the reactive lobes of these particles.

Part 2 describes one of these possible surface chemistries, namely Surface-Initiated Atom Transfer Radical Polymerization (SI-ATRP). This form of controlled radical polymerizations is exploited to modify (anisotropic) particles by grafting polymers from their surface. **Chapter 4** describes the theoretical and chemical details of this polymerization technique. These theoretical considerations are illustrated by experimental results on the grafting of polymers from the surface of polystyrene colloids. Due to the versatility of ATRP, a variety of (functional) polymers are tethered to the surface of polystyrene colloids. Post-functionalization reactions on the attached polymers widen the scope of ATRP as functionalization method even further, giving access to polymer brushes with engineered topology and functionality.

In **Chapter 5** we exploit SI-ATRP reactions to graft thermo-responsive poly(*N*-isopropylacrylamide) (pNIPAM) brushes on polystyrene particles. The resulting particles show thermo-reversible swelling and shrinking if dispersed in pure water. This behavior is caused by extension and collapse of the grafted pNIPAM polymers. The thermo-responsive behavior of pNIPAM originates from the polymer's lower critical solution temperature (LCST), below which the polymers are hydrophilic and extend into the aqueous continuous phase. Above the LCST, the polymers turn hydrophobic and collapse onto the polystyrene core.

At slightly elevated ionic strengths of the continuous medium, the pNIPAM grafted colloids show thermo-reversible aggregation. In the presence of salt, the surface charges present on the polystyrene cores are shielded. Consequently, the range of electro-static repulsion decreases. If virtually all electro-statics are shielded within the thickness of the collapsed, hydrophobic pNIPAM brushes, these brushes are freely to attract each other via a hydrophobic interaction. The aggregation process is reversible, since cooling of the system yields hydrophilic brushes and therefore a disappearance of the hydrophobic attraction. The particles can undergo many aggregation cycles without any significant hysteresis, making this system truly thermo-reversible.

Chapter 6 combines the principles and results obtained in Chapter 2, 3 and 5. By exploiting the reactive lobes of the chemically anisotropic dumbbells, ATRP initiators are introduced site-specifically. Subsequent ATRP of NIPAM yields dumbbell-shaped colloids of which only one lobe is grafted with a pNIPAM brush. The size of the grafted patch is tunable by both the geometry of the starting dumbbell and the grafting time. The partially grafted colloids form small colloidal clusters if dispersed in high ionic strength media. Under these conditions the larger polymer grafted patch

of the dumbbells remains stable, while the smaller bald protrusion turns attractive. Introducing attraction onto the smaller lobes of the dumbbells ensures a geometric constraint on the number of bonds per particle, ultimately yielding finite-sized clusters.

Formation of thermo-reversible clusters by exploiting the responsive properties of pNIPAM grafted patches (Chapter 5) is not achieved, since the pNIPAM patch was too large to limit the number of bonds per particle.

A final example of the versatility of ATRP as functionalization method is shown in **Chapter 7**. In this chapter, a colloidal system is developed which shows dissipative/out-of-equilibrium aggregation. The system comprises polystyrene particles grafted with block-copolymers with charged carboxylic acid end-segments. Addition of a strong methylating agent (chemical fuel) converts the carboxylic acids in the terminal block to methyl esters. This reaction increases the hydrophobicity of the polymer brush which consequently leads to an effective inter-particle attraction. Depletion of the fuel triggers spontaneous disassembly of the formed clusters by reintroducing the charged moieties on the grafted polymer hairs via base-catalyzed hydrolysis reactions, since the whole process is performed in a buffered basic reaction environment. Once the clusters are disassembled, the system returns to its equilibrium state. Subsequent fuel injections allow for a repetition of the dissipative cycle. This system is the first example of fuel-driven assembly of colloids and provides the basis for the development of colloidal model systems for out-of-equilibrium assembly processes observed in biology.

Part 3 focusses on tuning the surface charge of chlorinated polystyrene particles. Throughout this thesis, polystyrene particles with benzyl chloride moieties on their surface are extensively used. The benzyl chloride functionality provides a chemical handle for further modifications. Typically, these modifications are not conducted in water due to low conversions. Instead, polar aprotic solvents, such as dimethylformamide (DMF), are often employed. In **Chapter 8** we show that the use of chlorinated colloids in combination with DMF leads to an unexpected side reaction. DMF reacts with the benzyl chloride groups on the surface of the particles, eventually forming permanently positively charged quaternary amines. The introduction of these positively charged groups causes a complete overcharging of the initially negatively charged chlorinated particles. During the overcharging process, severe aggregation is observed near the iso-electric point. Surprisingly, stable dispersions are obtained after reaching sufficiently high positive surface potentials. Clearly, the particles are not trapped in an extremely deep potential minimum near the iso-electric point.

In principle, the surface reaction with DMF provides a procedure to tune the overall surface charge of the particles. However, quenching the reaction proved to be difficult, which limits the synthetic practicality. To circumvent this problem, a more controlled reaction was selected to tune the surface charge of the chlorinated colloids. In **Chapter 9**, the benzyl chloride groups are converted to quaternary amine via the

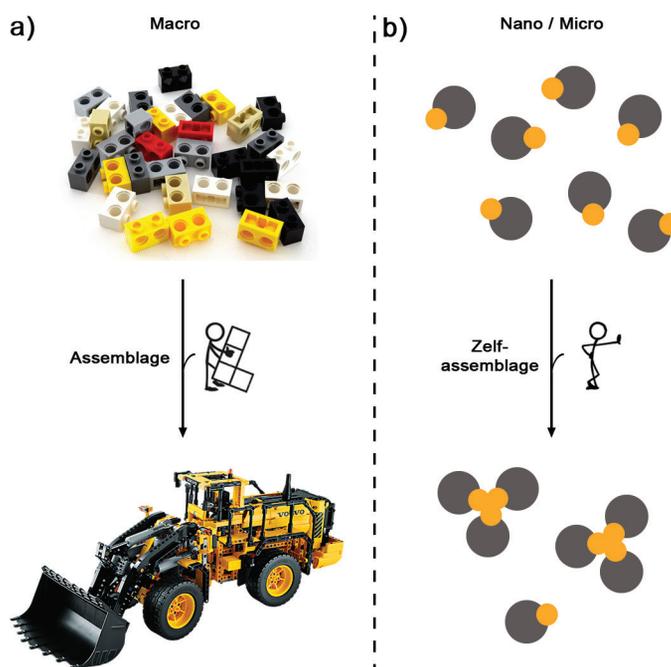
Menschutkin reaction. Unlike the harsh reaction conditions and complicated reaction mechanisms involved in the charge reversal reactions with DMF, a simple one-step procedure at low temperature proved to be sufficient to overcharge the chlorinated particles. Due to the simplicity of the reaction mechanism, the introduction of the positive charges was easily quenched. This method provides a robust way to tune the surface charge of polystyrene particles.

As example of an application for colloids with adjustable surface charge, we demonstrate the formation of organic–inorganic hybrid clusters via heterocoagulation with both nanometer- and micrometer-sized silica particles yielding raspberry-like particles and colloidal tetramers and trimers, respectively.

This thesis is concluded by **Part 4** which shows a completely different application of colloids with engineered surface properties. Chemically functional polystyrene particles are utilized as immobilization platform of a molecular transfer hydrogenation catalyst. Tethering of molecular catalyst to large carriers promotes recyclability. The additional advantage of carriers in the colloidal domain over macroscopic solids is the fact that colloids are still Brownian and therefore move through the reaction mixture. We hypothesized that this ensures intimate contact between catalyst and reactants and reduces loss of catalytic activity upon immobilization. The transfer hydrogenation of acetophenone is used as model reaction and the catalytic activity of the immobilized complex is compared to that of the homogeneous catalyst. Although a loss in catalytic activity is evident, full acetophenone conversion is still reachable within reasonable reaction times. Preliminary experiments show that recycling the catalyst by simple centrifugation of the colloids is feasible.

Samenvatting voor breder publiek

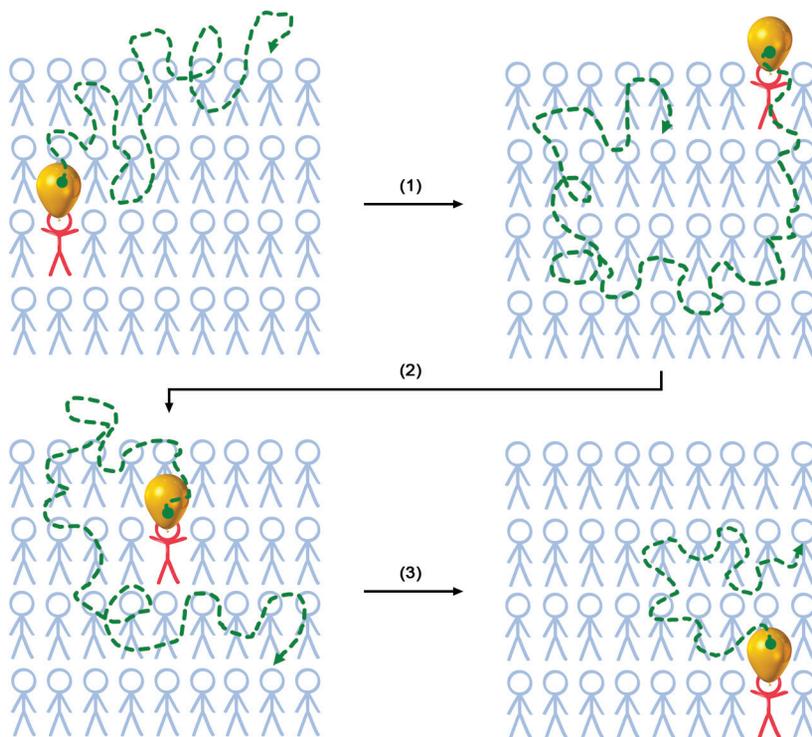
Zelf-organisatie of zelf-assemblage: het ontstaan van goed gedefinieerde en geordende systemen uit een chaotische begintoestand, komt enorm veel voor in de natuur. Vooral op de wat kleinere, moleculaire of atomaire schaal laat de natuur zien welke fascinerende structuren bereikbaar zijn als je bouwstenen op een goede manier in elkaar zet. Enkele voorbeelden van zelf-geassembleerde structuren zijn de vorming van ijskristallen uit watermoleculen, virussen uit losse eiwitten en erfelijk materiaal (DNA of RNA) en cel membranen uit zeepachtige vetmoleculen.



Figuur 1. (a) De assemblage van macroscopische bouwstenen (Lego steentjes) tot een volledige super-structuur. De super-structuur kan alleen verkregen worden als de bouwstenen actief bij elkaar gebracht worden. (b) Schematische weergave van een zelf-assemblage proces op de atomaire of moleculaire schaal. Door de kleine afmetingen, zijn de bouwstenen continu in beweging. Dit zorgt ervoor dat atomen of moleculen zich spontaan ordenen tot een super-structuur.

De assemblage van deze bouwstenen gebeurt spontaan; als je alle juiste ingrediënten bij elkaar stopt kun je na enige tijd de gevormde super-structuur terugvinden. Vandaar de term zelf-assemblage. Dit is anders voor een doos Lego. Hier zijn alle juiste bouwstenen wel aanwezig, maar ze zullen nooit vanzelf de mooie creatie vormen die voor op de doos staat (Figuur 1). In dit geval spreken we dan ook van assemblage in plaats van zelf-assemblage.

Een belangrijk verschil tussen de kleine moleculaire systemen en de macroscopische Lego steentjes is dat moleculen en atomen continu bewegen en dat de zwaartekracht op deze systemen verwaarloosbaar klein is. Deze bewegingen zijn te vergelijken met het traject dat een grote ballon aflegt wanneer deze op een grote menigte mensen wordt geworpen (Figuur 2). De mensen in de menigte zullen de ballon omhoog slaan waardoor de ballon een willekeurig pad aflegt (Figuur 2, groene stippellijn). Dit proces blijft zich herhalen wat er voor zorgt dat de ballon uiteindelijk de hele ruimte kan doorlopen. Wanneer je dus zeer kleine



Figuur 2. De continue beweging van moleculen, atomen en kleine deeltjes weergegeven aan de hand van een ballon die continu omhoog geslagen wordt door een persoon (rood mannetje) in een groep mensen (blauwe mannetjes). Na iedere stoot die de ballon krijgt legt deze een willekeurig pad af dat aangegeven is met de groene stippellijn. Als het aantal stootjes groot genoeg is, komt de ballon uiteindelijk overal.

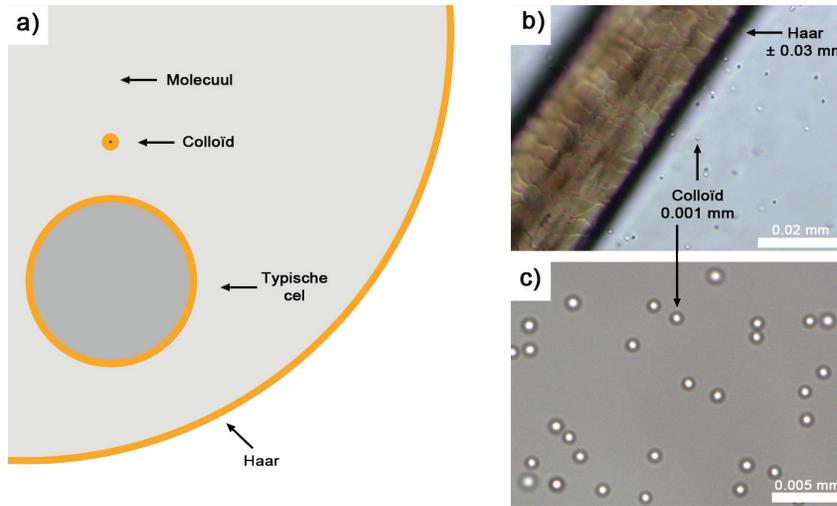
bouwstenen hebt die allemaal deze bewegingen spontaan uit voeren, dan zullen ze elkaar op een gegeven moment tegenkomen in de juiste oriëntatie ten opzichte van elkaar. Het gevolg is dat een binding gevormd wordt tussen de bouwstenen, net zo als het op elkaar zetten van twee Lego blokjes. Het aangaan van bindingen gaat door totdat de volledige structuur gevormd is.

Vanuit een fysisch oogpunt zijn deze processen zeer interessant. Als we de principes achter deze zelf-organisatie goed begrijpen snappen we bijvoorbeeld meer over de werkingen van cellen en hoe we ziektes kunnen voorkomen die het gevolg zijn van een fout in een assemblage proces. Ook vanuit technisch perspectief is kennis over zelf-assemblage processen enorm nuttig. Het fabriceren van de juiste bouwstenen kan immers leiden tot de spontane formatie van functionele materialen voor bijvoorbeeld coatings.

Een groot nadeel van het direct bestuderen van moleculaire of atomaire systemen is dat de bouwstenen (extreem) klein zijn. Moleculen zijn typisch niet groter dan 1 nanometer ($= 0.000000001 \text{ m} = 0.000001 \text{ mm}$). Om dit in perspectief te plaatsen; een typische cel in ons lichaam is 10000 keer zo groot en een menselijke haar is zelfs 50000 keer zo dik. In Figuur 3a is een poging gedaan om deze enorme verschillen in afmetingen weer te geven aan de hand van cirkels. De verhoudingen tussen de diameters van de cirkels zijn gelijk aan de verhoudingen tussen de afmetingen van de echte objecten. Zelfs als we de cirkel die correspondeert met de dikte van een haar enorm groot tekenen, resulteert dit in een onzichtbare kleine cirkel voor een molecuul.

Om de mechanismes achter zelf-organisatie processen toch te onderzoeken kunnen we gebruik maken van bouwstenen die net iets groter zijn dan de moleculaire/atomaire tegenhangers. Deze deeltjes, ook wel colloïden genoemd, hebben afmetingen tussen de 10 en 1000 nanometer ($= 0.00001\text{--}0.001 \text{ mm}$). Dat lijkt nog steeds heel erg klein, maar vooral als de deeltjes groter zijn dan enkele honderden nanometers worden de deeltjes *live* zichtbaar onder hedendaagse microscopen. Dit is duidelijk geïllustreerd in Figuur 3b en c. Figuur 3b laat een microscopie foto zien van colloïdale deeltjes in water die naast een haar liggen. Ondanks het feit dat de deeltjes significant kleiner zijn dan de haar, zijn ze duidelijk zichtbaar op deze foto. Wanneer we de vergroting van de microscoop opschroeven, zijn de deeltjes zeer goed zichtbaar (Figuur 3c), wat ons in staat stelt de deeltjes op individueel niveau te bestuderen. Zelfs bij deze grotere vergroting ziet de achtergrond van de foto er homogeen uit. Individuele water moleculen die zich rondom de deeltjes bevinden zijn simpelweg niet zichtbaar.

Omdat de deeltjes nog steeds relatief klein zijn, bewegen ze op een gelijksoortige manier als atomen en moleculen (Figuur 2). Deze eigenschap zorgt er eigenlijk voor dat we de deeltjes mogen gebruiken als modelsystemen voor moleculen en atomen. Maak je de deeltjes te groot en verlaat je het colloïdale regime dan verlies je de analogie met moleculaire systemen en begint het systeem zich te gedragen zoals Lego steentjes.



Figuur 3. (a) Schematische weergave van de relatieve afmetingen van een menselijke haar (± 0.05 mm), een typische cel uit ons lichaam (± 0.01 mm), een colloïdaal deeltje (± 0.001 mm) en een molecuul (± 0.000001 mm). (b) Microscopie foto van colloïdale deeltjes van 0.001 mm naast een van mijn haren met een dikte van ± 0.03 mm. (c) Dezelfde colloïden als weergeven in Figuur b, maar nu bij een grotere vergroting. Zelfs deze relatief kleine deeltjes zijn zeer goed zichtbaar met hedendaagse microscopen.

Naast het voordeel dat we deeltjes direct kunnen observeren en dus bestuderen, zijn (fysisch) chemici momenteel in staat vele soorten colloïden te maken. Je kunt daarbij denken aan variaties in vorm (bol, kubus, staafjes, plaatjes), maar ook in de manier waarop de deeltjes aan elkaar binden, oftewel interacties aangaan, kan beïnvloed worden. Verschillende vormen worden meestal verkregen door specifieke materialen en reactiecondities te kiezen. Bolvormige deeltjes zijn meestal vervaardigd van plastic of silica (zand). Kubische deeltjes zijn te maken uit hematiet, een speciale vorm van ijzeroxide (roest) en plaatjes/staafjes zijn bijvoorbeeld te vinden in klei.

Het instellen van wisselwerkingen, ook wel interacties genoemd, tussen de deeltjes wordt veelal gedaan door het introduceren van specifieke moleculen op het oppervlak van de deeltjes. Deze moleculen zorgen ervoor dat de deeltjes elkaar 'leuk' gaan vinden en elkaar dus gaan aantrekken. Het is eenvoudig voor te stellen dat wanneer deze moleculen overal op het deeltje aanwezig zijn er geen voorkeur is voor een bepaalde oriëntatie waarin de deeltjes binden. In moleculaire systemen is dit vaak niet het geval. De moleculaire bouwstenen bevatten stukjes die attractief zijn en andere stukjes die juist afstotend zijn. In welke richting en in welke oriëntatie bindingen gevormd worden zit min of meer verankerd in de structuur van het molecuul. Om dit gedrag

dus na te bootsen met onze colloïdale modelsystemen moet er ook een voorkeur voor bepaalde bindingsconfiguraties ingebouwd worden in de deeltjes die we gaan gebruiken. Deeltjes die deze eigenschap hebben worden vaak aangeduid als *patchy*. De deeltjes bevatten regio's (*patches*) die alleen interacties aangaan met *patches* van andere deeltjes. Dit is schematisch ook weergegeven in Figuur 1. Alleen de gele stukjes van de bouwstenen plakken aan elkaar in de uiteindelijke super-structuur. Het aantal bindingen dat één bouwsteen kan maken en de oriëntatie ten op zichte van andere deeltjes hangt respectievelijk af van het aantal *patches* en de verdeling van de *patches* over het oppervlak van ieder deeltje.

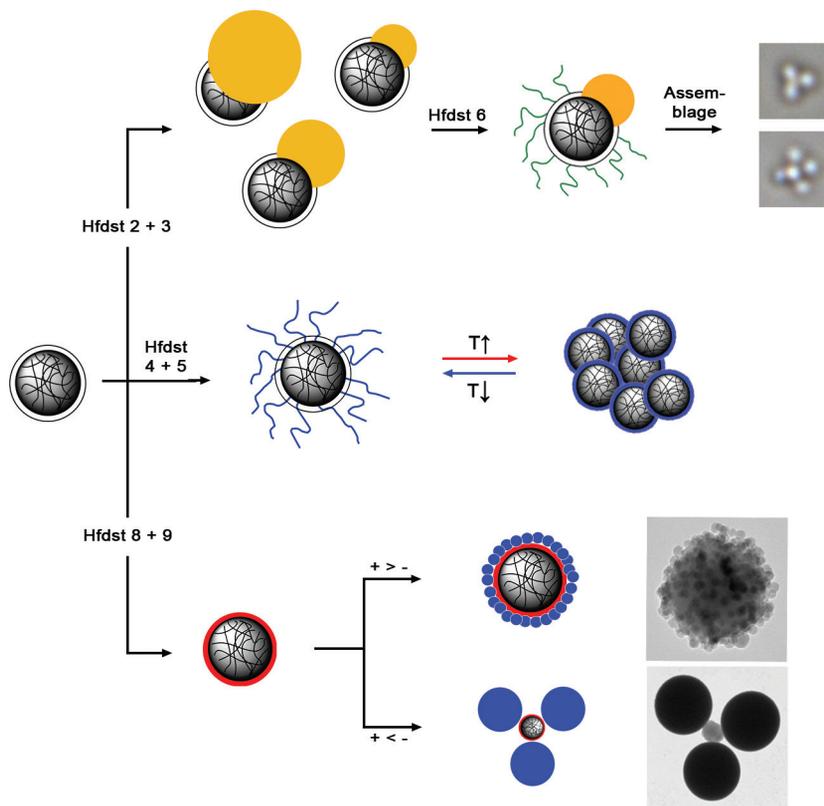
De controle over de vorm, interacties en voorkeur voor bindingsoriëntatie tussen de deeltjes stelt de (fysisch) chemicus in staat om bouwstenen te ontwerpen die een beoogde structuur vormen ten gevolge van een zelf-organisatie proces. Vervolgens kunnen vorm en interacties systematisch gevarieerd worden zodat een goed beeld ontstaat over welke elementen essentieel zijn voor succesvolle assemblage op colloïdale, maar dus ook op moleculair niveau.

Dit proefschrift beschrijft een aantal methodes om deeltjes te maken die wellicht gebruikt zouden kunnen worden voor dit soort modelstudies. In **Deel 1** van het proefschrift wordt de synthese van deeltjes met een sneeuwpopachtige of Barbapapa vorm beschreven (Schema 1, links boven). De procedure om deze deeltjes te synthetiseren begint met het maken van kleine plastic (polystyreen) bolletjes. Deze bolletjes kunnen gezien worden als kleine sponsjes die vloeistof op kunnen nemen. Wanneer de deeltjes zwellen met de toegevoegde vloeistof, ontstaat er elastische stress op het deeltje. Deze stress kan weggenomen worden door het systeem te verhitten. In feite wordt de spons leeg geknepen. Onder de juiste omstandigheden vormt de vloeistof een kleine druppel op het oppervlak van het bolvormige deeltje waarmee we zijn begonnen. In de laatste stap wordt de vloeibare druppel omgezet in een vast materiaal, zodat uiteindelijk een volledig sneeuwpopvormig deeltje gevormd wordt. Het speciale van deze deeltjes is dat het hoofd van de sneeuwpop chemisch gezien anders is dan zijn lijf (**Hoofdstuk 2**). In feite zijn deze sneeuwpoppen daarom deeltjes met één *patch*. Deze *patch* kan vervolgens gemodificeerd worden met allerlei functionele moleculen door gebruik te maken van zeer efficiënte koppelingsreacties.

In **Hoofdstuk 3** wordt beschreven hoe de geometrie, oftewel de verhouding tussen de afmeting van het hoofd en het lijf van de sneeuwpop, gevarieerd kan worden door het systematisch veranderen van relevante reactieparameters.

Samen leveren Hoofdstuk 2 en 3 synthese procedures op die als leidraad dienen voor de synthese van een breed scala aan *patchy* colloïden die op specifieke regio's gefunctionaliseerd kunnen worden. Deze deeltjes vormen daarmee een goed startpunt voor het ontwerp van colloïdale bouwstenen voor zelf-organisatie studies.

Schema 1. Schematisch overzicht van de onderwerpen die behandeld worden in dit proefschrift.^a



^a Hfdst 2 + 3 beschrijven de synthese van sneeuwpopvormige deeltjes beginnend vanuit bolvormige polystyreen (plastic) bolletjes. De verhouding tussen het lijf (grijs) en het hoofd (geel) van de sneeuwpop kan gevarieerd worden. Hfdst 4 + 5 beschrijven hoe bolvormige polystyreen colloïden gefunctionaliseerd kunnen worden met polymeren haren. Deze haren kunnen bijvoorbeeld gebruikt worden om de deeltjes reversibel te laten samenklonteren als de temperatuur van de omgeving veranderd wordt. Hfdst 6 beschrijft het specifiek introduceren van polymeren haren op het lijf van de sneeuwpop-vormige deeltjes. Deze deeltjes dienen vervolgens als bouwstenen voor de vorming van kleine clusters. Hfdst 8 + 9 beschrijven hoe de oppervlakte lading van polystyreen deeltjes gereguleerd kan worden. Positief geladen deeltjes (rode rand) worden vervolgens gemengd met negatief geladen deeltjes (blauw) wat resulteert in verschillende colloïdale clusters. Welk type cluster gevormd wordt hangt af van de relatieve afmetingen van beide deeltjes.

Deel 2 beschrijft een van de mogelijke methodes om deeltjes of *patches* van deeltjes te functionaliseren om ze zo te voorzien van de juiste fysische eigenschappen.

De methode die gebruikt wordt heet in het goed Nederlands *Atom Transfer Radical Polymerization* (ATRP). Deze techniek stelt ons in staat om lange moleculen, polymeren, vast te zetten op het oppervlak van een deeltje. De deeltjes die hiervoor gebruikt worden bevatten chemische groepen op het oppervlak die dienen als groeipunt voor de polymeren. Je zou de deeltjes kunnen zien als een hoofd waaruit haren, de polymeren, groeien gedurende de ATRP reacties. Omdat ATRP een relatief onbekende techniek is binnen de fysische chemie, is **Hoofdstuk 4** gewijd aan de theoretische principes en aspecten van deze methode. De theorie wordt gecombineerd met enkele experimenten om te laten zien hoe ATRP gecombineerd kan worden met colloïden en welke polymeren op een deeltje gezet kunnen worden. ATRP is een zeer veelzijdige techniek wat er voor zorgt dat er een grote variëteit aan polymeren haren gegroeid kan worden.

In **Hoofdstuk 5** wordt ATRP gebruikt om bolvormige deeltjes te functionaliseren met polymeren haren die reageren op temperatuursveranderingen van de waterige omgeving waarin de deeltjes rondzwemmen. Bij een lage omgevingstemperatuur zijn de polymeren hydrofiel. Dit betekent dat de polymeren graag oplossen in water en daarom steken ze in de waterige omgeving. Echter, wanneer de temperatuur omhoog gaat, ondergaan de polymeren een overgang waardoor ze hydrofoob worden. Dit zorgt voor een sterk verminderde wateroplosbaarheid en de polymeren haren krimpen ineen. Als het systeem afgekoeld wordt komt het hydrofiele karakter van de polymeren weer terug en zwellen de haren weer op. Met andere woorden, het proces is omkeerbaar of reversibel. Onder de juiste omstandigheden kan de plotselinge overgang van hydrofiele naar hydrofobe haren gebruikt worden om de deeltjes reversibel te laten samenklonteren, ook wel aggregeren genoemd. De hydrofobe deeltjes die verkregen worden bij verhoogde temperatuur willen immers niet graag in water zijn en trekken elkaar dus aan. De liefde tussen de deeltjes gaat snel over als de temperatuur weer verlaagd wordt, omdat de polymeren liever in contact staan met water dan met polymeren van andere deeltjes (Schema 1, midden).

De mogelijkheid om interacties tussen deeltjes aan en uit te zetten door eenvoudig de temperatuur te veranderen is een interessante optie voor het gecontroleerd starten of beëindigen van zelf-assemblage processen. Bovendien geeft dit de mogelijkheid om fouten in de verkregen super-structuren te repareren door de structuur tijdelijk op te breken en vervolgens weer te laten helen.

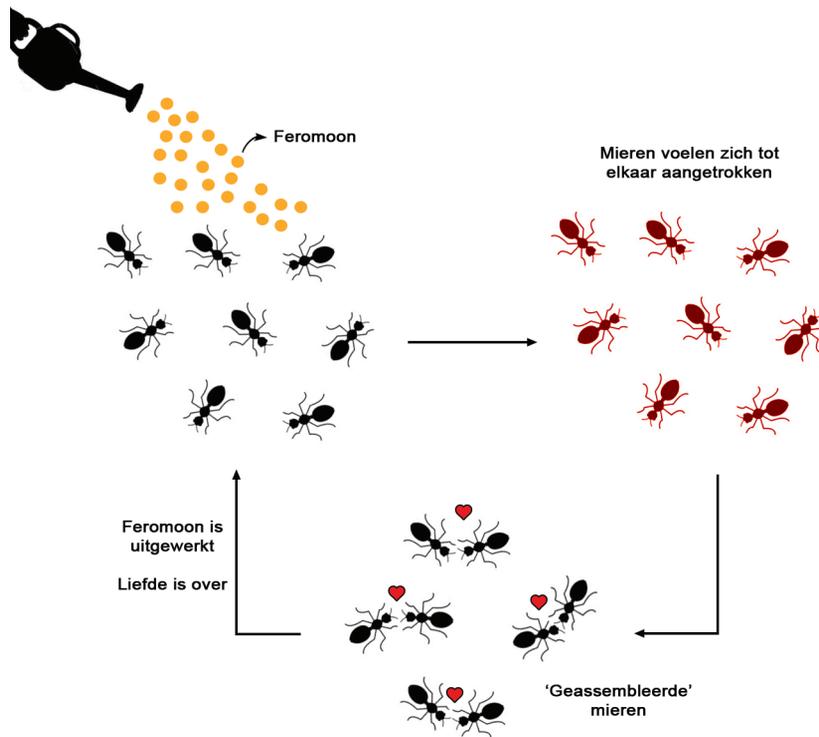
In Hoofdstuk 5 is gebruik gemaakt van bolvormige deeltjes. Als deze deeltjes elkaar aan gaan trekken door een verhoging in de temperatuur ontstaan er clusters van deeltjes waarin geen goed gedefinieerde structuur zit. De deeltjes plakken immers op alle plekken aan elkaar. Zoals eerder vermeld, kan dit probleem opgelost worden door gebruik te maken van *patchy* deeltjes. **Hoofdstuk 6** combineert de sneeuwpopvormige deeltjes uit Hoofdstuk 2 en 3 met de mogelijkheid om temperatuurgevoelige

polymeren op een deeltje te groeien door middel van ATRP (Hoofdstuk 5). Omdat de sneeuwpop deeltjes twee chemisch verschillende delen hebben, zijn we in staat om de polymeren haren slechts op één deel van deze sneeuwpoppen te groeien (Schema 1, rechts boven). Het resultaat na het groeien van de haren zijn sneeuwpoppen met of een behaard hoofd of een behaard lijfje. De deeltjes met een klein kaal hoofd en een groter behaard lijfje zijn in staat kleine clusters te vormen door hun hoofdjes bij elkaar te steken. Omdat de lijfjes groter zijn dan de hoofdjes, kunnen slechts drie tot vijf hoofdjes aan elkaar gaan zitten. Het volgende deeltje past er gewoonweg niet meer bij omdat de harige lijfjes van de deeltjes die zich al in het cluster bevinden in de weg zitten.

Deze clusters zijn echter niet reversibel; de clusters blijven permanent bestaan. Om reverseerbare clusters te maken zouden juist de harige regio's van de deeltjes attractief moeten worden. Zoals gezien in Hoofdstuk 5 kan deze aantrekking eenvoudig geïntroduceerd worden door de temperatuur van de omgeving te verhogen. Ook in het geval van de harige sneeuwpoppen blijkt dit te werken. Echter, in plaats van de beoogde kleine, goed gedefinieerde clusters die deeltjes met slechts één *patch* zouden moeten vormen, werden grote wanordelijke aggregaten gevormd. Onze verklaring voor deze waarneming is dat de *patch* waarop de temperatuurgevoelige polymeren zitten te groot is ten op zichte van het kale stukje van de sneeuwpop. De kleine kale regio kan niet voorkomen dat er steeds meer deeltjes aan elkaar binden. Uiteindelijk leidt dit tot zeer grote clusters met geen enkele structuur.

In **Hoofdstuk 7** laten we het laatste voorbeeld zien van hoe de combinatie tussen deeltjes en ATRP kan leiden tot nieuwe colloïdale systemen. Zoals besproken in het begin van deze samenvatting is zelf-organisatie een spontaan proces. Nadat je de bouwstenen hebt gemaakt en ze bij elkaar brengt ontstaat er vanzelf een grotere structuur. Wanneer we echter iets willen leren over hoe de natuur omgaat met het maken van geassembleerde structuren uit lossen bouwstenen, is deze spontane formatie niet altijd een goed model. Veel assemblage processen in de moleculaire biologie zijn namelijk niet spontaan, maar verlopen alleen als er energie wordt toegevoegd aan de bouwstenen. Zodra de energiebron op is of weggenomen wordt, stopt het assemblage proces en valt de gevormde structuur spontaan uiteen. De energie die nodig is om deze systemen te laten werken zit verpakt in moleculen. Door de concentratie en de positie van deze moleculen te reguleren zijn biologische systemen superieur in het controleren van assemblage processen.

Om dit principe wat concreter te maken zou je het kunnen vergelijken met mieren die zich tot elkaar aangetrokken voelen door tussenkomst van feromonen of signaalmoleculen (Figuur 4). In de begintoestand verdelen de mieren zich over alle beschikbare ruimte. Ze zijn niet geïnteresseerd in elkaar en geven elkaar de ruimte. Dit verandert echter wanneer een bioloog of biochemicus besluit om liefdesferomonen



Figuur 4. Energie-gedreven assemblage uitgelegd aan de hand mieren die zich tot elkaar aangetrokken voelen na toevoeging van feromonen. Onder normale omstandigheden zijn de mieren (bouwstenen) niet in elkaar geïnteresseerd en verdelen ze zich over de beschikbare ruimte. Wanneer een biochemicus/bioloog echter feromonen (energierijke brandstof) toevoegt, zullen de mieren zich tot elkaar aangetrokken voelen (attractieve, rode mieren). Dit leidt tot het aggregeren of assembleren van de mieren. Dit proces gaat door zolang er voldoende feromonen aanwezig zijn. Zodra de feromonen vervlogen zijn, verliezen de mieren interesse in elkaar en verspreiden ze zich weer.

te verspreiden in de mierenkolonie. Deze feromonen zorgen ervoor dat de mieren elkaar aantrekkelijk gaan vinden. In feite veranderen de mieren van repulsieve (zwarte mieren) naar attractieve bouwstenen (rode mieren). Dit leidt tot de vorming van liefdeskoppeltjes en dus kleine clusters van mieren. Het aggregatieproces gaat door zolang er voldoende feromonen aanwezig zijn. Zodra de feromonen vervlogen zijn verliezen de mieren hun wederzijdse interesse en breken de aggregaten van mieren spontaan weer op.

Synthetische systemen om deze energie-gedreven assemblage processen te bestuderen zijn tot op de dag van vandaag zeer zeldzaam. In Hoofdstuk 7 beschrijven

we de synthese van het eerste colloïdale systeem dat de elementaire eigenschappen heeft om deel te nemen aan een energie-gedreven assemblage proces. Om dit te realiseren, worden polymeren op colloïdale deeltjes gezet die negatief geladen zijn. Door de aanwezigheid van de lading stoten deeltjes elkaar af als ze elkaar tegen komen. De situatie verandert echter als we een extra component toevoegen aan het systeem. Deze component gaat een reactie aan met de polymeren haren op de deeltjes en zorgt ervoor dat de lading verdwijnt. Hiermee verdwijnt ook de onderlinge afstoting tussen de deeltjes dat clustering van de colloïden tot gevolg heeft. Dit aggregatie proces gaat door zolang de ladingen van de polymeren weggenomen worden. Op een gegeven moment is de extra component op en groeien de aggregaten niet meer. De chemische groepen die de lading wegnamen zijn echter niet stabiel onder de reactieomstandigheden. Langzaam worden de ladingen opnieuw gevormd op de polymeren haren. De deeltjes in een cluster beginnen elkaar dus weer af te stoten en uiteindelijk gaan we terug naar de beginsituatie waarin alle deeltjes los rond zwemmen. Deze hele cyclus kan herhaald worden door opnieuw de extra component toe te voegen.

In **Deel 3** wordt het reguleren van de oppervlakte lading van deeltjes besproken. Veruit de meeste deeltjes die gebruikt worden in het onderzoek dat staat beschreven in dit proefschrift, zijn geladen. Deze lading is nodig om de deeltjes uit elkaar te houden en dus te voorkomen dat ze aan elkaar plakken. Des te meer lading, des te sterker de afstoting tussen de deeltjes onderling en des te groter de gemiddelde afstand tussen de deeltjes. Niet in alle gevallen is een grote onderlinge afstoting wenselijk. Wanneer je deeltjes ontwerpt die in staat moeten zijn te assembleren in een grotere structuur, moeten de individuele deeltjes natuurlijk wel dicht genoeg bij elkaar kunnen komen. In dit soort situaties is minder lading per deeltje wenselijk. Het reguleren van oppervlakte ladingen is daarom een natuurlijke weg om de wisselwerking tussen deeltjes te sturen. In **Hoofdstuk 8** wordt de observatie beschreven dat negatief geladen plastic (polystyreen) bolletjes positief geladen worden door ze te in contact te brengen met het oplosmiddel dimethylformamide (DMF). DMF is in staat te reageren met het oppervlak van de polystyreen deeltjes wat de vorming van positief geladen chemische groepen ten gevolge heeft. Tijdens deze reactie blijven de negatieve groepen die al op het deeltje aanwezig waren ook bestaan. Halverwege de reactie ontstaat er dus de situatie dat er even veel negatieve als positieve groepen aanwezig zijn op het deeltje. Netto hebben de deeltjes geen lading en is aggregatie onvermijdelijk. Echter, wanneer de reactie verder verloopt, komen er meer positieve dan negatieve groepen en worden uiteindelijk deeltjes met een netto positieve lading gevormd. In principe geeft deze oppervlakte reactie dus een methode om de hoeveelheid lading en het teken van de lading te controleren door de reactie op een gewenst tijdstip te stoppen. Voor de reactie met DMF bleek dit echter niet heel goed te werken, omdat de reactie nog doorgaat na verwijdering van de DMF. Dit probleem kon worden opgelost door een beter gedefinieerde en mechanistisch

makkelijkere reactie te kiezen om de positieve groepen te introduceren (**Hoofdstuk 9**). Met deze vernieuwde methode was het mogelijk om de reactie op ieder punt snel te stoppen, zodat de lading van de deeltjes werkelijk controleerbaar was. Om aan te tonen dat de uiteindelijke deeltjes daadwerkelijk positief geladen zijn, werden deze op een gecontroleerde manier gemengd met negatief geladen deeltjes. De tegengesteld geladen deeltjes trekken elkaar aan wat resulteert in kleine clusters. Het soort cluster dat gevormd wordt hangt af van de relatieve afmetingen tussen de positief (Schema 1, rood deeltje onderaan) en negatief geladen deeltjes (Schema 1, blauw deeltje onderaan). Wanneer de positief geladen deeltjes veel groter zijn dan de negatief geladen deeltjes ontstaan er clusters waarin de positieve deeltjes compleet bedekt zijn met een groot aantal negatieve deeltjes. In de tegenovergestelde situatie, waarin de positieve deeltjes de kleinste zijn van de twee, binden er slechts twee of drie negatieve deeltjes aan één positief geladen colloïd.

Dit proefschrift wordt afgesloten met **Deel 4**, waarin een compleet andere toepassing van colloïdale deeltjes wordt beschreven. In **Hoofdstuk 10** worden colloïdale deeltjes gefunctionaliseerd met een katalysator. Vele reacties die chemici willen doen verlopen zeer traag of alleen bij hoge temperaturen en drukken. Om het leven van de chemicus wat aangener te maken kan hij of zij gebruiken maken van een katalysator. Een katalysator verlaagt de energiedrempel die je over moet om uiteindelijk bij het beoogde product te komen. Katalysatoren worden niet verbruikt tijdens de reactie en kunnen dus gerecycled worden. Een groot gedeelte van de beschikbare katalysatoren zijn echter kleine moleculen die zeer moeilijk te scheiden zijn van het reactiemengsel. Om dit probleem op te lossen kunnen katalysatoren geïmmobiliseerd worden op een drager, bijvoorbeeld een colloïdaal deeltje. De relatief grote afmeting zorgt ervoor dat scheiding van colloïden en dus ook de geïmmobiliseerde katalysator uit reactiemengsels gemakkelijk is. Bovendien zijn de deeltjes klein genoeg om nog door het reactiemengsel te bewegen. Dit zorgt voor intiem contact tussen de katalysator en de reactanten wat de opbrengst ten goede komt. In feite worden katalysatormobiliteit en mogelijkheid tot recyclen op een elegante manier gecombineerd.

Acknowledgments

As a Ph.D. student you are focused on one or two subjects for four years, trying to understand some (fundamental) problems and to contribute something to the scientific community. In practice it means countless hours of lab work, analyzing unexplainable results, writing reports and being frustrated because you have no clue how to proceed with the project. If you read this, you might think that doing a Ph.D. project is one of the worst things that can happen to you. Fortunately, the complete opposite is true. The last four years were really great and this is mainly because of all the people that made this work possible and supported me throughout this period. The classical stereotype of a lonely scientist that works alone in a dark basement is luckily long gone.

First of all I would like to thank my promotor and daily supervisor. Willem, thanks for giving me the opportunity to conduct my Ph.D. project with you. I appreciate your way of supervising. Although you have a clear scientific vision, you gave me enough freedom to pursue my own ideas and maybe sometimes ‘weird’ chemical tricks. I believe that our collaboration really worked both ways: I introduced you to the magical world of ATRP and particles with weird surface functionalities, while you taught me the physical aspects of the project. We stitched chemistry and physics together as it should in a group for Physical Chemistry. Before I came to Utrecht I promised myself to never do thermodynamics again, but you convinced me: thermodynamics are useful and yes, even elegant. I think this is the biggest compliment I can give you. Besides your scientific input, you provided always a relaxed and nice working atmosphere. Despite your busy agenda, you had always time to have a quick discussion about how to boost my results to the next level and to bombard me with a flood of new ideas.

Besides my daily supervisor there are of course other people with whom I have collaborated during this project. I would like to thank all these people for their fruitful and critical input regarding my results. In particular I would like to thank Marlous Kamp (UU) for taking beautiful confocal microscopy images of partially fluorescent dumbbells which made publication in *Chemistry of Materials* possible, Judith van Wijk (TU/e) for XPS analysis of the chlorinated polystyrene particles and the colloids with the immobilized transfer hydrogenation catalyst, Isja de Feijter, Neus Vilanova Garcia and Ilja Voets (TU/e) for working together on the BTA functionalized colloids. Although this work is not included in this thesis, I am confident that our results will

make up a nice story once finished. Wouter Hendriksen and Rienk Eelkema (TUD) are thanked for introducing me into the world of dissipative self-assembly and the fruitful collaboration that led to the results presented in Chapter 7. I am sure these results will be published in a nice journal soon.

During my Ph.D. project I also had the privilege to guide some students. I would like to thank you all for providing a lot of experimental data and exploration of new projects. Susan van Rossum, thanks a lot for the countless experiments conducted during your bachelor thesis on the preparation of chemically anisotropic dumbbells. Dirk-Jan Schild, your work on the immobilization of a transfer hydrogenation catalyst resulted in Chapter 10. A great achievement for a relatively short internship. I am pleased to see that you continued your educational career at Utrecht University and wish you all the best in the future. Finally, I was lucky enough to have Frans Dekker as master student. Frans, I admire your enthusiasm for research and in particular chemical synthesis. Your hard work resulted in almost the complete experimental part of Chapter 4 and your results served as inspiration for all the ATRP related chapters. Good luck with your own Ph.D. and of course many thanks for being my paranymph.

During my Ph.D. project I spend most of my time either in the lab (N724) or in my office (N731), so first of all I would like to thank the people with whom I had the pleasure to share these rooms: Yong, Mikal (lab) and Jaakko, Janne-Mieke, Esther, Jan, Antara, Ivan and Alvaro (office). Jan en Mikal, thanks for all the great music! The metal-sessions in N724 were legendary (you can ask some of the students who had to work in the room next to the lab)! I enjoy(ed) the game evenings after work: *All guns blazing & let's do this!!!*

Many thanks to all the other (former) colleagues at FCC for providing the perfect scientific and relaxed atmosphere: Anke, Samia, Ping, Laura, Joost, Chris, Jos, Julius, Pepijn (thank you for being my ünter), Jasper, Mark, Nina, Roel, Fuqiang, Burak, Susanne, Rocio, Rob, Gert-Jan, Hans, Henk, Jan Groenewold, Remco, Albert, Ben, Andrei and all the people I might forget. All the labuitjes, Borrels (special thanks to my über, Chris), New Year's dinners, conferences and whiskey nights we had together were great! The social activities of FCC are of equally high level as the scientific output. All I can ask is: 要啤酒吗? (Yong and Fuqiang will understand :)). Bonny, Kanvaly and Dominique are thanked for all the lab-related assistance. Marina, thanks for dealing with all the bureaucratic issues I faced throughout the past four years.

Hans and Chris, thanks for the assistance at the electron microscopes. I did not use the microscopes so often and you were always willing to help me if I forgot how to fix a small problem myself.

Of course I would also like to thank my parents and Maartje for the endless support and interest in my project. The weekends in Weert were relaxing and usually something completely different from my daily routine. Thanks for all the times we

chopped wood, cutted enormous trees and fixed my BMW (again :P). Although completely unrelated to chemistry, the pragmatic way of thinking and hard-working mentality you thought me brought me where I am today.

And as the very last, Sonja. The short way of saying this is: I love you! You were always there for me and helped me with everything one can imagine, from checking my not-so-flawless English to traveling with me to the end of the world and being my paranymph. With you around everything becomes much easier, better and more fun <3.

List of Publications

This thesis is based on the following publications:

- B. G. P. van Ravensteijn, W. K. Kegel, Colloids with continuously tunable surface charge. *Langmuir* **2014**, *30*, 10590–10599. (Chapter 8 and 9)
- B. G. P. van Ravensteijn, M. Kamp, A. van Blaaderen, W. K. Kegel, General route toward chemically anisotropic colloids. *Chem. Mater.* **2013**, *25*, 4348–4353. (Chapter 2)

Manuscripts submitted or in preparation:

- B. G. P. van Ravensteijn, W. K. Kegel, Tuning particle geometry of chemically anisotropic dumbbells. *In preparation*. (Chapter 3)
- B. G. P. van Ravensteijn, W. K. Kegel, Salt-dependent thermo-reversible aggregation of pNIPAM grafted colloids. *In preparation*. (Chapter 5)
- B. G. P. van Ravensteijn, W. K. Kegel, Colloidal dumbbells with tunable Janus balance via site-specific Atom Transfer Radical Polymerization. *In preparation*. (Chapter 6)
- B. G. P. van Ravensteijn, W. E. J. Hendriksen, J. H. van Esch, R. Eelkema, W. K. Kegel, Out-of-equilibrium aggregation of colloidal building blocks. *In preparation*. (Chapter 7)
- B. G. P. van Ravensteijn, D.-J. Schild, R. J. M. Klein Gebbink, W. K. Kegel, Immobilization of a transfer hydrogenation catalyst on colloidal particles. *In preparation*. (Chapter 10)

Other papers by the author:

- G. C. Sanders, B. G. P. van Ravensteijn, R. Duchateau, J. P. A. Heuts, The unexpected behaviour of epoxidised macromonomers derived from catalytic chain transfer during ring opening copolymerisation. *Polym. Chem.* **2012**, *3*, 2200–2208.

Curriculum Vitae

Bas van Ravensteijn was born on April 18, 1988 in Eindhoven, The Netherlands. After graduation from the Bisschoppelijk College in Weert in 2006, he started studying Chemical Engineering & Chemistry at the Eindhoven University of Technology (TU/e). In 2009 he obtained his Bachelor of Science degree after finishing a bachelor thesis on colloidosomes composed of sterically stabilized colloidal particles. This project was conducted at the department of Chemistry and Polymer Science, Stellenbosch University, South Africa under the supervision of Joris Salari and Bert Klumperman. In this year he also started the master program Molecular Engineering with a strong focus on polymer and organic chemistry. He performed his master thesis in the Polymer Chemistry group at the TU/e on the preparation of epoxidized macromonomers using catalytic chain transfer polymerization and their ring opening polymerization behavior. Supervision was provided by Gemma Sanders, Hans Heuts and Rob Duchateau. The master program was concluded (*cum laude*) by a four month internship at Icopal on the development of encapsulated fire retardants for bitumen roofing applications under supervision of Joris Salari, Judith van Wijk and Frits Zandvoort. In 2011 he moved to the Van 't Hoff Laboratory for Physical and Colloid Chemistry at Utrecht University to start his Ph.D. project supervised by Willem Kegel. The results of this project, of which parts are published in scientific journals and have been presented at both national and international conferences, are described in this thesis. Conferences where the author presented his work include the Graduate Research Seminar (part of International Polymer and Colloids Group Meeting 2013) in Shanghai, China and ACS Colloids & Interface Science Symposium 2014 in Philadelphia, United States. The presentation in Shanghai was rewarded with the prize: "Best oral presentation of the conference."

